University of Rome “Tor Vergata”

Consiglio Nazionale delle Ricerche

UNIVERSITY OF ROME “TOR VERGATA”

Dr. Vincenzo Baglio

Ph.D. course in “Materials for Environment and Energy”

(XVII cycle)

Preparation and characterization of components for Direct Methanol Fuel Cells

Supervisor:

Prof. Pier Luigi Antonucci

Director:

Prof. Enrico Traversa

TABLE OF CONTENTS

Summary pag. 4

CHAPTER I – Introduction pag. 5

I.1 – Introduction to Direct Methanol Fuel Cells pag. 5

I.2 – Fundamental Aspects pag. 6

I.2.1 – Anodic oxidation of methanol pag. 6

I.2.1.1 – *Overall reaction* pag. 6

I.2.1.2 – *Electrocatalysis* pag. 7

1.2.1 – General comments pag. 7

1.2.2 – Experimental methods pag. 8

1.2.3 – Structural effects and electrode-kinetics pag. 10

1.2.4 – Pt electrocatalysts pag. 11

1.2.5 – Pt-Ru binary alloy electrocatalysts pag. 13

1.2.6 – Promoting effects of Ru and Sn: bifunctional mechanism and ligand effect pag. 15

1.2.7 – Role of Ru-oxide in enhancing kinetics pag. 18

1.2.8 – Ternary alloy Pt-Ru-W and Pt-Ru-Mo electrocatalysts pag. 19

1.2.9 – Heteropolyacids as surface promoters pag. 20

1.2.10 – Alternative electrocatalysts to Platinum and their alloys pag. 21

I.2.1.3 – *Morphological aspects of electrocatalysts* pag. 23

1.3.1 – Role of surface area and metal loading pag. 23

1.3.2 – Role of carbon support pag. 24

1.3.3 – Preparation methods pag. 25

I.2.2 – Cathodic reduction of oxygen pag. 26

2.1 – General considerations pag. 26

2.2 – Oxygen electroreduction in DMFCs pag. 27

2.3 – Carbon supported electrocatalysts pag. 29

2.4 – Non-noble metal based electrocatalysts pag. 31

I.3 – Technology Development and its Prospects pag. 32

I.3.1 – Proton conducting membranes pag. 32

I.3.2 – Membrane and electrode assemblies pag. 34

I.3.3 – Single cell performance – Polarization behaviour pag. 36

3.1 – Dependence on kinetics of electro-oxidation of methanol and

oxygen reduction pag. 36
3.2 – Effect of methanol concentration, pressure and flow rates on DMFC performance pag. 38
3.3 – Effect of methanol cross-over pag. 39
3.4 – Flow fields pag. 41
I.4 – References pag. 43
CHAPTER II – Catalysts development and characterization pag. 51
II.1 – Effect of Pt-Ru alloy composition on high-temperature methanol electro-oxidation pag. 51
II.1.1 – Introduction pag. 51
II.1.2 – Experimental pag. 53
II.1.3 – Results and Discussion pag. 54
3.1 – Physico-chemical analysis pag. 54
3.2 – Electrochemical studies pag. 62
3.3 – Mechanism and kinetic equation pag. 66
II.1.4 Conclusions pag. 67
II.1.5 References pag. 69
II.2 – Analysis of the high temperature methanol oxidation behaviour at carbon supported Pt-Ru catalysts pag. 72
II.2.1 – Introduction pag. 72
II.2.2 – Experimental pag. 73
II.2.3 – Results and Discussion pag. 75
II.2.4 – References pag. 93
II.3 – Electrochemical analysis of high temperature methanol electro-oxidation at Pt-decorated Ru catalysts pag. 95
II.3.1 – Introduction pag. 95
II.3.2 – Experimental pag. 96
II.3.3 – Results and Discussion pag. 97
II.3.4 – Conclusions pag. 98
II.3.5 – References pag. 106
CHAPTER III – Membranes development and characterization pag. 107
III.1 – Influence of the acid base characteristics of inorganic fillers on the high temperature performance of composite membranes in direct methanol fuel cells pag. 107

III.1.1 – Introduction pag. 107
III.1.2 – Experimental pag. 109
III.1.3 – Results and Discussion pag. 111
III.1.4 – Conclusions pag. 132
III.1.5 – References pag. 134
III.2 – Influence of TiO_2 nanometric filler on the behaviour of a composite membrane for applications in direct methanol fuel cells pag. 136
III.2.1 – Introduction pag. 136
III.2.2 – Experimental pag. 136
III.2.3 – Results and Discussion pag. 138
III.2.4 – Conclusions pag. 151
III.2.5 – References pag. 152
III.3 – Zeolite-based composite membranes for high temperature direct methanol fuel cells pag. 153
III.3.1 – Introduction pag. 153
III.3.2 – Experimental pag. 153
III.3.3 – Results and Discussion pag. 155
III.3.4 – Conclusions pag. 161
III.3.5 – References pag. 162
Acknowledgements pag. 164

SUMMARY

Direct Methanol Fuel Cells (DMFCs) are becoming an important area of research, due to their potentialities for a wide application in the next future as electrical power generators because of their low environmental impact. The fields in which these devices may find application involve transportation, portable power sources and distributed generation of clean energy. Yet, the commercial application of these devices is limited by the presence of two main drawbacks that have hindered the achievement of high performances: (i) the slow methanol oxidation kinetics and (ii) the methanol cross-over through the perfluorosulfonic membranes commonly used as electrolyte in these systems. Thus, the topics of this PhD thesis, and, consequently, of my research activity, are concerning with:

a) analysis of high temperature methanol electro-oxidation at different Platinum-based catalysts, i. e. unsupported Pt-Ru alloys of various compositions in terms of metal atomic ratio, supported Pt-Ru catalysts varying by different concentrations of metallic phase on carbon support, Pt-decorated Ru catalysts;

b) composite Nafion membranes containing different hygroscopic ceramic oxides for high temperature DMFC operation (130-150°C).

The recent developments in both fundamental and technological aspects of Direct Methanol Fuel Cells are also described and included in Chapter I of this thesis.

The research activity concerning with the development of catalysts for the methanol electro-oxidation reaction and their physico-chemical and electrochemical characterization is reported in Chapter II.

The preparation and characterization of composite perfluorosulfonic membranes based on recast Nafion containing finely dispersed inorganic oxides is reported in Chapter III, togheter with an analysis of the mechanisms governing the conductivity/water retention properties relationship.

CHAPTER I

INTRODUCTION

I.1 Introduction to Direct Methanol Fuel Cells

Direct methanol fuel cells (DMFCs) working at low and intermediate temperatures (up to 150°C) and employing solid protonic electrolytes have been postulated as suitable systems for power generation in the field of electro-traction [1-6]. DMFCs utilize liquid fuel to deliver a continuos power but they have higher utilization efficiencies and intrinsically lower polluting emissions with respect to internal combustion engines. Since transportation represents a significant portion of world energy consumption and contributes considerably to atmospheric pollution, the development of an appropriate fuel cell system is an important issue from both economical and environmental point of views. In order to be competitive within the transport market, the DMFC must be reasonably cheap and capable of delivering high power densities. At present, there are a few challenging problems in the development of such systems [1-7]. These mainly consist in finding i) electrocatalysts which can effectively enhance the electrode-kinetics of methanol oxidation ii) electrolyte membranes which have high ionic conductivity and low-methanol cross-over and iii) methanol tolerant electrocatalysts with high activity for oxygen reduction. Furthermore, a significant relevance play all the aspects related to fuel cell stack development, in particular, materials and design of cell housing, bipolar plates, gaskets, and stack auxiliaries. All these materials and devices contribute to the final characteristics of practical devices determining the performance, efficiency and cost. At present, the cost of the entire system is mainly determined by the presence of noble metals in the catalyst and the use of Nafion membranes [3-5].

I.2 Fundamental Aspects

I.2.1 Anodic oxidation of methanol

I.2.1.1 Overall reaction

Most of fuel cell systems operate with hydrogen as a fuel. Electro-oxidation of hydrogen is a fast reaction on a low loading Pt electrocatalyst (0.05 to 0.1 mg cm^{-2}). On the other hand, the methanol oxidation reaction rate is at least three to four orders of magnitude slower on a high Pt-Ru loading (≈ 2 mg cm^{-2}) electrocatalyst. Although thermodynamic characteristics are similar to the hydrogen reaction, especially in terms of reversible oxidation potential, the methanol electro-oxidation reaction is a slow process and it involves the transfer of six electron to the electrode for a complete oxidation to carbon dioxide.

Thermodynamics of direct methanol fuel cell

Anode reaction: $CH_3OH + H_2O \longrightarrow CO_2 + 6H^+ + 6e^-$ (1)

Cathode reaction: $3/2\ O_2 + 6H^+ + 6e^- \longrightarrow 3\ H_2O$ (2)

Overall reaction: $3/2\ O_2 + CH_3OH \longrightarrow CO_2 + 2\ H_2O$ (3)

The free energy associated with the overall reaction at 25°C and 1 atm and the electromotive force are [2]:

$\Delta G = -686\ kJ\ mol^{-1}_{CH3OH};\quad \Delta E = 1.18\ V$ (4)

Various reaction intermediates may be formed during the methanol oxidation [8]. Some of these (CO-like) species are irreversibly adsorbed on the surface of the electrocatalyst and severely poison Pt for the occurrence of the overall reaction, which has the effect of significantly reducing the efficiency for fuel consumption and the power density of the fuel cell. Thus, it is vitally important to develop new electrocatalysts to inhibit the poisoning and increase the electro-oxidation rate by at least two-three orders of magnitude. Other species may be released with a consequent decrease of fuel efficiency, whereas, an efficient catalyst must allow a complete oxidation to CO_2. Principal by-products in the methanol oxidation are

formaldehyde and formic acid. Methyl formiate and other substances have been found in traces.

$CH_3OH \longrightarrow HCHO + 2H^+ + 2e^-$ (5)

$HCHO \longrightarrow HCOOH + 2H^+ + 2e^-$ (6)

$HCOOH \longrightarrow CO_2 + 2H^+ + 2e^-$ (7)

DMFCs are characterized by two slow reactions i.e. methanol electro-oxidation and oxygen reduction with the further drawback of the presence of a mixed potential at the cathode determined by the methanol cross-over. On the other hand, there are specific advantages in using methanol as direct fuel especially for what concerns costs, simplicity of design, large availability, easy handling and distribution. Another concern is that, even though significant progresses have been made in enhancing the electrocatalysis of the four-electron transfer oxygen reduction reaction at low temperatures, the overpotential of this reaction at desired current densities (e.g. 500 mA cm^{-2}) is still about 400 mV in H_2/air fuel cells and increases by about 50-100 mV in DMFCs because of the effect caused by methanol, which crosses over from the anode to the cathode [3-5].

I.2.1.2 Electrocatalysis

1.2.1 General comments

In the last few years, a significant amount of investigation has been carried out in the field of electro-oxidation of small organic molecules at low temperature [8]. Most of these fundamental studies have been conducted in half cell configuration and on smooth electrode surfaces, in order to individuate the best electrocatalyst composition [8]. Electrochemical investigations have been generally conducted in combination with spectroscopic techniques in order to elucidate the oxidation mechanism and to investigate the irreversibly adsorbed species on the electrode surface. From a general point of view, almost all electro-oxidation reactions involving low molecular weight organic molecules, such as CO, CH_3OH, C_2H_5OH, HCOOH, HCHO, require the presence of a Pt-based catalyst [4-8]. A second aspect is that all these electro-oxidation reactions give rise to the formation of strongly adsorbed CO species in linear or bridge-bonded form. Pt is involved in two key steps occurring during the oxidation route. One is the dehydrogenation step (eg. in the case of methanol) and the second one is the chemisorption of CO. Studies involving partial substitution of Pt with other transition metals like W, Pd, Ni, Ti, Rh, Mo have not yielded beneficial results [6-12]. Accordingly, most of the work has been addressed to the modification of the Pt environment by alloying it with

other elements or through the synthesis of multifunctional electrocatalysts. The alloying route has given until now the most successful results. It has been shown that the alloying of Sn and Ru with Pt gives rise to electrocatalysts which strongly promote the oxidation of both methanol and CO. Since the complete oxidation of methanol to CO_2 involves the transfer of 6 electrons to the electrode, the overall reaction mechanism involves several steps including dehydrogenation, chemisorption of methanolic residues, rearrangement of adsorbed residues, chemisorption of oxygenated species (preferentially on the alloying element) and surface reaction between CO and OH to give rise to CO_2.

The concept of realization of multifunctional catalysts (Pt-Ru-Mo, Pt-Ru-W, Pt-Ru-Sn, Pt-Ru-oxides, Pt-Ru-W-Sn) is based on the need to promote each reaction step through proper elements [13-16]. What is essentially required is the presence of :

1) dehydrogenation sites
2) labile-bonded CO chemisorption sites
3) labile-bonded OH chemisorption sites
4) redox functionalities.

At present, the rate determining step for methanol oxidation at suitable temperatures (T ≈ 90°C) on Pt-based catalysts is considered to be either the adsorption of OH species at low potentials or the surface reaction between OH and CO chemisorbed on neighbouring sites; at lower temperatures (T< 60°C), the dehydrogenation step could also influence the reaction rate [17]. The achievement of significant reaction rates requires the use of highly dispersed metal phase on electrically conductive carbon black support. In this latter system, the preparation procedure of the catalyst strongly influences its performance for methanol oxidation. In the following paragraphs all these aspects are discussed starting from the oxidation mechanism on Pt surface.

1.2.2 Experimental methods

The mechanism of methanol electro-oxidation was elucidated in the last three-four decades by using a variety of experimental procedures [4-8]. The electrochemical methods used for such investigation include mainly steady-state galvanostatic polarizations, cyclic voltammetry and electrochemical transients (chronoamperometry, chronopotentiometry) [4-8, 18-23]. Ac-impedance spectroscopy has been used to a less extent [24]. In general electrokinetic parameters i.e. Tafel slopes, activation energies, reaction orders etc., have been derived by galvanostatic steady-state polarizations and linear potential scans in presence of acidic liquid electrolytes in a temperature range from 25 to 80 °C [25-27]. In situ

spectroscopic analyses in conjunction with electrochemistry such as FTIR, mass spectrometry XAS etc. [21-22, 28-32] have been demonstrated very useful for the investigation of adsorbed species and for determination of intermediate compounds formed during the oxidation process. Ellipsometry has been particularly used to in-situ investigate the potentials at which water displacement was occurring especially on Pt-Ru surfaces [33]. The experimental techniques and the information acquired from them in relation to methanol oxidation have been reviewed in a few excellent papers [4-8]. Beside these methods, in the recent years additional techniques and/or methodologies of investigation of methanol electro-oxidation have been proposed. Among them, significant interest has arisen around the following procedures:

i) ultra high vacuum preparation of well defined catalyst surfaces for voltammetric analyses [19];

ii) in-situ electrochemical crystal microbalance based studies for detection of adsorbed species [34-35];

iii) in-situ viewing of catalysts surfaces during methanol oxidation by scanning tunneling microscopy [36];

iv) in-situ electrochemical NMR studies allowing electronic-level description of metallic-shells in nanoparticle catalysts [37];

v) in-situ carbon monoxide stripping voltammetry [38-41];

vi) rotating ring disk method with a recast film of catalyst particles/Nafion deposited on an inert glassy carbon electrode to screen electrocatalysts [42-43];

vii) combinatorial methods for the screening of a large variety of catalysts' formulations [44].

Some of these techniques are still dealing with smooth electrode surfaces. The acquired information serves mainly to understand the mechanism at a basic level. Yet, there is a need to develop methodologies which allow to get information on the mechanisms occurring at high surface area electrodes and during fuel cell operation. In this regard in-situ CO stripping voltammetry is a very interesting methodology for the characterization of the catalyst / solid polymer electrolyte interface under fuel cell conditions. The information acquired from it regards an evaluation of active surface area, intrinsic catalytic activity and in some cases information on the surface composition of the catalysts is derived [41]. The presence of a close relationship between the anodic shift of the peak potential of the CO stripping and the catalytic activity towards methanol oxidation provides a clear evidence that CO removal is a rate determining step in the methanol electro-oxidation process [41].

A particular importance is played by the combinatorial analysis. This method is addressed to the discovery of new catalyst formulations and it has recently attracted a significant interest [44]. These studies have pointed out the need of a systematic screening of a large number of combination of elements as a suitable route to address the problem of finding better catalysts for methanol oxidation. As a result of these studies Pt-Ru-Os was proposed as one of the most interesting catalyst formulations.

1.2.3 Structural effects and electrode-kinetics

The electrokinetic parameters have been mainly determined at Pt-based electrodes. A Tafel slope between 90 and 120 mV dec^{-1} was determined for the methanol oxidation reaction at Pt-based catalysts in the temperature range between 25 and 60 °C [15, 22, 29]. This may vary depending on the potential region where it is determined. The Tafel slope in the temperature range from 100 to 130 °C is around 130-140 mV dec^{-1}. If one takes into account the effect of temperature, the observed Tafel slopes under DMFC operation conditions at high temperatures are very close to those observed in presence of liquid electrolytes at smooth electrodes. A fractional positive reaction order with respect to methanol concentration has been observed in half cell studies in a range of concentrations from 0 to 2.5 M [27]. The Temkin adsorption isotherm has been often used to describe the adsorption of methanolic residues [27, 45, 46] and various kinetic equations describing the variation of current as function of potential, temperature, coverage of adsorbed species have been proposed [46-49]. Bagotzky and Vassilyev derived functional expressions for methanol electrocatalysis at Pt based electrodes for two potential regions characterized by significantly different rates in water discharging i.e. for slow and fast water discharging process on the surfaces [27]. At a fixed potential, the current density (i / mA cm^{-2}) varies with the coverage on the basis of the following relationships:

$$i = k\, \vartheta_{OH} \exp(\Upsilon_1 r_1 \vartheta_{Org}) \qquad \text{(low potentials)}$$

$$i = k \exp(\Upsilon_1 r_1 \vartheta_{Org}) \cdot \exp(\Upsilon_2 r_2 \vartheta_{OH}) \qquad \text{(high potentials)}$$

where k is a kinetic constant, ϑ_{Org} and ϑ_{OH} are the coverages of methanolic residues and oxygen species, respectively, Υ and r are electro-kinetic and Temkin parameters, respectively [27]. These latter take into account the effects of the heterogeneous surface and the interaction between adsorbates. The second relationship holds in the potential region where water displacement and consequent OH chemisorption on the catalyst surface occurs at acceptable rates. For a Pt-Ru surface this region shifts to very low potentials. Although more recent studies have proposed alternative and more complex equations [48, 49], the

functional expression proposed by Bagotzky and Vassilyev have been demonstrated useful in interpreting kinetic data for a wide variety of catalyst-electrolyte interfaces. The activation energy for methanol electro-oxidation strictly depends on the catalytic system; Pt-Ru shows activation energy of 30-65 kJ mol^{-1}[25, 26, 50]. Yet, this value is significantly high and it clearly indicates the need of high temperature operation. The exchange current density (Io) for methanol oxidation at various Pt-based catalysts is a few orders of magnitude lower than that of H_2 oxidation [2, 51]. Io is obtained by intersection of the Tafel line with reversible potential for the methanol electrooxidation. As opposite of other electro-catalytic reactions, this parameter is sparely used to quantify the electro-catalyst activity. More often, mass and specific activities at defined potentials, where the reaction is under kinetic control (e.g. 0.25 V - 0.35 V vs. RHE for high temperature operation) are utilized to assess catalysts' reactivity. This probably depends on the fact that it is not always possible to determine the Tafel slope and/or the Tafel slope changes in the various potential regions [23, 26, 49, 50].

Electro-oxidation of methanol is a structure sensitive reaction. The first studies carried out on Pt surfaces with different crystallographic orientations and for polycristalline Pt evidenced an increased reactivity for methanol oxidation at the Pt planes with (110) Miller indexes [52] and for rough surfaces [18, 29]. Yet, recently Wieckowski et al. [53, 54] showed for Pt-Ru surfaces that the catalytic activity is maximized by the presence of (111) crystallographic planes. These evidences may be explained by the fact that water displacement at Pt sites occurs very slowly at low electrode potentials. Thus, in the case of a pure Pt catalyst, there is a strong need of Pt sites with high coordination numbers or surfaces with a large number of defects. These sites are capable of chemisorbing oxygen molecules at lower potentials. As opposite, in the Pt-Ru system, the water displacement occur at low potentials on Ru sites whereas methanol chemisorption involves three neighbouring Pt sites. CO removal which is often the r.d.s. at Pt-Ru surfaces [41] requires the presence of OH species adsorbed on adjacent Ru sites. These latter processes are accelerated by the presence of low Miller index planes. Implications for the development of high surface area catalysts are discussed in a following paragraph.

1.2.4 Pt electrocatalysts

The electrochemical oxidation of methanol on Pt involves several intermediate steps, i.e. dehydrogenation, CO-like species chemisorption, OH (or H_2O) species adsorption, chemical interaction between adsorbed CO and OH compounds, and CO_2 evolution. One of these steps is the rate determining step (r.d.s.) depending on the operation temperature and

particular catalyst surface (crystallographic orientation, presence of defects, etc.). The state of the art electrocatalysts for the electro-oxidation of methanol in fuel cells are generally based on Pt alloys supported on carbon black [6,7,55], even if the use of high surface area unsupported catalysts has recently gained momentum [56, 57]. As stated above, the electrocatalytic activity of Pt is known to be promoted by the presence of a second metal, such as Ru or Sn, acting either as an adatom or a bimetal. The mechanism by which such synergistic promotion of the methanol oxidation reaction is brought about has been the subject of numerous studies during the last 30-40 years, in which various spectroscopic methods have been employed in conjuction with electrochemistry [4-8]. A combination of cyclic voltammetry [18], in-situ ellipsometry [33], X-ray absorption spectroscopy [31], on-line mass spectrometry [30] and in-situ FTIR spectroscopic studies [22, 28, 29], revealed that the electro-oxidation of methanol on Pt-based catalysts proceeds through the mechanism (sequence of non-elementary reaction steps) below described. First a sequence of dehydrogenation steps give rise to adsorbed methanolic residues, according to the following scheme:

$$CH_3OH + Pt \rightarrow Pt\text{-}CH_2OH + H^+ + 1\,e^- \qquad (8)$$

$$Pt\text{-}CH_2OH + Pt \rightarrow Pt\text{-}CHOH + H^+ + 1\,e^- \qquad (9)$$

$$Pt\text{-}CHOH + Pt \rightarrow PtCHO + H^+ + 1\,e^- \qquad (10)$$

A surface rearrangement of the methanol oxidation intermediates gives carbon monoxide, linearly or bridge-bonded to Pt sites, as following:

$$PtCHO \rightarrow Pt\text{–}C{\equiv}O + H^+ + 1e^- \qquad (11a)$$

or

$$PtCHO + Pt \rightarrow \begin{matrix} Pt \\ \rangle C{=}O \\ Pt \end{matrix} + H^+ + 1e^- \qquad (11b)$$

In absence of a promoting element, water displacement occurs at high anodic overpotentials on Pt with formation of Pt-OH species at the catalyst surface.

$$Pt + H_2O \rightarrow PtOH + H^+ + 1e^- \qquad (12)$$

The final step is the reaction of Pt-OH groups with neighbouring methanolic residues to give carbon dioxide:

$$PtOH + Pt\,CO \rightarrow 2Pt + CO_2 + H^+ + 1e^- \qquad (13)$$

The overall oxidation process of methanol to carbon dioxide proceeds through a six electron donation process; yet, the rate determining step, derived from electrochemical steady-

state measurements on Pt, through analysis of the Tafel slope, involves a one-electron step [22]. On a pure Pt surface, the dissociative chemisorption of water on Pt is the rate determining step at potentials below ≈ 0.7 V vs. RHE, i.e. in the potential region that is of technical interest [22]. It is generally accepted that an active catalyst for methanol oxidation should give rise to water displacement at low potentials and to "labile" CO chemisorption. Moreover, a good catalyst for methanol oxidation should also catalyze the oxidation of carbon monoxide.

Even if various theories have been put forward to explain the promoting effect of the additional elements [13, 23, 58, 59], the subject remains controversial. Transition metal promoters and adatoms are seen as a means to improve the electrocatalytic behaviour of electrodes, either by minimizing the poisoning reaction or enhancing the main oxidation reaction. Besides, three main hypotheses have been made. A first hyphothesis suggests that the metal promoters and adatoms either alter the electronic properties of the substrate or act as redox intermediates [59, 60, 61]. This hypothesis, supported by experimental evidences, also leads to the influence of a possible steric effect on the enhanced oxidation rate [61]. A second hypothesis envisages ad-atoms as blocking agents for the poison forming reaction, assumed to occur on a number of sites greater than those required for the main reaction [61]. A third hypothesis based on the bifunctional theory invokes a mechanism by which the oxidation reaction of either the fuel or the poisoning intermediate is enhanced by the adsorption of oxygen or hydroxyl radicals on promoters or adatoms adjacent to the reacting species [23]. Combining the electronic and bifunctional theories it is derived that the role of the second element is to increase the OH adsorption on the catalyst surface, at lower overpotentials, and to decrease the adsorption strength of the poisoning methanolic residues.

1.2.5 Pt-Ru binary alloy electrocatalysts

According to the mechanism shown above it is generally accepted that Pt sites in Pt-Ru alloys are especially involved in both the methanol dehydrogenation step and the strong chemisorption of methanol residues. At suitable electrode potentials (0.2 V vs. RHE), water discharging occurs on Ru sites with formation of Ru-OH groups at the catalyst surface [33]:

$$Ru + H_2O \rightarrow Ru\text{-}OH + H^+ + 1e^- \qquad (14)$$

The final step is the reaction of Ru-OH groups with neighboring methanolic residues adsorbed on Pt to give carbon dioxide:

$$Ru\text{-}OH + Pt\text{-}CO \rightarrow Ru + Pt + CO_2 + H^+ + 1e^- \qquad (15)$$

The chemisorption process of methanol on Ru sites is significantly less favored than on Pt sites, but it is strongly activated by the temperature [17]; methanol dehydrogenation occurs on Pt at potential values below 0.2 V vs. RHE [18]. Besides, the water displacement reaction, producing oxygen species chemisorbed on Ru sites, occurs at potentials as low as 0.2 V vs. NHE. Although at high temperatures (90 to 130 °C), Ru can participate in the methanol chemisorption process at low potentials, the chemisorption energy of oxygen on Ru surfaces is so high (330 $kJ \cdot mol^{-1}$) [62] to inhibit Ru sites to be covered by methanolic residues; hence, they can suitably chemisorb OH groups. The CO removal process is also activated by an increase in temperature and in overpotential [63].

Although, the argument remains still controversial [17, 23, 34, 35, 43, 64-67], an optimal Ru content in carbon supported Pt-Ru catalysts for the methanol oxidation reaction at high temperature 90-130°C has been found to be 50 at % [68, Chapter II of this thesis]. The optimum Ru surface composition is referable to the relevant synergism accomplished by a Pt-Ru surface with 50% atomic Ru in maximizing the product of θ_{OH} (OH coverage) and k (intrinsic rate constant), according to the assumption of the surface reaction between CO_{ads} and OH_{ads} as rds; on the other hand, methanol adsorption and dehydrogenation processes, as well as water discharging, are considered to be in equilibrium at high temperatures. At low temperatures the situation is somewhat different. Adsorption of methanol on Pt requires an ensemble of three neighbor atoms whereas oxidation of methanolic residues requires a chemical interaction with neighbor adsorbed OH groups on Ru sites. Gasteiger et al. [17] have observed that methanol oxidation occurs more readily at room temperature on pure Pt-Ru alloys having low Ru contents (≈ 10%) whereas at intermediate temperatures (60°C) the reaction is faster on alloys with increased Ru contents (≈ 33%). An optimal Ru content in unsupported Pt-Ru catalysts for the methanol oxidation reaction at 130 °C has been found to be about 50 at % [68]. These results can be suitably interpreted by considering that dehydrogenation of methanol is the rate determining step at room temperature. Thus, electrocatalysts having a good fraction of ensembles of three neighbor Pt sites appear to give higher electrochemical activities. At higher temperatures methanol dehydrogenation is thermally activated on Ru sites which participate more actively in the methanol chemisorption process. Under such conditions, the rate controlling steps become the water displacement on Ru sites and the chemical interaction between adsorbed methanolic residues and OH groups. Analysis of specific and mass activity of unsupported Pt-Ru catalysts with different composition at high temperature (130 °C) in a DMFC [68] indicates the presence of a maximum for a 1:1 Pt-Ru atomic ratio.

The synergistic promotion exerted by Pt-Ru alloys is supported by X-ray absorption analysis [59]. Accordingly, an increase of Pt d-band vacancies is produced by alloying with Ru; this possibly modifies the adsorption energy of methanolic residues on Pt. Such evidences suggest that the reaction rate is not only dictated by the bifunctional mechanism but it is also influenced by electronic effects occurring on account of the interaction between Pt and Ru [59-60]. These aspects are discussed more in detail in the next paragraph.

The achievement of significant reaction rates for the Pt-Ru system requires the use of highly dispersed metal phase on electrically conductive carbon black support. In this latter system, the preparation procedure of the electrocatalyst was found to strongly influence its performance for methanol oxidation [4, 43]. Following various studies carried out in this field, the starting point for the development of an active electrocatalyst for CH_3OH oxidation is to synthesize a suitable highly dispersed Pt-Ru phase. A few authors have pointed out the need to develop multifunctional catalysts, thus, often the Pt-Ru system is modified with the addition of a third functionality (Pt-Ru-Mo [2], Pt-Ru-W [69], Pt-Ru-Sn [14, 52], Pt-Ru-Os [44]).

1.2.6 Promoting effects of Ru and Sn: bifunctional mechanism and ligand effect

Both Pt-Ru and Pt-Sn systems have been reported to be promising catalysts for electro-oxidation of methanol in direct methanol fuel cells [8, 52, 70]. But although there is conclusive evidence on catalytic promotion of methanol electro-oxidation on the Pt-Ru system in relation to Pt, contradictory results have been reported in the literature on the promotional effect of tin for this reaction [13, 19, 71-73]. While Janssen and Moolhuysen [13] and Motoo et al. [73] have found a 50-100 times enhancement in the electrocatalytic activity of smooth and electrodeposited Pt electrodes on which Sn was deposited, several other authors [71, 72] have reported considerably smaller and even negative effects. For carbon-supported Pt-Sn electrodes, different methods of preparation are found to exhibit varying effects [74, 75] leading to different Pt-Sn surface properties. The surface characteristics of Pt-Ru and Pt-Sn are of considerable significance for the methanol-oxidation reaction. Since both Pt-Ru and Pt-Sn systems have been reported to promote electro-oxidation of methanol, different electronic environments around Pt-sites in Pt-Ru and Pt-Sn should imply different routes for methanol-oxidation reaction. As stated above, the most agreeable mechanism for methanol oxidation on Pt-alloys is based on the bifunctional theory [23]. According to this theory, Pt-sites adsorb methanol through a dehydrogenation step whereas the alloying element, namely Ru or Sn, adsorbs oxygenated species from water. The

methanolic residues adsorbed on Pt-sites react with the oxygenated species present on the neighbouring Ru or Sn sites in the alloy producing CO_2.

In a previous study [70], it was observed a 1.1 eV shift in the X-ray near edge spectrum (XANES) of the Pt-Sn/C catalyst with respect to the Pt/C catalyst, from which result one may infer that Sn atoms in the Pt-Sn alloy donate electrons to Pt-atoms and are thereby oxidized. This is in agreement with the electronegativity values for elemental Pt and Sn which differ appreciably. A noticeable charge transfer from Sn to Pt has been also found in an XPS analysis, as reflected by a negative shift in the Pt-4f binding energies of the Pt-Sn samples in relation to Pt/C electrocatalysts [76].

Recently, Mukerjee and McBreen [59, 77] have shown in their X-ray absorption spectroscopic studies on Pt-Ru/C and Pt-Sn/C electrocatalysts that alloying Sn with Pt causes partial filling of Pt 5d-bands and a consequent increase in the Pt-Pt bond distances with a contrary effect observed for Pt-Ru catalysts. However in other investigations, XPS data on Pt-Ru/C samples have not shown any evidence of modification in the Pt-4f spectra as compared with that in Pt/C samples, which showed consistently nearly the similar electronegativity values for elemental Pt (2.2) and Ru (2.1). Beside the work of Mukerjee and McBreen [59], some in situ experiments have also provided evidence for the influence of Ru on the electronic state of Pt [78]. Iwasita et al. [60] observed in their FTIR experiments a shift towards higher frequencies for the CO stretching on Pt-Ru with respect to Pt. This effect has been attributed to a lower chemisorption energy for CO on the Pt-Ru alloy. Frelink et al. [34, 35] measured the stretching frequency of linearly bonded CO as a function of coverage for the Pt and Pt-Ru electrodes. A shift to higher frequencies at various coverages was observed as a result of change in the CO binding strength to the surface induced by Ru through a ligand effect on Pt [34-35]. But, these authors have also shown by in-situ ellipsometric studies on Pt and Pt-Ru electrodes that the Ru-oxide film is removed by reaction with methanol during its electro-oxidation. This evidence supports the bifunctional mechanism. The latter findings were further corroborated by DEMS studies [34, 35]. In a recent article, Iwasita and co-workers have emphasized the bifunctional mechanism for methanol electro-oxidation on the Pt-Ru system [66]. In our opinion, it may be rationalized from the in-situ experiments described above that the promotional effect of Ru could be due to both the contribution of bifunctional and ligand effects. But, the ligand effect in the Pt-Ru system appears to be significantly less prominent and it has still not found support in the results obtained from a few surface techniques including XPS [76].

Further insight on the mechanism can be obtained by analysing the Pt-carbon monoxide bonding since CO removal from Pt surfaces plays a dominant role in methanol oxidation The nature of Pt-CO bond in platinum systems has been well documented in the literature [79]. It would, however, be in context to elucidate the nature of bonds formed between CO and Pt as well as between OH and Ru (or Sn) in the respective alloy systems. Chemisorption of CO on Pt involves donation of an electron pair from σ^* anti-bonding orbitals of CO to the unfilled 5d-orbitals of Pt. A back donation of electrons from the Pt metal to CO-orbitals further stabilizes their interaction. Accordingly, it is apparent that the dative electron donation from CO to Pt is a pre-requisite for a strong CO-chemisorption. If the Pt surface is partially oxidised, the Pt metal can more easily accommodate the electrons donated by CO in its unfilled orbitals. The increase in the Pt 5d-band vacancies produced by Ru atoms as interpreted by Mukerjee and McBreen [59], would imply an increase in Pt-CO bond strength which in effect would retard the methanol-oxidation reaction. On this basis, the promoting action of Ru arises mainly due to an easier chemisorption of oxygen from water at lower electrode potentials in accordance with the bifunctional theory. Nevertheless, some modifications of the electronic environment around Pt may occur during the interface formation, since the uptake of oxygen functionalities from water could modify the electron accepting characteristics of Ru atoms. On the other hand, a charge transfer from Sn to Pt in the Pt-Sn system, evidenced from XAS and XPS data, causes a substantial increase in electron density around Pt-sites resulting in a weaker chemisorption of CO. This combined with an easier adsorption of OH-species on the oxidized Sn-sites at lower electrode potentials would enhance the oxidation of irreversibly adsorbed CO to CO_2, and would thus promote the methanol-oxidation reaction. The electro-catalytic promotion of CO electro-oxidation on Pt-Sn alloy at low electrode potentials has been recently discussed by Markovic' et al. [80]. Accordingly, the Pt_3Sn bulk alloy was found significantly more active than the Pt-Ru system for CO oxidation. However, higher electrode potentials produce a negative effect due to strong adsorption of OH-species on Sn-sites and retard the methanol-oxidation reaction on Pt-Sn catalysts. In many cases formation of stable tin-oxide species on the surface during catalyst preparation or electrode activation procedures has been observed [70]. The presence of these compounds present on the electrode surface play a significant role during the methanol oxidation reaction since the electrocatalyst is operated in a potential regime in which oxide must not be present but where the supply of active oxygen is important. Formation of labile-bonded oxygen species more easily occurs on an oxide-free surface and in this context the water displacement reaction occurs more easily on Ru than Sn sites. Generally, the

achievement of properly reduced Pt-Sn surfaces is brought about with difficulty. In this context, Pt surface containing Sn ad-atoms often perform better than bulk or carbon supported Pt-Sn alloy catalysts [74].

From all these evidences, one may conclude that the addition of Ru to Pt markedly increases the electrocatalytic activity of Pt through the adsorption of oxygenated species on Ru-sites. By contrast, the promotion of CO oxidation reaction on Pt-Sn catalyst appears to be mainly due to a modification of the electronic environment around Pt-sites. It becomes clear that Pt-Ru catalysts are more effective for methanol oxidation since the reaction desires the electrocatalyst to be operated in a potential regime where labile-bonded oxygen should be present on the surface. In this situation, the supply of active oxygen to the surface is of paramount importance since this apparently would facilitate the oxidation of adsorbed methanolic residues to CO_2. The presence of strongly-bonded oxygen species on Sn-sites in the Pt-Sn system limits the oxidation of methanol to CO_2.

1.2.7 Role of Ru-oxide in enhancing kinetics

Some Pt-Ru catalysts show a lower Ru content in the Pt-Ru alloy (as detected by XRD) with respect to the nominal composition [57, 81]. In such cases, the remaining Ru atoms are present as RuO_x species that may be composed of crystalline tetragonal RuO_2 or amorphous Ru-oxide [57, 81, 82]. The oxide species are generally detected by XRD or TEM if they have a crystalline structure (frequently RuO_2 tetragonal), whereas X-ray absorption spectroscopy (both EXAFS and XANES) and in some cases XPS may give information on the amorphous Ru-oxide species. Often, TEM micrographs of the carbon supported Pt-Ru sample show some agglomeration of particles having similar dimension but characterized by a different atomic contrast [81]. The interlayer spacing of Pt-Ru alloy particles that may be observed at high magnification is about 2.25-2 Å, corresponding to the (111) planes of the Pt or Pt-Ru fcc lattice. The largest interlayer spacing of the RuO_2 structure is 3.17 Å and is comparable to the interlayer spacing d (002) of the graphitic carbon support but they cannot be confused since the carbon lattice is quite irregular like in an amorphous material and is continuous. Amorphous Ru-oxide particles of small size also can not be easily distinguished. In such case XAS and XPS analyses may indicate the presence of amorphous Ru-oxide; it must be noted that XPS gives information only on the outermost layers [81]. It was reported that formation of labile oxygen groups on Ru sites, not directly alloyed with Pt but close enough to Pt sites, can allow chemical interaction between these groups and the adsorbed methanolic residues to produce CO_2. The promoting effect of the RuO_x species

for methanol oxidation reaction has been extensively investigated by several authors [83-85]; recently, very high performances were obtained in a DMFC with unsupported Pt-RuO_x anode electrocatalyst [56]. It was suggested that facile oxygen transfer from Ru to Pt rich regions where adsorption of CO-like residues preferentially occurs, could enhance the catalytic oxidation of methanol [85]. But, oxygenated species, strongly held on Ru surfaces, cannot easily migrate on the surface. In general XPS analysis has revealed the presence of Ru(IV) and Ru(VI) species. The oxygen transfer mechanism requires an open oxy-hydroxide structure with a significant number of free Ru-OH bonds [81]. Thus, such mechanism operates better on Ru(IV) that on Ru(VI) species since the formation of labile oxygen bonds occurs preferentially on the first sites. It is thought that both mechanisms involving Pt-Ru alloys and RuO_x species could actively participate in the methanol oxidation reaction. Yet, the absence of an atomic mixing of Pt with RuO_x species probably imposes an activation barrier for the migration of adsorbed intermediates. In order to assess which mechanism is more effective, in a recent study the methanol oxidation behaviour on a pure Pt-Ru alloy and a Pt-RuOx electrocatalyst, with comparable particle sizes, have been compared at high temperatures (130 °C) [84, 86, Chapter II of this thesis]. It was observed that both electrocatalysts are active for the methanol oxidation reaction but the electrocatalyst containing a lower amount of oxidized Ru species and characterized by a smaller Ru-O bond strength performed better [84, 86].

1.2.8 Ternary alloy Pt-Ru-W and Pt-Ru-Mo electrocatalysts

The Pt-Ru formulation suffers the lack of other elements able to promote a "labile" adsorption of carbon monoxide-like species and /or to oxidize these methanolic species by an effective redox mechanism. In this light, an interesting approach is the formulation of new electrocatalysts that, although based on Pt-Ru alloy (this has demonstrated irreplaceable characteristics in matching the above requirements), would take advantage of proper surface promoters able to facilitate labile adsorption of methanol residues and their oxidation through redox functionalities. In recent years, electrocatalyst formulations which includes tungsten and molybdenum have been proposed [2, 14, 69, 87]. In an acid electrolyte environment, these elements are generally stable in one or more oxidized forms such as WO_2/WO_3 or WO_2/WO_3 and can easily exchange oxidation states by adsorbing hydroxyl ions from water and donate these species to methanol residues adsorbed on Pt. Recently, Tseung et al. [69] have shown that the Pt-Ru-W system shows superior electrocatalytic activity, if W is present in a reduced form, for CO oxidation. Similar evidences were found for the ternary system

containing molybdenum [87]. But in this latter system, the electrochemical stability of molybdenum, under prolonged operation conditions, has still not been demonstrated.

Tungsten has the ability of coordinating water and a high mobility of hydroxyl species in the WO_3/WO_2 system in the region near the reversible potential for the oxidation of methanol, i.e. 0.04 V vs. NHE. The formation of hydrogen tungsten bronze, H_xWO_3, during the dehydrogenation process of methanol was observed for Pt/WO_3 electrocatalysts [88]. The presence of a "spillover" effect has a significant influence on the activity of the catalysts. Tungsten oxide-containing electrocatalysts produce an enhancement of the reaction rate by the continuous formation and oxidation of H_xWO_3 during the dehydrogenation of methanol. Furthermore, water is adsorbed on WO_3 at low overpotentials and may interact with CO adsorbed on Pt, thus facilitating its oxidation to CO_2.

Polyfunctionality is thought to be a prerequisite for oxidation of methanol, since it involves a series of intermediate steps. Whilst CO chemisorption is affected by the electronic environment and will be governed by the electron accepting-donating characteristics of Ru and W on Pt, including the promoting effect on the water discharge reaction at low potentials, the dehydrogenation process requires Pt with the added benefit of a significant spillover. The development of an active multifunctional catalyst, combining a redox functionality to the dehydrogenation step on Pt sites and the dehydroxylation step on Ru sites, is expected to constitute a fundamental "breakthrough" for DMFCs.

1.2.9 Heteropolyacids as surface promoters

A parallel strategy to the development of a new electrocatalyst for methanol electro-oxidation would be to employ co-catalysts or catalytic enhancers; accordingly, heteropolyacids have been demonstrated to be potential candidates in this approach [63, 89]. In the last few years, research on heteropolyacids has been a topic of remarkable and widespreading technological interest. The source of this interest mainly lies upon their unique structural and chemical characteristics, as well as on their capacity to exert various catalytic functions. In a previous study, it was shown that the electro-oxidation of methanol is promoted by an heteropolyacid, i.e. silicotungstic acid, but not by other inorganic acidic electrolytes, such as sulfuric acid [89]. More recently, other authors have shown that the enhancing behaviour of $H_4SiW_{12}O_{40}$ for methanol electro-oxidation is still present even when the heteropolyacid is dissolved in small amounts in sulfuric acid [90]. The observed improvements in the methanol oxidation activity in the presence of $H_4SiW_{12}O_{40}$ may be due to different factors, including the redox behavior of heteropolyacids at potentials close to

those of methanol adsorption, which thereby promotes the oxidation of strongly adsorbed methanolic residues. These results were supported by the improved kinetics of the electro-oxidation of carbon monoxide in phosphotungstic acid (PWA) electrolyte [63] over that in sulfuric acid. In particular, PWA was proven to enhance the water discharging process and the oxidation of CO species strongly bonded to the Pt electrocatalyst [63]. Heteropolyacids have also been used as surface promoters for another irreversible, electrochemical reaction (the oxygen reduction) when used as aqueous liquid electrolytes [91]. Recently, it was shown that heteropolyacids can be suitably anchored on active carbon supports and used as catalysts in heterogeneous oxidation reactions [92]. Tungstic acid (H_2WO_4) has been employed as a catalytic enhancer of Pt in phosphoric acid fuel cells by a simple blending procedure during electrode preparation [93]. Such evidences suggest that a novel route to increase the overall reaction rate may be based on the use of heteropoly-metallates as substrate species in conjunction with Pt-Ru catalysts.

1.2.10 Alternative electrocatalysts to platinum and their alloys

Only a few electrocatalyst formulations, alternative to Pt, have been proposed for methanol electro-oxidation. In most cases, the alternatives contain noble metals like gold, which does not solve the problem of the high cost of the materials employed in DMFCs. Only, a few formulations without noble metals have been tested: these are mainly based on transition metal alloys like NiZr [11], transition metal oxides and tungsten based compounds [9,10, 94]. All these materials showed lower reaction rates than Pt-based electrocatalyst and thus such unsatisfactory preliminary results have not stimulated much work in these directions.

Although many studies have been directed to the investigation and optimization of noble metals electrocatalysts, little work has been devoted to explore the possibility of using transition metal oxides as anodes. Transition metal oxides can play a role through their electron accepting and donating sites on the surface, and thereby adsorb methanol and CO related species. As an example, an oxidation mechanism, already proposed in gas-phase heterogeneous catalysis [95], is as follows:

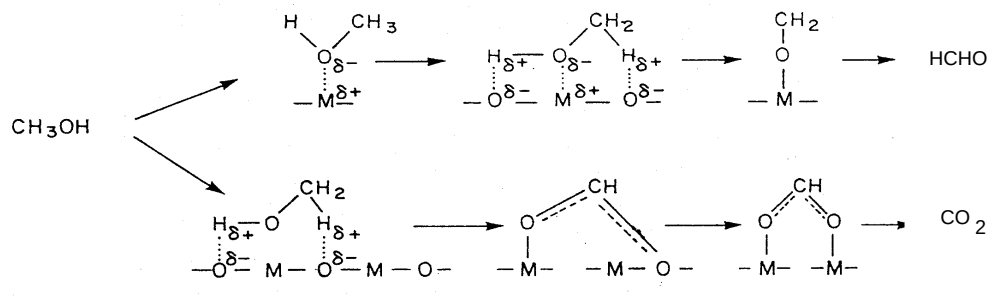

(16)

Transition metal oxides, because of their partially filled orbitals, may be ideal for a labile interaction with carbon monoxide and also be able to chemisorb hydroxyl species on neighbour sites. So far, the investigation of transition metals and metal oxide as electrocatalysts in DMFCs has been hampered by the corrosive characteristics of sulfuric and phosphoric acid electrolytes. However, the promising performance characteristics of DMFCs based on solid polymer electrolytes stimulate a reconsideration of non stoichiometric metal oxides, in view of their ability to oxidize water at low potentials, which is an essential feature for methanol oxidation. As transition metal oxide compounds intrinsically possess the thermodynamic characteristics which predict water displacement at low overpotentials, one could expect that, their wide range of potential for electro-reduction might meet the demand for the essential reaction through a surface oxygen vacancy mechanism.

In the following, a scheme of the thermodynamic potentials (E°) for the interaction of water with a few transition metal/metal oxides is presented and compared to that on Pt [96]:

$$Pt + H_2O \rightarrow PtO + 2H^+ + 2e- \quad E° = 0.99 \quad (17)$$

$$Mo + 3H_2O \rightarrow MoO_3 + 6H^+ + 6e- \quad E° = 0.25 \quad (18)$$

$$W + 2\,H_2O \rightarrow WO_2 + 4H^+ + 4e- \quad E° = -0.05 \quad (19)$$

$$W + 3H_2O \rightarrow WO_3 + 6H^+ + 6e- \quad E° = 0.09 \quad (20)$$

The considerable lower values of E° for the Mo/MoOx and W/WOx redox complexes than that for the Pt/PtO one, enhances the ability of coordinating water (at any significant concentration) by the metallic site and generating mobile hydroxyl species. As the most favourable condition for water displacement occurs in the region near to the reversible potential for oxidation of methanol, i.e. 0.04 V vs. RHE, transition metals like Mo and W appear ideally suitable for accelerating the rate of methanol oxidation. In particular, tungsten oxides show similar behaviour at different oxidation states. The doping of tungsten oxide with

rare earth elements or Na-alkali increases the rate of oxidation of pure carbon monoxide and of CO in reformed gas in a fuel cell [97]. This will open favourable perspectives, depending upon the degree of reduction of the bronzes, and whether water chemisorption can be tuned and the OH mobility adjusted through regulation of density of oxygen vacancies. Beside tungsten oxides, tungsten carbide is also known to possess intrinsic catalytic activity for electro-oxidation reactions such as hydrogen oxidation [10]. Although WO_2 was demonstrated to be very active for CO oxidation in a fuel cell as early as 1969 [9], it has only recently been shown that tungsten oxides and bronzes also have electrocatalytic activity for this reaction as well as methanol oxidation [98]. Furthermore, the concentration of oxygen vacancies on the electrocatalyst surface of tungsten bronzes can be appropriately adjusted by the addition of sodium or rare earth elements, so as to attain the desired range of potential for oxidative removal of the adsorbed CO by the active species generated on the surface of the electrocatalyst [97, 98]. According to the premises, the development of an active multifunctional catalyst, combining the dehydrogenation step promoted by tungsten carbide with a dehydroxylation step on the transition metal oxide site, may constitute the required "breakthrough" required for the reduction of noble metal loading in the anode and for further progress to make DMFCs commercially viable.

I.2.1.3 Morphological aspects of electrocatalysts

1.3.1 Role of surface area and metal loading

As discussed above, the main requirement for an optimal alloy electrocatalyst, such as Pt-Ru, is to synthesize it, highly dispersed on a carbon support. The mass activity (A/g Pt) of the catalyst for methanol electro-oxidation is strictly related to the degree of dispersion, since the reaction rate is generally proportional to its active surface area. In the case of an oxygen reduction electrocatalyst, it was found, after analysing a wide range of Pt and Pt alloy electrocatalysts, that there is an optimum particle size for the metallic phase (about 30 Å), which corresponds to a significantly high mass activity [99]. For this reaction it was found that the specific activity (mA cm^{-2} real surface area) increases with the particle size, but simultaneously decreases with the active surface area. The best compromise was achieved at about 30 Å Pt particle size [99].

In the case of methanol electro-oxidation on carbon supported Pt electrocatalyst, two different trends were observed. Mc Nicol et al. [4] observed for their Pt electrocatalysts a maximum activity at about 80 m^2/g surface area. Recently, another group has shown that the

specific activity increases as a function of particle size [100]. Thus, a maximum in mass activity vs. particle size should be observed as in the case of oxygen reduction. On the other hand, Watanabe et al. [101] found that the specific activity for methanol oxidation on a carbon supported Pt electrocatalyst does not change for a particle size above 20 Å (Pt fcc structure); thus, the mass activity increases as the dispersion of the metal phase is increased [101]. These latter findings have been in part confirmed for the Pt-Ru system for a particle sizes above 30 Å [102]. Not much work has been carried out on electrocatalysts with particle sizes below 20 Å or catalyst formed by an amorphous phase. Generally, most of the Pt-Ru fuel cell electrocatalysts have particle sizes above 20 Å, which are crystalline with a face centered cubic (fcc) structure. Below 20 Å, the distinction between amorphous and crystalline is not so evident. For particles with 10-15 Å size about 50% of the atoms are on the surface and thus there is no ordered structure. Some recent kinetic investigations by Wieckoski et al. [53, 54] on Pt surfaces covered with Ru ad-atoms have shown that the surface composed by the (111) Pt crystallographic plane covered by Ru ad-atoms performs better than any other Pt/Ru ad-atoms crystallographic plane. Thus extending these considerations to high surface area Pt-Ru electrocatalysts, the specific activity should increase with the particle size. In fact, a large-size particle possess a high surface content of (111) planes [99]. Accordingly, a maximum in the electrocatalytic activity should be observed as a function of particle size. In effect the data shown by Ren et al. [102] may be fitted as well with a "volcano" relationship with maximum at 3 nm and shape similar to that generally observed for oxygen reduction. Unfortunately, the scattering due to a variable composition of the Pt-Ru surface, in high surface area electrocatalysts, does not allow to distinguish a clear behaviour. A second aspect concerns the loading of the metal phase on the carbon support. A high wt. percent of Pt on the carbon substrate will significantly decrease the anode thickness for the same Pt loading per geometric electrode area (eg. 1 mg cm^2). Using this approach, it will be possible to enhance mass transport through the electrode and simultaneously reduce the ohmic drop. However, it has been found that an increase of the Pt loading (above 40 % wt.) on the carbon support decreases the dispersion of the electrocatalyst, probably due to some particle agglomeration.

1.3.2 Role of carbon support

In general preparation procedures, such as impregnation, colloidal deposition, surface reaction involve the adsorption step of active compounds on a carbon black surface. The synthesis of a highly dispersed electrocatalyst phase in conjuction with a high metal loading on carbon support has been one of the goals of the recent activity in the field of DMFCs. In

this regard it is of interest to determine which carbon black is most suitable as the support. In recent reports [103- 105], the mostly used carbon blacks were: Acetylene Black (BET Area: 50 m^2/g), Vulcan XC-72 (BET Area: 250 m^2/g) and KETJEN Black (BET Area: 1000 m^2/g).

All these materials have optimal electronic conductivity but, as denoted above, they differ for the BET surface area and thus very probably in the morphology. A low surface area carbon black (such as Acetylene Black) will not allow high dispersion of the metal phase, especially for a high metal loading (low carbon content); on the other hand, it does not have micropores in the structure, which could hinder mass transport through the electrocatalytic layer. A high surface area carbon black can easily accommodate a high amount of metal phase, with a high degree of dispersion but, at the same time, the significant amount of micropores on the carbon support will not allow a homogeneous distribution of the electrocatalytic phase through the support, which could lead to mass transport limitations of the reactant as well as its limited access to the inner electrocatalytic sites. Vulcan XC appears to be the best compromise with the presence of a small amount of micropores and a reasonable high surface area sufficient to accommodate a high loading of the metal phase. Up to now, this carbon black is the most used carbon support for the preparation of DMFCs catalysts.

1.3.3 Preparation methods

There are various routes for the synthesis of the Pt-Ru/carbon black electrocatalyst; these can be grouped into two main type, i.e., impregnation and a colloidal procedure. An impregnation procedure is characterized by an impregnation step of Pt and Ru precursors (e.g. H_2PtCl_6, Ru Cl_3, $Pt(NH_3)_2(OH)_2$, Ru_3CO_{12}, $Pt(NH_3)_2(NO)_2$ etc.) which is followed by a final reduction step. This can be a chemical reduction of the electrocatalyst slurry in aqueous solution by using N_2H_4, NaS_2O_5, NaS_2O_3, $NaBH_4$ (liquid-phase-reduction) or gas-phase reduction of the impregnated carbon black by a flowing hydrogen stream. It has been shown that the impregnation method can be used for the synthesis of a multifunctional system, e.g. from a bimetallic to a quaternary electrocatalyst (Pt-Ru-Sn-W) [15]. However, it requires the use of high surface area carbon black such as Ketjen black whose limitations for the operation of a methanol fuel cell have been pointed out above. Furthermore, this procedure does not allow one to obtain high dispersions in presence of high metal loadings.

There are various colloidal deposition routes, as, for example, used by Jalan [106], Bonneman et al. [107], Petrow and Allen [108], etc. The advantages of these preparation

routes consist in the attainment of significantly high surface areas in the presence of high metal loading on carbon. The main disadvantages are the presence of some complex preparation steps in the overall synthesis, the use in some cases of organic compounds/solvents and the increase of costs of production. An additional method is based on the thermal decomposition. In this case unsupported high surface area electrocatalysts are obtained by thermal decomposition of appropriate high molecular weight Pt-precursors such as Pt-carbonyl compounds [109]. Other methods, such as co-precipitation sol-gel or physical methods (e.g., sputtering [110]) have not stimulated much interest in the past but they are now becoming interesting for the synthesis of catalysts for portable power sources [110]. The choice of the most appropriate preparation procedure relies on the following considerations. It is well known that the preparation procedure of electrocatalysts influences their physico-chemical properties and thus their activity for methanol oxidation reaction and the oxygen reduction. The performance characteristics of an electrocatalyst depend on its chemical composition (surface and bulk), structure and morphology. Accordingly, the selected methodology of electrocatalyst synthesis should allow one to address the process for the attainment of a proper structure (crystalline or amorphous) and with a chemical composition on the surface as close as possible to the nominal or bulk composition. Since the rate of all electrocatalytic reactions is strictly related to the active surface area besides surface chemistry, the morphology of the electrocatalyst needs to be tailored. Morphology is not only related to the metal-phase area but also to the presence of micro and macro pores in the electrocatalyst support which could facilitate or hinder the mass transport properties. All these characteristics determine the cell performance even if the relative influence of each parameter is still not known in detail. It is thus necessary to select appropriate procedures for an optimization of these characteristics i.e. composition, structure, particle size, porosity etc. Generally a combination of physico-chemical and electrochemical analyses carried out on electrocatalysts with different characteristics indicates the system that better suits the scope of application in a DMFC.

I.2.2 Cathodic reduction of oxygen

2.1 General considerations

Although Pt/C electrocatalysts are, at present, the most widely used materials as cathodes in low temperature fuel cells, due to their intrinsic activity and stability in acidic solutions, there is still great enthusiasm to develop more active, selective and less expensive

electrocatalysts for oxygen reduction. Since it is widely established that Pt cannot be easily replaced (at least for the moment) by other electrocatalysts for the oxygen reduction reaction (ORR), there are a few directions that can be investigated to reduce the costs and to improve the electrocatalytic activity, especially in the presence of methanol cross-over. One is to increase Pt utilization. This can be achieved either by increasing its dispersion on carbon and the interfacial region with the electrolyte. Another successful approach to enhance the electrocatalysis of O_2 reduction is by alloying of Pt with transition metals. This enhancement in electrocatalytic activity has been differently interpreted, and several studies were made to analyze in depth the surface properties of the proposed alloys combinations [111-115]. Although a comprehensive understanding of the numerous reported evidences has not yet been reached, the observed electrocatalytic effects have been ascribed to several factors (interatomic spacing, preferred orientation, electronic interactions) which play, under fuel cell conditions, a favourable role in enhancing the ORR rate [116-120]. High specific activities of Pt-Cr and Pt-Cr-Co alloy electrocatalysts for oxygen reduction as compared with that on platinum were observed in H_2-air polymer electrolyte membrane fuel cells (PEMFCs) [111,120]. The formation of a tetragonal ordered structure upon thermal treatment, in the case Pt-Co-Cr, leads to a more active electrocatalyst than that with a Pt fcc structure [116-120]. Moreover, even in the presence of methanol cross-over, the performance of highly selective electrocatalysts for oxygen reduction would be (in theory) less affected by poisoning phenomena on account of the lower chemisorption energy of methanol on the alloys in comparison with that on Pt. Another goal in this field is to obtain very small sizes for the Pt alloy particles supported on carbon. In the case of Pt-Co-Cr particles with a tetragonal structure, the state of art electrocatalysts have a particle size of 6 nm [116-120]. In addition to the coprecipitation and impregnation methods for preparation of these alloys on a carbon support, colloidal preparation procedures have also been recently investigated [121].

2.2 Oxygen electroreduction in DMFCs

For the development of cathode electrocatalysts for DMFCs, two main aspects should be taken into account. The electrocatalysts should be very selective for oxygen chemisorption and thus highly active for oxygen electroreduction. In other words, the electrocatalysts should have a composition which will not be poisoned by the methanol crossing over from anode to cathode while maintaining high reaction rates for oxygen reduction. In most cases, a compromise between electrocatalytic activity and resistance to poisoning is necessary. The

most widely used electrocatalysts employed in low temperature fuel cells for the oxygen reduction are based on platinum. As discussed in a previous section, various studies conducted in the past, especially on carbon supported Pt electrocatalysts for oxygen reduction in phosphoric acid fuel cells, showed that the electrocatalytic activity (mass activity, mA g^{-1} Pt, and specific activity, mA cm^{-2} Pt) depends on the mean particle size. The mass activity for oxygen reduction reaches a maximum at a mean particle size of 30 Å, corresponding closely to the particle size at which there is a maximum in the fraction of (111) and (100) surface atoms on Pt particles of cubo-octahedral geometry [99]. On the other hand, the specific activity increases gradually with an increase in the Pt particle size and closely follows the trend observed between the surface fraction of (111) and (100) Pt atoms and the particle size. These results have indicated that the (111) and (100) surface atoms are more electro-catalytically active than Pt atoms located on high Miller index planes [99]. Platinum atoms at edge and corner sites are considered to be less active than Pt atoms on the crystal faces. Accordingly, the mass and specific activity should decrease significantly as the relative fraction of atoms at edge and corner sites approach unity [99]. This situation occurs with Pt particles smaller than 10 Å diameter. Most of the experimental evidence observed in PEMFCs, shows that crystalline electrocatalysts with about 25-30 Å particle size have higher activities than amorphous particles and also electrocatalysts with larger crystallite sizes [122].

In the case of DMFCs, an additional aspect should be considered; this is in regard to the methanol cross-over through the membrane. Methanol oxidation and oxygen reduction in the cathode compartment compete for the same sites producing a mixed potential which reduces the cell open circuit potential. In order to better understand these effects, it is worthwhile considering the mechanism for methanol oxidation and oxygen reduction; possible mechanisms are presented below.

Oxygen reduction:

$$O_2 + Pt \rightarrow Pt\text{-}O_2 \qquad (21)$$

$$Pt\text{-}O_2 + H^+ + 1e^- \rightarrow Pt\text{-}HO_2 \qquad (22)$$

$$Pt\text{-}HO_2 + Pt \xrightarrow{rds} Pt\text{-}OH + Pt\text{-}O \qquad (23)$$

$$Pt\text{-}OH + Pt\text{-}O + 3H^+ + 3e^- \rightarrow 2Pt + 2\,H_2O \qquad (24)$$

Equation (23) indicates an intermediate step requiring a dual-site reaction, and if it is the rate-determining step, it is more affected by particle size than intermediate step represented by equation (22). When the particle size becomes very small, then only the inactive edge and corner atoms will be present and dual sites of the proper orientation would not be available. Thus the activity of the particle should be lower. According to the observed variation of the

reaction rate with particle size, one may conclude that the rate-determining step is represented by Eq. 23 [121].

Methanol oxidation:

$$CH_3OH+3Pt \rightarrow Pt_3\text{-}COH \quad (25)$$

$$Pt_3COH \rightarrow Pt\text{-}CO+H^+ +2Pt \quad (26)$$

$$Pt+H_2O \rightarrow Pt\text{-}OH+H^+ +1e \quad (27)$$

$$Pt\text{-}OH+PtCO \rightarrow 2Pt+CO_2 \quad (28)$$

In the case of methanol oxidation at the cathode, three neighboring Pt sites in a proper crystallographic arrangement will favour the methanol chemisorption. Since at high cathodic potentials the water discharging reaction (eq. 27) is largely favoured, oxidation of the methanolic residues adsorbed on the surface proceeds very fast producing a parasitic anodic current on this electrode.

When the particle size of the electrocatalyst is very small or one has an amorphous Pt electrocatalyst for the oxygen reduction, methanol chemisorption energy could be lower and hence the cathode less poisonable. But, at the same time, due to the fact that only the inactive edge and corner atoms will be present and dual sites of the proper orientation will not be available, the activity of such electrocatalyst for oxygen reduction will be lower. The best compromise is to modulate the structure and the particle size between amorphous and crystalline in order to decrease the poisoning by methanol and enhance oxygen reduction.

A second possibility is to use a promoting element for oxygen reduction which simultaneously hinders the methanol chemisorption still maintaining the proper structure and particle size.

2.3 Carbon supported electrocatalysts

In order to enhance the resistance to methanol poisoning of the cathode, research activities based on the modification of Pt electrocatalyst by addition of transition metals were recently initiated in various laboratories [121, 123]. In phosphoric acid and PEMFCs the intrinsic electrocatalytic activity of Pt alloys (Pt-Cr, Pt-Ni, Pt-Cr, Pt-Cu, Pt-Fe), with a lattice parameter smaller than that of Pt, is higher than on the base metal [111-120]. This effect is related to the nearest neighbour distance of Pt-Pt atoms on the surface of the fcc crystals. Since it has already been observed that the rate determining step involves the rupture of the O-O bond through a dual site mechanism, a decrease of the Pt-Pt distance favours the dual site O_2 adsorption. Most of these evidences are derived from studies carried out in phosphoric acid fuel cells. In such cases leaching of non-noble elements produces a surface roughening with a

corresponding increase of the Pt surface area. A considerably lower number of studies has been carried out on Pt-alloys as electrocatalysts for ORR in PEMFCs [111, 120, 122]. In this case, since the electrolyte anions are chemically bound to the backbone of perfluorosulfonic acid membranes and the cell temperature is relatively low, corrosion problems are minimised compared to phosphoric acid fuel cells. Also in the case of PEMFCs, there is specific evidence for an enhancement of the reaction rate for O_2 reduction on a Pt- alloy electrocatalyst [111, 120, 122]. As pointed out in a previous sub-section, methanol chemisorption and oxygen reduction reactions require an appropriate geometrical arrangement of Pt atoms. Both processes are favoured on a Pt (111) surface, which possesses the reasonable nearest Pt-Pt interatomic distance. Thus, the poisoning effect of methanol cross-over should be more significant on the Pt (111) surface. The lack of information in this field, however, does not allow one to quantify the compensation effect due to the increased methanol oxidation rate at the sites where oxygen reduction is favoured. Beside these aspects, recent work has also taken into consideration the role played by the promoting element (Co, Cr) for the removal of strongly bonded oxygenated species on Pt through an intra-alloy electron transfer [123]. Chemisorption of oxygen molecules occur more easily on oxide-free Pt surfaces [123]. But, as well documented by cyclicvoltammetric analyses [18], methanol adsorption and oxidation are favoured on a reduced Pt surface rather than on platinum oxide. In other words, the addition of Co and Cr to Pt, simultaneously favours the oxygen reduction and methanol oxidation reactions. Furthermore, the presence of electropositive elements, alloyed to Pt, favours the chemisorption of OH species on Pt neighbouring sites. In the absence of oxygen, a small but noticeable promoting effect for methanol oxidation in a wide range of anodic overpotentials has been observed by Cr, Fe and other elements usually selected as catalytic enhancers for the oxygen reduction reaction in PEMFCs [6]. At present, it is difficult to establish if the beneficial effect on oxygen reduction is prevailing with respect to the promoting effect on methanol oxidation at DMFC cathode. In a recent paper, a limited enhancement of ORR was shown when a Pt-alloy instead of Pt was used in DMFCs [121], whereas in other cases, it was observed that Pt-alloys are less tolerant than Pt alone to methanol.

The preparation of cathodic Pt-based electrocatalysts for DMFCs are pratically the same as for the anodic electrocatalysts. However, there are some differences in terms of the thermal treatment of a Pt-Ru or Pt-Sn alloy for methanol oxidation and that of a Pt-Cr, Pt-Co, Pt-Co-Cr electrocatalysts for oxygen reduction [111-120]. In the latter case, the activation temperature is significantly higher, around 700-900 °C, compared to 100-400°C adopted for

the anodic alloy. In the case of the cathode electrocatalyst, a complete alloying is generally accompanied, in most cases, by a phase transition from fcc (cubic) to an ordered tetragonal (fct) structure. This treatment causes an increase of the mean particle size. Thus, the increase of intrinsic electrocatalytic activity is counteracted by the decrease of the surface area of the electrocatalysts.

2.4 Non-noble metal based electrocatalysts

As an alternative to using platinum, an interesting approach is directed towards the use of organic transition metal complexes as electrocatalysts for the oxygen reduction reaction. Transition metals, such as iron or cobalt organic macrocycles from the families of phenylporphyrins, phthalocyanines, and azoannulenes have been tested as O_2-reduction electrocatalysts in fuel cells [124-128]. One major problem with these metal organic macrocyclics is their chemical stability under operation of fuel cells at high potentials. In many cases, the metal ions are irreversibly dissolved in the acid electrolyte. However, if the metal-organic macrocyclic is supported on a high surface area carbon and it is then treated at about 500 to 800 °C, the residue exhibits electrocatalytic activity comparable to that on Pt, without any degradation in performance from which one may infer the stability of the metal in the electrocatalyst [127]. Recently, Savinell and co-workers [127] showed interesting results for the operation of these compounds in solid polymer electrolyte fuel cells and a high selectivity for oxygen.

In some other studies, a few inorganic materials have recently been proposed as suitable substitutes for Platinum in methanol fuel cells due to their selectivity for oxygen reduction, even in the presence of methanol, at significant rates. These materials mainly consist of the Chevrel-phase type ($Mo_4Ru_2Se_8$), transition metal sulfides ($Mo_xRu_yS_z$, $Mo_xRh_yS_z$) or other transition metal chalcogenides ($(Ru_{1-x}Mo_x)SeO_z$) [129-130]. Some of these materials possess semiconducting properties, thus, in theory, they could introduce an additional ohmic drop in the electrode. Their activities for oxygen reduction are significantly lower than Pt [2, 4]. Beside these materials, carbon supported Ru electrocatalysts have also exhibited high selectivity for oxygen reduction in the presence of methanol but their activities are quite low [131]. The mechanism by which these materials are tolerant of methanol is due to the absence of adsorption sites for methanol dehydrogenation. In the case of Ru/carbon, at high potentials, the surface is mainly covered by Ru oxides on which methanol chemisorption is hampered [131]. The same mechanism is also effective for Pt but to a less extent. In a previous study [24], we have shown that in the presence of methanol, the Tafel slope for

oxygen reduction at 60 °C on a Pt surface is pratically unaltered at high potentials (-60 mV/dec), i.e., in the region where the surface is mainly composed of Pt-oxides. At lower potentials, where the metallic surface is exposed, methanol is effectively oxidized in the presence of oxygen. This parasitic reaction determines an increase of the Tafel slope (Fig. 6) which changes from 130 to 170 mV/dec [24] . This effect is the same as that observed in classical cyclic voltammetry of methanol at Pt electrodes [18]. The methanol oxidation peak in the anodic scan is followed by a sharp decrease of current due to the formation of a strong Pt-oxide layer on the surface before oxygen evolution. This evidence show that the presence of oxides on the surface of the electrocatalysts in DMFCs make them more tolerant than the metal to methanol in respect to the kinetics of ORR. This is also one of the reasons why Pt-Cr, Pt-Co, Pt-Co-Cr have shown only limited or no enhancement of oxygen reduction kinetics in DMFCs, as compared to that in H_2-air SPEFCs. In general, Co, Cr interact with Pt in the alloy by electron donation to 5d Pt orbitals due to their electropositive character [123]. Thus, they remove the strongly bonded oxygen species from Pt sites thus favouring methanol chemisorption on Pt [123].

I.3 Technology Development and its Prospects

I.3.1 Proton conducting membranes

Nafion membranes are currently used as electrolytes in DMFCs; yet, since methanol is rapidly transported across perfluorinated membranes, commonly used in polymer electrolyte membrane fuel cells, and is chemically oxidized to CO_2 and H_2O at the cathode, there is a significant decrease in the coulombic efficiency for methanol consumption in the fuel cell by as much as 20% at technical operation conditions [132]. Thus, it is vitally important to modify these membranes by, as example, developing composites or finding alternative proton conductors with the capability of inhibiting methanol transport. It is generally accepted that a solid-state proton conductor is preferable for liquid fuel fed DMFCs because it limits corrosion and rejects carbon dioxide (produced during the methanol oxidation). The polymer electrolyte should have a high ionic conductivity ($5 \cdot 10^{-2}$ ohm^{-1} cm^{-1}) under working conditions and low permeability to methanol (less than 10^{-6} moles min^{-1} cm^{-2}). Further it must be chemically and electrochemically stable under operating conditions. These requirements appear to be potentially met by new classes of solid polymer electrolytes that show promising properties even though there has been no clear demonstration of their use in

DMFC. Some of the membranes investigated so far are: sulfonated poly (ether ether ketone) and poly (ether sulfone) [133], polyvinylidene fluoride [134], styrene grafted and sulfonated membranes [135], zeolites gel films (tin mordenite) and/or membranes doped with heteropolyanions [136].

Sulfonated poly (ether ether ketone) and poly(ether sulfone) electrolytes show promising characteristics in terms of (i) mechanical strength even when these are prepared in thin films (10-50 μm) and (ii) acceptable conductivity in their protonic form with low resistance to ion transport and reduced cross-over of methanol. The perspectives of preparing these materials as very thin films by casting them on electrodes from solution containing the polymer precursors offer considerable advantages in respect reducing ohmic overpotentials in DMFCs, as compared with perfluorinated sulfonic membranes with higher thickness (e. g. Nafion 117). The properties of sulfonated poly ether ether ketones and poly ether sulfones, as ascertained in DMFCs, are at the present at an insufficient stage with respect to the requirements of stability and conductivity. The evidence to date indicates instability of the materials in (hot) methanol, which is further increased by sulfonation of the materials; but, sulfonation is necessary to obtain the desired level of conductivity [135]. One approach to solve the above-mentioned problems is to cast the membranes and then cross-link the polymers. Suitable compounds for carrying out the cross-linking are aliphatic and cyclic diamines, such as diazobicyclooctane and aminopyridine (the chain length of the diamines can be varied and optimised so as to minimise the methanol flow through the membrane). An appropriate compromise between sulfonation and cross-linking procedures is generally required to obtain membranes with high ionic conductivity, good mechanical resistivity and low methanol cross-over [135]. Alternatives to these membranes and Nafion are acid-doped polyacrylamid and polybenzoimidazole [137]. The main question about these membranes is the extent of leaching of acids of small molecular weight (H_3PO_4) entrapped in the polymer, during operation of a fuel cell using a hot methanol/water mixtures as the anode reactant. In fact these polymers usually swell at high temperatures in the presence of water and methanol. Probably these problems may be better addressed by using a high molecular weight super acid (such as phosphotungstic acid) that may be physically entrapped in the polymer structure. However, in this case, the uptake of water by the polymer should not be significantly reduced since water is essential for the protonic conduction.

An interesting field regards the development of composite membranes [134, 138-140]. Composite recast Nafion-silica membranes have shown excellent properties in terms of mechanical characteristics, water retention at high temperature, resilience to methanol cross-

over and ionic conductivity [139]. These electrolytes allow DMFCs operation at 145 °C with a significant enhancement of methanol oxidation kinetics [139]. The only drawback, at the present time, appears to be the high cost of production, primarily determined by the expensive perfluorinated ionomer necessary for their fabrication. Few variations of this procedure include the use of heteropolyacid doped silica entrapped into recast Nafion or zirconium phosphate/extruded Nafion membranes [140]. Recent investigations from our group have shown interesting perspective for the use of these composite electrolytes in DMFCs [140].

I.3.2 Membrane and electrode assemblies

The performance of a DMFC is strongly affected by the fabrication procedure of the membrane-electrode assembly (MEA). The conventional technology, that was used until a few years ago, consisted of the preparation of gas-diffusion electrodes having suitable polytetrafluoroethylene (PTFE) contents in both diffusion and catalyst layers. Nafion® ionomer was spread onto the electrocatalyst layer, followed by the preparation of membrane-electrode assembling by a hot-pressing procedure [141]. A disadvantage of this procedure is that the Nafion® impregnated into the active layer of the electrode has a limited penetration depth. This drawback reduces the electrochemically active area which is between electrocatalyst particles and ionomer, thus decreasing the catalyst utilization [142]. The function of PTFE in the catalyst layer is to provide a network for gas transport and to give structural integrity to the layer. However, it has been evidenced that the ionic path in the electrocatalytic layer due to the recast ionomer is hindered on the surface of the electrocatalysts and pores covered and/or blocked by PTFE particles [142]. To avoid these drawbacks, modified electrode preparation methods have been developed. These methods are characterized by a procedure involving a direct mixing of the ionomer with the electrocatalyst. Both direct mixing of electrocatalyst with ionomer and appropriate solvent like glycerol or a “paste process” procedure based on the addition of a colloidal ionomer to the electrocatalytic layer have been successfully developed for use in DMFCs to obtain PTFE-free electrocatalytic layers [142-145]. Such fabrication methods do not require a laborious procedure. The optimization of the structure of the electrode and/or MEAs requires an appropriate investigation of the microstructure of the carbon support, in order to ideally distribute the ionomer on the carbon surface containing Pt or Pt-Ru particles. The main problem of direct mixing or “paste process” procedures is that the ionomer does not soak

deeply into the smaller pores of the active layer, as it would in the case of a liquid electrolyte. Thus, the reaction area is limited to an interface between Pt particles distributed on the outer surface of carbon agglomerates and ionomer [146]. As example, the electrochemical active surface area (ECA) of a highly dispersed carbon supported Pt-Ru catalyst, as determined by the CO stripping analysis under fuel cell configuration (catalyst-ionomer composite), and in the presence of high Pt loadings (1-2 mg Pt cm^{-2} as typically occurs in a DMFC) is about 50% of that determined by XRD or TEM analyses (MSA). The Pt loading could be significantly reduced if the Pt utilization increases. The enhancement of Pt utilization could be optimally achieved if both the anode and cathode electrocatalysts are tailored to be distributed on the outer surface of the carbon agglomerate; furthermore, an increase of the dimension of carbon pores and a decrease in the size of ionomer micelles are needed to increase the contact region with the ionomer.

Operation of DMFCs with air feed imposes an appropriate development of the cathode layer that takes into account requirements different from that of an oxygen-fed electrode. When air is fed to the cathode side, while oxygen reacts to produce water, the nitrogen contained in the feed stream remains entrapped in the pores of the electrode; the entrapped nitrogen is a diffusion barrier for the incoming oxygen, and results in mass transport overpotential performance losses even at intermediate current densities. Furthemore, although it is known that oxygen permeability through the ionomer is high, at high current densities, transport of this gas to the reaction sites is retarded by flooding of the electrocatalyst layer [141]. Due to this flooding of the active layer, the ionomer swells until it is saturated with water, thus increasing the hydrophilicity of the layer. Such drawbacks have been conveniently reduced in air feed-SPE fuel cells by using thin film electrodes having low electrocatalyst loadings (0.05 - 0.1 mg cm^{-2}) [143]. Due to the lower performance of the oxygen electrode with such low Pt loadings in DMFCs, alternative solutions should be investigated.

A few directions have been addressed as alternatives to the conventional preparation procedure of the electrocatalyst layer to enhance the oxygen transport properties when air is used as feed stream. Gas channels allowing the fast transport of the reaction gas to the ionomer and the easy removal of the excess N_2, can be realized in the cathode layer by means of PTFE-carbon composite ducts [144]. These ducts inside the electrocatalytic layer have been realized by ultrasonically mixing the electro catalyst-ionomer mixture with appropriate amounts of a PTFE-carbon composite before spreading resulting paste onto carbon cloth or carbon paper. The PTFE in this case does not cover Pt sites, being only loaded on the carbon

black; at the same time, the PTFE-C mixture contains a significant number of dry pores, thus enhancing the mass transport properties of the gas; its function will be to supply the reacting gas to the electrocatalytic sites and to exhaust the product water as well as the excess nitrogen [144]. As a consequence, this configuration does not affect the electrocatalyst utilization and the continuity of ionomer in the catalyst layer, thus improving the mass-transport properties of the electrode.

A second approach is to the modify the hydrophobic-hydrophilic properties of the ionomer in the electrocatalyst layer. As example, Nafion ionomer in solution is characterized by a rod-like structure in the form of direct micelles with the perfluorinated matrix forming the inner part and ionic sulfonate groups on the surface. In a completely hydrophilic layer, the gas is not easily provided in the absence of a network of hydrophobic pores within the electrocatalyst layer. Accordingly, gas transport through pores filled with ionomer and/or water will not be a limiting step if it only occurs over short distances. This is the case of thin film electrodes employed in SPEFCs. A complete hydrophilic layer could become a problem for gas transport in DMFCs since these devices require significant electrocatalyst loadings and, consequently, thick electrodes are generally used. To overcome these problems, the recast Nafion gel inside the electrocatalytic layer is thus modified by annealing at moderate temperatures (150-180°C). The thermal treatment degrades a significant fraction of sulfonic acid groups increasing the degree of hydrophobicity of the layer. This partially hydrophobic layer improves the mass transport properties at high currents and the removal of product water [142].

A third approach is to use pore formers such as $(NH_4)_2CO_3$ to increase the level of porosity in the active layer of the cathode, as recently suggested by Wendt and co-workers [147] and by Appleby et al. [148]. This approach has already shown interesting results for air feed DMFCs. Each of these procedures has shown specific advantages depending on the operating conditions e.g. operation temperature, air pressure, level of humidification etc.

I.3.3 Single cell performance – Polarization behaviour

3.1 Dependence on kinetics of electro-oxidation of methanol and oxygen reduction

The polarization behaviour of a DMFC is predominatly controlled by the cross-over of the methanol from anode to cathode and the slow kinetics of its electro-oxidation at the anode, when compared to that of a H_2/air PEMFC [56, 81, 149-156]. Most of the present DMFCs are based on Pt-Ru as anode electrocatalyst. The observed open circuit potentials in the present

DMFC are about 150 to 200 mV lower than those observed in PEMFCs, with similar oxygen pressure and cell temperature conditions, even though the reversible potential for methanol oxidation differs by only 40 mV from that of the reversible hydrogen electrode (RHE) [141]. The characteristic polarization curves of DMFCs at suitable temperatures of 90 °C -130 °C show an open circuit voltage ranging from 0.7 to 0.9 V, depending on the electrocatalyst, membrane and operating conditions. A potential drop of about 0.15-0.2 V, observed at very low current density can be ascribed to the methanol oxidation reaction and methanol cross-over [81]. Thereafter, the current density increases markedly with decrease in cell potential. This behavior is related to a first methanol dehydrogenation step which occurs at low anodic potentials but which gives rise to an almost complete monolayer of CO coverage on the surface on a Pt electrocatalyst. Oxidation of chemisorbed residues occurs as the anode overpotential becomes sufficiently high for a fast water discharge reaction on Ru sites producing OH species [81]. According to previous studies in the literature [81], the decrease in cell potential with increase in current density in the activation controlled region of the polarization curves suggests that water displacement occurs quite slowly at high cell potentials. On the other hand, at intermediate and low cell potentials, the observed variation of the fuel cell performance with methanol concentration indicates that the reaction rate is directly related to the coverage of methanolic residues. These evidences suggest that the rate of methanol oxidation depends on a suitable coverage of both OH and CO-like species on the anode surface. At the potential corresponding to the maximum power output, the rate of the water discharging process is extremely fast due to the high anode overpotential. Hence, the surface reaction between Pt-bonded CO-like species and OH species adsorbed on Ru sites could become the rate determining step of the overall process. The chemical interaction between these adsorbed intermediates requires a good atomic mixing between Pt and Ru sites. In general when a significant fraction of Ru atoms are alloyed with Pt these sites actively contribute to accelerate the methanol oxidation reaction. The oxygen reduction process is affected by methanol cross-over especially at high cell voltages where mixed potential at the cathode determines low OCV values. At high current densities due to the fact that methanol is readily consumed at the anode, the overpotential for oxygen reduction in a DMFC is not significantly higher than in the case of a H_2/air fuel cell.

The performance of a DMFC is generally reported in terms of maximum power density and power density at a particular cell voltage e.g. 0.5 V. It strongly depends on the operating conditions (working temperature, type of oxidant i.e. air or oxygen, back-pressures, mass transport conditions, M&E assembly conditioning) and on the characteristics of the fuel

cell components (catalyst loading, fabrication procedures of electrodes and M&E assembly, membrane conductivity, flow-fields). It is very difficult to make a comparison among the various polarization data reported in the literature mainly due to the fact that the operating conditions are not chosen following a general protocol. The best single cell (5-50 cm^2 active area) DMFC performances, achieved by various groups in the last five years, are 300-450 mW cm^{-2} and 200-300 mW cm^{-2} as maximum power density, in the presence of oxygen and air feed at the cathode, respectively [6, 56, 86, 102, 104, 149, 151-156]. These performances have been obtained at temperatures close or above 100 °C, with overall Pt loadings of 2-5 mg cm^{-2} and, in most cases, under pressurized conditions. At a cell voltage of 0.5 V, the best performances in presence of air as oxidant are 150-200 mW cm^{-2}. If the DMFC is operated at room temperature and under air breathing conditions the performances become less than one-tenth of those achieved under the above conditions.

3.2 Effect of methanol concentration, pressure and flow rates on DMFC performance

The variation of electrochemical performance of the DMFC with methanol concentration, generally reflects two phenomena. By increasing the methanol concentration, the coverage of the electrocatalyst sites by methanolic residues increases, but, it simultaneously decreases the water concentration in the solution. In this regard a reaction order of 0.5 with respect to methanol concentration has been observed in half-cell polarization experiments up to 2.5 M concentration [27]. During operation in a fuel cell, a high methanol concentration in the anode feed determines a high concentration gradient across the interface with consequent increase of the cross-over through the Nafion® membrane. Thus, a delicate balance among the effects of methanol oxidation kinetics and methanol cross-over is required to enhance the performance in the activation and ohmic-controlled regions [81]. On the other hand, the polarization behavior in the mass transfer controlled region is directly related to the methanol concentration. By increasing the methanol concentration, a corresponding increase of limiting current density in the I-V characteristics is generally observed [81]. Generally the highest power densities have been observed with 1 to 2 M methanol concentrations; 1 M methanol is preferable in presence of an air-fed DMFC because the effects of methanol cross-over on the cathode polarization and fuel efficiency are less with a lower methanol concentration.

High cathode back pressures are desirable to achieve suitable oxygen reduction rates in the presence of methanol cross-over. A high oxygen partial pressure is favourable due to the positive reaction order and to impede methanol chemisorption on the cathode surface

[149]. High air flow rates counteract the negative effects of cross-over by increasing the efficiency of oxidation of organic molecules [149]. Yet, a stack operation at high pressures of 2-3 atm and under high flow rates requires the use of a suitable compressor which consumes from 10 to 20% of the output power for a 5 kW stack [3]. Whereas for operation at much lower pressures (1.5 atm) with suitable air stoichiometries, an air blower is sufficient with a significant reduction in energy consumption and cost. Suitable anode back pressures are necessary for high temperature operation. This aspect is crucial to maintain a good level of hydration of membrane. The energy consumption of the liquid pump is much lower with respect to the air compressor.

3.3 Effect of methanol cross-over

Methanol cross-over through the polymer membrane is known to be one of the most challenging problems affecting the performance of DMFCs [102, 132]. The overall efficiency of a methanol fuel cell is determined by both the voltage efficiency and faradaic efficiency for consumption of methanol [150]. The faradaic efficiency is mainly influenced by the methanol cross-over through the membrane. If we express the methanol cross-over in terms of current density that is practically lost in the parasitic reaction occurring at the cathode, $I_{cross\text{-}over}$, the faradaic efficiency is determined by :

$$\eta_{fuel} = \frac{I_{cell}}{I_{cross-over} + I_{cell}} \qquad (29)$$

The methanol cross-over is measured indirectly by determining the CO_2 produced at the cathode by the electro-oxidation of methanol on the Pt surface [102, 132]. This CO_2 can be monitored on line by using an IR-detector or by chromatographic analysis of aliquot samples of cathode outlet stream [132, 139]. The latter method is more precise but is more time consuming and requires a more expensive apparatus. Chromatographic analysis of the cathode outlets reveals the presence of small but still detectable amounts of unreacted methanol [139]. Yet, this latter is often neglected since it is generally less that a few percents of the total cross-over i.e. comparable to the accuracy level of the IR-sensor for CO_2. The cross-over of methanol is influenced by the membrane characteristics and by the temperature, but a significant effect is also dependent on the operating current density [102, 132]. In general, an increase of temperature causes an increase of the diffusion coefficient of methanol and causes a swelling of the polymer membrane. Both effects contribute to an increase of the rate of methanol cross-over. The cross-over includes both methanol permeability due to a

concentration gradient and molecular transport caused by electro-osmotic drag. The latter is directly related to the proton migration through the membrane and it depends directly on the current density i.e. it increases with the current density [157]. The methanol permeability, caused by the concentration gradient at the interface, is also dependent on the operating current density in an indirect manner. In a polarization curve, the onset of diffusional limitation occurs when the rate of reactant supply is lower than the rate of electrochemical consumption. Thus, if the anode is sufficiently active to oxidize methanol electrochemically to CO_2 at a rate comparable to or higher than the rate of methanol supply, the concentration gradient at the electrode/membrane interface could decrease to zero [102, 132, 149]. This condition can be realized in presence of electrodes in which there is an extension of the electrocatalyst/electrolyte interface in the electrocatalytic layer (i.e. a composite catalytic layer containing catalyst and micelles of the ionomer) at a current density close to the limiting value in the DMFC. Some authors have shown this result by an appropriate tailoring of the experimental conditions (e.g. methanol flow feed, current density and temperature) in DMFCs with Nafion 117 membranes [102, 132]. Membranes with such large thicknesses are effective barriers for reducing methanol cross-over; conversely an increase in thickness causes an increase of ohmic overpotentials. In some cases, it may be more productive to use thinner membrane with reduced ohmic limitations and to select appropriate operating conditions which limit the methanol cross-over. At 90 °C, the methanol cross-over through Nafion 117 at open circuit conditions is larger than 100 mA cm^{-2} (equivalent current density), but it decreases to less that 40 mA cm^{-2} (equivalent current density) at about 300 mA cm^{-2} [102, 132]. Nafion 112 membrane with 50μm thickness shows a few hundreds of mA of equivalent current density for methanol cross-over close to the open circuit conditions, but this reduces to 60 mA cm^{-2} at a current density of 500 mA cm^{-2} (electric output rate of DMFC) in the presence of electrodes allowing efficient methanol consumption and with moderate methanol feed rates [102, 149]. This means that a faradaic efficiency close to 90% can be achieved with thin membranes with consequent benefits in terms of reduced ohmic drops.

Modified composite silica-Nafion membranes with silica particles (about 7 nm size) entrapped in the polymer structure show lower methanol cross-over (40 mA cm^{-2} equivalent current density at 145 °C and 500 mA cm^{-2}) cell current [139]. In this case, the silica acts as a physical barrier, especially if its action is further supported by an increase of the crystalline properties of the polymer. In general a perfluorinated membrane with a higher degree of crystalline region with respect to the amorphous region should show reduced methanol cross-over. This does not necessarily occurs at the expenses of ionic conductivity as one may

expect since this latter is mainly determined by the water retention properties of the membrane which are enhanced by the addition of hygroscopic inorganic materials [139].

Recently, the usual method of measuring the cross-over has been criticized [158]. Since some fraction of the CO_2 produced at the anode during cell operation can permeate through the membrane, the level of methanol cross-over especially at high current densities may be significantly affected by this phenomenon. In effect some curves reporting the variation of equivalent current density vs. cell current do not show a progressive decrease of methanol cross-over as the current density increases but at high current density an asymptotic behavior towards a constant value of equivalent current density is observed [102]. This would indicate the presence of some background which may be related to the permeation of CO_2. These conjectures are still not adequately supported by appropriate experimental evidences, but if they are true, the fuel efficiency of a DMFC must be higher than that calculated up to now and it will approach 95% or more. At present, studies carried out at the University of California indicate a fuel utilization of 80-90% under optimum overall conversion efficiency conditions [150].

3.4 Flow fields

The increasing levels of performance that have recently been reached in DMFCs are often associated with a reduction of kinetic and ohmic limitations [56]; there is now an increase of interest on reducing mass-transport limitations. In this regard, some progress has been obtained by improving the characteristics of the backing layer in terms of composition and thickness. Recent investigations have focused on design of the reactant flow fields [149, 159]. The most widely employed flow field in highly advanced fuel cells is based on the serpentine configuration. In such a configuration, the reactant is constrained to flow in a zig-zag way along parallel channels which are machined in a graphite plate in contact with the electrode backing layer. Such a design has often been adopted for stacked cells. The reactant molecules have access to the electrocatalytic sites through diffusion across the so-called diffusion layer, i.e. the backing layer, made of carbon cloth and carbon black, hydrophobized by appropriate addition of polytetrafluoroethylene (PTFE).

Recently, a different approach for the flow of reactants and products within the electrode structure, i.e. an interdigitated design, was proposed by Nguyen [160] and by Wilson et al. [161] for H_2-O_2 solid polymer electrolyte fuel cells (SPEFCs). In practice, the reactant gases are forced to enter into the electrode pores and exit from them under a gradient pressure by making the inlet and outlet channels dead-ended. As pointed out by Nguyen

[160], the flow through the electrode, in the presence of the interdigitated design, is no more governed by diffusion but becomes convective in nature. This particular design was selected for H_2-air SPE fuel cells in order to avoid the water flooding problem at the cathode and to facilitate the removal of inert nitrogen molecules, which accumulate in the pores of the active layer and consequently produces a diffusion barrier [160]. The forced-flow-through characteristics created by the interdigitated flow fields in SPEFCs have been recently investigated for DMFCs [149]. In general, it has been shown that enhanced mass transfer characteristics are achieved with the interdigitated flow field in DMFCs but these beneficial effects are especially observed only at high current densities corresponding to low values of cell potential. At high cell potentials, i.e. under practical operation conditions (above 0.5 V), a higher efficiency for fuel utilization is obtained with the classical serpentine flow fields due to the lower effect on methanol cross-over. This problem does not affect the cathode, thus an optimised condition may be represented by a serpentine flow field at the anode and an interdigitated flow field at the cathode.

In the fuel cell stacks of significant sizes, graphite bipolar plates are being replaced with the more economic carbon based composite materials or by metallic foams [162, 163]. In the presence of composite materials, the same design of graphite plates may be reproduced whereas the metallic foam conceptually operates under conditions similar to serpentine flow fields where the reactant distribution over the electrocatalyst layer is controlled by diffusion. Alternative designs have been investigated by Scott and co-workers [159]. These authors have analyzed the possibility of using more open structures at the anode (e.g. dots or open channels) to favor the diffusion of methanol. In other cases, the parallel flow channels pattern has been preferred due to an optimal combination of simplicity of design and suitable performance. Graphite or carbon composite based bipolar plates exhibit minimal corrosion. In the case of stainless-steel or metallic alloys based materials, an appropriate evaluation of the chemical and electrochemical stability in the presence of hot methanol/water mixtures is necessary. In some cases surface treatments or special alloys are required to minimize corrosion.

I.4 References

[1] K. Kordesch and G. Simader, Fuel Cells and their Applications, WILEY-VCH, Weinheim, 1996.

[2] J. O'M. Bockris and S. Srinivasan, Fuel Cells: Their Electrochemistry, McGraw- Hill Book Company, New York, 1969.

[3] A. K. Shukla, A. S. Aricò, V. Antonucci, Renewable & Sustainable Energy Reviews, 2000, 4.

[4] B. D. McNicol, D. A. J. Rand, K. R. Williams, J. Power Sources 1999, 83, 15.

[5] S. Wasmus and A. Kuver, J. Electroanal. Chemistry 1999, 461, 14.

[6] A. Hamnett, Catalysis Today 1997, 39, 445.

[7] M. P. Hogarth and G. A. Hards, Platinum Metal Rev. 1996, 40, 150.

[8] R. Parsons, T. Van der Noot, J. Electroanal. Chem. 1988, 257, 9.

[9] L. W. Niedrach and H. I. Zeliger, J. Electrochem. Soc. 1969, 116, 152.

[10] H. Okamoto, G. Kawamura, A. Ishikawa, T. Kudo, J. Electrochem. Soc. 1987, 134, 1645.

[11] C. C. Hays, R. Manoharan, J. B. Goodenough, J. Power Sources 1993, 45, 291.

[12] P.L. Antonucci, A. S. Aricò, E. Modica, V. Antonucci, J. Solid State Electrochemistry 1999, 3, 205 .

[13] M. M. P. Janssen, J. Moolhuysen, Electrochim. Acta 1976, 21, 861.

[14] M. Gotz and H. Wendt, Electrochim. Acta 1998, 43, 3637.

[15] A. S. Aricò, Z. Poltarzewski, H. Kim, A. Morana, N. Giordano and V. Antonucci. J. Power Sources 1995, 55, 159.

[16] K. Lasch, L. Jorissen, J. Garche, Proceedings of the Workshop "Electrocatalysis in Indirect and Direct Methanol PEM Fuel Cells", (Eds C. Lamy and H. Wendt), Sept. 12-14 Portoroz, Slovenia, 1999, p. 104.

[17] H. A Gasteiger, N. Markovic, P. N. Ross, Jr., and E. J. Cairns, J. Electrochem. Soc. 1994, 141, 1795.

[18] D. Pletcher and V. Solis, Electrochim. Acta, 1982, 27, 775.

[19] K. Wang, H. A. Gasteiger, N.M. Markovic and P. N. Ross Jr., Electrochim. Acta, 1996, 41, 2587.

[20] J. B. Goodenough, A. Hamnett, B. J. Kennedy, R. Manoharan and S. Weeks, J. Electroanal. Chem. 1988, 240, 133.

[21] B. Beden, F. Kardigan, C. Lamy, J. M. Leger, J. Electroanal. Chem. 1981, 127, 75.

[22] K. Chandrasekaran, J. C. Wass, and J. O' M. Bockris, J. Electrochem. Soc. 1990, 137, 518.

[23] M. Watanabe and S. Motoo, J. Electroanal. Chem. 1975, 60, 275.

[24] A. S. Aricò, V. Antonucci, V. Alderucci, E. Modica and N. Giordano J. Appl. Electrochem. 1993, 23 , 1107.

[25] G. Méli, J.-M. Léger, C. Lamy and R. Durand, J. Appl. Electrochem. 1993, 23, 197.

[26] A. Aramata, T. Kodera and M. Masuda, J. Appl. Electrochem. 1988, 18, 577.

[27] V. S. Bagotzky and Yu. B. Vassiliev, Electrochim. Acta 1967, 12, 1323.

[28] J. Clavilier, C. Lamy, and J. M. Leger, J. Electroanal. Chem. 1981, 125, 249.

[29] P. A. Christensen, A. Hamnett and G. L. Troughton, J. Electroanal. Chem. 1993, 362, 207.

[30] X. H. Xia, T. Iwasita, F. Ge and W. Vielstich, Electrochim. Acta 1996, 41, 711.

[31] R. A. Lampitt, L. P .L. Carrette, M. P. Hogarth, A. E. Russell, J. Electroanal. Chem. 1999, 460, 80.

[32] W. Vielstich, P. A. Christensen, S. A. Weeks and A. Hamnett, J. Electroanal. Chem. 1988, 242, 327.

[33] E. Ticianelli, J. G. Berry, M. T. Paffet, and S. Gottesfeld, J. Electroanal. Chem. 81, 229, 1977.

[34] T. Frelink, W. Visscher, J.A.R. van Veen, Surface Sci. 1995, 335, 353.

[35] T. Frelink, W. Visscher, J.A.R. van Veen, Langmuir 1996, 12, 3702.

[36] T. Iwasita, H. Hoster, A. John-Anacker, W. F. Lin and W. Vielstich, Langmuir 2000, 16, 522.

[37] Y. Y. Tong, C. Rice, A. Wieckowski and E. Oldfield, J. Am. Chem. Soc. 2000, 122, 1123.

[38] H. A. Gasteiger, N. Markovic, P. N. Ross, E. J. Cairns Jr, J Phys. Chem. 1994, 98, 617.

[39] A. K. Friedrich, K. P. Geyzers, U. Linke, U. Stimming, and J. Stumper J. Electroanal. Chem. 1996, 402, 123.

[40] T. J. Schmidt, M. Noeske, H. A. Gasteiger, R. J. Behm. P. Britz, W. Brijoux and H. Bonnemann, Langmuir 1997, 14, 2591.

[41] H. N. Dinh, X. Ren, F. H. Garzon, P. Zelenay and S. Gottesfeld, J. Electroanal. Chem 2000, 491, 222.

[42] T. J. Schmidt, H. A. Gasteiger and R. J. Behm, Electrochemistry Communications 1998, 1, 1.

[43] Y. Takasu, T. Fujiwara, Y. Murakami, K. Sasaki, M. Oguri, T. Asaki and W. Sugimoto, J. Electrochem. Soc. 2000, 147, 4421.

[44] B. Gurau, R. Viswanathan, R. X. Liu, T. J. Lafrenz, K. L. Ley, E. S. Smotkin E. Reddington, E. A. Sapienza , B.C. Chan, T. E. Mallouk, S. Sarangapani, J. of Phys. Chem. B 1998, 102, 9997.

[45] A. S. Aricò, E. Modica, E. Passalacqua, V. Antonucci and P. L. Antonucci, J. Appl. Electrochem. 1997, 27, 1275.

[46] S. Swathirajan and Y. M. Mikhail, J. Electrochem. Soc. 1991, 138, 1321.

[47] A. Aramata, M. Masuda, T. Kodera, J. Electrochem. Soc. 1989, 136, 3288.

[48] J.-M. Léger, Proceedings of the Workshop "Electrocatalysis in Indirect and Direct Methanol PEM Fuel Cells", (Eds. C. Lamy and H. Wendt), Sept. 12-14 Portoroz, Slovenia 1999, p. 9.

[49] R. Inada, K. Shimazu and H. Kita, J. Electroanal. Chem. 1990, 277, 315.

[50] A. Aramata and M. Masuda, J. Electrochem. Soc. 1991, 138, 1949.

[51] A. K. Shukla, M. K. Ravikumar, A. S. Aricò, V. Antonucci, N. Giordano and A. Hamnett, J. Appl. Electrochem., 1995, 25, 528.

[52] H. Kita, Y. Gao, T. Nakato, H. Hattori, J Electroanal. Chem. 1994, 373, 177.

[53] W. Chrzanowski and A. Wieckowski, Langmuir, 1998, 14, 1967.

[54] H. Kim and A. Wieckowski, Third International Symp. On New Materials for Fuel Cells and Modern Battery Systems, (Ed. O. Savadogo) , Montrèal, Canada, 1999, pp. 125-126

[55] L. Liu, C. Pu, R. Viswanathan, Q. Fan, R. Liu and E.S. Smotkin, Electrochim. Acta 1998, 43, 3657.

[56] X. Ren, M. S. Wilson and S. Gottesfeld, J. Electrochem. Soc. 1996, 143, L12.

[57] A. S. Aricò, A. K. Shukla, K. M. el-Khatib, P. Creti, V. Antonucci, J. Appl. Electrochem., 1999, 29, 671.

[58] A. B. Anderson, E. Grantscharova and S. Seong, J. Electrochem. Soc. 1996, 143 , 2075.

[59] J. Mc Breen and S. Mukerjee, J. Electrochem. Soc. 1995, 142, 3399.

[60] T. Iwasita, F. C. Nart, and W. Vielstich, Ber. Bunsenges Phys. Chem. 1990, 94, 1030 .

[61] M. Shibata, S. Motoo, J. Electroanal. Chem. 1985, 194, 261.

[62] T. E. Madey, H. A. Engelhardt and D. Menzel, Surf. Sci. 1975, 48, 304.

[63] A. S. Aricò, E. Modica, P. Cretì, P. L. Antonucci, and V. Antonucci, J. New Mat. Electrochem. Systems, 2000, 3, 207.

[64] J. B. Goodenough, R. Manoharan, A. K. Shukla, and K. V. Ramesh, Chemistry of Materials, 1989, 1, 391.

[65] D. Chu and S. Gilman, J. Electrochem. Soc. 1996, 143, 1685.
[66] T. Iwasita, H. Hoster, A. John-Anacker, W. F. Lin, and W. Vielstich, Langmuir 2000, 16, 522.
[67] B. D. McNicol and R.T. Short, J. Electroanal. Chem. 1977, 81, 249.
[68] A. S. Aricò, V. Baglio, P. Cretì and V. Antonucci, 2000 Fuel Cell Seminar Abstracts, October 30-November 2, 2000, Portland, Oregon, pp. 75-78
[69] K.Y Chen, Z. Sun, A. C. C. Tseung, Electrochem. Solid State Lett. 2000, 3, 10.
[70] A. S. Aricò, V. Antonucci, N. Giordano, A. K. Shukla, M. K. Ravikumar, A. Roy, S. R. Barman, D. D. Sarma, J. Power Sources 1994, 50, 295.
[71] S. A. Campbell, R. Parsons, J. Chem. Soc. Faraday Trans. 1992, 88, 833.
[72] A. N. Haner, P. N. Ross, J. Phys. Chem. 1991, 95, 3740.
[73] M. Watanabe, Y. Furuuchi, S. Motoo, J. Electroanal. Chem. 1985, 191, 367.
[74] T. Frelink, W. Visscher, J. A. R. van Veen, Electrochim. Acta 1994, 39, 1871.
[75] B. Bittins-Cattaneo, T. Iwasita, J. Electroanal. Chem. 1987, 238, 151.
[76] A. K. Shukla, A. S. Aricò, K. M. el-Khatib, H. Kim, P. L. Antonucci, V. Antonucci, Appl. Surf. Sci. 1999, 137, 20.
[77] S. Mukerjee, J. McBreen, Proc. 2nd International Symp. on New Materials for Fuel Cells and Modern Battery Systems, (Eds. O. Savadogo and P. R. Roberge) Montréal, Canada, 1977, pp.548-559.
[78] R. Ianniello, V. M. Schmidt, U. Stimming, J. Stumper and A. Wallau, Electrochim. Acta 1994, 39, 1863.
[79] F. A. Cotton, G. Wilkinson, Advanced Inorganic Chemistry, Wiley-Interscience, New York, 1980.
[80] N. Markovic', A. Widelov, P. N. Ross, O. R. Monteiro, I. G. Brown, Catal. Lett. 1997, 43, 161.
[81] A. S. Aricò, P. Creti, H. Kim, R. Mantegna, N. Giordano and V. Antonucci, J. Electrochem. Soc. 1996, 143, 3950.
[82] D. R. Rolison, P. L. Hagans, K. E. Swider and J. W. Long, Langmuir, 1999, 15, 774.
[83] A. N. Buckley and B. J. Kennedy, J. Electroanal. Chem. 1991, 302, 261.
[84] A. S. Aricò, G. Monforte, E. Modica, P. L. Antonucci and V. Antonucci, Electrochemistry Communications 2000, 2, 466.
[85] A. Hamnett, B. J. Kennedy, and F. E. Wagner, J. Catal. 1990, 124, 30.
[86] A. S. Aricò, P. Cretì, E. Modica, G. Monforte, V. Baglio and V. Antonucci Electrochim. Acta 2000, 45, 4319.

[87] C. Lamy and J-M. Léger, Proc. Second International Symp. On New Materials for Fuel Cells and Modern Battery Systems, (Eds. O. Savadogo and P. R. Roberge), Montrèal, Canada, 1997, pp.477-487.

[88] P. Shen, K. Chen, and A. C.C. Tseung, J. Chem. Soc. Faraday Trans. 1994, 90, 3089.

[89] A. S. Aricò, H. Kim, A. K. Shukla, M. K. Ravikumar, V. Antonucci and N. Giordano, Electrochim. Acta, 1994, 39, 691.

[90] A. R. J. Kucernak, C. J. Barnett, G. T. Burstein and K. R. Williams, in Proceedings of the first international symposium on new materials for fuel cell systems; (Eds. O. Savadogo, P. R. Roberge, T. N. Veziroglu), July 9-13, Montreal Quebec, Canada, 1995.

[91] N. Giordano, S. Hocevar, P. Staiti and A. S. Aricò, Electrochim. Acta, 1996, 41, 397.

[92] M. A. Schwegler, P. Vinke, M. va der Eijk and H. Bekkum, Appl. Catal. A, 1992, 80, 41.

[93] A. Essalik, O. Savadogo, F. Ajersch, J. Electrochem. Soc. 1995, 142, 1368.

[94] H. Okamoto, G. Kawamura, A. Ishikawa, T. Kudo, J. Electrochem. Soc. 1987, 134, 1645.

[95] M. Boudart and G. G. Djega Mariadassou, Kinetics of Heterogeneous Catalytic Reactions, Princeton University Press, 1984.

[96] M. S. Antelman, The encyclopedia of the chemical electrode potentials, Plenum, NewYork 1982.

[97] A. C. C. Tseung, P. K. Shen, K. Y. Chen, J. Power Sources 1996, 61, 223.

[98] P. K. Shen and A.C.C. Tseung, 183st Meeting of the Electrochemical Society. Extended Abstract N° 1778, p. 2426, Honolulu, Hawaii, May 16-21-1993.

[99] N. Giordano, E. Passalacqua, L. Pino, A. S. Aricò, V. Antonucci, M. Vivaldi and K. Kinoshita, Electrochimica Acta 1991, 36, 1979.

[100] J. A. Poirier, The Electrochemical Society Interface, Winter 1994, p. 49.

[101] M. Watanabe S. Saegusa, and P. Stonehart, J. Electroanal. Chem. 1989, 271, 213.

[102] X. Ren, P. Zelenay, S. Thomas, J. Davey, and S. Gottesfeld, J. Power Sources 2000, 86, 111.

[103] P. S. Kaurenan and E. Skou, J. Electroanal. Chem. 1996, 408, 189.

[104] M. K. Ravikumar and A. K. Shukla, J. Electrochem. Soc. 1996, 143, 2601.

[105] J. B. Goodenough, A. Hamnett, B. J. Kennedy, S. A. Weeks, Electrochim. Acta 1987, 32 1233.

[106] V. Jalan, Extended Abstracts, Electrochemical Society, Los Angeles, CA, Fall Meeting, Abstract 192 (October 1979).

[107] H. Bonnemann, R. Brinkmann, W. Brijoux, E. Dinjus, T. Joussen, B. Korall, Angew. Chem. 1991, 103, 1344.

[108] H. G. Petrow and R. J. Allen, U.S. Pat. 3, 992, 331, 1976.

[109] K. Machida, A. Fukuoka, M. Ichikawa and M. Enyo, J. Electrochem. Soc., 1991, 138, 1958.

[110] C. K. Witham, W. Chun, T. I. Valdez and S. R. Narayanan, Electrochem. Solid-State Lett. 2000, 3, 497.

[111] S. Mukerjee, S. Srinivasan, J. Electroanal. Chem. 1993, 357, 201.

[112] T. R. Ralph, G. A. Hards, S. D. Flint, J. M. Gascoyane, Fuel Cell Seminar Abstracts, p. 536, Palm Springs, CA, Nov. 16-19, 1998.

[113] M. T. Paffet, G. J. Beery, S. Gottesfeld, J. Electrochem. Soc. 1998, 135, 1431.

[114] M. Watanabe, K. Tsurumi, T. Mizukami, T. Nakamura, P. Stonehart, J. Electrochem. Soc. 1994, 141, 2659.

[115] A. Freund, J. Lang, T. Lehman, K. A. Starz, Cat. Today 1996, 27, 279.

[116] V. Jalan, E. J. Taylor, J. Electrochem. Soc. 1983, 130, 2299.

[117] S. Gottesfeld, M. T. Paffett, A. Redondo, J. Electroanal. Chem. 1986, 205, 163.

[118] B. C. Beard, P. N. Ross, J. Electrochem. Soc. 1970, 137, 3368.

[119] K. T. Kim, J. T. Whang, Y. G. Kim, J. S. Chung, J. Electrochem. Soc. 1993, 140, 31.

[120] S. Mukerjee, S. Srinivasan, M. P. Soriaga, J. McBreen, J. Electrochem. Soc. 1995, 142, 1409.

[121] M. Neergat, A. K. Shukla, K. S. Gandhi, J. Appl. Electrochem. 2001, 31, In press.

[122] Y. Takasu, T. Iwazaki, W. Sugimoto and Y. Murakami, Electrochemistry Communications 2000, 2, 671.

[123] A. S. Aricò, A. K. Shukla, H. Kim, S. Park, M. Min and V. Antonucci, Appl. Surf. Sci. 2001, 172, 33.

[124] R. Jasinski, J. Electrochem. Soc. 1965, 112, 526.

[125] R. Franke, D. Ohms, K. Wiesener, J. Electroanal. Chem., 1989, 260, 63.

[126] G. Faubert, G. Lalande, R. Coté, D. Guay, J. P. Dodelet, L. T. Weng, P. Bertrand, G. Dénés, Electrochim. Acta , 1996, 41, 1689.

[127] G. R. Sun, J. T. Wang, R. F. Savinell, J. Appl. Electrochem. 1998, 28, 1087.

[128] A. Elzing, A. Van der Putten, W. Visscher and E. Barendrecht, J. Electroanal. Chem. 1987, 233, 113.

[129] N. Alonso-Vante, H. Tributsch, Nature (London) 1986, 323, 431.

[130] R. W. Reeve, P. A. Christensen, A. Hamnett, S. A. Haydock, S. C. Roy, J. Electrochem. Soc. 1998, 145, 3463.

[131] T. J. Schmidt, U. A. Paulus, H. A. Gasteiger, N. Alonso-Vante, R. J. Behm, J. Electrochem. Soc. 2000, 147, 2620.

[132] S. Cleghorn, X. Ren, S. Thomas and S. Gottesfeld, Book of Extended Abstracts, 1997 ISE-ECS Joint Symposium, Paris, Sept. 1997, Abstract n. 182, p. 218-219.

[133] B. Bauer, D. J. Jones, J. Roziere, L. Tchicaya, G. Alberti, M. Casciola, l. Massinelli, A. Peraio, S. Besse and E. Ramunni, J. New Materials for Electrochemical Systems 2000, 3, 93.

[134] E. Peled, T. Duvdevani, A. Aharon and A. Melman, Electrochem. Solid-State Lett., 2000, 3, 525.

[135] S. Hietala, M. Koel, E. Skou, M. Elomaa, F. Sundholm, J. Mater. Chem. 1998, 8, 1127.

[136] A. S. Aricò, P. L. Antonucci, N. Giordano and V. Antonucci. Material Letters 1995, 24, 399.

[137] J. Wang, S. Wasmus, and R. F. Savinell, J. Electrochem. Soc. 1995, 142, 4218.

[138] D. A. Boysen, C. R. I. Chisholm, S. M. Haile, and S. R. Narayanan, J. Electrochem. Soc. 2000, 147, 3610.

[139] A. S. Aricò, P. Creti, P. L. Antonucci and V. Antonucci, Electrochem. Solid-State Lett. 1998, 1, 66.

[140] C. Yang, S. Srinivasan, A. S. Aricò, P. Cretì, V. Baglio and V. Antonucci, Electrochemical and Solid-State Letters 2001, 4, A31.

[141] S. Srinivasan, R. Mosdale, P. Stevens, and C. Yang, Annu. Rev. Energy Environ. 1999, 24, 281.

[142] A. S. Aricò, P. Creti, N. Giordano, V. Antonucci, P.L. Antonucci and A. Chuvilin, J. Appl. Electrochem. 1996, 26, 959.

[143] M. S. Wilson and S. Gottesfeld, J. Appl. Electrochem., 1992, 22, 1.

[144]. A. K. Shukla, P. Stevens, A. Hamnett, and J. B. Goodenough, J. Appl. Electrochem 1989, 19, 383.

[145] M. Uchida, Y. Aoyama, N. Eda, and A. Ohta, J. Electrochem. Soc., 1995, 142, 463.

[146] A. S. Aricò, P. Creti, P. L. Antonucci, J. Cho, H. Kim and V. Antonucci, Electrochim. Acta, 1998, 43, 3719.

[147] A. Fisher, J. Jindra and H. Wendt, J. Appl. Electrochem. 1998, 28, 277.

[148] S. Gamburzev, C. Boyer, and A. J. Appleby, in Proton Conducting Membrane Fuel Cells II -Second International Symposium, (Eds. S. Gottesfeld, T. F. Fuller), Proceedings Volume 98-27, pp. 23-29, Electrochemical Society, Pennington, New Jersey, 1999.

[149] A. S. Aricò, P. Cretì, V. Baglio, E. Modica and V. Antonucci, J. Power Sources 2000, 91, 202.
[150] R. M. Moore, S. Gottesfeld and P. Zelenay in Proton Conducting Membrane Fuel Cells - Second International Symposium, (Eds. S. Gottesfeld, T. F. Fuller), Proceedings Volume 98-27, pp. 365-379, Electrochemical Society, Pennington, New Jersey, 1999.
[151] S. R. Narayanan, W. Chun, T. I. Valdez, B. Jeffries-Nakamura, H. Frank, S. Surampudi, G. Halpert, J. Kosek, C. Cropley, A. B. LaConti, M. Smart, Q. Wang, G. Surya Prakash and G.A. Olah, Program and Abstracts, Fuel Cell Seminar 1996 pp. 525 - 528.
[152] M. Baldauf and W. Preidel, J. Power Sources 1999, 84, 161.
[153] A. K. Shukla, P. A. Christensen, A. Hamnett and M. P. Hogarth, J. Power Sources 1995, 55, 87.
[154] K. Scott, W. M. Taama, P. Argyropoulos, K. Sundmacher, J. Power Sources, 1999, 83, 204.
[155] D. H. Jung, C. H. Lee, C. S. Kim, and D. R. Shin, J. Power Sources, 1998, 71, 169.
[156] M. K. Ravikumar and A. K. Shukla, J. Electrochem. Soc., 1996, 143, 2601.
[157] X. Ren, T. E. Sringer and S. Gottesfeld in Proton Conducting Membrane Fuel Cells - Second International Symposium, (Eds. S. Gottesfeld, T. F. Fuller), Proceedings Volume 98-27, pp. 341-357, Electrochemical Society, Pennington, New Jersey, 1999.
[158] H. Dohle, J. Divisek, J. Mergel, H. F. Oetjen, C. Zingler, D. Stolten, Fuel Cell Seminar Abstracts, October 30-November 2, 2000, Portland, Oregon, pp. 126-129.
[159] K. Scott, W. M. Taama, and P. Argyropoulos J. Applied Electrochem. 1998, 28, 1389.
[160] T. V. Nguyen, J. Electrochem. Soc. 1996, 143, L103.
[161] M. S. Wilson, T. E. Sringer, J. R. Davey and S. Gottesfeld, in Proton Conducting Membrane Fuel Cells I, PV 95-23, (Eds. S. Gottesfeld, G. Halpert and A. Langrebe). The Electrochemical Society Proceedings Series, Pennington, NJ, 1995 p.115.
[162] D. N. Busick and M. Wilson in Proton Conducting Membrane Fuel Cells - Second International Symposium, (Eds. S. Gottesfeld, T. F. Fuller), Proceedings Volume 98-27, pp. 435-445, Electrochemical Society, Pennington, New Jersey, 1999.
[163] C. Zawodzinski, M. S. Wilson and S. Gottesfeld, in Proton Conducting Membrane Fuel Cells - Second International Symposium, (Eds. S. Gottesfeld, T. F. Fuller), Proceedings Volume 98-27, pp. 446-456, Electrochemical Society, Pennington, New Jersey, 1999.

CHAPTER II

CATALYSTS DEVELOPMENT AND CHARACTERIZATION

II.1 Effect of Pt-Ru alloy composition on high-temperature methanol electro-oxidation*

II.1.1 Introduction

Carbon supported and unsupported Pt-Ru alloys are currently being used as electro-catalysts for methanol oxidation in direct methanol fuel cells (DMFCs) [1-16]. A significant number of studies have been carried out to find appropriate synthesis procedures for production of these catalysts with suitable dispersions [17-21] and various investigations have been addressed to understand the properties of such systems, as well as their promoting effect towards methanol electro-oxidation [23-31]. In general, the preparation of Pt-Ru electro-catalysts with high surface area (80-140 m^2 g^{-1}) is not difficult, especially on carbon-supports [17-22]. In the literature [29-32], both the bulk and surface chemistry of these materials has been extensively investigated. Most of the electro-catalysts form solid solutions of platinum and ruthenium with face-centered-cubic structure but some of these contain bulk and surface Ru oxides [16,31]. So far as the synergistic promotion mechanism is concerned, it is widely accepted that Ru atoms promote the formation of labile bonded oxygenated species in proximity of methanolic residues adsorbed on Pt sites, facilitating them to be oxidised as carbon dioxide [25]. Moreover, the effect of modification in Pt electronic environment, induced by Ru through increase in Pt d-band vacancies, has been emphasied [32]. Accordingly, Pt-Ru interaction should alter the strength of the Pt-CO bond involved in the oxidation mechanism [33].

Various studies have shown a "volcano-shape" relationship between the methanol electro-oxidation rate at low temperatures (< 80 °C) and Ru atomic fraction in the alloy. However,

* A paper based on this study has been published on **Electrochimica Acta 47 (2002) 3723-3732**

there is no conclusive evidence in the literature on the optimal Ru composition which maximises the oxidation rate at temperatures higher than 100 °C. Watanabe *et al*. [19] have shown that the highest rate for methanol oxidation in sulphuric acid at 40-60°C is achieved in the presence of 50% Ru atomic fraction on high surface-area carbon-supported Pt-Ru electro-catalysts and on Ru ad-atoms covered Pt electrodes with 50% surface coverage. Accordingly, they assumed that the surface composition of carbon supported Pt-Ru catalysts was similar to that of electrodes with deposited Ru ad-atoms. A 1:1 Pt/Ru atomic ratio was identified by Goodenough and co-workers [34] as the most appropriate bulk composition for methanol oxidation on Pt-Ru/C electro-catalysts obtained by impregnation. More recently, Gasteiger *et al.* [26] made a systematic investigation of methanol oxidation on well characterised Pt-Ru alloy surfaces. They observed that the maximum in the electro-catalytic activity for CH_3OH oxidation in H_2SO_4 shifted from 10 to 33 at. % Ru surface content as the temperature was increased from 25 to 60-80°C. This would suggest that the operation temperature influences the optimal Pt-Ru composition for methanol oxidation. Differently, Chu and Gilman [35] found a maximum in activity for Pt:Ru 50:50 in the bulk, between 25 and 60°C in the presence of sulphuric acid. Frelink *et al.* [28] investigated the surface of their electrodeposited Pt-Ru electrodes by an electro-chemical crystal microbalance technique. They found an optimal Ru surface composition of 15% for methanol oxidation at room temperature. A broad maximum in activity at room temperature in $HClO_4$ electrolyte was found between 10% and 40% surface Ru content for smooth Pt-Ru alloys by Iwasita and co-workers [36]. An investigation of methanol oxidation in phosphoric acid at 180 °C showed a better performance for Pt-Ru (1:1) vs. Pt-Ru (5:2) catalyst [22]. A surface enrichment has been reported by McNicol and Short for carbon-supported Pt-Ru alloys [37]; this points out the need of a careful catalyst characterisation in terms of both surface and bulk compositions. From the analysis of the data available in the literature, it appears that the optimal Ru content for CH_3OH oxidation depends, besides operation temperature, on the preparation of the Pt-Ru catalysts and on the electrolyte.

High Pt-loadings (1-2 mg cm^{-2}) are currently necessary for the methanol electro-oxidation reaction to proceed at acceptable rates [3-16]. There are various limitations in the use of catalyst layers of large thickness in fuel cells; they reduce the electro-catalyst utilisation [4] and cause an increase in ohmic and mass-transport polarizations; these aspects have prompted studies on unsupported high surface area Pt-Ru electro-catalysts [4, 6,16,31]. Systematic investigations of methanol electrooxidation on well characterized Pt-Ru catalysts have been mainly carried out at low temperature [26,28,35-36]. The increasing use of thermally-stable

polymeric proton conducting electrolytes with non-volatile solvents [12], as well as composite membranes [15], capable of retaining water even under low-humidity conditions**,** has given new emphasis to the studies dealing with methanol electro-oxidation at high temperature. Thus, it is of interest to investigate catalytic activity under these conditions and to relate it with bulk and surface properties of the materials. In this study, both mass and specific activity of unsupported Pt-Ru alloys of varying compositions have been investigated for methanol electro-oxidation at 130°C and in the presence of a perfluoro-sulfonic polymer electrolyte.

II.1.2 Experimental

Unsupported Pt-Ru electrocatalysts of various compositions were synthesized in-house by using an identical colloidal procedure based on the "Prototech method" developed by Petrow and Allen [17]. Sulfite complexes of Pt or Pt and Ru, in appropriate amounts, were decomposed by hydrogen peroxide to form aqueous colloidal solutions of Pt and Ru oxides. The colloidal Pt and Pt-Ru particles were precipitated from the solution at pH ≈5. The resulting amorphous oxides were reduced in a hydrogen stream at 100°C. In a similar manner colloidal Pt particles were adsorbed on a carbon black to form a 90 % Pt/Vulcan XC 72 catalyst which was employed for cathode fabrication.

Powder X-ray diffraction (XRD) patterns for these catalysts were obtained on a Philips X-Pert X-ray Diffractometer using CuK_{α}-source operating at 40 kV and 30 mA. The peak profiles of (111), (200) and (220) reflections of the face-centered-cubic (fcc) structure, in the XRD patterns of the respective catalysts, were obtained by the Marquardt algorithm [14]. Instrumental broadening was determined by using a standard platinum sample. Energy Dispersive Analyses by X-rays (EDAX) of the catalysts were carried out on a Philips XL-20 Scanning Electron Microscope equipped with LaB_6-filament and operating at an acceleration voltage of 20 kV.

X-ray photoelectron spectroscopy (XPS) measurements were performed by using a VSW Scientific Instruments (Manchester, England) spectrometer; X-ray source was Al Kα at a power of 150 W. Spectra were obtained with pass energy of 90 eV for wide scans and 44 eV per individual elements. The pressure in the analysis chamber of the spectrometer was $5 \cdot 10^{-10}$ mbar (Ti sublimation pump) and $5 \cdot 10^{-9}$ mbar during the measurements. The samples were introduced into the spectrometer using a separate differentially pumped fast entry chamber, then into the desorption chamber in ultrahigh vacuum for desorption of high volatile species adsorbed on carbon support, and finally into the analyzer chamber. The Pt $4f_{7/2}$ and $4f_{5/2}$ peaks

of a Pt foil were taken, after argon sputtering, for calibration of the binding energy (B.E.) scale. The background correction was performed by the Shirley method and curve fitting by Gauss-Lorentz routines. The quantitative evaluation of each peak was obtained by dividing the integrated peak area by atomic sensitivity factors which were calculated from the ionization cross-sections, the mean free electron escape depth and the measured transmission functions of the spectrometer.

The electrodes were prepared according to the procedure described in Ref. [16]; they consisted of carbon cloth, diffusion and catalytic layers. Nafion® ionomer content in the catalytic layer was 15% wt. The Pt loading in each electrode was 2 mg cm^{-2}. Unsupported Pt and Pt-Ru catalysts were employed at the anode, whereas carbon supported 90% Pt/Vulcan-XC was utilized for cathode fabrication. Membrane-electrode assemblies (MEAs) were formed by a hot-pressing procedure [16] and subsequently installed in a fuel cell test fixture of 5 cm^2 active area. The cell fixture (Globe Tech Inc., College Station, TX) was equipped with serpentine graphite flow fields having machined reference electrode ports [6]. The dynamic hydrogen reference electrode system consisted of two small Pt/C electrodes placed on the opposite sides of the Nafion membrane and distant about 1 mm from the working electrodes; a small current was applied by a galvanostat (AMEL model 549) to allow the hydrogen evolution on the reference electrode located on the anodic side. The single cell test fixture was connected to a test station including an HP6060B electronic load. The cell temperature was measured by a thermocouple embedded in the anodic graphite plate, close to the MEA. Preheated aqueous methanol was fed to the anode chamber of DMFC through a peristaltic pump; humidified oxygen pre-heated at 100°C was circulated through the cathode chamber. Pressure in the anode and cathode compartments were 2.5 and 3 atm, respectively. Reactant flow rates were 2 ml min^{-1} and 500 ml min^{-1} for the methanol/water mixture and oxygen stream, respectively. Single cell and anode performances were investigated by steady-state galvanostatic measurements.

II.1.3 Results and Discussion

3.1 Physico-chemical analysis

The XRD patterns for Pt-Ru and Pt catalysts are shown in Fig. 1. All catalysts exhibit the diffraction peaks of the face centered cubic structure (fcc). A distinct shift to higher Bragg angles and an increase of peak broadening were observed as the nominal content of Ru in the samples was increased (Fig. 1), indicating a decrease of both lattice parameter and mean

particle size (Table 1). No distinct presence of elemental Ru, RuO_2 or amorphous phases is observed; this denotes a high degree of alloying. The structural changes occurring in one exemplary catalyst during the preparation were monitored. A comparison between the XRD patterns for completely amorphous, partially reduced and completely alloyed unsupported Pt-Ru catalyst (sample 3 in Table 1) is shown in Fig. 2.

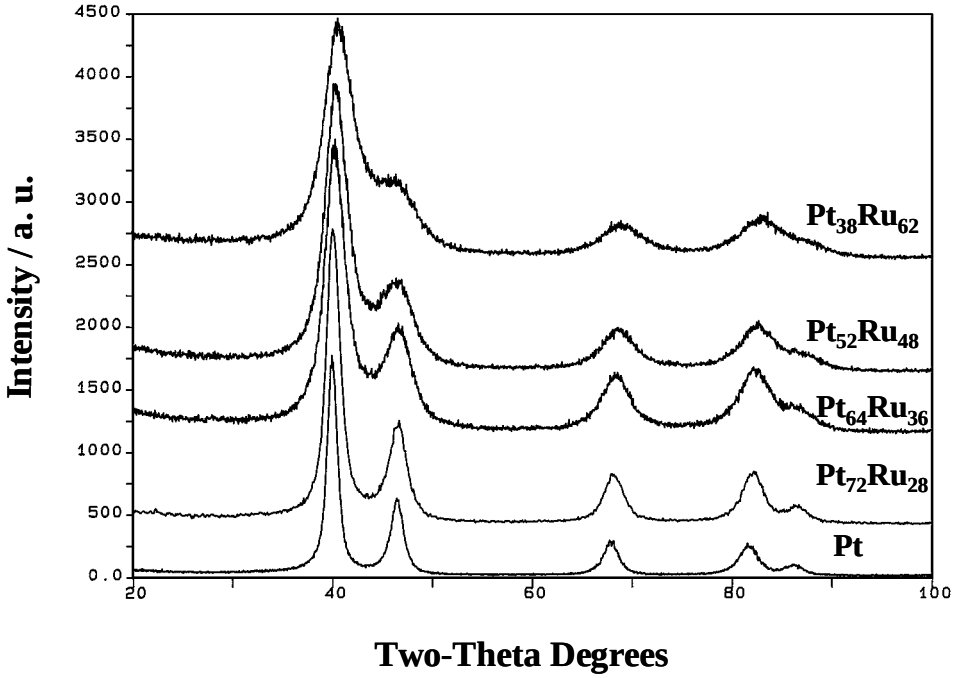

Fig. 1. X-ray diffraction patterns of unsupported Pt and Pt-Ru catalysts. The reported compositions were determined from the lattice parameters.

Sample	Nominal Composition At. %	XRD-derived Composition At. % (± 2%)	EDAX-derived Composition At. % (± 4%)	Lattice Parameter Å (± 0.002Å)	Mean particle size Å (± 2 Å)	XRD-derived Density g cm^{-3}	Metal Surface Area m^2 g^{-1}	Dispersion %	<111>/<200>
1	Pt	Pt	Pt	3.923	51	21.46	55	21	2.36
2	$Pt_{75}Ru_{25}$	$Pt_{72}Ru_{28}$	$Pt_{79}Ru_{21}$	3.891	41	19	77	27	2.37
3	$Pt_{65}Ru_{35}$	$Pt_{64}Ru_{36}$	$Pt_{68}Ru_{32}$	3.881	28	18.19	116	39	2.17
4	$Pt_{50}Ru_{50}$	$Pt_{52}Ru_{48}$	$Pt_{54}Ru_{46}$	3.866	26	17.22	134	42	2.5
5	$Pt_{40}Ru_{60}$	$Pt_{38}Ru_{62}$	$Pt_{41}Ru_{59}$	3.848	21	15.91	184	54	2.7

Table 1. Bulk composition and physico-chemical properties of unsupported Pt-Ru catalysts

The unreduced material shows the amorphous scattering of disordered Pt and Ru oxide phases [16,38]. The amorphous components decrease in intensity upon reduction and disappear in the completely alloyed materials. Interestingly, the position of diffraction peaks does not change significantly from the first reduction step up to the end of the reduction process. Accordingly, the first alloy particles formed during this process have the same bulk composition of completely reduced samples. This reveals a high degree of homogeneity for the alloy, which is probably due to the presence of an intimate mixture of Pt-Ru (atomic mixing) in the amorphous oxide precursor. The lattice parameter for the fcc structure (a_{fcc}) varied between 3.923 to 3.848 Å, in accordance with the Vergard's law, as the nominal Ru content was increased from 0 to about 60 % (Table 1). Catalysts having Ru nominal contents larger than 65% have been discarded because of the presence of Ru hexagonal phase.

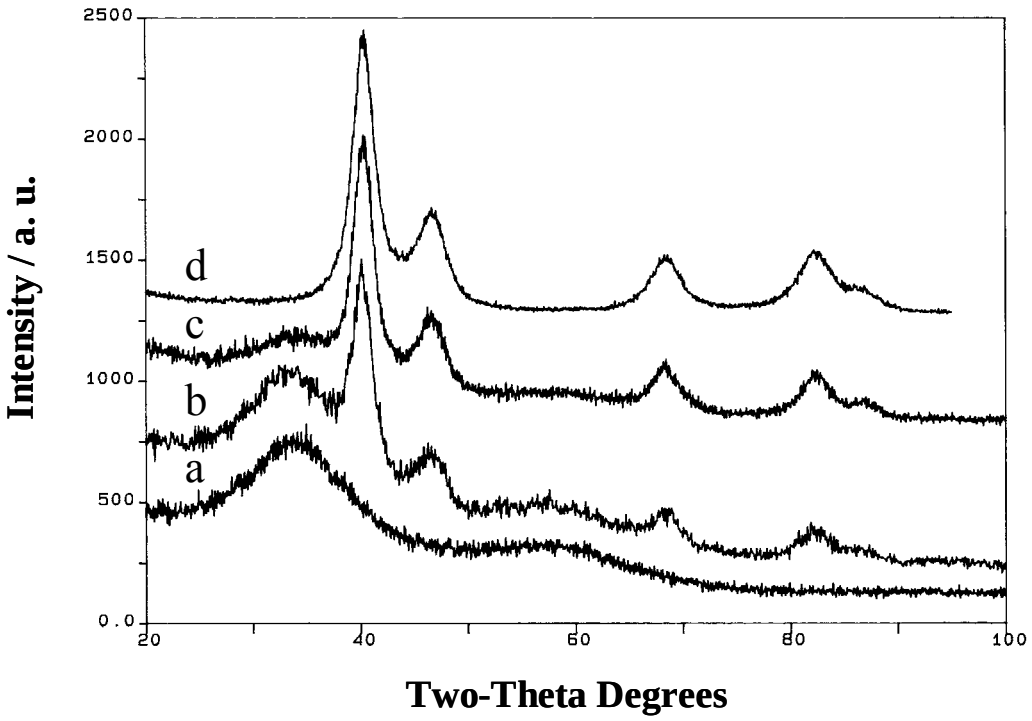

Fig. 2. X-ray diffraction pattern of an amorphous Pt-Ru oxide catalyst precursor (a), and Pt-Ru samples subjected to reduction treatments for different periods: (b) 10 min; (c) 20 min; (d) 60 min. Nominal composition: Pt_{65}-Ru_{35}.

Linear relationships between lattice parameter and bulk composition for Pt-Ru alloys were previously determined by Watanabe *et al.* [19] and Gasteiger *et al.* [39]; these relationships have been used to derive the XRD bulk composition for our catalysts. Atomic compositions of completely alloyed Pt-Ru catalysts are reported in Table 1 together with relative contents of (111) and (200) reflections. The latters were obtained by integration of the respective areas

after peak deconvolution by using the Marquardt algorithm [31]. It should be pointed out that the results of (111) and (200) peaks' deconvolution are affected by high level of uncertainty when a strong overlap of these reflections occurs, as in the case of the Ru-rich sample (sample 5 in Table 1). The ratio between (111) and (200) areas does not change significantly in these samples, within the error of the determination, indicating the absence of any preferential orientation. The average size of the Pt-Ru particles in all catalysts was estimated from the broadening of 220 reflection [14,30]. The particle sizes were found to vary between 21 and 51 Å as the Ru content (XRD) decreases from 62 to 0 %. The 90% Pt/C catalyst employed in the fabrication of the cathode showed an average particle size of 37 Å [40].

EDAX spectra of reduced catalysts (not shown) denoted the presence of Pt and Ru, only; by contrast, the unreduced samples evidenced the presence of oxygen too. The Pt/Ru atomic ratios determined by EDAX analysis were slightly higher than those derived from XRD data (Table 1); such deviations are attributed to both deconvolution of EDAX spectra and particle size effects [41] in XRD patterns.

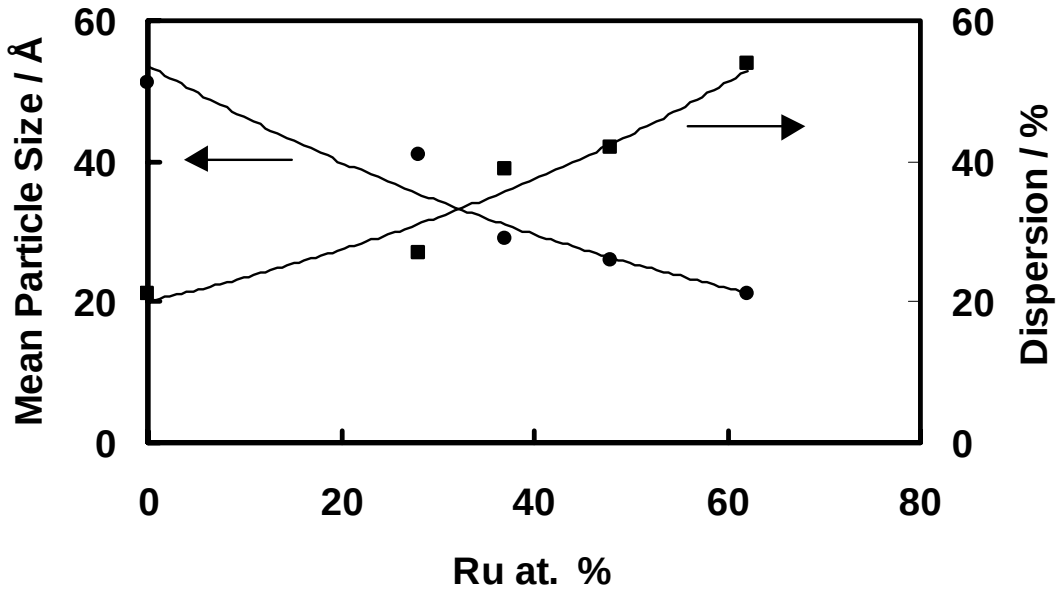

Fig. 3. Variation of the dispersion and mean particle size in the Pt-Ru samples as a function of XRD-determined composition.

XRD results show that the catalyst particle size significantly decreases as the Ru content increases. Since an identical preparation procedure was used for each catalyst composition, the above evidence reflects an increase of the activation energy for the reduction of the amorphous oxides mixture induced by Ru [42]. In fact Ru, being less noble than Pt

absorbs much of the heat produced in the Pt exothermic reduction reaction and undergoes a change from oxidized to metallic state; this effect hinders the growth of Pt particles. Information on the relative surface/bulk distribution of Pt and Ru atoms in the various alloys was obtained by the following formula [43]:

$$D=Ns/Nt=11/d; \quad (1)$$

where D is the dispersion, Ns is the number of atoms on the surface of the particle, Nt the total number of atoms in the particle and d (Å) is the mean particle size. It is observed that dispersions around 40-50% are achieved for atomic Ru contents above 35 % (Fig. 3).

The metal surface area (MSA / $m^2\ g^{-1}$) was obtained from the XRD mean particle size:

$$MSA= 6\ 10^4 / (\rho \cdot d) \quad (3)$$

where ρ (g cm^{-3}) is the density of Pt-Ru alloy and d (Å) is the average particle size. The ρ values for each composition are derived from XRD data as follows:

$$\rho=\text{Unit cell weight/ Unit cell volume} = 4\cdot 10^{24}\cdot((X_{Pt}\cdot FW_{Pt})+(X_{Ru}\cdot FW_{Ru}))/((a_{fcc})^3 \cdot N_A)) \quad (4)$$

where X_{Pt} and X_{Ru} are the atomic fractions of Pt and Ru, FW_{Pt} and FW_{Ru} are the formula weights (g $mol.^{-1}$) of Pt and Ru, a_{fcc} (Å) is the lattice parameter, N_A (mol^{-1}) is the Avogadro number. The values of metal surface area and alloy density have been reported in Fig. 4 for the various catalyst compositions. The alloy density decreases linearly as the Ru atomic content increases. This effect is due to a larger contribution of the decrease in average formula weight with respect to lattice contraction; accordingly, the surface area of a Ru-rich Pt-Ru catalyst is significantly larger with respect to a pure Pt catalyst with the same mean particle size. Thus, the catalyst surface area increases almost exponentially with increase in its Ru content (Fig. 4) as a result of two effects: (i) decrease of alloy density, and (ii) decrease of the mean particle size.

An XPS analysis was carried out on the unsupported Pt-Ru catalysts to obtain information on surface composition and oxidation states of Pt and Ru. As an example, the Pt 4f XP spectrum of sample 4 in Table 1 is reported in Fig. 5. The Pt 4f signal in all samples derives from the contribution of three doublets. The Pt $4f_{7/2}$ line occurs at B.E. of 71.3 ± 0.3 eV, 72.6 ± 0.3 eV and 74.1 ± 0.3 eV, attributable to Pt°, Pt(2^+), and Pt(4^+) species, respectively [14]. The relative concentration of Pt° species in all the samples is larger than 75%. Only small differences are observed in terms of B.E. and relative concentration of valence states among the unsupported Pt and Pt-Ru samples, suggesting that no strong modification of the electronic environment of Pt surface sites is occurring as a consequence of Ru alloying.

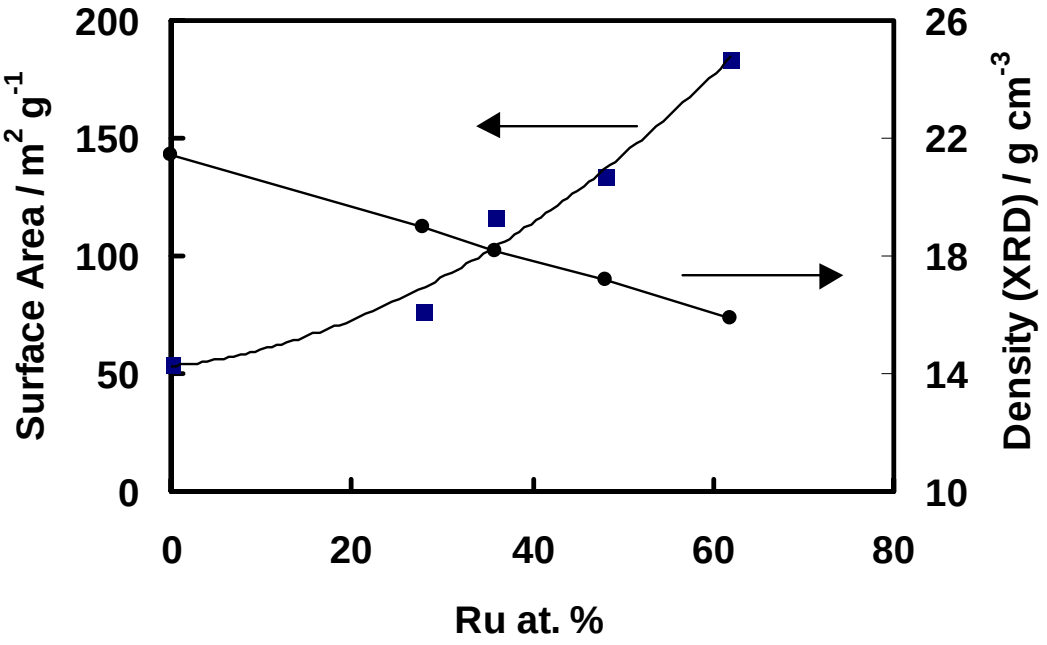

Fig. 4. Variation of the XRD-determined metal surface area and alloy density in the Pt-Ru samples versus XRD-determined composition.

The Ru surface species were investigated by analyzing the Ru $3p_{3/2}$ line in order to avoid the interference of C1s signal from adventitious carbon on the more intense Ru 3d line.

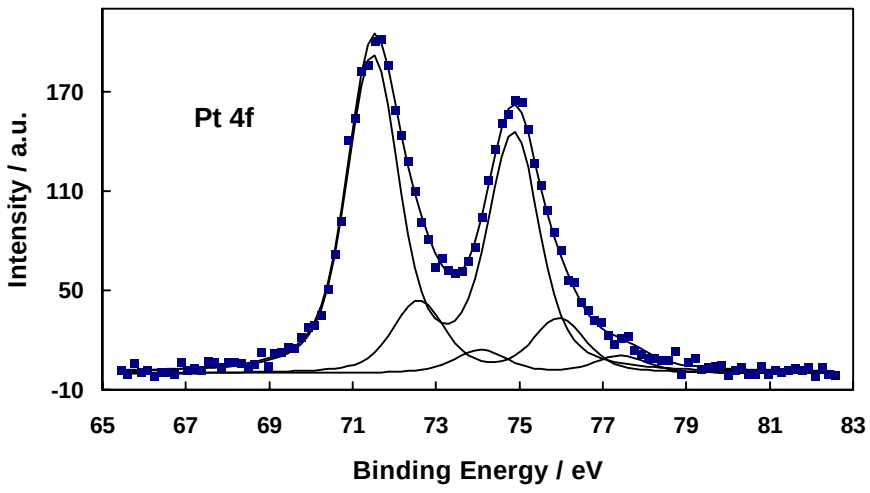

Fig. 5. Pt 4f X-ray photoelectron spectrum of the unsupported Pt_{50}-Ru_{50} catalyst.

These spectra are shown in Fig. 6 for three unsupported Pt-Ru catalysts. In all cases the main peak is observed at 461.7 ± 0.2 eV which is very close to metallic Ru [31]. A slight shoulder at higher B.E. is observed at about 464 eV that is indicative of Ru(4^+) species [31], but its contribution is around 20%. The relative content of surface Ru sites and their B.E. as a function of bulk Ru content are reported in Fig. 7.

A Pt surface enrichment is observed for the samples with low Ru content in the bulk and with large particle size, whereas no significant enrichment in one of the two elements is observed for the samples with high Ru content in the bulk and high degree of dispersion (compare Table 1 and 2). This effect may be attributed to a highly exothermic reduction process for the samples with low Ru content, producing both particle sintering and Pt surface enrichment.

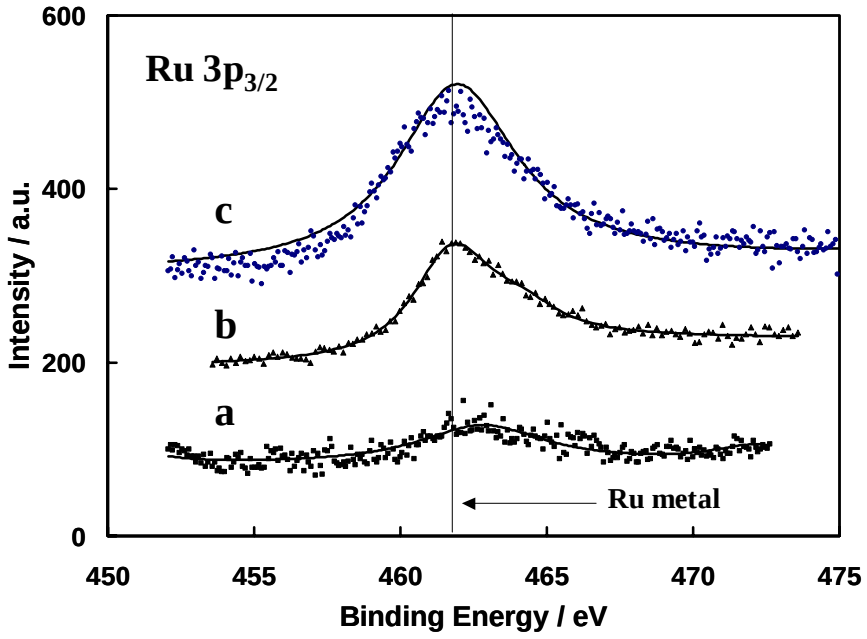

Fig. 6. Ru $3p_{3/2}$ X-ray photoelectron spectra of the catalysts with the following nominal composition; a) Pt_{75}-Ru_{25}, b) Pt_{50}-Ru_{50}, c) Pt_{40}-Ru_{60}.

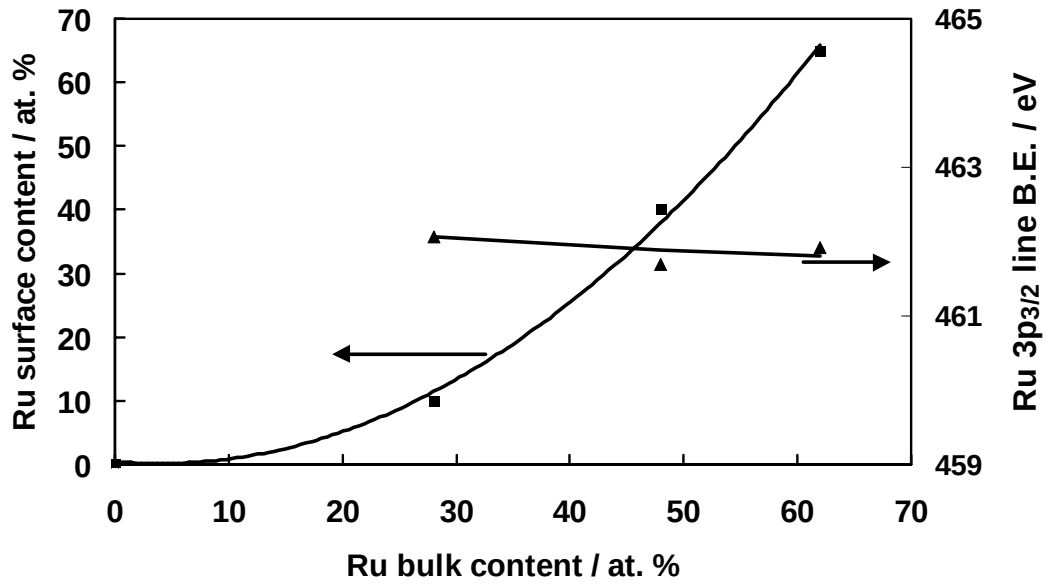

Fig. 7. Surface vs. bulk Ru content and Ru $3p_{3/2}$ B.E. in the unsupported Pt-Ru catalysts.

Sample	XRD-derived Composition At. % (± 2%)	XPS-derived Composition At. % (± 5 %)	Power Density @ 0.5 V mW cm^{-2}	Maximum power density mW cm^{-2}
DMFC1	Pt	-	20	75
DMFC2	$Pt_{72}Ru_{28}$	$Pt_{90}Ru_{10}$	85	190
DMFC3	$Pt_{64}Ru_{36}$	-	155	250
DMFC4	$Pt_{52}Ru_{48}$	$Pt_{60}Ru_{40}$	275	390
DMFC5	$Pt_{38}Ru_{62}$	$Pt_{35}Ru_{65}$	175	260

Table 2. Electrochemical parameters for the direct methanol fuel cells based on various unsupported Pt-Ru catalysts.

3.2 Electrochemical studies

The electrocatalytic activity for methanol oxidation of the various unsupported Pt-Ru samples was investigated in a direct methanol fuel cell at 130 °C. Nafion® 112 electrolyte was selected in these experiments in order to reduce the contribution of ohmic drop.

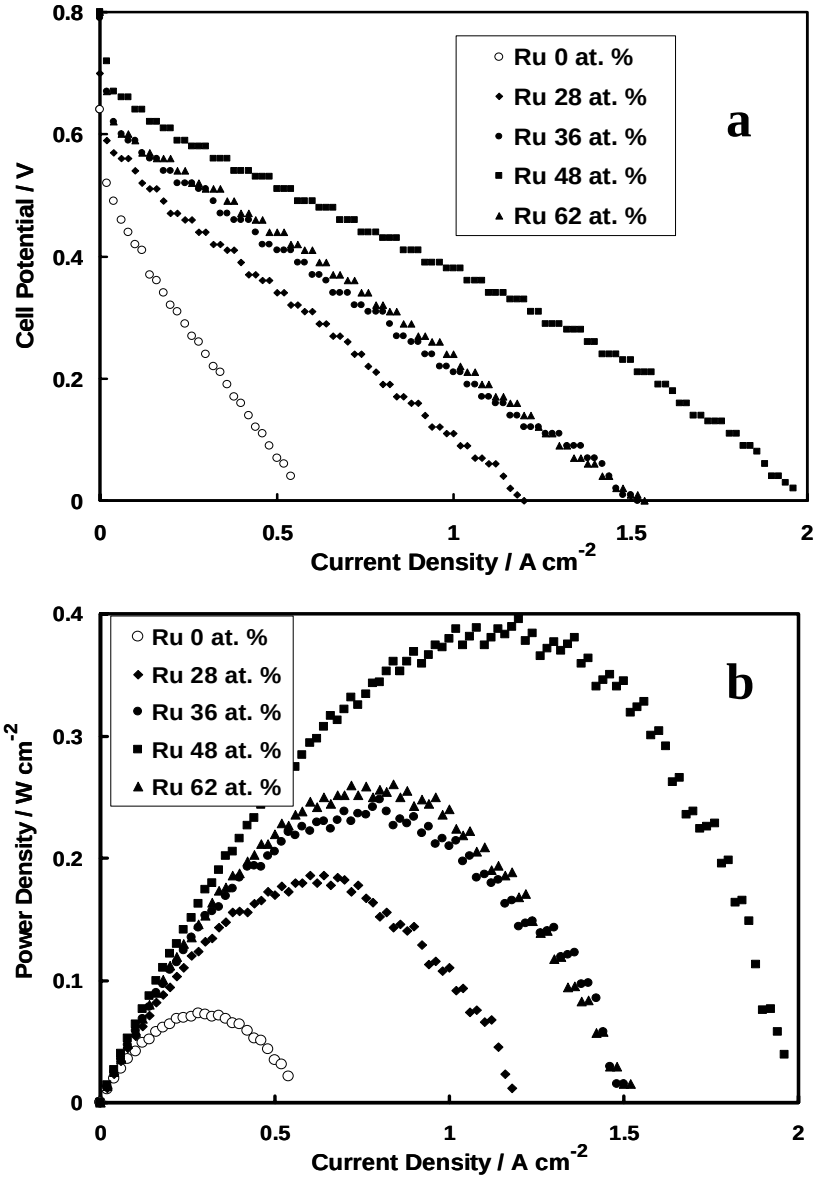

Fig. 8. Polarization (a) and (b) power density curves for a DMFC equipped with different Pt Ru anodic catalysts (the legend reports the XRD-determined composition). Operating conditions: 130°C; 2 mg Pt cm^{-2}; 2 M CH_3OH, 2.5 atm; oxygen feed, 3 atm; Nafion® 112 membrane.

The DMFC was first conditioned by operation with 0.5 M methanol solution at 90 °C up to obtain a steady-state performance; thereafter, experiments were carried out at 130 °C in the presence of 2 M methanol. Fig. 8 a-b shows the galvanostatic polarization data and their corresponding power density curves obtained at 130°C and with 2 M methanol feed for the MEAs employing unsupported Pt and Pt-Ru anode catalysts of various compositions. The MEA based on the unsupported Pt catalyst shows lower open-circuit potential and significantly larger voltage losses in the activation controlled region with respect to the Pt-Ru catalysts. The voltage drop at very low current densities is also significant for the Pt-Ru catalysts; this effect is due to the contribution of two main factors, i.e. anode polarization losses due to the slow methanol oxidation at the anode and mixed potential at the cathode caused by methanol cross-over. The DMFC performance increases as the Ru content in the anode catalyst becomes larger up to about 50% Ru, and decreases for the Ru-rich sample. This trend appears to originate from a different behavior of the various catalysts in the activation-controlled region, which is related to a different electrocatalytic activity. Maximum power densities and power outputs at 0.5 V cell voltage for the various DMFCs are reported in Table 2. At a cell voltage of 0.5 V, the power density varies by more than one order of magnitude from Pt (20 mW cm^{-2}) to Pt-Ru 1:1 (275 mW cm^{-2}). The maximum power densities are obtained at very high current densities and correspondingly low cell voltages; thus, these are of limited technical interest from the point of view of efficiency. These values range between 70 and 390 mW cm^{-2}, with the highest value obtained for the 1:1 Pt-Ru atomic ratio (Table 2).

Anodic polarization curves were obtained at 130 °C during single cell experiments by employing a reference electrode located in the anode compartment (Fig. 9). The rest potential significantly shifts to lower values as the Ru content in the catalyst is increased; however, it is almost similar for catalyst compositions above 35 at. % Ru. The Pt-Ru (1:1) catalyst shows the lowest overpotential. Catalysts having Ru bulk contents of 36 and 62 at. % show comparable performance, whereas the highest polarization losses were recorded for the pure unsupported Pt catalyst (Fig. 9).

The mass activities (A g^{-1}_{Pt+Ru}) observed at constant potentials of 0.2 V and 0.3 V vs. RHE, i.e. in the region of technical interest, have been plotted vs. the Ru at. % content in the catalysts (Fig. 10a). A “volcano-shape” relationship was observed with maximum activity at about 50:50 Pt-Ru bulk composition. This relationship is similar to that obtained by Watanabe *et al*. [19] for carbon supported, high surface area Pt-Ru catalysts at 60 °C in H_2SO_4; yet, the observed mass activities are significantly higher in the present experiments, mainly due to the

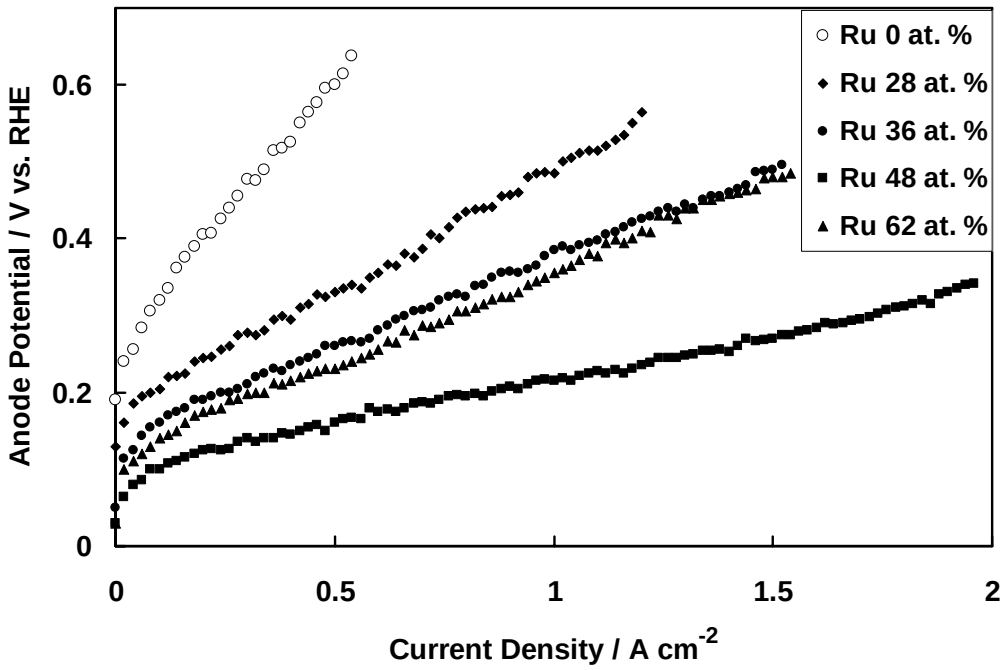

Fig. 9. Anode polarization curves for methanol electro-oxidation at 130°C in direct methanol fuel cell. Legend and operating conditions as in Fig. 8.

higher operation temperature (130 °C) and the presence of Nafion®. In fact, Nafion® does not give rise to significant anion adsorption on the catalyst surface, unlike sulfate anions. The similar trend of catalytic activity vs. Ru content in the Pt-Ru alloy at 60 and 130 °C for high surface area catalysts would indicate an identical methanol oxidation mechanism.

Specific activity (A m^{-2}_{Pt+Ru}) was derived by normalizing mass activity with respect to the surface area. The active catalyst surface area in a DMFC anode is influenced by various factors involving catalyst morphology, extension of electrode/electrolyte interface, operating conditions, etc. In our experiments we have used suitable ionomer content in the catalytic layer, as well as anode back-pressure, in order to maintain an optimal concentration of liquid phase inside the catalytic layer which allows a high degree of catalyst utilization. The determination of active catalyst surface area in a Pt-Ru electrode under fuel cell operation at 130°C is fraught with difficulty. Hydrogen desorption peaks in cyclic voltammograms of Pt-Ru samples are affected by interference of Ru-oxide formation at relatively low potentials. On the other hand, determination of surface area by CO stripping voltammetry at 130°C is adversely affected by two main uncertainties: i) both linear and bridge-bonded chemisorbed CO may occur on the surface, ii) the CO coverage at this temperature does not reach a monolayer unless a high CO partial pressure is used. Thus, both chemisorption stoichiometry and degree of coverage can not be exactly determined; these characteristics may vary for

catalysts with different Pt-Ru compositions. Accordingly, in the following calculations the surface area values determined by XRD have been utilized. By doing this, a similar "volcano-shape" relationship was obtained for specific activity vs. composition (Fig. 10b). The influence of Pt and Pt-Ru catalyst surface area towards methanol oxidation for catalysts of identical composition has been largely investigated [44-48]. The present results of mass and specific activity appear to indicate that the composition plays a prevailing role with respect to the catalyst surface area in the investigated range.

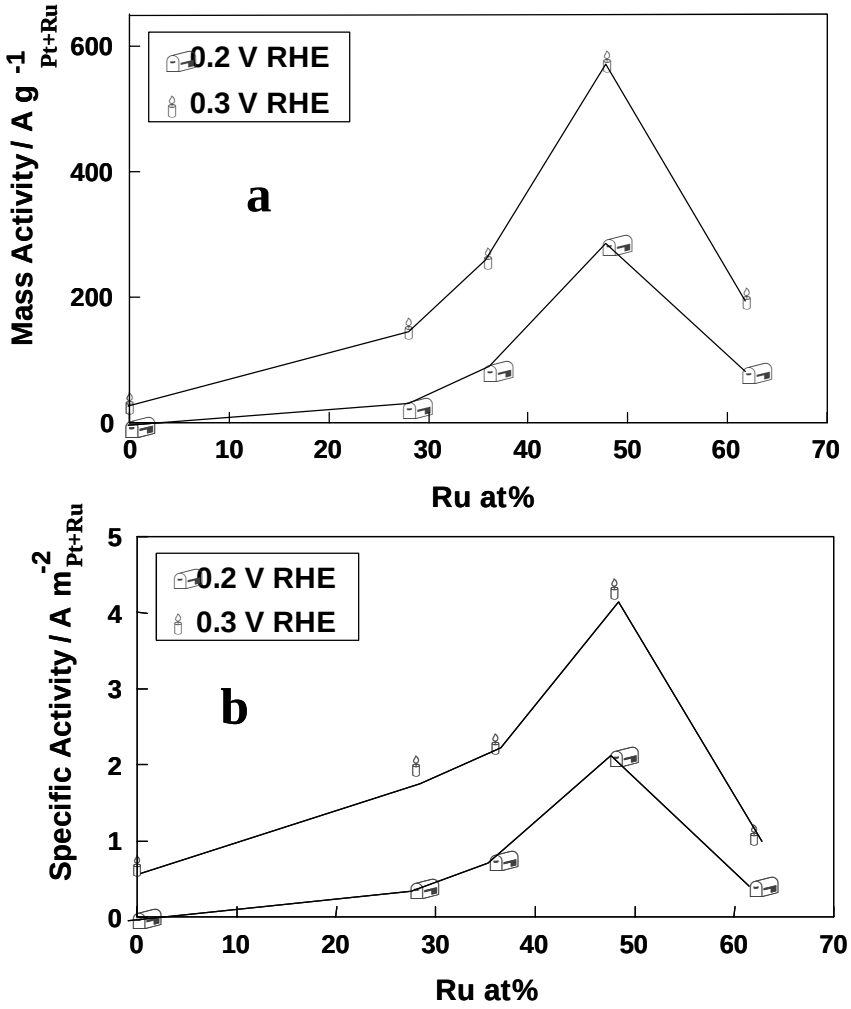

Fig. 10. Mass and specific activities for methanol electro-oxidation at 130°C versus XRD-determined bulk composition. The activities were calculated on the basis of the Pt+Ru total loading.

3.3 Mechanism and kinetic equation

Semi-logarithm plots of mass and specific activity vs. composition show a linear trend up to 50% Ru, indicating a direct relationship between composition and intrinsic activity (Fig. 11). These results may be interpreted on the basis of the well known bifunctional mechanism of methanol oxidation [24-28,33,35,37,39,45,49,50]. These anodic polarization data show very low onset potentials, thus the water discharging process appears to be favored by operation at 130°C even if the reaction rate is low in the potential region close to RHE. The adsorption energy of CH_3OH intermediates (CO-like species) is 120 kJ mol^{-1} on both Pt and Ru surfaces [51], whereas the adsorption energy of oxygen species on Ru sites is significantly larger (330 kJ mol^{-1}) [52,53]. Thus, it is thought that at 130°C, at low overpotentials, a significant fraction of Ru sites is not covered by methanolic residues; hence, they can suitably chemisorb OH groups from water. Both water discharging and carbon monoxide are favoured as the overpotential increases. Yet, at low overpotentials, the observed variation of the catalytic activity with Ru content up to 50% indicates that the reaction rate is directly related to the coverage of oxygen species on Ru sites. On the other hand, the surface reaction between Pt-bonded CO-like species and OH species adsorbed on Ru sites appears to be the rate determining step when a suitable coverage of both OH species and methanolic residues is present on the surface; this occurs for our series of catalysts at about 50:50 bulk and 60:40 Pt:Ru surface composition. At high Ru contents the coverage of oxygen species on the catalyst surface appears prevailing, limiting the adsorption of CH_3OH.

Assuming that the coverage of OH species is directly proportional to the Ru content and that for alloy compositions varying between 0 and 50% Ru the organic residues cover almost all Pt sites, the curves shown in Fig. 11 appear to follow the relationship of Bagotzky and Vassilyev [24]. Accordingly, at a fixed potential and at medium surface coverage of both ϑ_{OH} and ϑ_{Org}, the current density (i / mA cm^{-2}) increases exponentially with the coverage [24]:

$$i = k \exp(\Upsilon_1 r_1 \vartheta_{Org}) \cdot \exp(\Upsilon_2 r_2 \vartheta_{OH}) \qquad (5)$$

where k is a kinetic constant, ϑ_{Org} and ϑ_{OH} are the coverages of methanolic residues and oxygen species, Υ and r are electro-kinetic and Temkin parameters; these latters take into account the effects of surface heterogeneity and interaction between adsorbates. This relationship holds in the potential region where water displacement and consequent OH chemisorption on the catalyst surface occurs at acceptable rates. Thus, it appears that the Temkin isotherm, that was previously found to match well the data at temperatures around 60°C [54-56] applies in a more extended temperature range.

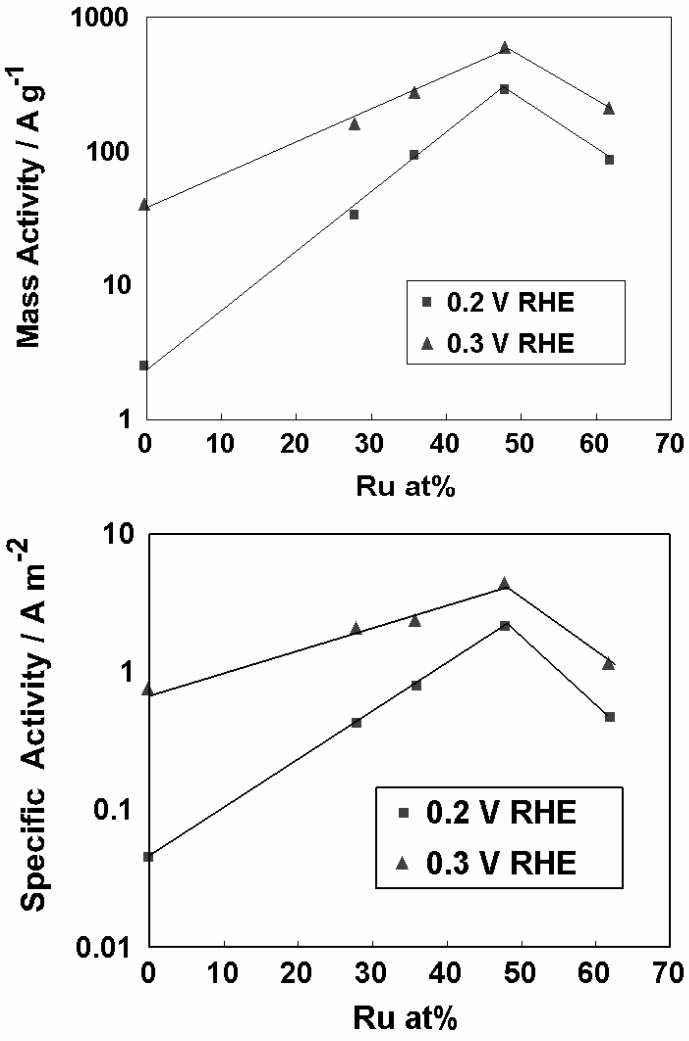

Fig. 11. Logarithm variation of mass and specific activities for methanol electro-oxidation at 130°C as a function of XRD-determined bulk composition.

II.1.4 Conclusions

An "in-situ" investigation of the electrocatalytic activity of Pt-Ru catalysts of different compositions for methanol oxidation was carried out under fuel cell operation at 130°C. The results have been correlated with bulk and surface properties of the materials. Operation at high temperature (~130°C) represents an ideal condition for application of DMFCs in

electro-traction; thus, there is a strong interest in a detailed understanding of the catalyst behavior under such conditions.

A good agreement was found between the nominal and XRD derived compositions in the present Pt-Ru catalysts, suggesting a high degree of alloying for such materials. A decrease in particle size with the increase in Ru content was observed. XPS analysis indicated the presence of a Pt surface enrichment for bulk Pt-rich catalysts, whereas this effect was less significant or absent for catalysts with high bulk Ru content and small particle size (20Å). The following conclusions may be drawn from the observed results:

a) the catalytic activity is mainly determined by the Pt/Ru atomic ratio in the alloy;
b) a volcano-shaped curve for catalytic activity versus composition was observed at 130 °C indicating a behavior similar to that observed for operation at lower temperatures (60-80°); accordingly, the data may be interpreted on the basis of the bifunctional theory;
c) a linear relationship between the logarithm of specific activity and Ru content (up to 40-50%) appears to account for a Temkin adsorption isotherm of oxygen-containing species on Ru sites.
d) water displacement on Ru sites significantly limits the electro-oxidation of methanol at very low overpotentials, especially for Pt-rich samples; however, the rate determining step at suitable overpotentials (0.2-0.3 V vs. RHE) and in the presence of an optimal composition (50% Ru) appears to involve a surface reaction between methanolic residues and oxygen-containing species adsorbed on neighboring Pt and Ru sites.

II.1.5 References

[1] S. Srinivasan, R. Mosdale, P. Stevens, C. Yang, Annu. Rev. Energy Environ. 24 (1999) 281.

[2] S. Wasmus, A. Kuver, J. Electroanal. Chemistry 461 (1999) 14.

[3] A.K. Shukla, P. A. Christensen, A. Hamnett, M.P. Hogarth, J. Power Sources 55 (1995) 87.

[4] X. Ren, M.S. Wilson, S. Gottesfeld, J. Electrochem. Soc. 143 (1996) L12.

[5] M. Baldauf, W. Preidel, J. Power Sources 84 (1999) 161.

[6] L. Liu, C. Pu, R. Viswanathan, Q. Fan, R. Liu, E.S. Smotkin, Electrochim. Acta 43 (1998) 3657.

[7] S.R. Narayanan, W. Chun, T.I. Valdez, B. Jeffries-Nakamura, H. Frank, S. Surampudi, G. Halpert, J. Kosek, C. Cropley, A.B. LaConti, M. Smart, Q. Wang, G. Surya Prakash, G.A. Olah, Program and Abstracts, Fuel Cell Seminar (1996), pp. 525 - 528.

[8] M.K. Ravikumar, A.K. Shukla, J. Electrochem. Soc. 143 (1996) 2601.

[9] P.S. Kaurenan, E. Skou, J. Electroanal. Chem. 408 (1996) 189.

[10] K. Scott, W.M. Taama, P. Argyropoulos, K. Sundmacher, J. Power Sources 83 (1999) 204.

[11] M. Gotz, H. Wendt, Electrochim. Acta, 43 (1998) 3637.

[12] J. Wang, S. Wasmus, R.F. Savinell, J. Electrochem. Soc. 142 (1995) 4218.

[13] D.H. Jung, C.H. Lee, C.S. Kim, D.R. Shin, J. Power Sources 71 (1998) 169.

[14] A.S. Aricò, P. Creti, H. Kim, R. Mantegna, N. Giordano, V. Antonucci, J. Electrochem. Soc. 143 (1996) 3950.

[15] A.S. Aricò, P. Creti, P.L. Antonucci, V. Antonucci, Electrochem. Solid State Lett. 1 (1998) 4.

[16] A.S. Aricò, A.K. Shukla, K.M. el-Khatib, P. Creti, and V. Antonucci, J. Appl. Electrochem. 29 (1999) 671.

[17] H.G. Petrow and R.J. Allen, U.S. Pat. 3, 992, 331 (1976).

[18] V. Jalan, Extended Abstracts, Electrochemical Society, Los Angeles, CA, Fall Meeting, Abstract 192 (October 1979).

[19] M. Watanabe, M. Uchida, S. Motoo, J. Electroanal. Chem. 22 (1987) 395.

[20] K. Lasch, L. Jorissen, J. Garche, Proceedings of Proceedings of the Workshop "Electrocatalysis in Indirect and Direct Methanol PEM Fuel Cells", C. Lamy, H. Wendt (Eds.), Sept. 12-14 Portoroz, Slovenia 1999, p. 104.

[21] T.J. Schmidt, M. Noeske, H.A. Gasteiger, R.J. Behm. P. Britz, W. Brijoux, H.

Bonnemann, Langmuir 14 (1997) 2591.
[22] C. He, H.R. Kunz, J.M. Fenton, J. Electrochem. Soc. 144 (1997) 970.
[23] W. Chrzanowski, H. Kim, A. Wieckowski, Catal. Lett. 50 (1998) 69.
[24] V.S. Bagotzky, Yu. B. Vassiliev, Electrochim. Acta 12 (1967) 1323.
[25] M. Watanabe, S. Motoo, J. Electroanal. Chem. 60 (1975) 275.
[26] H.A. Gasteiger, N. Markovic, P.N. Ross Jr., E.J. Cairns, J. Electrochem. Soc. 141 (1994) 1795.
[27] K.A. Friedrich, K.P. Geyzers, U. Linke, U. Stimming, J. Stumper, J. Electroanal. Chem. 402 (1996) 123.
[28] T. Frelink, W. Visscher, J.A.R. van Veen, Langmuir 12 (1996) 3702.
[29] A.K. Shukla, A.S. Aricò, K. M. el-Khatib, H. Kim, P.L. Antonucci, V. Antonucci, Applied Surface Science 137 (1999) 20.
[30] V. Radmilovic, H.A. Gasteiger, P.N. Ross, Jr., J. Catal. 154 (1995) 98.
[31] A.S. Aricò, G. Monforte, E. Modica, P.L. Antonucci, V. Antonucci, Electrochemistry Communications, 2 (2000) 466.
[32] J. Mc Breen, S. Mukerjee, J. Electrochem. Soc. 142 (1995) 3399.
[33] T. Iwasita, F.C. Nart, W. Vielstich, Ber. Bunsenges Phys. Chem. 94 (1990) 1030.
[34] J.B. Goodenough, R. Manoharan, A.K. Shukla, and K.V. Ramesh, Chemistry of Materials 1 (1989) 391.
[35] D. Chu, S. Gilman, J. Electrochem. Soc., 143 (1996) 1685.
[36] T. Iwasita, H. Hoster, A. John-Anacker, W. F. Lin, W. Vielstich, Langmuir 16 (2000) 522.
[37] B.D. McNicol, R.T. Short, J. Electroanal. Chem. 81 (1977) 249.
[38] R.A. Lampitt, L.P.L. Carrette, M.P. Hogarth, A.E. Russell, J. Electroanal. Chem. 460 (1999) 80.
[39] H.A. Gasteiger, P.N. Ross Jr., E. Cairns, J. Surf. Sci. 67 (1993) 293.
[40] A.S. Aricò, P. Cretì, V. Baglio, E. Modica, V. Antonucci, J. Power Sources 91 (2000) 202.
[41] J.A. Poirier, The Electrochemical Society Interface, Winter 1994, p. 49.
[42] B. D. McNicol, R.T. Short, J. Electroanal. Chem. 92 (1978) 115.
[43] K.A. Starz, E. Auer, Th. Lehmann, R. Zuber, J. Power Sources 84 (1999) 167.
[44] M. Watanabe, S. Saegusa, P. Stonehart, J. Electroanal. Chem. 271 (1989) 213.
[45] B.D. McNicol, D.A.J. Rand, K.R. Williams, J. Power Sources 83 (1999) 15.
[46] K. Kinoshita, J. Electrochem. Soc. 137 (1990) 845.

[47] G. Hoogers, D. Thompsett, CAT-THEC 3 (2000) 107.

[48] X. Ren, P. Zelenay, S. Thomas, J. Davey, S. Gottesfeld, J. Power Sources 86 (2000) 111.

[49] K. Chandrasekaran, J.C. Wass, J.O' M. Bockris, J. Electrochem. Soc. 137 (1990) 518.

[50] J. Clavilier, C. Lamy, J.M. Leger, J. Electroanal. Chem. 125 (1981) 249.

[51] T. Engel, G. Ertl, Adv. Catal. 28 (1979) 1.

[52] E. Ticianelli, J.G. Berry, M.T. Paffet, S. Gottesfeld, J. Electroanal. Chem. 81 (1977) 229.

[53] T.E. Madey, H.A. Engelhardt, D. Menzel, Surf. Sci. 48 (1975) 304.

[54] A.S. Aricò, P.L. Antonucci, E. Modica, E. Passalacqua, V. Antonucci, J. Appl. Electrochem. 27 (1997) 1275.

[55] A.S. Aricò, E. Modica, P. Cretì, P.L. Antonucci, V. Antonucci, J. New Materials for Electrochemical Systems 3 (2000) 207.

[56] S. Swathirajan, Y.M. Mikhail, J. Electrochem. Soc. 138 (1991) 1321.

II.2 Analysis of the high temperature methanol oxidation behaviour at carbon supported Pt-Ru catalysts*

II.2.1 Introduction

A direct methanol fuel cell based on a high temperature proton conducting membrane with suitable conductivity and stability up to 130°-150 °C and characterized by low thermal and water management constraints would become a viable system for mobile applications [1-5]. However, methanol electro-oxidation at 130 °C is an activation controlled reaction with a Tafel slope of 130 mV/dec [6]; the optimal Pt/Ru relative composition in the bulk and on the surface is about 1:1 [7, 8]. The bifunctional effect appears to govern the reaction mechanism at high temperatures, with the removal of adsorbed carbon monoxide species being the rate determining step [6-8]. At present, most of the efforts have been addressed towards the development of high temperature membranes since this is a key aspect to achieve good performance and prolonged life-time [5, 8, 9, Chapter III]. Yet, although interesting results have been obtained by high temperature operation, the significant amount of the required noble metal loading (1-2 mg cm^{-2}) [1] indicates that further development of the anodic catalyst is needed. This aspect may be addressed through a better comprehension of the high temperature behaviour and a deep analysis of the various factors influencing the performance.

One of the main disadvantages of high temperature operation is the high pressure requirement to maintain a good hydration level inside the membrane. Besides these aspects, the pressure is expected to have a significant influence on the coverage of reacting molecules and intermediate species. Previous works have shown that a Temkin adsorption isotherm governs the electro-adsorption of CO species on Pt-Ru/C catalysts at low temperatures and a reaction order of 0.5 has been observed for CO oxidation with respect to its partial pressure [10]. On the other hand, it should be considered that the coverage of CO species on smooth Pt surfaces strongly decreases in the temperature range from 25°C to 150 °C as opposite of hydrogen coverage [11]. Both aspects are relevant for the methanol reaction. In fact, methanol electro-oxidation on Pt-Ru catalysts occurs through a first dehydrogenation step at Pt sites followed by removal of adsorbed CO-like reaction intermediates by OH species adsorbed on the neighbouring Ru sites [12]. Accordingly, an increase of operation temperature would play a favourable role for the initial dehydrogenation of methanol and it would facilitate the CO

* A paper based on this study has been published on **J. Electroanalytical Chemistry 557 (2003) 167-176**

desorption decreasing the coverage of irreversibly adsorbed species. In order to get an experimental evidence of these conjectures and to derive insights on high temperature methanol electro-oxidation, various Pt-Ru/C catalysts were selected and the influence of temperature and pressure on the methanol stripping behaviour was analysed. An attempt to correlate the electrochemical behaviour with the physico-chemical properties of the catalysts is made.

Carbon supported catalysts were singled out in the present analysis due to their better potentialities with respect to the unsupported ones for application in low noble metal loading electrodes. To compare the properties of different catalysts, standard commercial Nafion membranes have been used. The maximum operating temperature of these membranes is 130°C. However, although cell operation at 150 °C is considered ideal, 120-130 °C are still suitable operating temperatures for DMFC application in electro-traction.

II.2.2 Experimental

Three carbon supported Pt-Ru catalysts for methanol oxidation have been selected. A 85% Pt-Ru (1:1)/Vulcan XC 72 catalyst was prepared in-house by a sulphite complex route [13]. 30% and 60% Pt-Ru (1:1)/Vulcan XC 72 were provided by E-TEK (USA). A 60% Pt/Vulcan XC 72, in-house prepared by the sulphite complex route, has also been investigated and used for the oxygen reduction reaction. This cathode catalyst was suitable for operation in high temperature DMFC.

The in-house made catalysts were prepared as follows. Sulfite complexes of Pt and Ru, in appropriate amounts, were decomposed by hydrogen peroxide to form aqueous colloidal solutions of Pt and Ru oxides. These particles were adsorbed on a carbon black to form a 85% Pt-RuOx/Vulcan XC 72 catalyst. The amorphous oxides on carbon were reduced in a hydrogen stream to form a metallic alloy. The 60% Pt/Vulcan XC 72 catalyst was synthesized in a similar way. It was used as cathode in all experiments.

X-ray diffraction powder (XRD) patterns for these catalysts were obtained on a Philips X'Pert X-ray Diffractometer using CuK_{α}-source operating at 40 kV and 30 mA. The peak profiles of the (220) reflection in the face-centered-cubic (fcc) structure were obtained by using the Marquardt algorithm [14]. Instrumental broadening was determined by using a standard platinum sample. X-ray fluorescence analysis of the catalysts was carried out by a Bruker AXS S4 Explorer spectrometer operating at a power of 1 kW and equipped with a Rh X-ray source, a LiF 220 crystal analyser and a 0.12° divergence collimator. The Pt/Ru atomic

ratio was determined by using Pt Lα and Ru Lα emission lines after appropriate calibration with standard samples. TEM analysis was made by first dispersing the catalyst powder in isopropyl alcohol. A few drops of these solutions were deposited on carbon film coated Cu grids and analysed with a Philips CM12 microscope. X-ray photoelectron spectroscopy (XPS) measurements were performed by using a Physical Electronics (PHI) 5800-01 spectrometer. A monochromatic Al Kα X-ray source was used at a power of 350 W. Spectra were obtained with pass energies of 58.7 eV for elemental analysis (composition) and 11.75 eV for the determination of the oxidation states. The pressure in the analysis chamber of the spectrometer was $1 \cdot 10^{-9}$ Torr during the measurements. The Ag $3d_{5/2}$ peak of an Ag foil was taken, after argon sputtering, for checking the calibration of the binding energy (B.E.) scale. The quantitative evaluation of each peak was obtained by dividing the integrated peak area by atomic sensitivity factors which were calculated from the ionization cross-sections, the mean free electron escape depth and the measured transmission functions of the spectrometer. XPS data have been interpreted by using the on-line library of oxidation states implemented in the PHI Multipak 6.1 software and the PHI Handbook of X-ray photoelectron spectroscopy [15].

The electrodes were prepared according to the procedure described in a previous paper [16]; they consisted of carbon cloth, diffusion and catalytic layers. The Pt loading in each electrode was 2 mg cm^{-2}. Pt-Ru/Vulcan XC catalysts were employed at the anode, whereas Pt/Vulcan-XC was utilized for cathode fabrication. A Nafion 117 membrane was used as electrolyte. Membrane-electrode assemblies (MEAs) were formed by a hot-pressing procedure [16] and subsequently installed in a fuel cell test fixture of 5 cm^2 active area. This latter was connected to a test station including an HP6060B electronic load or to an EG&G electrochemical apparatus consisting of a PAR 273 A Potentiostat/Galvanostat and a 20A Current Booster. The cell temperature was measured by a thermocouple embedded in the anodic graphite plate, close to the MEA. For single and half-cell polarization experiments, preheated aqueous methanol (1M) was fed to the anode chamber of DMFC through a peristaltic pump; humidified air, pre-heated at 100°C, was fed to the cathode. Pressure in the anode compartment was varied between 1 and 3 atm. rel., whereas, it was set to 2.5 atm in the cathode compartment. Reactant flow rates were 2 ml min^{-1} and 500 ml min^{-1} for methanol/water mixture and air stream, respectively. Single cell performances were investigated by steady-state galvanostatic measurements. In half cell polarization studies a three-electrode configuration was used. Hydrogen (1 atm. rel.) was fed to the cathode that was used as both counter and reference electrode. These measurements were carried out by both potentiodynamic sweeps at a scan rate of 5 mV s^{-1} or by steady-state galvanostatic

measurements. Data have not been corrected for the IR-drop. The cell resistance was the same (within the experimental error) for all MEAs at each temperature, it varied as a function of temperature, i.e. 0.12 ohm cm^2 at 90 °C, 0.1 ohm cm^2 at 110 °C and 0.09 ohm cm^2 at 130 °C.

In-situ methanol and CO stripping voltammetries were carried out at various temperatures under DMFC configuration at both carbon supported Pt and Pt-Ru catalysts/Nafion 117 membrane interfaces. For CO stripping, the first, second and third cycles were recorded at 50 mV s^{-1}, after adsorption from 2% CO in Ar at 0.1 V for 30 min and subsequent purging in Ar atmosphere. Adsorption times longer than 30 min at 0.1 V did not appear to produce in our experiments any significant change in the stripping potentials and charge. The same procedure was adopted for the stripping of adsorbed methanolic residues. After the adsorption step, the anode was in-situ washed by flowing deaerated water through the electrode. In some cases small amounts of residual adsorbed CO was detected in the second scan. This residual amount was taken into account for a proper determination of the stripping charge.

II.2.3 Results and discussion

All the catalysts have same nominal 1:1 composition. XRF analysis indicates similar bulk composition (Table 1). X-ray diffraction analysis (Fig. 1) of the various carbon supported catalysts shows for all samples the cubic fcc crystallographic structure of the Pt-Ru alloy. A shift towards higher Bragg angles is observed in the XRD patterns of the 85% Pt-Ru/C catalyst with respect to the other carbon supported catalysts; this, indicates a higher degree of alloying in the sample. Crystallographic parameters, mean particle size and degree of alloying, this latter calculated according to the relationship described in Ref [17], are reported in Table 1. The particle size, determined by the Debye-Sherrer equation, is smaller in the highly dispersed 30% Pt-Ru/C catalyst. An amorphous halo is evident in this latter catalyst at about 34°-35° Bragg angles. This effect may be due to the presence of amorphous $RuO_2 \cdot xH_2O$, also reported in the literature as RuO_xH_y [18, 19]. TEM observation of the catalysts (see Fig. 2) clearly indicates a significantly higher degree of agglomeration for the 85% Pt-Ru/C catalyst and a lower metal-support interaction in comparison with the other samples. These latter show primary Pt-Ru particles well anchored to the carbon black surface.

Catalyst	Bulk Composition (XRF) (±2%)	Alloy Composition (XRD) (±2%)	Surface Composition (XPS) (±5%)	Particle size Å (±2Å)
30% Pt-Ru/C	$Pt_{48}Ru_{52}$	$Pt_{69}Ru_{31}$	$Pt_{52}Ru_{48}$	18
60% Pt-Ru/C	$Pt_{50}Ru_{50}$	$Pt_{59}Ru_{41}$	$Pt_{51}Ru_{49}$	22
85% Pt-Ru/C	$Pt_{51}Ru_{49}$	$Pt_{47}Ru_{53}$	$Pt_{55}Ru_{45}$	21
60 % Pt/C	-	-	-	37

Table 1. Physico-chemical characteristics of the carbon supported Pt-Ru catalysts.

XPS analysis of Pt 4f, Ru 3d and Ru $3p_{3/2}$ spectra (Figs. 3-5) shows a shift to higher binding energies with a larger fraction of oxidized species for the catalysts with lower concentration of metallic phase on carbon, i.e. 30% Pt-Ru/C and 60% Pt-Ru/C (Table 2). As example, by comparing the Pt 4f spectra of the various catalysts (Fig. 3), it is observed that the 30% Pt-Ru/C sample has a significantly higher content of oxidized Pt species (Table 2). In fact, this sample shows a larger broadening of the peaks and a shift towards higher binding energies. The Pt 4f components are attributed to Pt°, Pt^{2+} and Pt^{4+} species [15]. However, a shift by about 0.5 eV of the Pt 4f signal with respect to a previously investigated unsupported Pt-Ru catalyst with the same bulk composition and lattice parameter is observed [20]. Such effect may be tentatively attributed to metal-support interaction.

XP spectra for the Ru 3d-C1s region are shown in Fig. 4. The C1s peak from graphitic carbon occurs at 284.55 eV in all samples in good agreement with the literature [15]. This peak entirely covers the Ru $3d_{3/2}$ signal and it partially overlaps to the Ru $3d_{5/2}$. Accordingly, a quantitative estimation of the oxidation states is not possible from these spectra. However, from a qualitative point of view, it can be easily observed in the $3d_{5/2}$ region the presence of two peaks at low (280.3 eV) and high (281.5 eV) B.E. assigned to Ru° [15, 21] and anhydrous

RuO_2 [15, 19], respectively. These peaks appears to be shifted by about 0.3 eV towards higher B.E. with respect to the corresponding values in the literature [15, 19], probably due to a large C1s peak tail. The Ru 3d signal from hydrous amorphous $RuO_2 \cdot xH_2O$ occurs at B.E. about 1 eV higher than anhydrous RuO_2. The presence of $RuO_2 \cdot xH_2O$ is not excluded in the present catalysts, but the overlapping with the large C1s peak from graphitic carbon makes difficult its clear identification. Accordingly, the Ru $3p_{3/2}$ peak signal was analysed to get rid of the interference from graphitic carbon [14, 15, 22]. Ru $3p_{3/2}$ spectra are reported in Fig. 5. The 85% Pt-Ru/C catalyst shows a prevailing presence of the metallic component; whereas, the Ru $3p_{3/2}$ peak in the 30% and 60% Pt-Ru/C catalysts is located at significantly higher B.E. values.

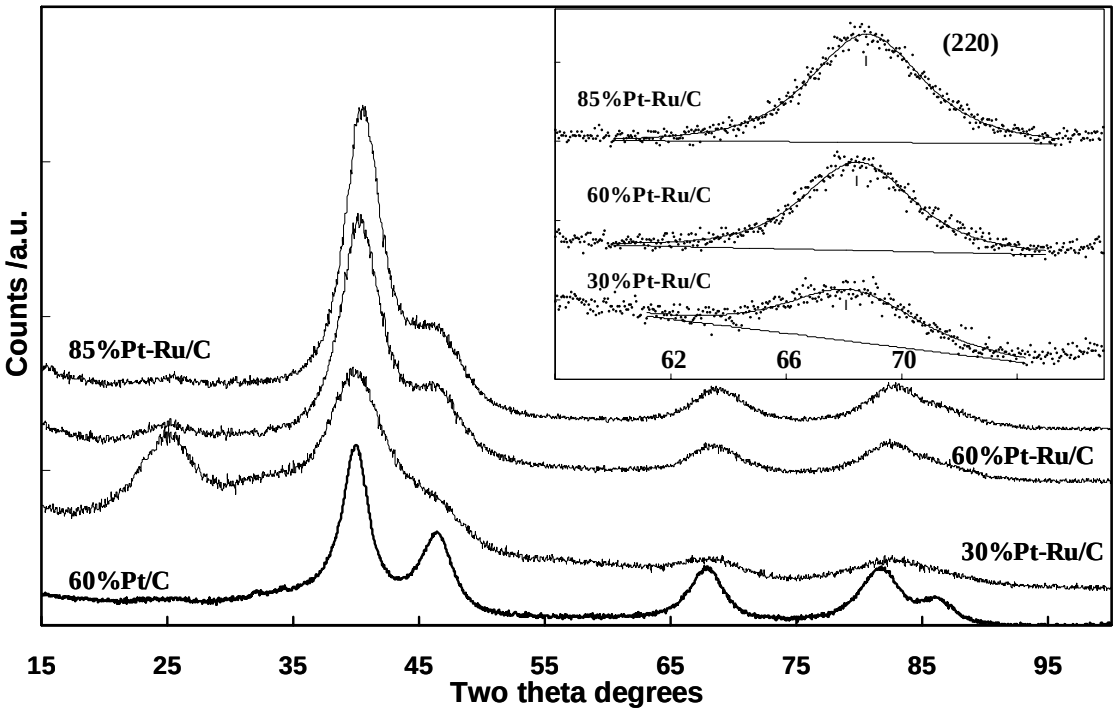

Fig. 1. XRD patterns of carbon supported supported Pt-Ru catalysts.

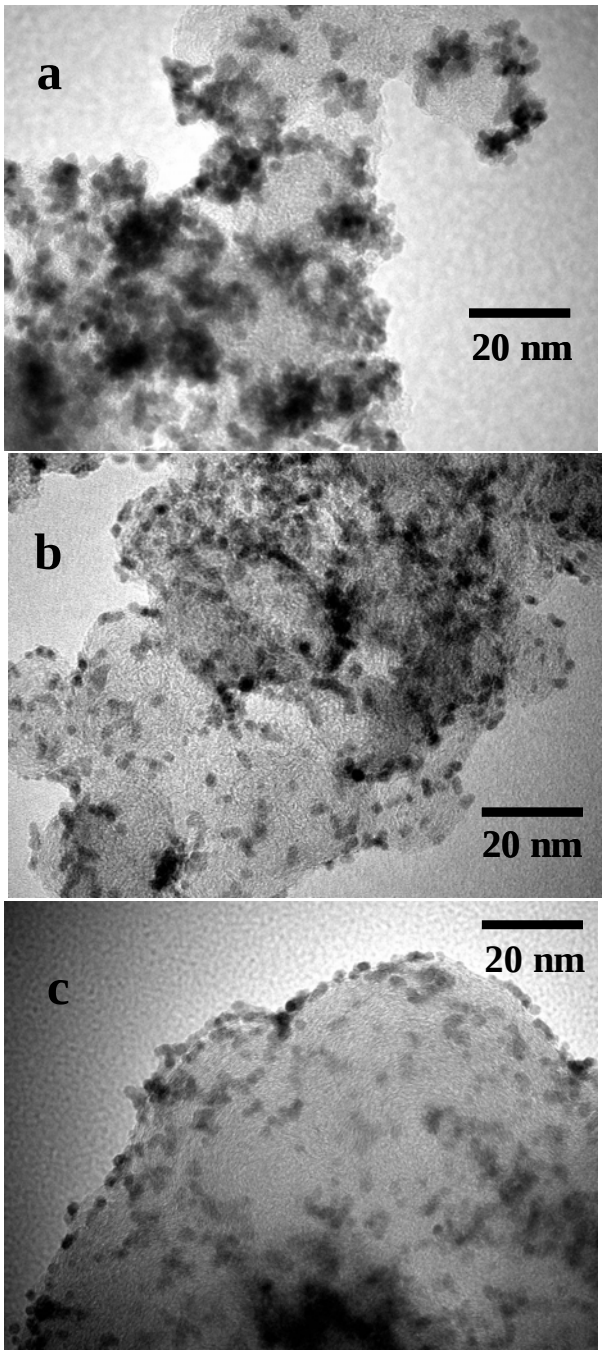

Fig. 2. Transmission electron micrographs of carbon supported supported Pt-Ru catalysts; a) 85 % Pt-Ru/C catalyst; b) 60 % Pt-Ru/C catalyst; c) 30 % Pt-Ru/C catalyst .

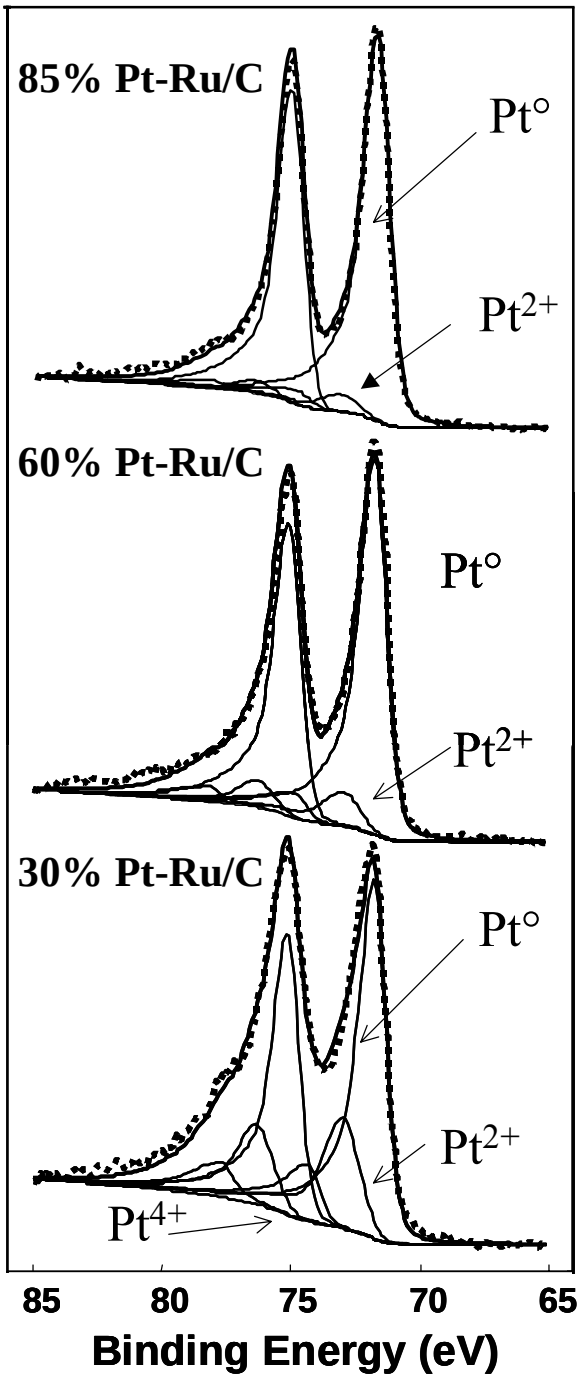

Fig. 3. X-ray photoelectron spectra of Pt-Ru catalysts (Pt 4f doublet).

This indicates that a larger fraction of oxidation state species is present in the 60% Pt-Ru/C as well as in the 30% Pt-Ru/C sample. In these latter catalysts there is a significant interaction of Pt and Ru with carbon functional groups (metal-support interaction) which being more electronegative than Pt and Ru, share part of their electron clouds. The three Ru $3p_{3/2}$ components (Fig. 5) are attributed to Ru° [14, 15, 22], anhydrous RuO_2 [14, 15, 22] and

hydrous amorphous $RuO_2 \cdot xH_2O$. As stated by Rolison et al. [19], the RuO_3 species should be excluded in favour of the hydrous amorphous $RuO_2 \cdot xH_2O$ since the RuO_3 is not thermodynamically stable under the present conditions. Nevertheless, the surface characteristics of a catalyst do not always reflect the thermodynamic data. XPS analysis of O1s and C1s (not shown) reveals a significant presence of oxygenated functional groups (e.g., -CO as well as –COO- like species) which may be responsible of such interaction.

A comparison of the in-situ stripping behaviour of adsorbed methanolic residues for the three Pt-Ru/C catalysts at various temperatures is shown in Fig. 6. It is clearly evident that, as the temperature is increased above 90 °C, the methanolic residues stripping area progressively decreases for all catalysts, whereas, the peak shifts towards lower potentials on account of the decrease of the activation energy for CO removal. By comparing the behaviour of the various catalysts, it is observed that the 30 % Pt-Ru/C sample has the larger stripping area per unit of weight. Such evidence indicates that a larger amount of catalytic sites are covered by methanolic residues in this sample. Yet, the stripping peak potential at each temperature is more shifted towards negative values for the 85% PtRu/C catalyst. Furthermore, the stripping peaks are significantly sharper for this latter catalyst indicating higher intrinsic catalytic activity and faster charge transfer kinetics.

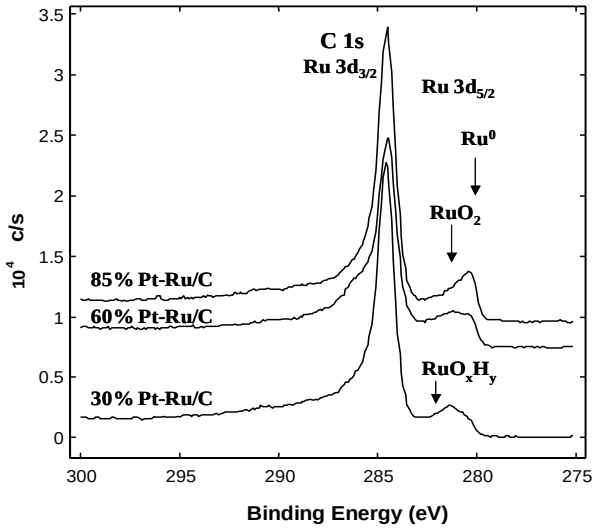

Fig. 4. X-ray photoelectron spectra of Pt-Ru catalysts (C1s and Ru 3d regions).

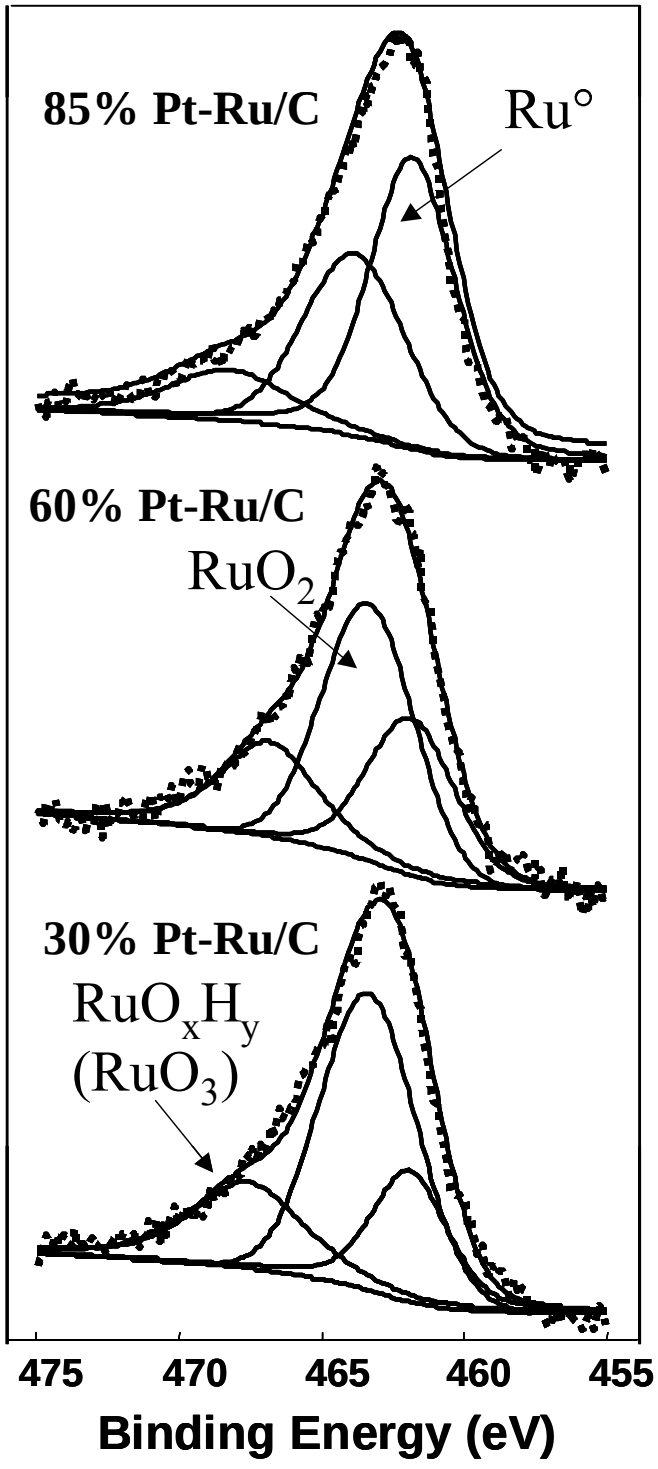

Fig. 5. X-ray photoelectron spectra of Pt-Ru catalysts (Ru $3p_{3/2}$ line).

Species	Binding Energy (eV)		Relative peak area (%)
85% Pt-Ru/C			
Pt 4f	$4f_{7/2}$	$4f_{5/2}$	
	71.70	75.05	90.09
	73.10	76.45	5.49
	74.80	78.15	4.42
Ru 3p	$3p_{3/2}$		
	461.85		51.57
	463.65		37.60
	467.85		10.83
60% Pt-Ru/C			
Pt 4f	$4f_{7/2}$	$4f_{5/2}$	
	71.70	75.05	81.18
	72.90	76.25	10.73
	74.80	78.15	8.09
Ru 3p	$3p_{3/2}$		
	461.90		29.20
	463.40		47.27
	467.10		23.53
30% Pt-Ru/C			
Pt 4f	$4f_{7/2}$	$4f_{5/2}$	
	71.70	75.05	81.18
	72.90	76.25	8.09
	74.80	78.15	10.73
Ru 3p	$3p_{3/2}$		
	461.95		21.08
	464.39		53.96
	467.62		24.96

Table 2. Binding energy and relative intensities of different species from curve-fitted XPS spectra in the various Pt-Ru/C catalysts.

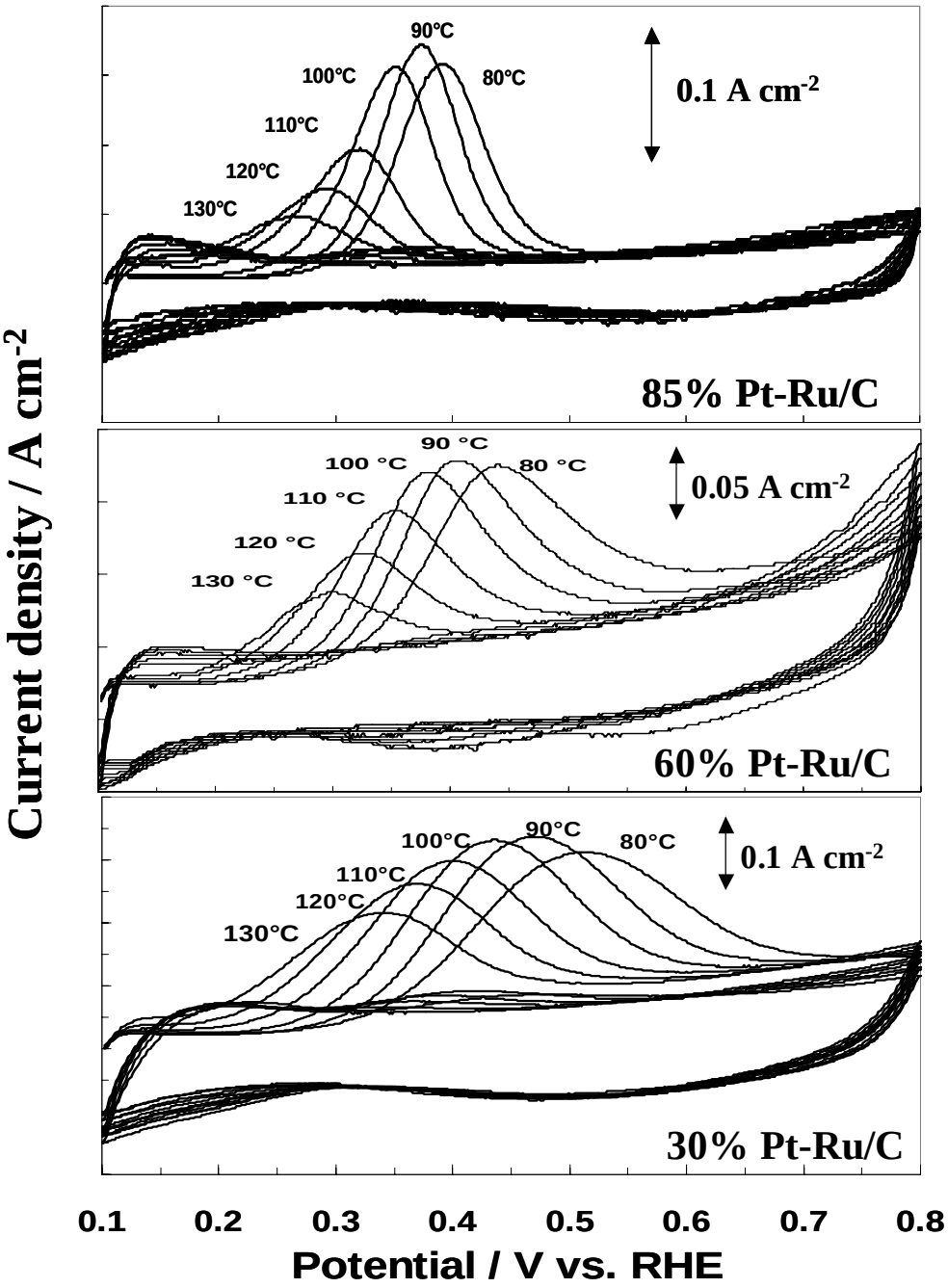

Fig. 6. In-situ methanol residues stripping voltammetry at the various carbon supported Pt-Ru catalyst/Nafion 117 membrane interface, at various temperatures under DMFC configuration. Anode: 1 M methanol, 1 atm. rel. adsorbed for 30 min; cathode: H_2 feed 1 atm. rel.

The Pt/C catalyst (Fig. 7) shows similar methanolic residues stripping behaviour as function of temperature with respect to Pt-Ru/C catalysts. However, the large mean particle size (37 Å) and its poor catalytic activity produce small peak areas and significant shift of the stripping potentials towards positive values. In order to understand if the adsorbed methanolic residues stripping behaviour is related to the removal of carbon monoxide [23], the CO

stripping process was investigated on the 85% Pt-Ru/C catalyst (Fig. 8). At high temperature, the limited amount of water in the humidified CO stream does not allow for a sufficient humidification of the electrolyte membrane; thus, this analysis was carried out up to 110 °C. The CO stripping behaviour (Fig. 8) appears very similar to the methanolic residues stripping process. The CO and methanolic residues stripping peak potentials are similar for the 85% Pt-Ru/C catalyst (Fig. 9a). The adsorbed methanolic residues stripping peaks are slightly broader, but, the number of catalytic sites involved in the stripping process are larger for carbon monoxide with respect to the methanolic residues stripping (Fig. 9b).

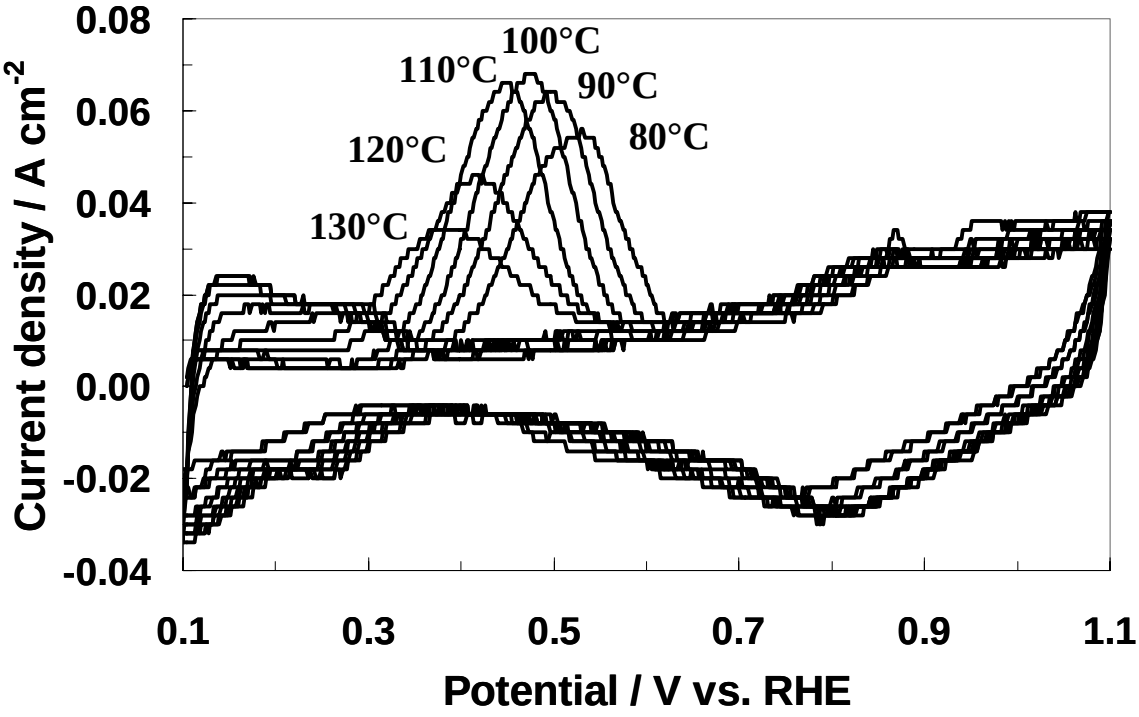

Fig. 7. In-situ methanol residues stripping voltammetry at the carbon supported Pt catalyst/Nafion 117 membrane interface, at various temperatures under DMFC configuration. Anode: 1 M methanol, 1 atm. rel. adsorbed for 30 min; cathode: H_2 feed 1 atm. rel.

The variation of the stripping potentials as a function of temperature is almost linear for all the catalysts in the investigated range (Fig. 9a). The stripping peak potentials are shifted towards the reversible methanol electro-oxidation potential as the temperature is increased and for the catalysts with higher metallic character (85% Pt-Ru/C).

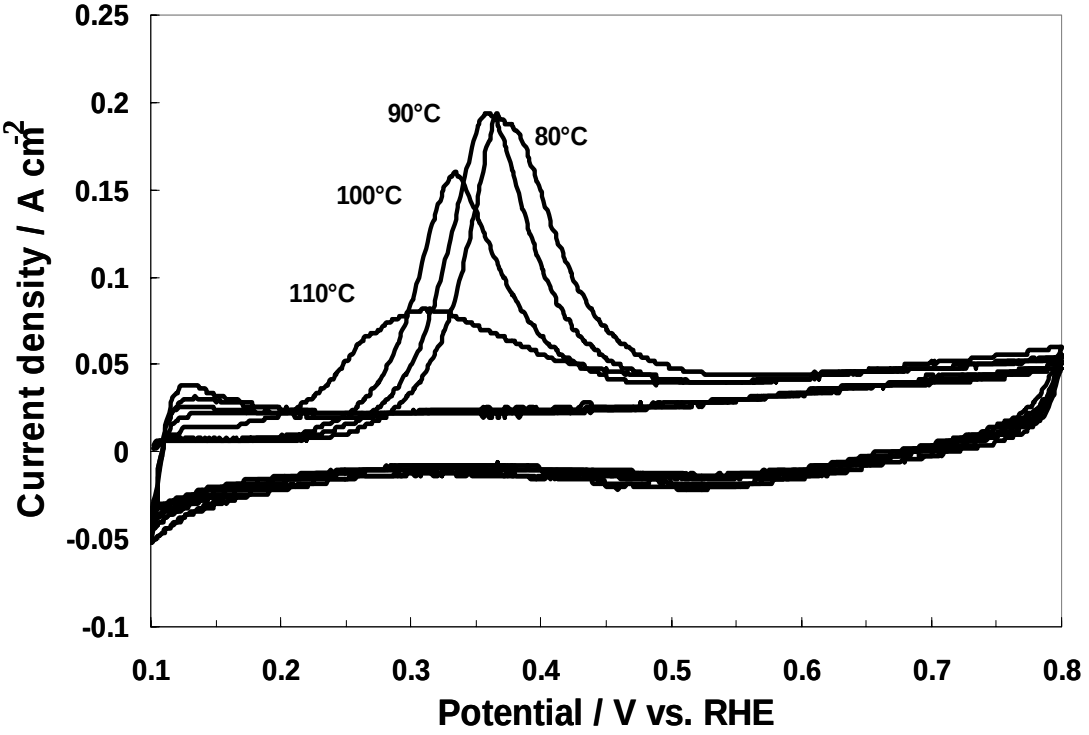

Fig. 8. In-situ CO stripping voltammetry at a carbon supported 85 % Pt-Ru catalyst/Nafion 117 membrane interface, at various temperatures under DMFC configuration. Anode: 2% CO in Ar, 1 atm. rel., adsorbed for 30 min; cathode: H_2 feed 1 atm. rel.

A large number of investigations have been reported in the literature on the methanol and CO oxidation mechanisms at low temperature on Pt-based catalysts (see Ref. [6] and references herein reported). Accordingly, three Pt reaction sites are involved in the initial stage of methanol adsorption, whereas, in the case of CO adsorption mainly linear-bonded species have been detected. The stripping behaviour is related to CO removal in both cases [23, 24], but the steady-state coverage is influenced by "steric" effects occurring in the first phase of the methanol adsorption process. When the number of reaction sites, per unit weight of Pt, which are involved in the stripping behaviour is expressed in terms of m^2/g, the Pt surface area involved in the stripping behaviour decreases with temperature above 90 °C with a trend similar for all catalysts (Fig. 9b). It appears clear that the number of reaction sites, expressed as m^2/g, at T > 90 °C can not be assumed as a quantification of the electrochemical available surface area. Probably, the same parameter determined at lower temperatures, e.g. 50° or 80 °C in the CO stripping process could be a good estimation of the active surface area. The trend represented in Fig. 9b is strictly related to the variation of coverage of electro-adsorbed species with temperature. By comparing the value of stripping

peak area, expressed as m^2/g, for methanol and CO stripping processes on the same catalyst (85% Pt-Ru/C) at 80 °C, it is derived that only 65 % of the reaction sites available for CO adsorption are effectively involved in the adsorption of methanolic residues. At higher temperatures, the number of catalytic sites occupied by methanolic residues should approach the value determined for the CO adsorption process (see Fig. 9b). At low temperature CO adsorption occurs at both Pt and Ru sites whereas methanol dehydrogenation occurs preferably at three neighbouring Pt sites. However, at high temperature also the Ru sites participate to methanol dehydrogenation [6]. Accordingly, the number of occupied sites in the CO and methanol desorption process becomes similar.

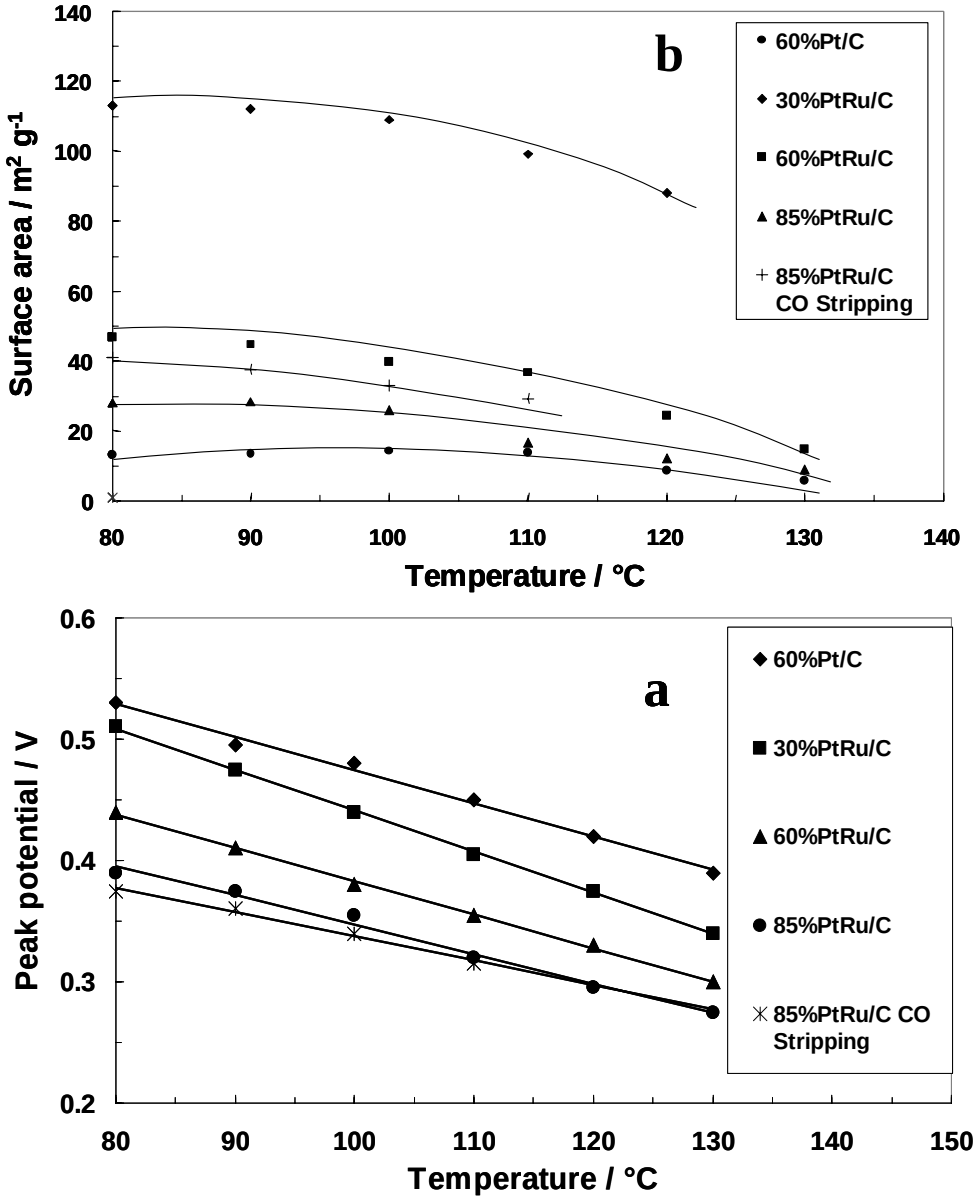

Fig. 9. Variation of the stripping peak potentials (a) and integrated methanol residues-CO stripping peak areas (b) as a function of temperature for various catalysts.

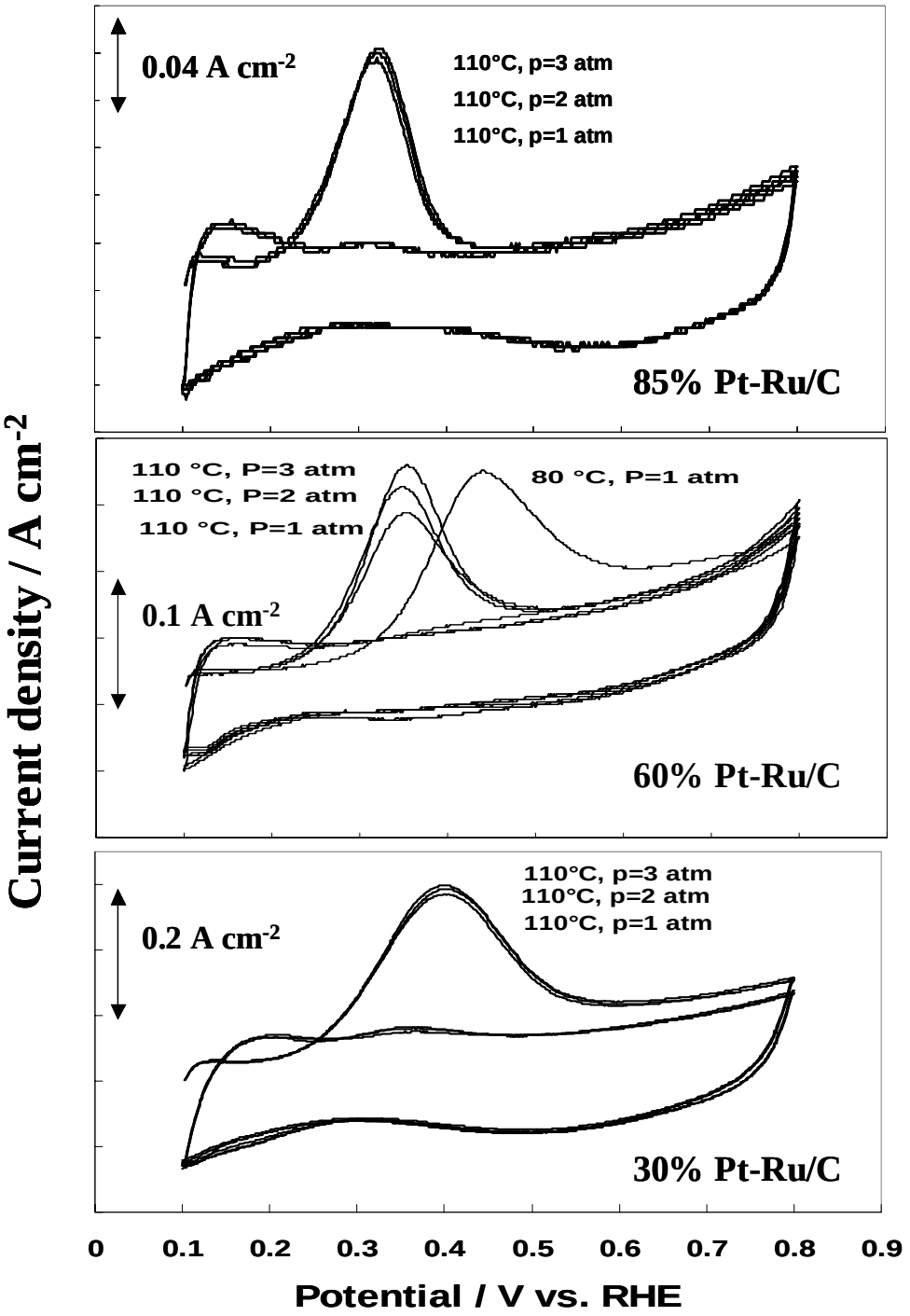

Fig. 10. In-situ methanol residues stripping voltammetry at the various carbon supported Pt-Ru catalyst/Nafion 117 membrane interface, at different pressures under DMFC configuration. Anode: 1 M methanol, adsorbed for 30 min; cathode: H_2 feed 1 atm. rel.

From a technical point of view it is interesting to investigate the influence of the anode compartment pressure on the stripping behaviour. Below 90°C, no effect of pressure is observed on the stripping behaviour (not shown). Similar evidence is observed for the 30% Pt-Ru/C catalyst at 110°C, whereas a slight influence is observed for the other catalysts at this temperature (Fig. 10). In the stripping voltammograms of the 60% Pt-Ru/C catalyst which shows the most significant influence, it is clearly evidenced that even at high pressure (3 atm), the coverage of methanolic residues is quite smaller than that observed for the same catalysts at 80 °C and 1 atm (Fig. 10).

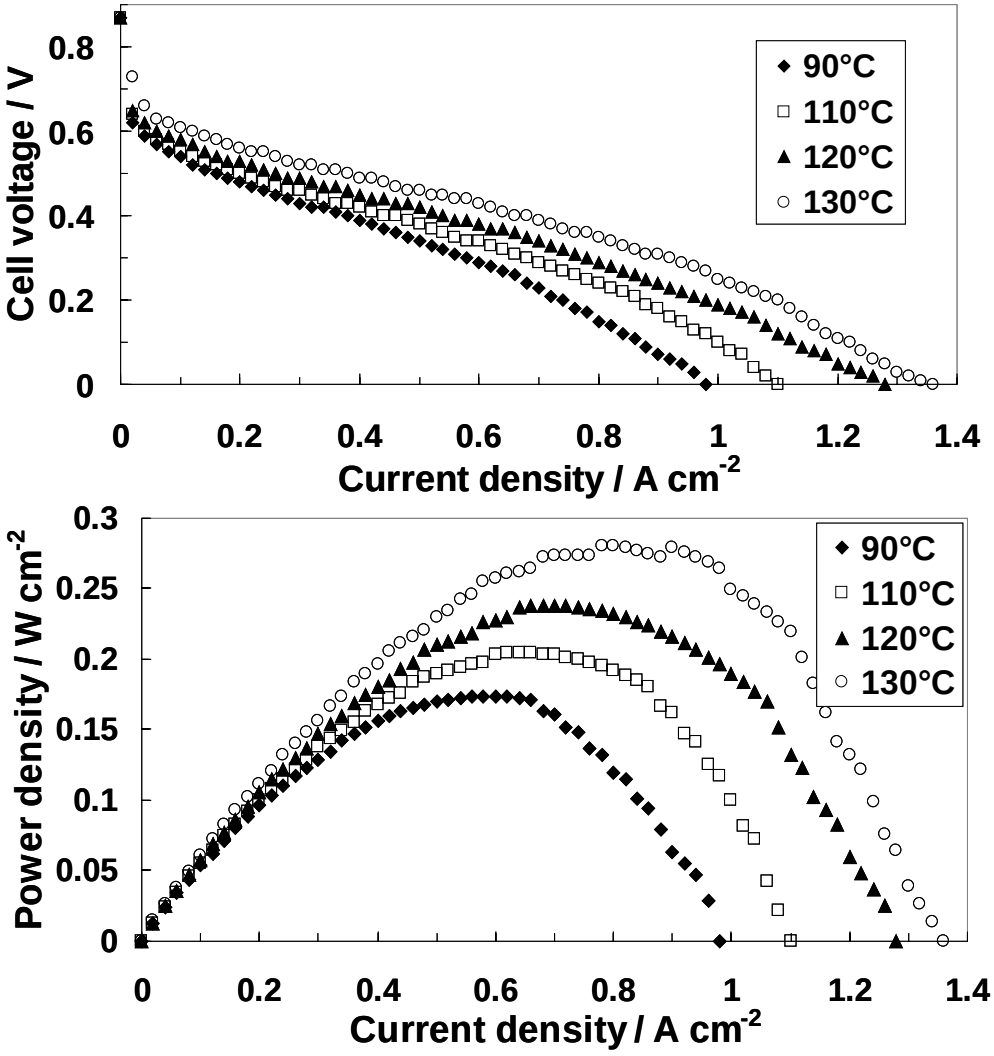

Fig. 11. DMFC polarization and power density curves at various temperatures for the assembly equipped with the 85% Pt-Ru/C anode catalyst; anode, 1 M methanol, 1 atm. rel.; cathode, air feed 2.5 atm.

Polarization and power density curves for the DMFC including the 85% Pt-Ru/C catalyst at anode show a significant increase of performance with temperature (Fig. 11). This is in good part related to the decrease of overpotential for the half cell anodic reaction as function of temperature (Fig. 12 a). The half cell polarization curves in Fig. 12a indicate that passing from 90 to 110 °C, the reaction rate is strongly enhanced. On the other hand, at higher temperatures the decrease of activation barrier for the reaction is counteracted by a significant decrease of coverage of reacting species. Thus, only a limited enhancement is recorded. This is in contrast with the results of the single cell polarization curves where a significant increase in DMFC performance is also registered in the high temperature range.

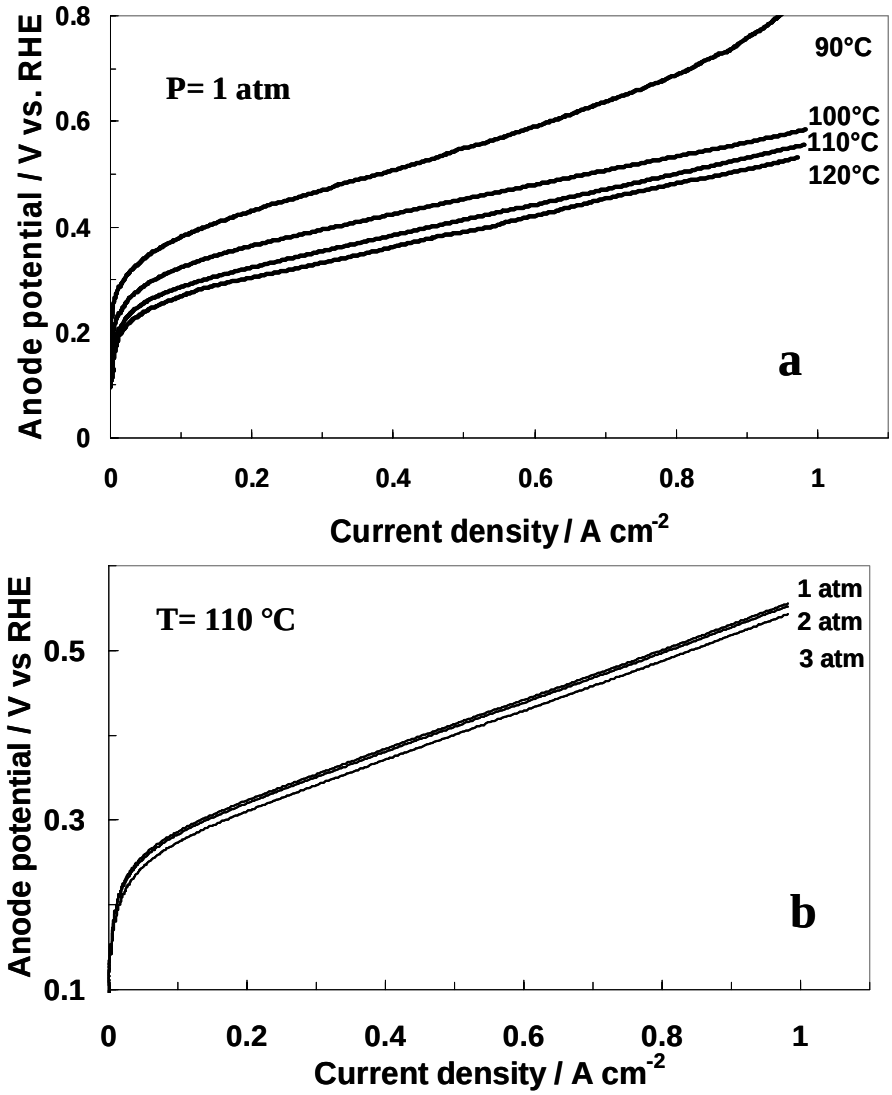

Fig. 12. Potentiodynamic anodic polarization curves for the 85% Pt-Ru/C catalyst/Nafion 117 interface at various temperatures (a) and pressures (b). Anode: 1 M methanol; cathode: H_2 feed 1 atm. rel.

Such enhancement can be hardly attributed to the electrolyte behaviour or to the water availability at the anode since the ohmic resistance does not decrease significantly in the range between 110° and 130 °C and the water is fed to the anode in a molar ratio with respect to methanol of about 54:1 (1M CH_3OH). A slight shift of the hydrogen reversible potential, used as reference electrode, with the temperature should be considered. However, passing from 110° to 130 °C the RHE varies only by about a few mV. Another effect is due to the enhancement of the cathode reaction by the increase in temperature. However, beside these aspects, it should be also considered the effect of the decrease of the coverage of methanolic residues on the cathode at high temperatures (Fig. 7). Thus, although methanol cross-over generally increases with temperature, its effects are less significant in terms of coverage and, consequently, the cathode is less poisoned. Such aspects are of particular relevance when the DMFC is operated with air feed. Due to the low oxygen partial pressure, methanol molecules crossing the membrane strongly compete with oxygen for the reaction sites. Accordingly, the increase of cell performance in the high temperature range in the presence of air feed may be due to an enhanced methanol tolerance at the cathode. Enhancement of mass transfer at high temperature should also be taken into account but these effects are observed only at very high current densities.

Fig. 12b shows that the anode pressure does not influence significantly the polarization curves; thus, the reaction rate does not appear altered. This is also accounted by the small variation of coverage as the anode pressure is changed, as previously observed in the stripping analysis. Generally, a high pressure in the anodic compartment is necessary to maintain good membrane humidification at high temperatures and low ohmic losses. Accordingly, DMFC operation at high anodic pressures above 100 °C produces beneficial effects only for membrane hydration.

By comparing the behaviour of the three different catalysts either in terms of single cell and half cell polarization curves at 90° and 120 °C (Figs. 13 and 14), it is derived that better performances are achieved for the catalyst showing both lower stripping peak potentials (as expected) but also lower coverage of methanolic residues. Thus, especially at 90 °C, the higher intrinsic catalytic activity (lower activation barrier) appears to be more relevant than the catalyst dispersion. The physico-chemical properties of the catalysts have less influence on the anode electrochemical behaviour at high temperatures (e.g. 120 °C) since CO poisoning is alleviated under such conditions. The variation in intrinsic activity for the present catalysts arises from the different bulk and surface properties. Higher degree of alloying and lower content of oxidation states (especially for Ru) have been recognised to

play a favourable role in enhancing the rate of methanol electro-oxidation [20, 23, 25]. Furthermore, in situ XANES spectroscopic analysis of a highly performing Pt-Ru/C catalyst has shown metallic characteristics under operation in reformate-air polymer electrolyte fuel cells [26]. The sharp profile of the methanol stripping peaks for the 85% Pt-Ru/C catalyst, compared to the other catalysts, would indicate that a single type reaction sites (i.e. Pt-Ru pairs in the alloy) is involved in the electrochemical process [27]. On the other hand, the broadened profile prevailingly observed for the 30% Pt-Ru/C catalyst, may indicate the participation to the process of both Pt-Ru alloy and Pt-RuOx as well as PtOx species.

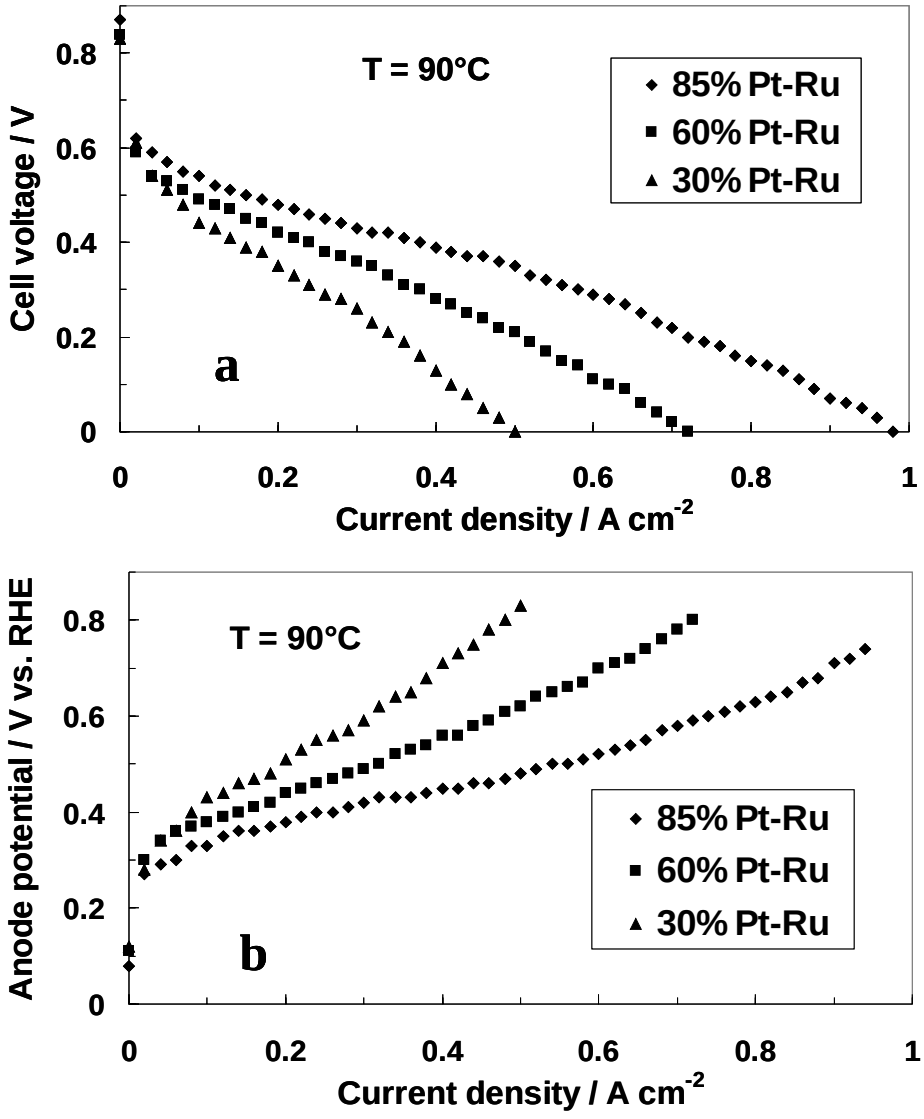

Fig. 13. DMFC single cell (a) and anodic half cell polarization behaviour (b) at 90 °C for various Pt-Ru/C catalysts. Anode: 1 M methanol, 1 atm. rel.; cathode: air feed 2.5 atm (a), H_2 feed 1 atm. rel. (b).

It would be of interest to synthesise Pt-Ru catalysts which associate high degree of dispersion to a prevailing metallic behaviour for the active phase; in this regard, the choice of carbon support and the preparation procedure for the deposition of the metal phase on the support may play an important role. To achieve this scope, one should select carbon supports and preparation procedures which do not favour the formation of a strong metal-support interaction through surface functional groups [28].

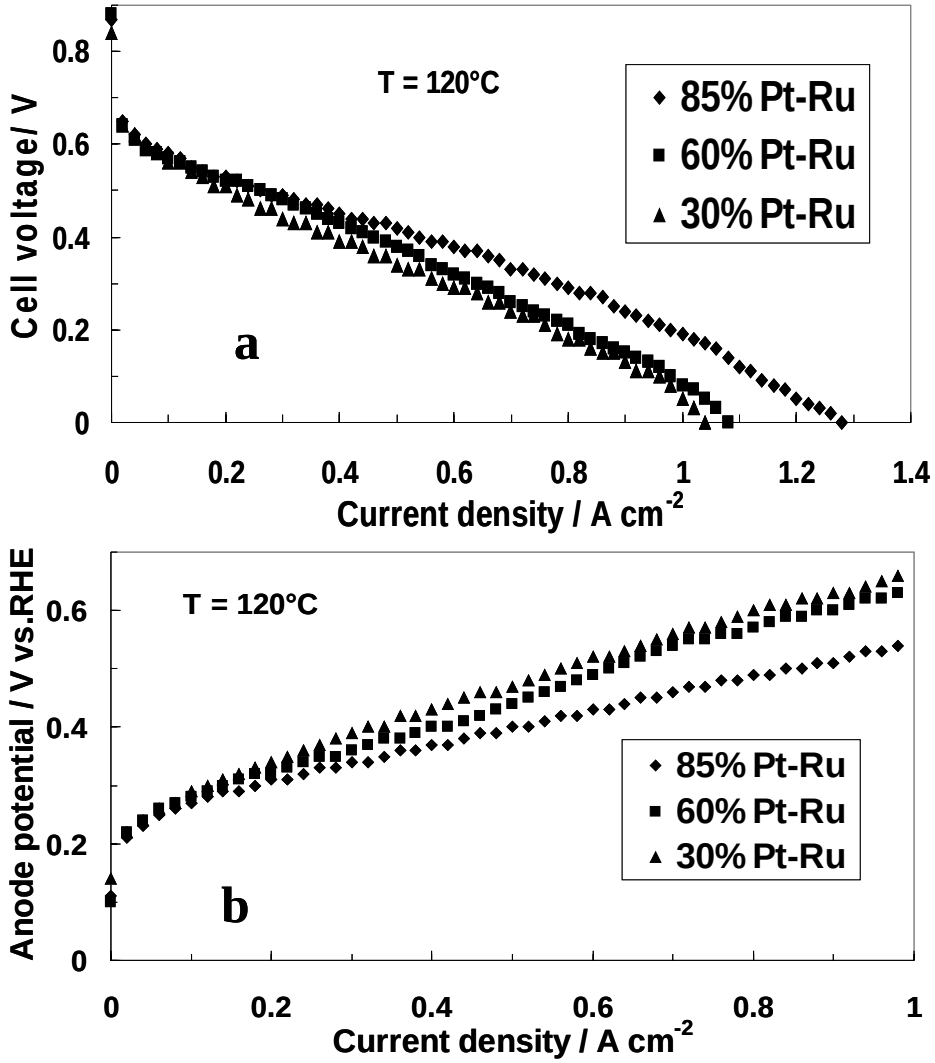

Fig. 14. DMFC single cell (a) and anodic half-cell polarization behaviour (b) at 120 °C for various Pt-Ru/C catalysts. Anode: 1 M methanol, 1 atm. rel.; cathode: air feed 2.5 atm (a), H_2 feed 1 atm. rel. (b).

II.2.4 References

[1] M. Neergat, D. Leveratto, U. Stimming, Fuel Cells 2 (2002) 25.

[2] M.K. Ravikumar, A.K. Shukla, J. Electrochem. Soc. 143 (1996) 2601.

[3] L. Liu, C. Pu, R. Viswanathan, Q. Fan, R. Liu, E.S. Smotkin, Electrochim. Acta 43 (1998) 3657.

[4] X. Ren, M.S. Wilson, S. Gottesfeld, J. Electrochem. Soc. 143 (1996) L12.

[5] A.S. Aricò, P. Creti, P.L. Antonucci, V. Antonucci, Electrochem. Solid-State Lett. 1 (1998) 66.

[6] A.S. Aricò, S. Srinivasan, V. Antonucci, Fuel Cells 1 (2001) 133.

[7] Z. Jusys, J. Kaiser, R. J. Behm, Electrochim. Acta 47 (2002) 3693.

[8] A.S. Aricò, P.L. Antonucci, E. Modica, V. Baglio, H. Kim, V. Antonucci, Electrochim. Acta 47 (2002) 3723.

[9] J. Wang, S. Wasmus, R.F. Savinell, J. Electrochem. Soc., 142 (1995) 4218.

[10] A.S. Aricò, E. Modica, E. Passalacqua, V. Antonucci, P.L. Antonucci, J. Applied Electrochem. 27 (1997) 1275.

[11] K.T. Adjemian, S.L. Lee, S. Srinivasan, J. Benziger, A.B. Bocarsly, J. Electrochem. Soc. 149 (2002) A256.

[12] M. Watanabe, S. Motoo, J. Electroanal. Chem. 60 (1975) 267.

[13] H.G. Petrow and R.J. Allen, U.S. Pat. 3, 992, 331 (1976).

[14] A.S. Aricò, P. Creti, H. Kim, R. Mantegna, N. Giordano and V. Antonucci, J. Electrochem. Soc. 143 (1996) 3950.

[15] J.F. Moulder, W.F. Stickle, P.E. Sobol, K.D. Bomben, Handbook of X-ray Photoelectron Spectroscopy, ed. Physical Electronics, Inc., ISBN: 0-9648124-1-X, Eden Prairie, Minnesota, USA (1995).

[16] A.S. Aricò, A.K. Shukla, K.M. el-Khatib, P. Creti, V. Antonucci, J. Appl. Electrochem., 29 (1999) 671.

[17] H.A. Gasteiger, P.N. Ross Jr., E. Cairns, J. Surf. Sci. 67 (1993) 293.

[18] W. Dmowski, T. Egami, K.E. Swider-Lyons, C.T. Love, D.R. Rolison, J. Phys. Chem. B 106 (2002) 12677.

[19] D.R. Rolison, P.L. Hagans, K.E. Swider, J.W. Long, Langmuir 15 (1999) 774.

[20] A.S. Aricò, G. Monforte, E. Modica, P.L. Antonucci, V. Antonucci, Electrochemistry Communications 2 (2000) 466.

[21] B. Gurau, R. Viswanathan, R. Liu, T.J. Lafrenz, K.L. Ley, E.S. Smotkin, E. Reddington, A. Sapienza, B.C. Chan, T.E. Mallouk, S. Sarangapani, J. Phys. Chem. B 102 (1998) 9997.

[22] C. Cattaneo, M.I. Sanchez de Pinto, H. Mishima, B.A. Lopez de Mishima, D. Lescano, L. Cornaglia, J. Electroanal. Chem. 461 (1999) 32.

[23] H.N. Dinh, X. Ren, F.H. Garzon, P. Zelenay, S. Gottesfeld, J. Electroanal. Chem. 491 (2000), 222.

[24] P. Waszczuk, A. Wieckowski, P. Zelenay, S. Gottesfeld, C. Coutanceau, J.-M. Léger, C. Lamy, J. Electroanal. Chem 511 (2001), 55.

[25] T. Iwasita, Electrochim. Acta 47 (2002) 3663.

[26] R. Viswanathan, G. Hou, R. Liu, S.R. Bare, F. Modica, G. Mickelson, C.U. Segre, N. Leyarovska, E.S. Smotkin, J. Phys. Chem. B 106 (2002) 3458.

[27] A.V. Tripkovic', K.D. Popovic', B.N. Grgur, B. Blizanac, P.N. Ross, N.M. Marcovic', Electrochim. Acta 47 (2002) 3714.

[28] A.S. Aricò, P.L. Antonucci, V. Antonucci in "Catalysis and Electrocatalysis at Nanoparticle Surfaces" edited by A. Wieckowski, E. R. Savinova and C. G. Vayenas, ISBN: 0-8247-0879-2, Marcel Dekker. Inc. New York USA (2003), p. 613.

II.3 Electrochemical analysis of high temperature methanol electro-oxidation at Pt-decorated Ru catalysts*

II.3.1 Introduction

Several drawbacks have hindered the large-scale diffusion of Direct Methanol Fuel Cells, in particular the significant cost of these devices. In fact, a large Pt loading in the electrodes (1-2 mg cm^{-2}) is needed to achieve suitable performances [1-3]. Less expensive methanol tolerant materials based on transition metal chalcogenides [4] or iron-cobalt organic macrocycles from the families of phenylporphyrins and phthalocyanines [5] have been proposed to replace Pt-based catalysts at the cathode. On the other hand, the presence of Pt appears to be necessary in the DMFC anode due to its excellent dehydrogenation properties at low temperatures. The electro-oxidation process of methanol to CO_2 occurs through an initial dehydrogenation step [3]. Low temperature methanol dehydrogenation is promoted by Pt or other high cost noble metal catalysts with similar properties e.g. Ir, Pd [6]. Previous attempts to replace Pt in DMFC anodes with non-noble metal catalysts have not allowed to achieve performances compatible with the commercialisation requirements [7,8]. Alternatively, a multilayer sputtering process has been investigated to reduce the Pt content in the DMFC electrodes [9]. Ultra-low Pt loading electrodes (Pt content $\leq$ 0.1 mg cm^{-2}) have been successfully developed for H_2-air PEMFCs [10-11]; yet, their stability in presence of significant CO contents in the anode stream has still to be demonstrated. An interesting approach has been recently proposed to reduce the Pt loading in PEMFCs anodes by depositing a Pt submonolayer on Ru nanoparticles [12]. This class of catalysts, including also Pt samples containing Ru submonolayers on the surface [13], has shown good potentialities even in presence of reformate-gas feed but no attempts have been made to investigate their behaviour in DMFCs.

As opposite of PEMFCs, DMFCs devices being fed with significant amounts of water at the anode (1M methanol in water) can be suitably operated up to 130 °C with a certain number of polymer membranes without significant dehydration effects [14]. Operation at 130 °C is considered ideal for application of these devices in transportation and it allows to enhance the methanol oxidation rate [3]. In the present study, we have investigated the high temperature performance of DMFCs based on Pt-decorated unsupported Ru anode catalysts.

* A paper based on this study has been published on **Electrochemistry Communications 6 (2004) 164-169**

These catalysts may represent a possible approach to significantly reduce the Pt content in the anode. As first attempt, we have achieved at 130 °C performances about 35% lower than the state of art commercial Pt-Ru (1:1)/C catalysts (2 mg Pt cm^{-2}), despite of the fact that the Platinum loading in the decorated catalyst-based electrode was 20 times smaller (i.e. 0.1 mg cm^{-2}). To get insights into the properties of the decorated catalyst with respect to conventional carbon supported Pt-Ru alloy and unsupported Ru catalysts we have in-situ investigated their electrocatalytic activity by adsorbed methanolic residues stripping voltammetry [15].

II.3.2 Experimental

Three anode catalyst formulations have been investigated for methanol oxidation. A 2 wt.% Pt-decorated unsupported Ru catalyst was prepared in-house by impregnation of an amorphous Ru-oxide with a diluted 1mM H_2PtCl_6 solution and successive reduction of the impregnated catalyst in a hydrogen stream. An unsupported Ru catalyst without Pt impregnation was prepared using the same procedure and investigated for comparison. The amorphous Ru-oxide was prepared by dissolving a Ru-sulphite precursor in a diluted H_2SO_4 solution and subsequently decomposing the sulphite complex by H_2O_2 addition to form a colloidal suspension of RuOx particles. The pH was thus adjusted to allow the complete precipitation of amorphous RuOx particles. A 60 wt.% Pt-Ru (1:1)/Vulcan XC 72 anode catalyst was purchased from E-TEK (USA). For the oxygen reduction reaction, a 30 wt.% Pt/Vulcan XC 72 was purchased from E-TEK and was used as cathode in all experiments.

X-ray diffraction powder (XRD) patterns of the anode catalysts were obtained on a Philips X'Pert X-ray Diffractometer using a CuK_α-source. The analysis was made by using a grazing angle set-up to enhance the X-ray scattering from the sample surface. Bulk X-ray fluorescence analysis of the catalysts was carried out by a Bruker AXS S4 Explorer spectrometer. TEM analysis was carried out by a Philips CM12 microscope. The electrodes and membrane-electrode assemblies (MEAs) were prepared according to the procedure described in a previous paper [16]. The Pt loading was 2 mg cm^{-2} in the electrodes based on commercial 60% Pt-Ru/Vulcan XC anode and 30% Pt/ Vulcan-XC cathode catalysts. Whereas, the Pt loading was 0.1 mg cm^{-2} in the 2% Pt decorated unsupported Ru. The Ru loading in the bare unsupported Ru catalyst used for comparison was 4.9 mg cm^{-2}. A Nafion 117 membrane was used as electrolyte. In single cell polarization experiments, preheated aqueous methanol (1M) was fed to the anode chamber of DMFC whereas humidified air, pre-heated at 100°C, was fed to the cathode. The pressure in the anode compartment was

varied between 1 and 2 atm. rel. as the temperature was increased from 90° to 130 °C; whereas, it was fixed at 2.5 atm in the cathode compartment. Stripping voltammetry of adsorbed methanolic residues and carbon monoxide has been carried out as described in Ref. [15]. The pressure in the anode and cathode compartment was maintained fixed at 1 atm.

II.3.3 Results and Discussion

The Pt/Ru atomic ratio in the commercial and in-house made Pt decorated catalysts was determined by using Pt Mα and Ru Lα emission lines in the XRF spectra (Fig. 1) after proper calibration with standard samples.

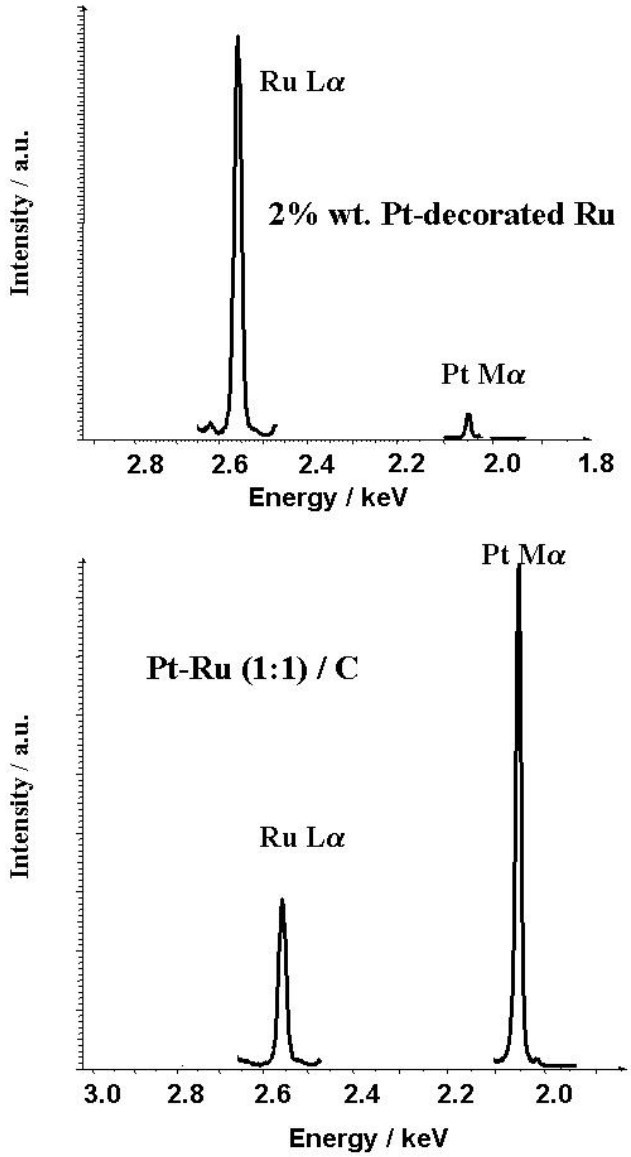

Fig. 1. XRF spectra of Pt-decorated unsupported Ru and Pt-Ru (1:1)/C catalysts.

Fig. 2 shows a comparison between the XRD patterns of the reduced bare unsupported Ru and Pt-decorated catalyst. Both Pt and Ru in the catalysts are in the metallic form. The fcc crystallographic structure of Pt (continuous lines in Fig. 2) is overlapping to the hexagonal structure of unsupported Ru (dashed lines). The presence of sharp peaks for the Pt fcc structure indicates large crystallite size for Pt particles whereas the Ru peaks are more broadened. An estimation of the Pt particle size is not possible from this analysis due to the convolution of Pt and Ru peaks belonging to different crystallographic phases. The XRD pattern of the commercial Pt-Ru/C catalyst is reported in Ref. [15]. This sample is characterised by the presence of a Pt-Ru alloy. Transmission electron micrographs of the bare unsupported Ru and Pt decorated catalysts are shown in Fig. 3a-b; a micrograph of the commercial 60% Pt-Ru/C catalyst is reported in Ref. [15]. A dispersion of fine particles is shown in the bare unsupported Ru catalyst with a mean particle size of about 30 Å. These particles form agglomerates with suitable porous structure. In the 2% Pt/Ru catalyst (Fig. 3b), it is observed that the Pt particles decorate the edges of large Ru agglomerates. In this latter case the average size of Pt particles is about 70 Å. A clear identification of the Pt particles is allowed by measuring the Pt (111) lattice distances at high magnification.

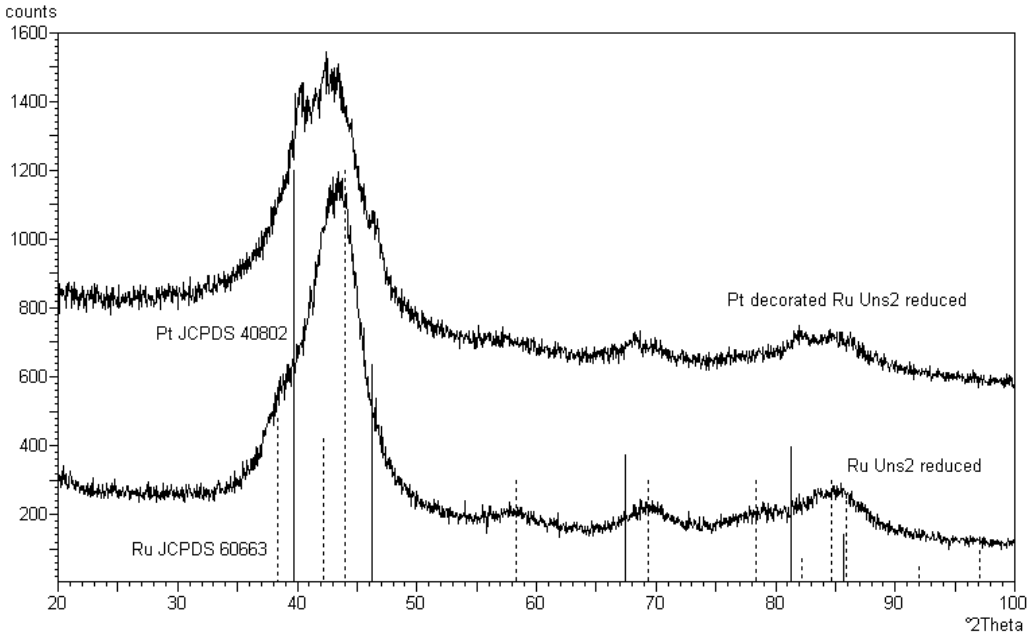

Fig. 2. XRD spectra of Pt-decorated Ru (a) and bare unsupported Ru (b) catalysts. Dashed lines indicate the reflections from the Ru hexagonal structure.

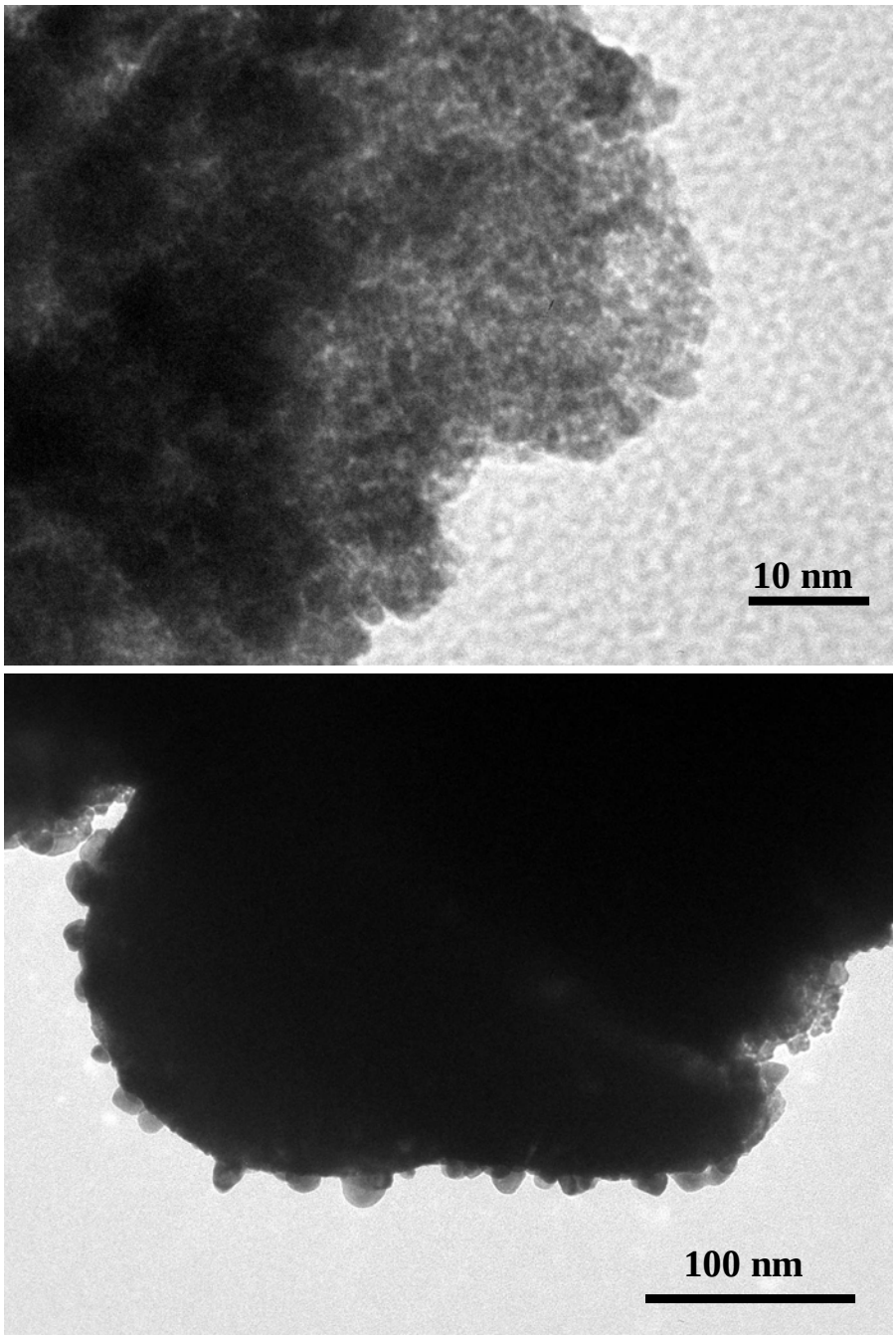

Fig. 3. Transmission electron micrographs of bare unsupported Ru (a) and Pt-decorated Ru (b) catalysts.

Fig. 4 shows the galvanostatic polarization curves for the DMFC based on the unsupported Ru catalyst decorated with Pt (2 wt.%) at different temperatures. Open circuit voltage and performance significantly increase with an increase of the operating temperature. It is derived that the methanol electro-oxidation reaction on the Pt decorated catalyst is strongly activated by the temperature. It has been reported that the methanol dehydrogenation at low temperature occurs mainly on Pt sites; whereas, Ru sites start to participate to the dehydrogenation process as the temperature is increased [17].

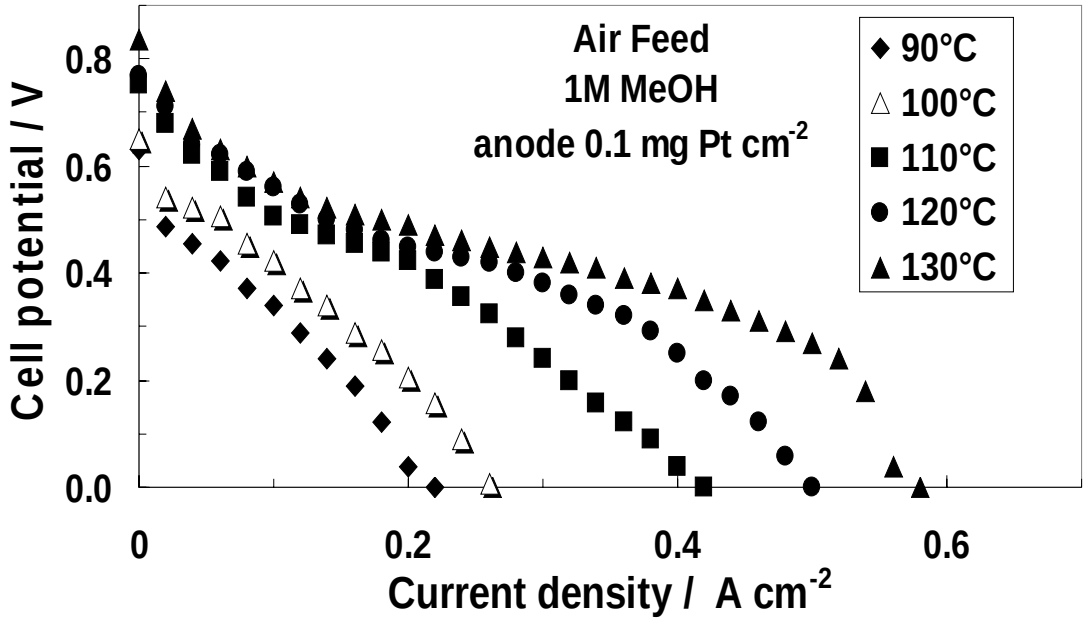

Fig. 4. DMFC single cell polarizations at various temperatures for the Pt-decorated unsupported Ru catalyst. Anode: 1 M methanol, 1-2 atm. rel.; cathode: air feed 2.5 atm.

A comparison of the DMFC polarization curves for unsupported Ru, Pt-decorated and commercial Pt-Ru/C catalysts at 130 °C is reported in Fig. 5. The Pt loading in decorated catalyst based anode was 0.1 mg cm^{-2}, i.e. 20 times lower than the loading usually used with conventional PtRu/C catalysts (i. e. 2 mg cm^{-2}). The Ru content was 4.9 mg cm^{-2}. The commercial cathode catalyst had 2 mg cm^{-2} Pt loading. The Pt decorated-Ru catalyst with 0.1 mg cm^{-2} Pt loading achieved about 150 mW cm^{-2} maximum power density (Fig. 5), which is not significantly lower than that achieved by the commercial Pt-Ru (1:1)/C catalyst with 2 mg Pt cm^{-2} (i.e. 230 mW cm^{-2}) under similar conditions, despite the fact that the Pt loading was 20 times less. The performance of the bare unsupported Ru (50 mW cm^{-2}) was significantly lower than that of the decorated catalyst. This clearly indicates a promoting effect of the decorating Pt particles in enhancing the performance.

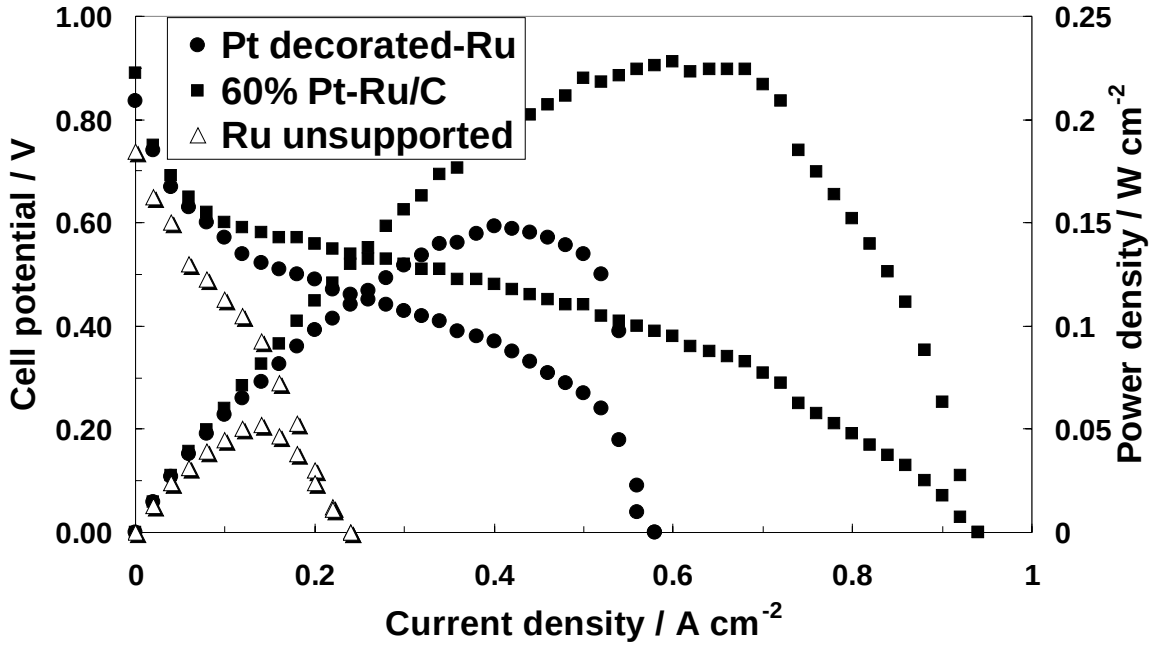

Fig. 5. DMFC single cell polarizations at 130 °C for commercial Pt-Ru/C, Pt-decorated and bare unsupported Ru catalysts. Anode: 1 M methanol, 2 atm. rel.; cathode: air feed 2.5 atm.

The adsorbed methanolic residues stripping voltammetry results for the three investigated anode catalysts are shown in Fig. 6. The decorated catalyst shows more positive stripping potentials with respect to the carbon supported Pt-Ru alloy (60% Pt-Ru/C) and close to the bare unsupported Ru. This indicates a lower intrinsic catalytic activity with respect to the Pt-Ru alloy. But, the stripping charge decreases much more significantly with the temperature in the carbon supported Pt-Ru alloy than in the decorated catalyst. In effect, the stripping charge is significantly larger in the decorated catalyst than in the Pt-Ru/C as well as in the unsupported Ru catalyst at high temperatures. The anodic shift of the stripping potential for methanolic residues adsorbed on the surface of the decorated and bare unsupported Ru catalysts with respect to the carbon supported Pt-Ru alloy reflects a stronger adsorption strength in the latter two catalysts for the CO-like species.

In order to get information on the catalyst dispersion, the low temperature (80 °C) carbon monoxide stripping behaviour was investigated. In fact, it is known that the coverage of carbon monoxide on Pt-Ru catalysts decreases as the temperature is increased [15]. The CO stripping profiles (not shown) were similar to those related to the removal of methanolic residues. The charge associated with the stripping of adsorbed CO molecules and methanolic residues for the investigated catalysts is reported in Table 1. The stripping charge in the CO

chemisorption process is from 10 to 20% larger than that associated with the stripping of methanolic residues, as previously reported for Pt-Ru alloys [15]. Assuming that adsorbed CO molecules are linearly bonded to both Pt and Ru sites [18], the catalyst dispersion is calculated as the ratio between the number of sites involved in the low temperature CO electro-chemisorption process and the total number of Pt and Ru atoms in the electrode. Interestingly, the calculated catalyst dispersion is similar for the three samples. This result is explained by the large contribution of the surface Ru atoms in the decorated and unsupported Ru catalysts to the CO chemisorption.

	60% Pt-Ru/C E-TEK	Pt-decorated Ru	Ru unsupported
Adsorbed methanolic residues stripping charge (80°)	130 $C \cdot g^{-1}_{Pt+Ru}$	179 $C \cdot g^{-1}_{Pt+Ru}$	173 $C \cdot g^{-1}_{Ru}$
Adsorbed methanolic residues stripping charge (120°)	68 $C \cdot g^{-1}_{Pt+Ru}$	170 $C \cdot g^{-1}_{Pt+Ru}$	130 $C \cdot g^{-1}_{Ru}$
Adsorbed carbon monoxide stripping charge (80°)	145 $C \cdot g^{-1}_{Pt+Ru}$	218 $C \cdot g^{-1}_{Pt+Ru}$	199 $C \cdot g^{-1}_{Ru}$
Catalyst dispersion as determined from CO adsorption at 80 °C	11%	11%	10%

Table 1. Stripping charge of CO-like residues and catalyst dispersion

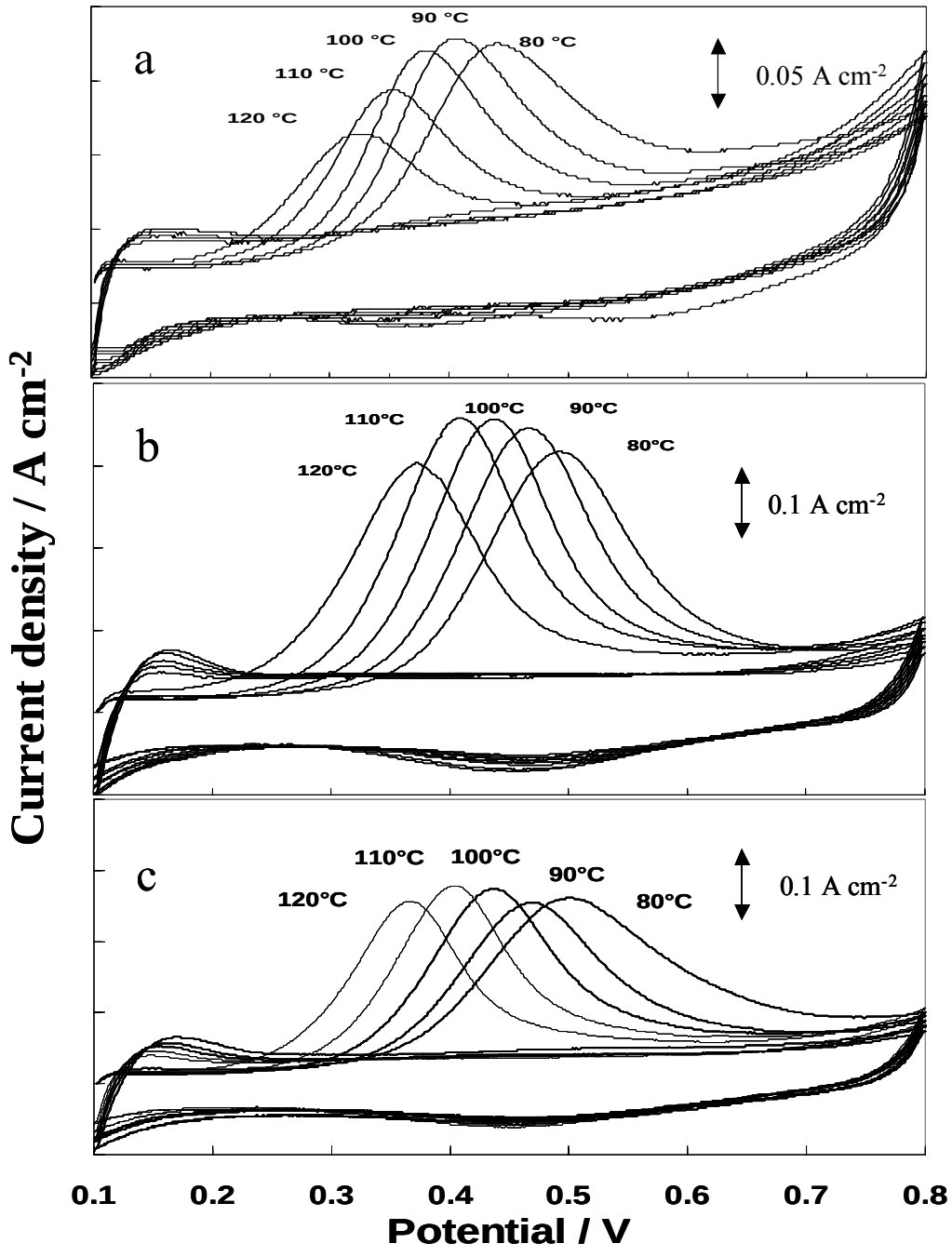

Fig. 6. In-situ methanol residues stripping voltammetry for commercial Pt-Ru/C (a), Pt-decorated (b) and bare unsupported Ru (c) catalysts, at various temperatures under DMFC configuration. Anode: 1 M methanol, 1 atm. rel. adsorbed for 30 min; cathode: H_2 feed 1 atm. rel.

Lin et al. [18] observed in their FTIR experiments a shift towards higher frequencies for the CO stretching on Pt-Ru alloys with respect to bare Pt and Ru metals. This effect has been attributed to a lower chemisorption energy for CO on the Pt-Ru alloy. Frelink et al. [19] measured the stretching frequency of linearly bonded CO as a function of coverage for the Pt and Pt-Ru electrodes. A shift to higher frequencies at various coverages was observed as a result of change in the CO binding strength to the surface induced by Ru through a ligand effect on Pt [19]. Accordingly, the Pt-Ru alloy favours the formation of less strongly adsorbed CO. On the other hand the bare Ru catalyst is not so active as Pt towards methanol dehydrogenation. It is known from the literature that the methanol dehydrogenation on Ru sites is strongly activated by the temperature [17], but the present results indicate a lower intrinsic catalytic activity even at 130 °C. Effectively, the affinity of Ru sites towards oxygen species is significantly larger than for methanol whereas different seems to be the case for CO-like species or methanolic residues. CO-like species may compete at the same extent of oxygen species for the adsorption on Ru sites [3,6]. Thus, it appears that the Pt particles localised on the surface of the Ru agglomerates promote the dehydrogenation of methanol with a consequent migration of the so formed methanolic residues (CO-like species) on the Ru sites. This latter phenomenon is probably activated by the temperature as it was above envisaged from the analysis of polarization curves. The superior performance of the decorated catalyst with respect to bare Ru, despite of the similar methanolic residues stripping potentials, mainly relies on the better dehydrogenation properties of Pt. However, a contribution may be due to the larger CO-like species coverage at high temperature (Table 1). In fact, differently from the reformate gas electro-oxidation process, where adsorbed CO-like species constitute a poisoning agent [20, 21], in the methanol electro-oxidation they are the intermediate species formed in the fuel oxidation process [22]. Accordingly, the electro-oxidation rate is directly proportional to their coverage on the surface [23]. Thus, if the adsorption strength is similar, a suitable coverage of intermediate species may increase the reaction rate.

II.3.4 Conclusions

Suitable DMFC performances have been achieved in presence of ultra-low Pt loading in the anode at high temperatures. Twenty times reduction of the Pt loading in the anodes produces a loss of power density of about 35%. From the point of view of intrinsic catalytic activity the Pt-Ru/C alloy appears to be superior to the decorated catalysts; however, the

effect of Pt decoration is to significantly enhance methanol dehydrogenation and consequently to increase the steady-state coverage of methanolic residues on the catalyst surface. The present results indicate that, being the methanol electro-oxidation governed by surface phenomena, catalysts containing small amounts of Pt nano-particles on the surface of a less expensive metal, which participate to the reaction, may represent a useful approach to reduce the incidence of the catalyst on the cost of DMFC devices.

II.3.5 References

[1] M. Neergat, D. Leveratto, U. Stimming, Fuel Cells 2 (2002) 25.

[2] X. Ren, M.S. Wilson, S. Gottesfeld, J. Electrochem. Soc. 143 (1996) L12.

[2] A.S. Aricò, S. Srinivasan, V. Antonucci, Fuel Cells 1 (2001) 133.

[4] N. Alonso-Vante, H. Tributsch, Nature (London) 323 (1986) 431.

[5] G. R. Sun, J. T. Wang, R. F. Savinell, J. Appl. Electrochem. 28 (1998) 1087.

[6] S. Wasmus and A. Kuver, J. Electroanal. Chem. 461 (1999) 14.

[7] C. C. Hays, R. Manoharan, J. B. Goodenough, J. Power Sources 45 (1993) 291.

[8] T. Shobha, C. L. Aravinda, L. Gomathi Devi, S. M. Mayanna, J. Solid State Electrochem. 7 (2003) 451.

[9] C. K. Witham, W. Chum, T. I. Valdez, S. R. Narayanan, Electrochem. Solid-State Lett., 3 (2000) 497.

[10] M. S. Wilson, S. Gottesfeld, J. Electrochem. Soc. 139 (1992) L45.

[11] G. Sasi Kumar, M. Raja and S. Parthasarathy, Electrochim. Acta 40 (1995) 285.

[12] S. R. Brankovic, J. X. Wang, R.R. Adzic, Electrochem. Solid-State Lett. 4 (2001) A217.

[13] W. Chrzanowski and A. Wieckowski, Langmuir 15 (1999) 4944.

[14] A.S. Aricò, V. Baglio, A. Di Blasi V. Antonucci, Electrochem. Commun. 5 (2003) 862.

[15] A.S. Aricò, V. Baglio, A. Di Blasi, E. Modica, P.L. Antonucci and V. Antonucci, J. Electroanal. Chem, 557 (2003) 167.

[16] A. S. Aricò, A. K. Shukla, K. M. el-Khatib, P. Cretì, V. Antonucci, J. Appl. Electrochem. 29 (1999) 671.

[17] H. A Gasteiger, N. Markovic, P. N. Ross, Jr., E. J. Cairns, J. Electrochem. Soc. 141 (1994) 1795.

[18] W. F. Lin, T. Iwashita, W. Viestich, J. Phys. Chem. 103 (1999) 3250.

[19] T. Frelink, W. Visscher, J.A.R. van Veen, Langmuir 12 (1996) 3702.

[20] T. J. Schmidt, H. A. Gasteiger and R. J. Behm, Electrochem.Commun. 1 (1998) 1.

[21] A. M. Castro Luna, G. A. Camara, V. A. Paganin, E. A. Ticianelli, E. R. Gonzalez, Electrochem. Commun. 2 (2000) 222.

[22] H. N. Dinh, X. Ren, F. H. Garzon, P. Zelenay and S. Gottesfeld, J. Electroanal. Chem. 491 (2000) 222.

[23] J.-M. Léger, Proceedings of the Workshop "Electrocatalysis in Indirect and Direct Methanol PEM Fuel Cells", (Eds. C. Lamy and H. Wendt), Sept. 12-14 Portoroz, Slovenia 1999, p. 9.

CHAPTER III

MEMBRANES DEVELOPMENT AND CHARACTERIZATION

III.1 Influence of the acid-base characteristics of inorganic fillers on the high temperature performance of composite membranes in direct methanol fuel cells*

III.1.1 Introduction

In recent years increasing interest has been devoted to the development of high temperature proton conducting polymer electrolyte fuel cell systems [1-7]. A low cost and high temperature membrane, with suitable ionic conductivity and stability up to 150 °C, would be a potential solution to some of the drawbacks presently affecting reformate-fuelled polymer electrolytes (PEMFCs) as well as direct methanol fuel cells (DMFCs). Fuel cell operation at elevated temperatures will limit the effects of electrode poisoning by adsorbed CO molecules, increase both methanol oxidation and oxygen reduction kinetics and reduce water and thermal managements. Furthermore, the high temperature operation will reduce the complexity of the reforming reactor employed for PEMFCs [2,6]. An operating range between 130° and 150 °C would be ideal for application of these systems in electric vehicles and for distributed power generation. These devices would not require, in any case, prolonged start-up and shut-down cycles and they may operate with suitable efficiency and performance.

Various polymer electrolyte materials have been proposed for high temperature operation. Differentiation into two categories can be made on the basis of the water-presence requirements for the proton conduction [1,3]. Polymer electrolytes involving water molecules in the proton mobility mechanism (e.g. perfluorosulfonic membranes) need humidification to maintain or increase the conductivity characteristics. The level of humidification may vary

* Three papers based on this study have been published on **Solid State Ionics 161 (2003) 251-265**, **Electrochemistry Communications 5 (2003) 862-866**, **J. Power Sources 128 (2004) 113-118**

depending on the operating temperature, membrane properties and it influences size and complexity of the device. Some other electrolytes which do not necessarily involve water molecules in the mechanism of proton conduction (e.g. PBI/H_3PO_4 [5], blends of PBI and polysulfone [8], hybrids of polymers and proton conducting inorganic compounds such as $Zr(HPO_4)_2$ [4] etc.) do not strictly need humidification. Yet, some aspects related to the short-term stability of such systems, problems of phosphoric acid leakage, poor extension of the three-phase reaction zone inside the electrodes, reduced conductivity levels for inorganic proton conductors have moderated the enthusiasm related to the development of water-free protonic electrolytes. Alternatively, composite perfluorosulfonic membranes based on recast Nafion® containing hygroscopic ceramic oxides have been demonstrated to operate up to about 150 °C both in direct methanol [6,9] and hydrogen-air [2,10,11] polymer electrolyte fuel cells with reduced preheating temperature for the reactants (85 °C). As opposite, bare or recast Nafion membranes without ceramic fillers may operate only up to 130 °C [6] under elevated pressures (4 atm abs.) and with higher reactants preheating temperature (120-140 °C).

The presence of hygroscopic inorganic oxides inside the composite membrane enhances water retention at high temperatures extending the operation range of perfluorosulfonic membranes (e.g. Nafion®) and reduces the cross-over effects [6] which are particularly serious at high temperature in DMFC systems. Yet, these membranes require significant operating pressures for both anode and cathode compartments to maintain a suitable content of liquid water inside the assembly. Cathode operation at high pressure reduces system efficiency because of power consumption by the air compressor, whereas less remarkable is the power loss for the liquid pump at the anode. The high pressure requirement, is actually the main feature limiting a wide diffusion of such composite electrolytes.

Significant progress has been achieved, in the last few years, on the development of composite membrane based systems [6,9]. Yet, most of the efforts have been addressed to technical aspects and limited attention has been devoted to an in-depth analysis of the basic operation mechanism of such materials. A better understanding of the effects enhancing the proton conductivity at 150 °C in these hybrid-membrane systems could suggest new routes to enhance conductivity and reduce pressure requirements.

In the present study, various composite membranes based on recast Nafion containing inorganic nanoparticle fillers (SiO_2, phosphotungstic acid-impregnated SiO_2, ZrO_2, Al_2O_3) varying by their surface chemistry and acid-base characteristics have been prepared and investigated in DMFC devices. It has been observed that the surface acid-base properties of

the inorganic fillers play a fundamental role in determining the conductivity characteristics at high temperature and fuel cell performance. Appropriate tailoring of the surface chemistry in these nanoparticles appears to be a key step to enhance water retention at high temperature.

III.1.2 Experimental

SiO_2, b Al_2O_3 and n Al_2O_3 ceramic oxide fillers have been purchased from Cabot, Aldrich and Baker, respectively. ZrO_2 was synthesized at Rome Tor Vergata University [12] and SiO_2-PWA (phosphotungstic acid) was prepared as described in Ref. [9]. X-ray diffraction analysis (XRD) of the fillers was carried out on a Philips X'Pert diffractometer equipped with a CuKα X-ray source. Transmission electron microscopy (TEM) was carried out on a Philips CM12 microscope equipped with LaB_6 filament. XRF analysis was carried out by a Bruker S4 Explorer Instrument. BET surface area measurements in the inorganic fillers were made by a Thermoquest 1990 series Sorptomatic. The fillers were compacted into pellets at 50 Mpa and completely degassed in a sample holder at 160 °C under vacuum before the measurement. The pH of slurry was measured at room temperature by an ATC compensated pH probe (Orion). The slurry was composed by 0.5 g powder per 0.1 l of bi-distilled water. The slurry was stirred for about 24 hrs. in presence of nitrogen bubbling to obtain a steady-state pH value. Potentiometric titrations of the inorganic fillers were carried out following the procedures reported in Ref. [13]. A Metrohm automated titration system equipped with an ATC compensated pH probe was used. The inorganic powder was suspended in an aqueous electrolyte (KNO_3, 0.1 M) and continuously stirred in presence of N_2 purging. A defined amount of KOH (0.1 N) was added for each sample and the slurry back-titrated with HNO_3 (0.1 N). The steady-state pH value was measured per each addition of HNO_3.The acid-base surface functional groups were determined from these measurements by the WinZPC software (Costech International). X-ray photoelectron spectroscopy (XPS) measurements were performed by using a Physical Electronics (PHI) 5800-01 spectrometer. A monochromatic Al Kα X-ray source was used at a power of 350 W. Spectra were obtained with pass energy of 11.75 eV. The Ag $3d_{5/2}$ peak of an Ag foil was taken, after argon sputtering, for checking the calibration of the binding energy (B.E.) scale. FTIR measurements were carried out in the transmission mode on a Bruker Equinox 55 spectrometer by diluting the filler powder (1% wt.) in a KBr pellet. Operating conditions were 2 cm^{-1} resolution, 32 accumulating sweeps and high sensitivity DLATGS detector.

The membranes were prepared by using a recast procedure described in Ref. [6]. The maximum temperature reached during the membrane preparation was 160 °C. The thickness of the membranes was about 100 μm. Small angle X-ray scattering (SAXS) analysis on the membranes was carried out by using a diffractometer equipped with CuKα source and Kratky chamber. The samples were analysed both in dry form (under vacuum) and immersed in water in a sample holder at room temperature. The Kratky chamber was always maintained under vacuum. Wide angle X-ray scattering (WAXS) analysis on the dried membranes was carried out on a X'Pert diffractometer.

Water retention/uptake properties of the various membranes were investigated in the temperature range from 155° to 45°C by using a method similar to that developed by Kreuer et al. [14] to investigate the hydration behaviour of high temperature inorganic proton conductors. Accordingly, the membranes were heated in the measurement crucible of a Netzsch TG/DSC/DTA analyser under constant R.H. (30%) up to 155 °C (sweep rate 10°C/ min) and left at this temperature for 10 min. No further weigh loss was recorded in the last minutes of such treatment at 160 °C. The temperature was thus decreased at constant sweep rate (2°C/ min), under 30% R.H., up to 45° and the mass increment due to the water uptake was measured by the thermobalance for each sample. Pulse-field-gradient nuclear magnetic resonance (PFG-NMR) experiments were performed on some selected membranes in the temperature range up to 140 °C in order to determine the self-diffusion coefficients of water. The membranes were firstly swelled in water at room temperature; they were then removed from water, the surface was dried with a paper tissue and loaded in a sample holder where they were allowed to equilibrate under constant R.H. (30%) for 48 hrs at 20 °C. The sample holder was then sealed and measurements were performed with a Varian 400 spectrometer. The stimulated spin-echo pulse sequence $\pi/2$-G(δ) -$\pi/2$-τ- G(δ)-(echo) was used to probe the water mobility.

Membrane and electrode (M&E) assemblies were prepared following the procedure described in Ref. [6]. Fuel cell experiments were carried out in a 5 cm^2 single cell (GlobeTech, Inc.). 2M aqueous solution of methanol and oxygen were preheated at 85°C and fed to the cell. The catalyst employed for methanol oxidation was a 60% Pt-Ru (1:1)/Vulcan XC (E-TEK), whereas a 30% Pt/Vulcan XC (E-TEK) was used for oxygen reduction. The platinum loading for all the electrodes was 2 mg cm^{-2}. Cell resistance measurements under fuel cell operation have been carried out by the current interrupter method using a digital memory oscilloscope.

III.1.3 Results and discussion

The inorganic fillers selected for the composite membranes are characterized by different chemistry and acid-base behaviour (Table 1). Silica and zirconia oxides are acidic in nature, whereas, alumina oxides are characterized by basic (b Al_2O_3) and neutral (n Al_2O_3) properties on the surface. To extend the acid-base range of the present investigation, PWA was adsorbed on the silica surface [9]. The PWA compound is known to possess superacid behaviour and its use as electrolyte in fuel cells has already been investigated [15]. The acid-base properties of the inorganic oxides are mainly determined by the number (concentration) and strength of functional groups present on their surface (Table 1) as determined by the potentiometric titrations; no relationship is envisaged between BET surface area and concentration of acid-base surface groups in these inorganic fillers (Table 1). The surface characteristics of most of the selected oxides are known from the literature since they find wide application as catalyst supports in heterogeneous catalytic reactions. Silica surface is mainly characterized by the presence of silanol (-Si-OH) and siloxane (-Si-O-Si) groups with the first having higher acidic strength [16]. Similar surface characteristics are present on the alumina [17]; ZrO_2 surface is characterized by surface defects often saturated by strongly bonded hydrogen forming OH species [18]. In the case of alumina, the relative concentration of OH groups and bridge-bonded oxygen species imparts prevailingly acid or basic characteristics [17], whereas, significantly high acidic strength of the silanol groups mainly imparts acid properties to silica. However, structural effects as well as the chemical environment surrounding the functional groups may influence the polarization of the O-H bond as well as the electron-accepting or donation characteristics (Lewis acid-base behaviour) of the surface functionalities.

The pH of slurry is an important parameter to assess the surface acid-base behaviour of these solids since it reflects both the strength and the concentration of the surface groups. In the present oxides, the pH of slurry roughly increases from acidic to neutral-basic range as the electronegativity of the element to which oxygen is bonded decreases (Si>Zr≥Al). This would be expected for particles with similar surface area and type/concentration of surface groups. However, the surface characteristics may be modified by chemical or thermal treatments. As example, a thermal treatment in inert atmosphere at high temperatures increases the number of basic groups in alumina.

As proposed above, in order to obtain insoluble nanoparticle fillers with strong acidic properties, the silica powder was impregnated with PWA up to a weight percent of 30%. This

is really a good compromise to achieve high surface coverage while avoiding significant crystallization of PWA on the surface. Such effect would facilitate the acid leaching by the water environment during operation [9].

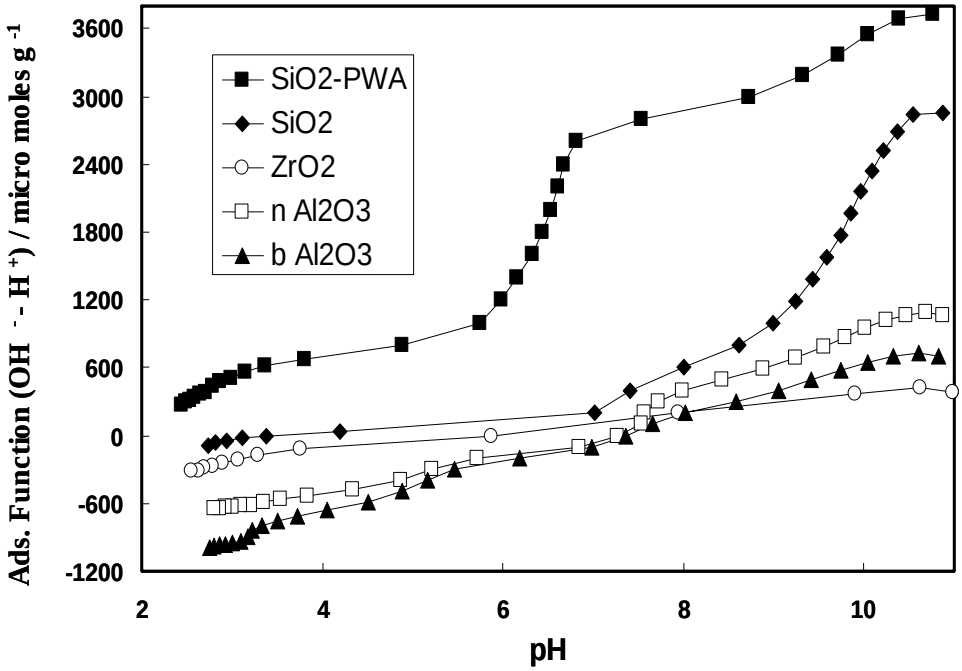

Fig. 1. Variation of the Adsorption Density Function versus pH for various inorganic fillers.

Filler	Crystallographic structure	Mean particle size nm	pH of slurry	BET Surface Area (m^2/g)	Basic or Acidic Functional Group Dissociation Costants	Basic or Acidic Functional Group Amounts (meq/g)
SiO_2	Amorphous	7.0[a]	4.75	324.11	pKa= 4.76	0.086
SiO_2/PWA	Amorphous	20.0[b]	2.54	166.28	pKa= 6.59 pKa= 3.34	1.480 0.760
ZrO_2	Cubic fluorite Monoclinic	7.5[c]	5.35	96.03	pKa= 6.24	0.067
n Al_2O_3	γ-Alumina α-$Al(OH)_3$	6.1[c]	7.5	109.1	pKa= 7.65 pKb= 6.98 pKb= 8.86	0.525 0.150 0.350
b Al_2O_3	γ-Alumina δ-Alumina	5.4[c]	8.2	152.17	pKa= 7.78 pKb= 7.02 pKb= 8.87	0.275 0.200 0.425

Table 1. Physico-chemical properties of inorganic fillers.

The host environment of the inorganic filler particles may be considered, in a first approximation, as a solution of a diluted strong acid. The conductivity of Nafion® 1100 is at room temperature almost one order of magnitude lower than a 0.5 M H_2SO_4 solution (6 10^{-2} S cm^{-1} vs. 4 10^{-1} S cm^{-1}) [19]. Accordingly, the adsorption density of OH^- species in the pH range around pH=2 may be indicative of the capability of the filler to adsorb water on the surface. It is clearly observed in Fig. 1 that the adsorption density (OH^- - H^+) varies in the low pH range according to the following series: SiO_2-PWA>SiO_2>ZrO_2> n Al_2O_3> b Al_2O_3. The adsorption density appears much more related to the amount and strength of functional groups than to the BET surface area (see, as an example, the SiO_2-PWA vs. SiO_2). With the exception of ZrO_2, the adsorption density series for OH^- species in the basic range (Fig. 1) is similar to that of the acid range (SiO_2-PWA>SiO_2> n Al_2O_3> b Al_2O_3> ZrO_2).

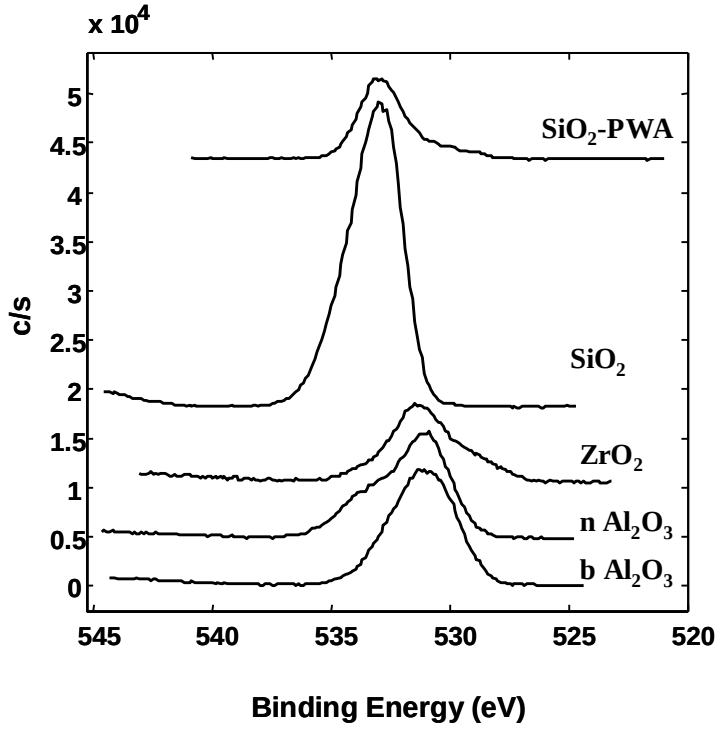

Fig. 2. Comparison of the O1s X-ray photoelectron peak for various inorganic fillers.

Fig. 2 shows the O1s XP spectra for the various inorganic fillers; the O1s peak position shifts towards higher B.E. values for the materials with stronger acidic character. The series of O1s B.E. (SiO_2-PWA>SiO_2>ZrO_2> n Al_2O_3> b Al_2O_3) is essentially the same to that observed for the pH of slurry and adsorption density at low pH values. The shift towards higher binding energy of more than 2 eV for the O 1s orbital passing from b Al_2O_3 to SiO_2-PWA is associated to a strong electronegative effect of the chemical species bonded to the

acidic surface oxygen sites which, attracting the electron clouds of these latter, increase the bond polarization with the terminal hydrogen atoms. Thus, the O1s peak shift towards high B.E. is indicative of a more acidic behaviour.

Two specific aspects concerning the XPS analysis should be discussed in detail. The analysis depth in the present investigation (about 50 Å) is larger than a few surface monolayers; accordingly, the information reflects in part the chemistry of the layers underlaying the surface which are not responsible for the water adsorption during operation. The peak broadening for the O1s signal in the various samples indicates the presence of more than one oxygenated functional group in each material; however, only in the case of neutral Al_2O_3 two distinct contributions to the XP signal are clearly observed, since these oxides possess groups with significantly different acid-base behaviour. For the other fillers, the XP signals associated to each group tend to overlap. Appropriate deconvolution of such peaks is not straightforward since it would require appropriate calibration of the B.E. for each functionality. In this regard, it may be stated that the potentiometric titration technique is more surface selective than XPS since it detects only the top layers, allowing a proper separation of the surface groups on the basis of their different acid-base behaviour. The difference in O1s B.E. between SiO_2-PWA and SiO_2 is not very significant (0.2 eV) as one would expect from the acid-base properties. A significant contribution of the Si 2p-2s signals beside the W 4f signal is observed in the XP survey spectrum of SiO_2-PWA powder (not shown), indicating that either the analysis depth is very large (SiO_2 and SiO_2-PWA particles range between 7 and 20 nm, as indicated by TEM observation) or the coverage of the silica particles by PWA is not complete. The second hypothesis seems to be ruled out by the potentiometric titration results which do not give evidence of a significant number of functional groups with surface acid constant similar to that for the functionalities present in the bare silica. Nevertheless, the XPS results corroborate the findings of the acid-base potentiometric and pH of slurry analyses.

X-ray diffraction analysis of the nanoparticle fillers (Fig. 3) shows an amorphous structure for SiO_2 whereas ZrO_2 and Al_2O_3 are crystalline. ZrO_2 shows both monoclinic and cubic structure. Typical Bragg angles (CuKα) for the monoclinic structure are 24.4°, 28.3° and 31.5° (2θ), whereas, typical Bragg angles for the cubic structure are 30.2°, 34.8° and 50.5°. Basic and neutral alumina show mainly the structure of γ-Al_2O_3. Yet, n Al_2O_3 also shows the presence of small peaks at low Bragg angles (14.4° and 20.3°) related to α-$Al(OH)_3$. Average particle sizes for these inorganic fillers, as provided by the suppliers or XRD/TEM-determined, are reported in Table 1. They range between about 5 and 20 nm. No

significant degree of agglomeration inside the membrane was evident under optical microscope observation for all the composite membranes. The SiO_2-PWA powder reveals the presence of a few PWA crystallographic peaks. The PWA does not appear from the XRD pattern to be in a well crystallized form although its concentration (confirmed by XRF) is 30% in weight with respect to the oxide. These evidences would suggest that PWA interacts with the SiO_2 surface, probably through an acid-base reaction, establishing strong bonding properties. On the other side, the very low pH of slurry of this material accounts for a prevailing surface effect by PWA.

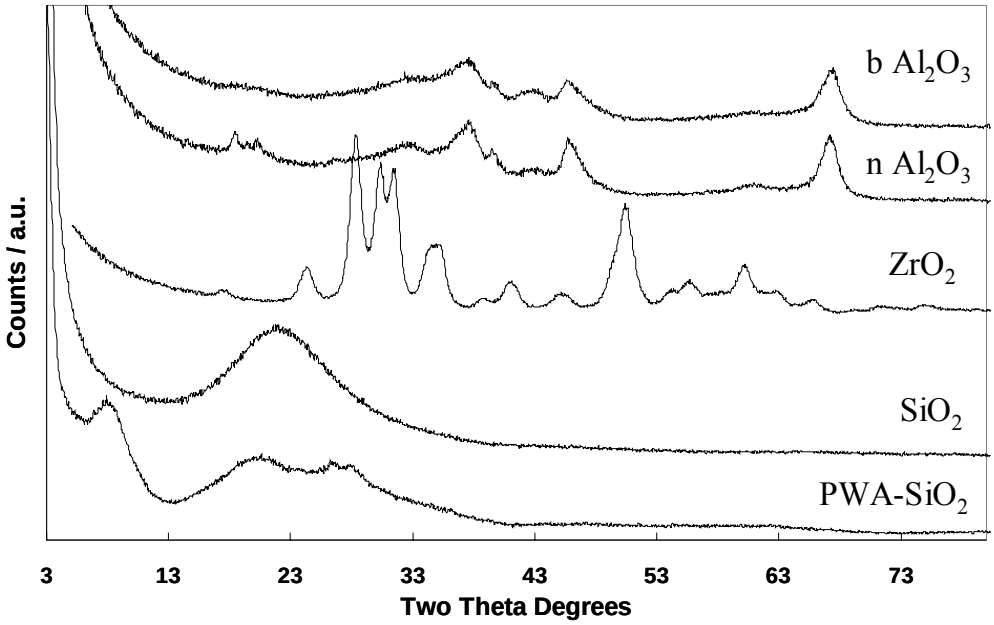

Fig. 3. X-ray diffraction analysis of various inorganic fillers employed in the preparation of composite Nafion recast membranes.

TEM micrographs of the various samples are shown in Fig. 4a-f. The estimated mean particle size is reported in Table 1. It is observed that the silica particles containing adsorbed PWA have an average size larger than bare SiO_2. The primary particles in the PWA-SiO_2 sample are well separated, whereas, the bare silica particles are joined to each other forming a continuous network without significant agglomeration. The other samples (ZrO_2, n Al_2O_3, b Al_2O_3) show a higher degree of agglomeration.

Fig. 5 shows the variation of cell resistance versus temperature in the range between 90° and 145°C. These values were determined under cell operation since water produced by the oxygen reduction enhances membrane humidification at the cathodic side. The cell resistance varies from 0.13 to 0.05 ohm cm^2 at 145 °C as the pH of slurry of the oxide filler

changes from 8.2 to 2.5. Practically, all oxide fillers here investigated enhance membrane water retention properties since recast Nafion does not allow to operate at 145 °C (Fig. 5).

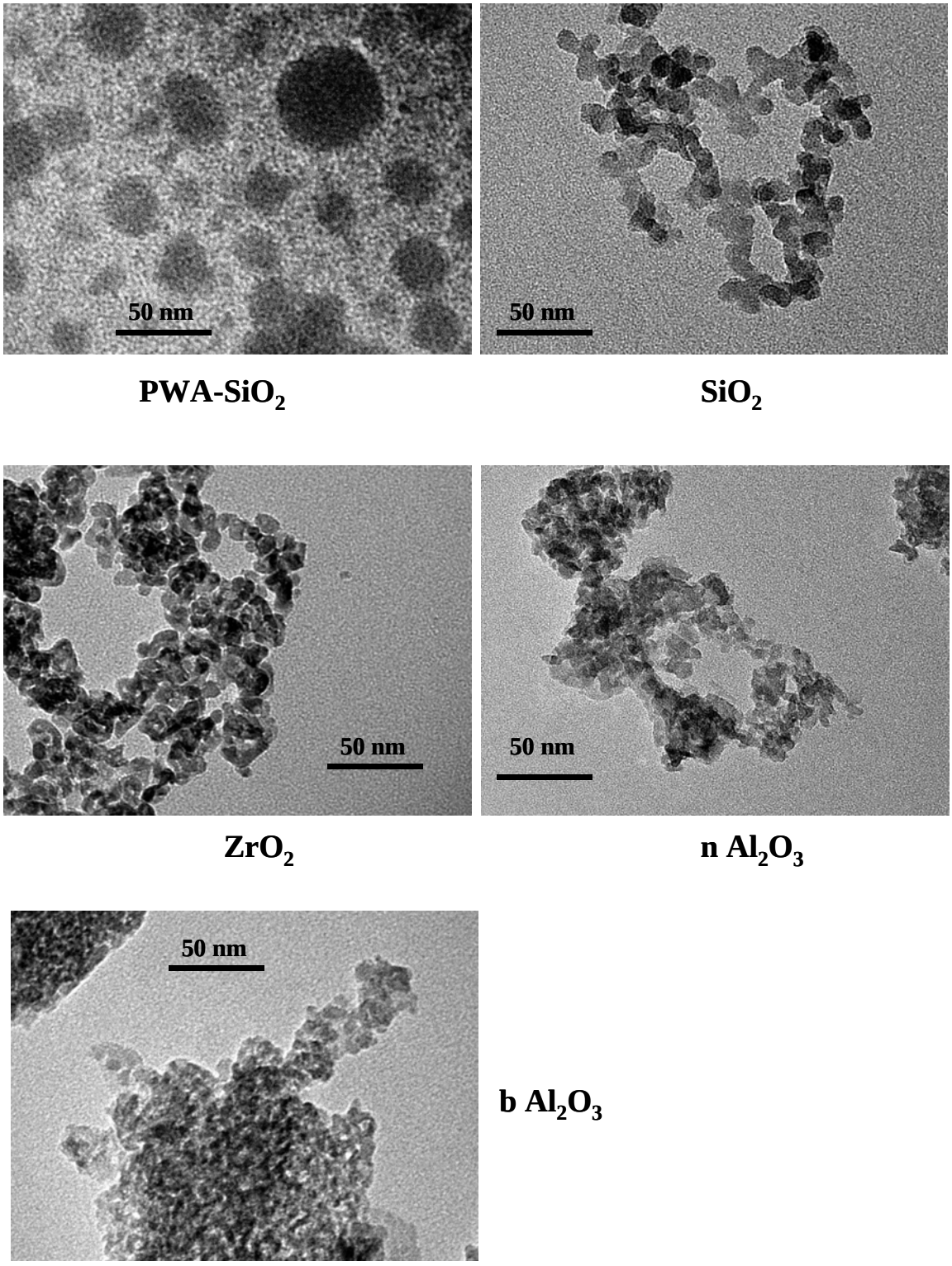

Fig. 4. Transmission electron micrographs of various inorganic fillers employed in the preparation of composite Nafion recast membranes.

The cell resistance behaviour is almost the same for all membranes but less evident in ZrO_2. The cell resistance decreases up to 130°-140°C and it increases again at 145 °C. It seems evident that above 130-140 °C, water retention inside the membrane is no more favoured. Desorption of H_2O molecules from the inorganic filler surface produces an increase of cell resistance. Such behaviour is not much different from that of strongly desiccant materials (e.g. silica gels, molecular sieves) after they have been water-saturated. These materials are generally reactivated (re-dried) at 130°-140° C. In the case of ZrO_2, the progressive increase of cell resistance would indicate a slightly different mechanism or a shift in the water desorption temperature. The water uptake properties of ZrO_2 appear to be better than alumina due to its more acidic surface characteristics.

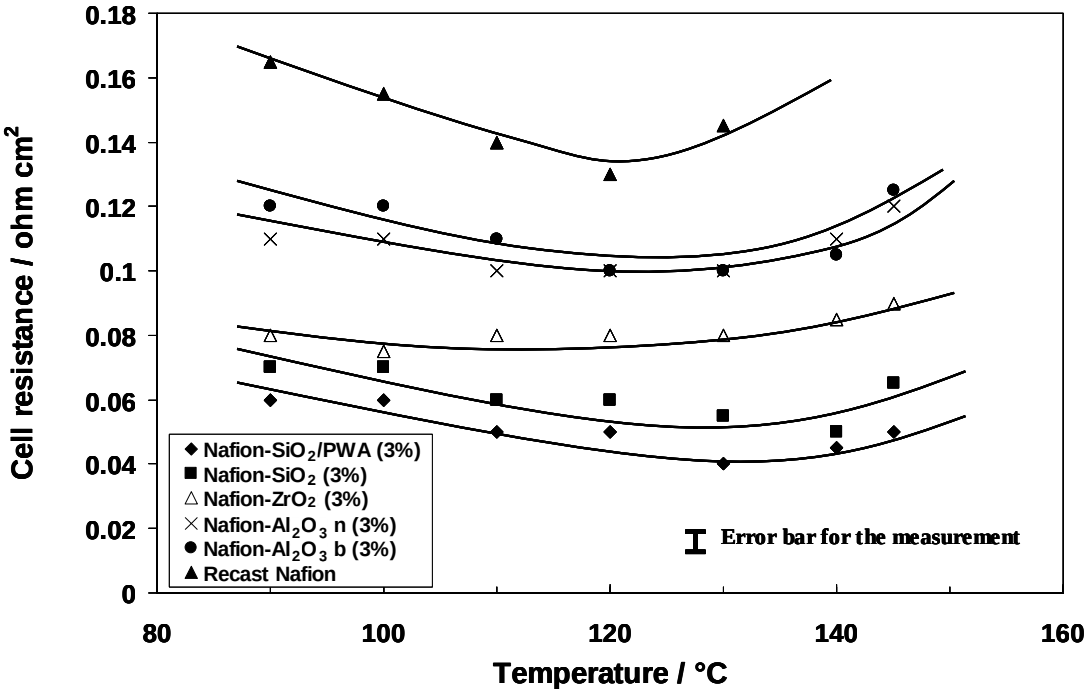

Fig. 5. Variation of cell resistance values as a function of the operating temperature for DMFCs employing different Nafion recast composite membranes.

By considering that at 145 °C, the cell resistance of PWA-SiO_2 based cell is about 0.05 ohm cm^2 with a membrane thickness of 100 μm, a rough conductivity value of 0.2 S cm^{-1} is derived. This calculation does not take into consideration the effects of electrode resistance, contact resistance and the slight reduction of membrane thickness after M&E assembly fabrication and cell tightening. These effects probably compensate each other. Conductivity values are also calculated for the other composite membranes and favourably compare to bare recast Nafion (Fig. 5).

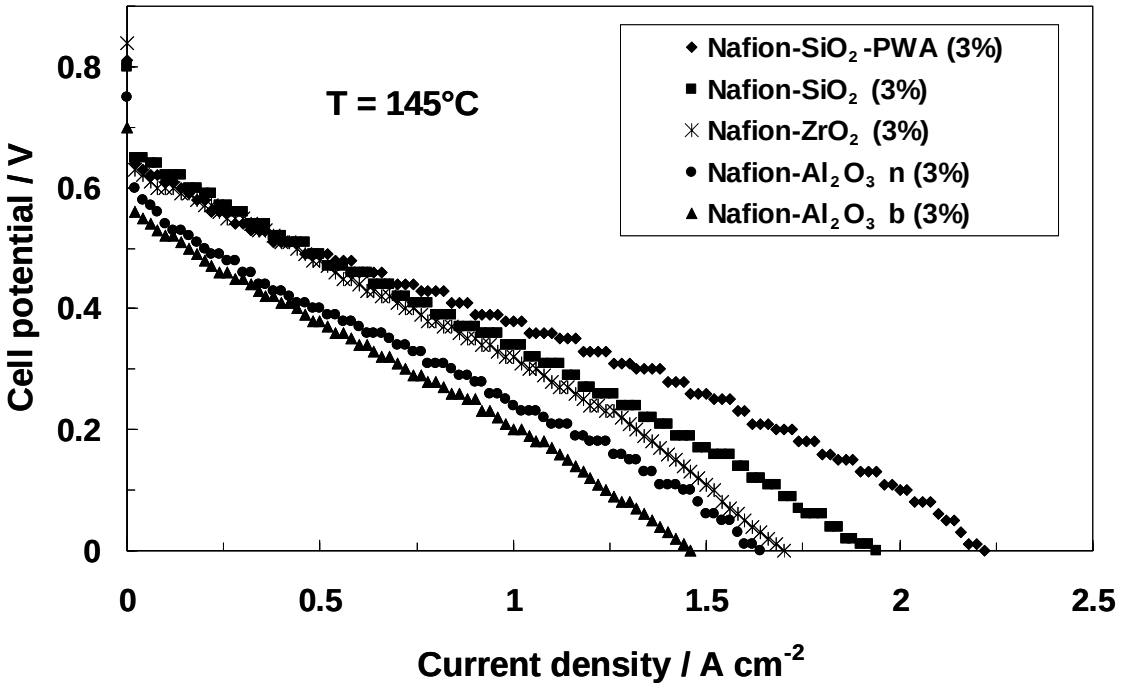

Fig. 6. DMFC polarization curves at 145 °C for various membrane-electrode assemblies equipped with composite Nafion recast membranes. Methanol feed 2M, 2.5 atm; oxygen feed 2.5 atm. Pt loading 2 mg cm^{-2}.

The DMFC polarization characteristics and power density curves at 145 °C (Figs. 6-7) closely reflect the trend observed in the cell resistance diagram (Fig. 5). Significantly lower potential losses are observed in the ohmic and mass transfer controlled regions of the polarization curves (i.e. above 0.5 A cm^{-2}) for the MEAs based on the more conductive membranes (i.e. those containing acidic fillers). Interestingly, smaller potential losses are observed in the activation controlled region, at low current density, for the acidic with respect to neutral or basic oxide fillers-based MEAs. The latter effect can only be related to the rate of electrode reactions. Probably, basic or neutral particles give rise to an acid-base reaction with Nafion sulfonic groups decreasing proton activity close to the cathode-electrolyte interface. It is well known that the concentration of hydrogen ions plays a significant role in the oxygen reduction mechanism contributing to increase the reaction rate [15].

Maximum power densities are recorded at currents between 0.8 and 1.3 A cm^{-2} i.e. in the region where membrane conductivity effects are dominant (Fig. 7). Accordingly, these performances reflect the cell resistance values in Fig. 5. A twice increase in cell resistance in b Al_2O_3/Nafion with respect to the SiO_2-PWA/Nafion corresponds to a half power density. As said above, a slight contribution from the inhibition of cathode electrode reaction due to

decreased proton activity induced by neutral or basic oxide fillers should not be discarded even at high currents.

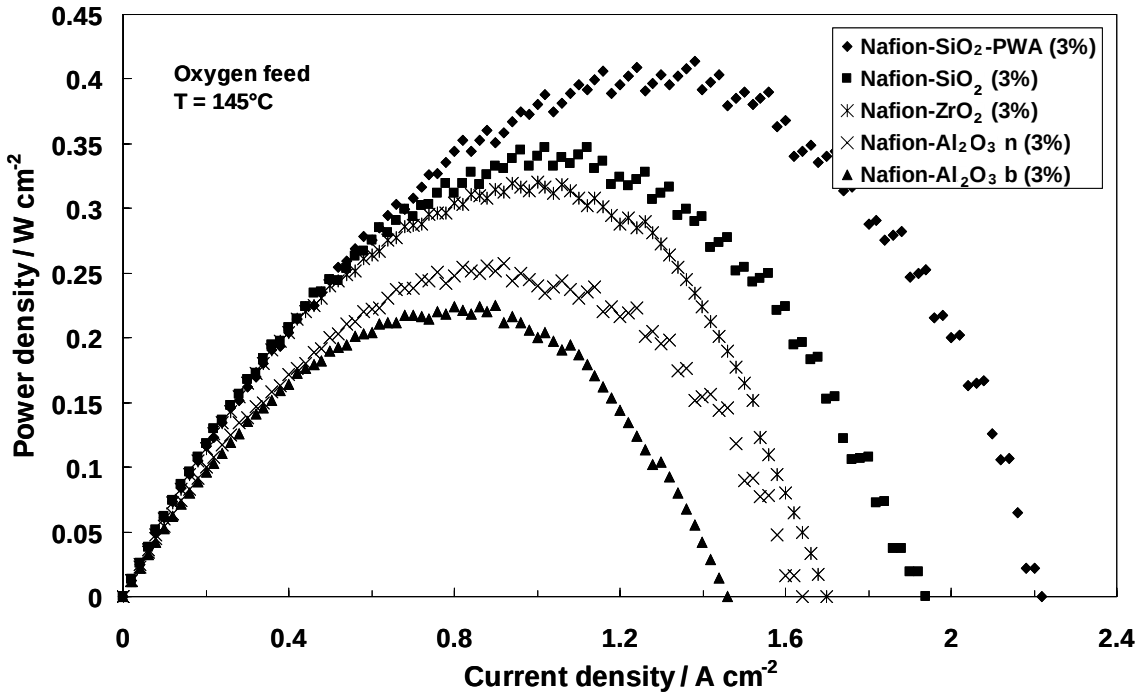

Fig. 7. DMFC power density curves at 145 °C for various membrane-electrode assemblies equipped with composite Nafion recast membranes. Methanol feed 2M, 2.5 atm; oxygen feed 2.5 atm. Pt loading 2 mg cm^{-2}.

The above discussed effects are summarised in Fig. 8. An increase of cell resistance and a linear decrease of maximum power density as a function of the pH of slurry of the inorganic fillers are observed. Such trends indicate that the acid-base behaviour of the oxide filler plays a key role in determining the electrochemical properties. Clearly, these oxide materials (including the one containing adsorbed PWA) do not possess elevated intrinsic protonic activity at 145 °C as well as their low weight content does not allow to justify a significant contribution as proton conductor. Their effect is mainly due to the hygroscopic characteristics and the large surface area. These properties enable suitable water adsorption on the surface and enhance water retention characteristics of the membranes. Such behaviour is essentially present in all the investigated oxides, but, those possessing strong acidic surface functionalities are capable of larger water retention and do not participate in neutralization reactions with sulfonic groups as in the case of neutral or basic functionalities.

These conjectures are confirmed by thermogravimetric analysis. Water uptake was

measured by recording thermogravimetric (TG) curves from 155 °C up to 45°C under constant R.H. on both bare recast Nafion and composite membranes previously dried to a constant weight at 155 °C (Fig. 9). Although the TG experiments have been carried out in conditions different than the fuel cell operation where water is both fed to the anode and produced at the cathode by the electrochemical reaction, these measurements reveal that the composite membranes are characterised by a larger water uptake/retention in the high temperature range than the bare perfluorosulfonic membrane (Fig. 9). The water retention capability appears to be directly related to the surface acid-base properties of the inorganic fillers (compare Fig. 9 and Table 1).

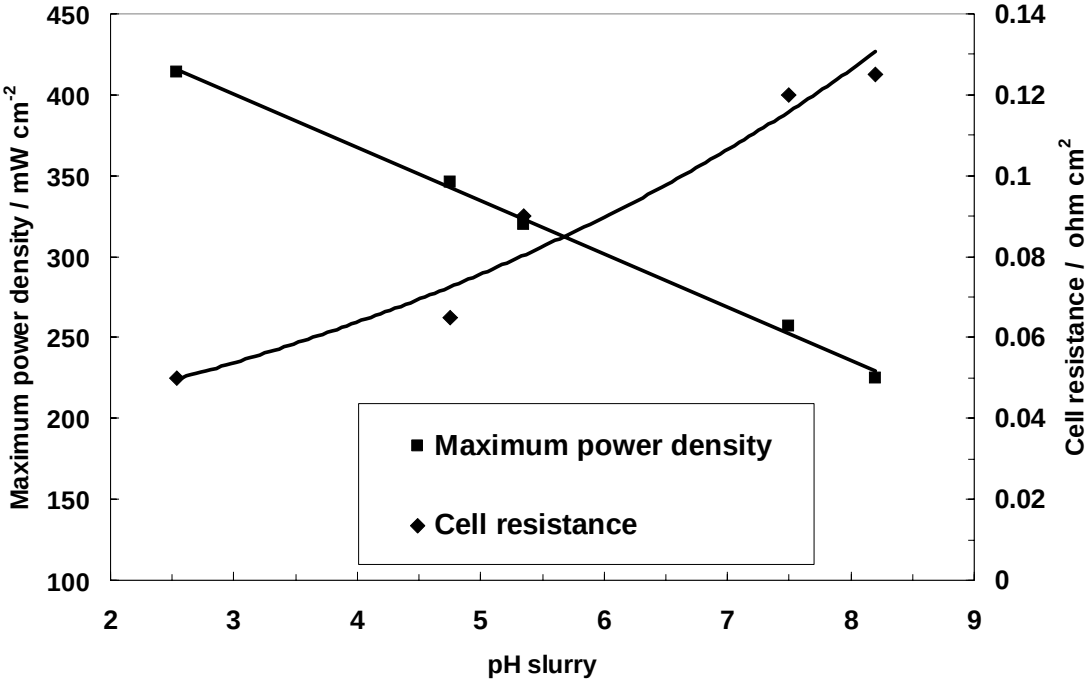

Fig. 8. Variation of the maximum power density and cell resistance of composite membranes-based DMFC at 145 °C as a function of the pH of slurry of the inorganic filler.

The wide number of literature reports on the surface characteristics of such materials allows to derive some interpretations on their behaviour under fuel cell operation. Phosphotungstic acid crystallizes in its solid form with 36 water molecules [15] at room temperature ($H_3PW_{12}O_{40}$ 36 H_2O); thus, it possess the strongest water retention characteristics since water is present in the crystallographic structure. In a previous study [20], a fast water uptake-release in a composite zeolite-PWA powder was observed by X-ray diffraction analysis at room temperature as a function of the relative humidity. This phenomenon was associated to a variation of the PWA crystallographic structure on the basis

of the number of water molecules coordinated by the acid. In a recent study of PWA-doped polymer membranes it has been observed a rapid decay of membrane conductivity around 140 °C [21]. Thermal analysis investigation allowed to attribute this behaviour to the rapid water loss from the heteropolyacid under these conditions [21].

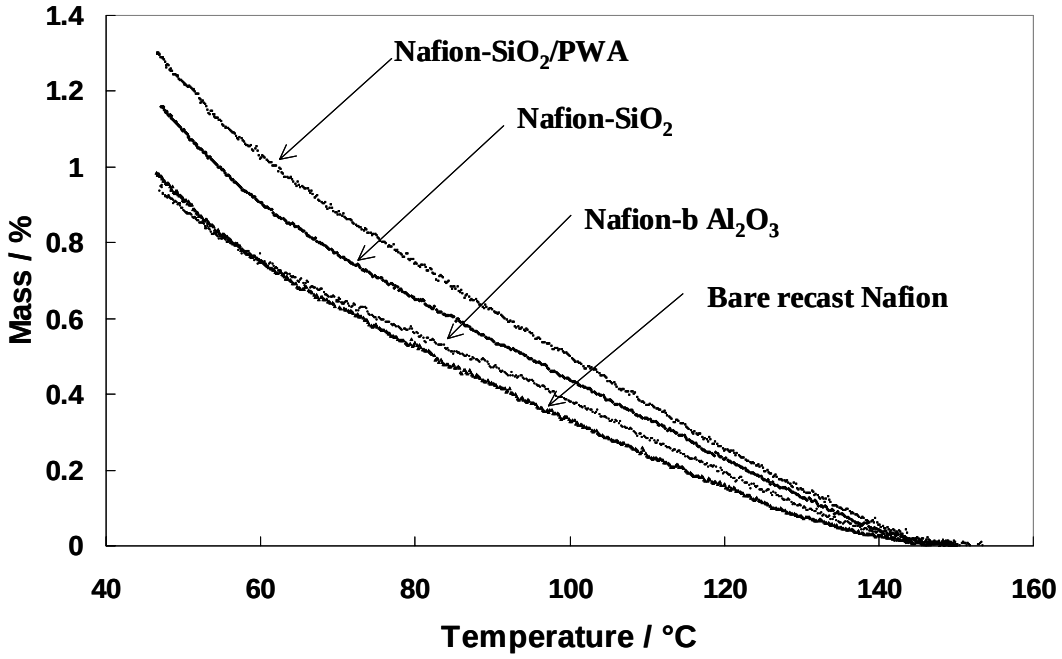

Fig. 9. Thermo-gravimetric analysis of the water uptake by the recast membranes (R.H. = 30%); thermal sweep from 155 °C to 45 °C.

Amorphous silica, such as Aerosil or Cabosil, is widely used in catalysis. Its surface functionalities have been investigated by infrared spectroscopy [16]. Typical silica surface groups are reported in Fig. 10 a-b-c. These functional groups are mainly silanol groups which may be isolated, geminal or connected by hydrogen bonding. Siloxane groups may be also present in the surface but in a lower amount. These latter form on the surface after dehydration above 200 °C. FT-IR investigations [16] have evidenced that Cabosil is characterized by a large content of isolated silanol groups both on the surface and in the bulk with respect to other amorphous silica materials. The silica dehydration is known to occur through the following steps [16]: a) evaporation of water formed in the silica pores by capillary condensation occurs below 140 °C in the presence of dry nitrogen stream (this effect should be less significant for well dispersed spherical silica particles); b) desorption of physically adsorbed water occurs at 140-150 °C leaving a large content of silanol groups on the surface; c) the silanol groups desorb in the temperature range between 150° and 800 °C

depending on their characteristics (e.g. isolated, geminal) and environment, forming siloxane groups and releasing water. At 800 °C, the surface of silica is almost all covered by siloxane groups showing hydrophobic properties and basic surface characteristics as opposite of hydrophilic characteristics of silica covered by silanol groups (acidic surface). It is derived that the presence of acidic silanol groups is essential for the water uptake and the desorption of physically adsorbed water gives rise to the minimum in the cell resistance behaviour observed in Fig. 5.

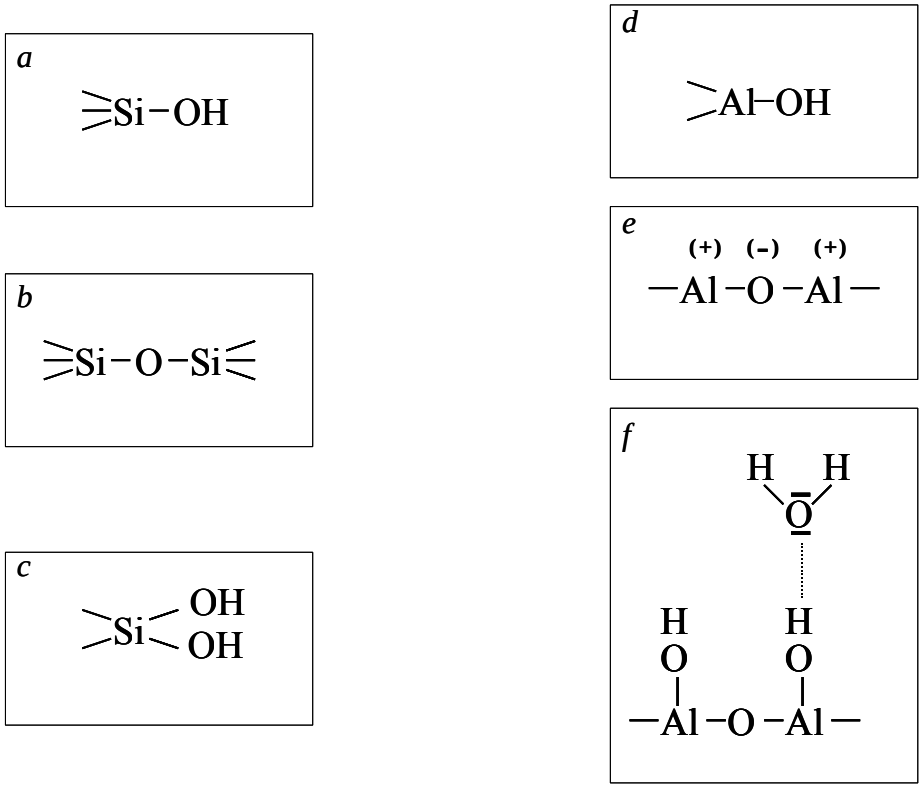

Fig. 10. Surface functional groups in SiO_2 and Al_2O_3 materials involved in the water retention mechanism.

As for silica, the surface properties of γ-alumina are well known from the literature being this material widely used as catalyst support (see Fig. 10 d,e,f). Accordingly, water is bonded to the alumina surface under various forms. Physically and chemically adsorbed water desorb at T>120°C and T>300°C, respectively [17]. OH groups (Fig. 10 d) chemically bonded to the surface desorb at T> 400°C realising water molecules. Such groups generally impart weakly acid properties to the surface whereas bridge bonded oxygen sites (Fig. 10 e) show mainly Lewis basic behaviour. Elevated thermal treatments in inert atmosphere determine a prevailing basic behaviour.

From the above picture, silica and alumina show similar surface properties and dehydration behaviour. The surface characteristics depend in both cases by the concentration and acid-base strength of functional groups which are influenced by the chemical environment and may be modified by surface reactions as well as thermal treatments. Large concentration of acidic groups as well as high acidic strength (larger polarization of the OH dipoles) produce significant amount of physically adsorbed water in both silica and alumina [16]. A typical example is represented in Fig. 10f. Yet, OH groups bonded to silicon are more acidic than those bonded to Al being this latter characterized by lower electronegativity. This effect is well known in zeolites where dealumination produces an increase of acid properties [20]. Characteristic water loss temperature in PWA appears to coincide with that of SiO_2 and Al_2O_3 giving rise to a similar behaviour; however, PWA is charaterized by larger water uptake. Whereas, the behaviour of ZrO_2 in Fig. 5 indicates a smooth release of the water coordinated by acidic OH groups originated by surface defects without any characteristic desorption temperature.

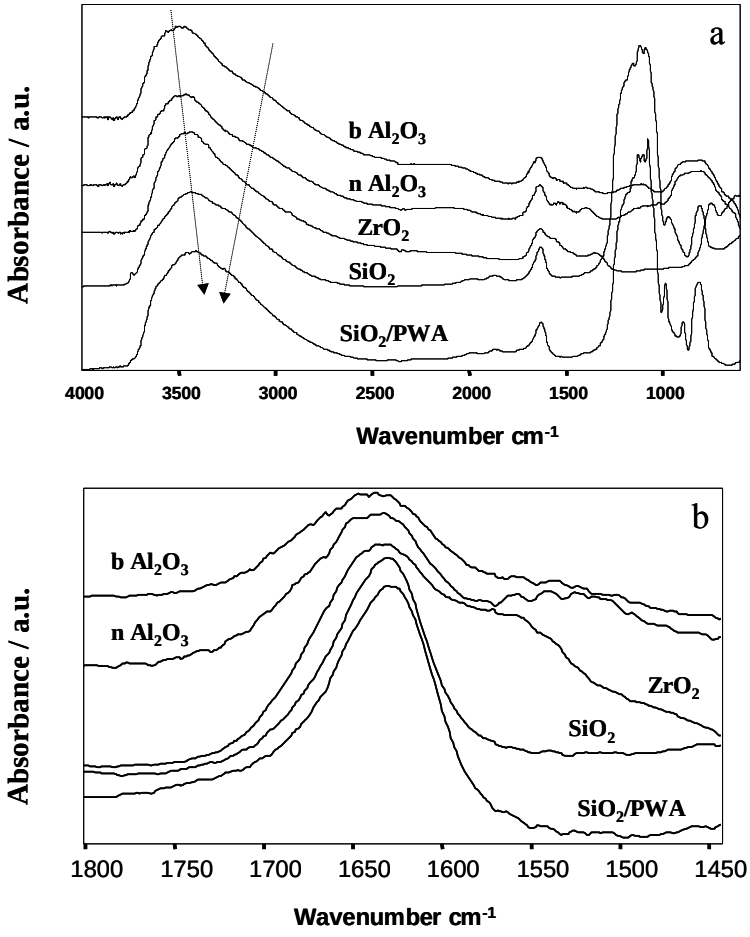

Fig. 11. FTIR spectra (a) with enlarged water bending vibrations region (b) for the inorganic fillers.

Fig. 11a shows a comparison of the IR spectra for the as-received or prepared inorganic fillers. The IR region from 600 up to about 1500 cm^{-1} reflects both the bulk and surface chemistry of the filler. In the case of SiO_2, the IR-bands in this region are assigned to the O-H bending mode of hydrogen-bonded (813 cm^{-1}) and isolated (972 cm^{-1}) silanolic groups and to the stretching mode of Si-O (1116 cm^{-1}) in the silica frame [2, 22]; this latter is characterised by an intense absorption. The peak at 1632 cm^{-1} (Fig. 11b) is due to the bending vibrations of physically adsorbed water [22]. Overtones modes of silica frame appear in the region between 1800 and 2100 cm^{-1} [23]. The broad absorption band from about 2500 cm^{-1} up to about 3750 cm^{-1} is assigned to the stretching vibrations of hydrogen-bonded silanols and water physically adsorbed on the surface [23]. The stretching vibration characteristics of isolated hydroxil groups (sharp band at 3750 cm^{-1} [2]) are not detected in the spectra. By comparison, ZrO_2 as well as n Al_2O_3 and b Al_2O_3 show Zr-O and Al-O bending vibrations absorption bands below 1000 cm^{-1} and overtone modes of zirconia and alumina frames up to about 1600 cm^{-1}. The filler obtained by impregnation of Cabosil with phosphotungstic acid (SiO_2-PWA) possesses both SiO_2 and PWA characteristics. The absorption bands at 813 cm^{-1} is assigned to the bending mode of silanol groups [22], the peak at 892 cm^{-1} is assigned to the stretching mode of W-O-W bonds [24], whereas, the peak at 982 cm^{-1} is due to the stretching vibrations of W=O in the Keggin structure [24]. A further peak typical of the Keggin structure (asymmetric stretching vibration of the central PO_4 tetrahedron) at 1081 cm^{-1} [24] is partially overlayed by the Si-O frame vibrations. It appears that the molecular structure of PWA is retained after adsorption on the silica surface. The most important features for the filler application in composite membranes are related to the adsorption properties of water on the surface. In this regard, the broad band in the O-H stretching vibration region at 2500-3800 cm^{-1} appears to be mainly composed by two overlapping peaks occurring in the ranges: 3040-3240 cm^{-1} and 3400-3540 cm^{-1}. It is observed that the main peak (3400 –3540 cm^{-1}) shifts to lower frequencies as the surface acidity of the filler increases as reflected by the pH of slurry (Fig. 11a). It is well known that the O-H stretching vibration frequency of surface acidic groups increases as a function of the acidic character whereas the stretching frequency of O-H in water, in its non bonded state, occurs at 3651 cm^{-1} (ν symmetric) and 3756 cm^{-1} (ν asymmetric) [25]. Formation of strong H-bonds with surface groups for the physically adsorbed water shifts the stretching frequencies to much lower energies [26]. Thus, we identify the high frequency peak as due to H-bonded physically adsorbed water and the shoulder at lower frequency to the surface acid-base (O-H) functionalities in the fillers. FTIR

measurements of the filler powders subjected to hydration-dehydration treatments (not shown) further supported this assignment.

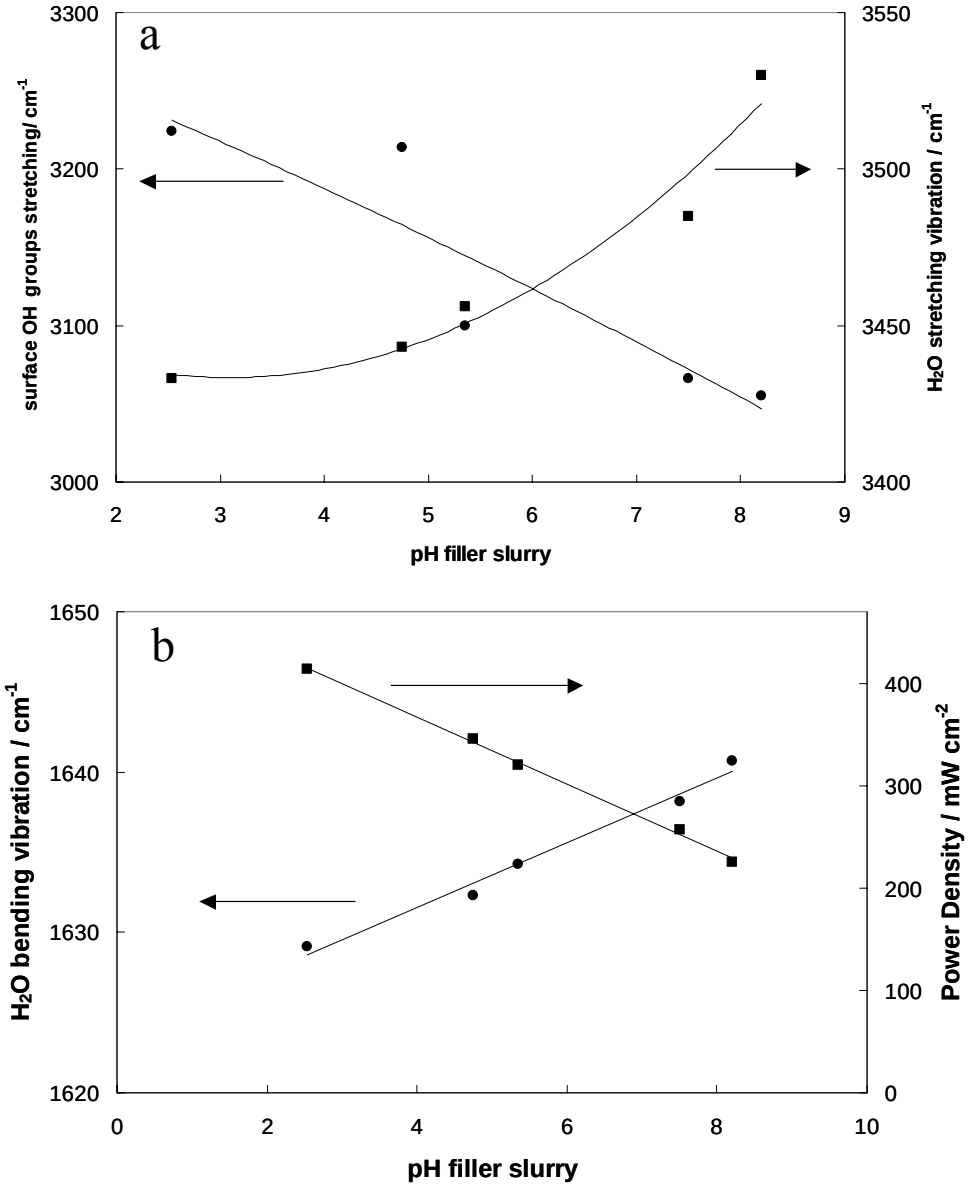

Fig. 12. Variation of O-H stretching vibration frequencies for surface OH functionalities and physically adsorbed water versus the pH of slurry of the fillers (a); variation of O-H bending vibration frequencies of physically adsorbed water and DMFC maximum power density versus the pH of slurry of the fillers (b).

An increase of the polarization bonding in the O-H surface functionalities, associated to a more acidic character, reflects a larger bond strength with a consequent increase of the vibration frequency. On the other hand, the decrease of the frequency associated with the O-H stretching mode of adsorbed water, as the pH of slurry decreases, reflects a strong interaction

of water with the surface of acidic fillers through hydrogen bonds (Fig. 11a). This latter aspect is further corroborated by the decrease of the water bending frequencies with the increase of the acidic character of the filler (Fig. 11b). Accordingly, the electrons associated to the hydrogen atoms in the adsorbed water are shared between two oxygen atoms with a consequent decrease of the energy associated to each bond. As above observed from thermal analysis measurements, the water uptake is larger for the membranes containing acidic fillers; from the FTIR measurements, we can associate such behaviour to a stronger interaction of water with the surface of the acidic filler probably due to the larger electrostatic field locally produced by strongly polarised acidic groups on the surface. Thus, acidic groups interact more strongly with water and they are able to retain more consistently water at high temperatures by effect of a strong hydrogen bond formation. According to the so called "vehicle mechanism", a large uptake of water is essential for a fast proton conduction [27]. It is thought that the water physically adsorbed on the surface of the igroscopic oxides can be reversibly released and re-adsorbed allowing proton transport through the membrane. On the other hand, due to the presence of hydrogen bonds between the surface functionalities and the physically asdorbed water, a conduction mechanism by hydrogen ions hopping , similarly to the Grotthus mechanism [27] may not be excluded even at high temperature. The increase of the membrane conductivity in the overall temperature range with the decrease of the pH of the filler may be thus associated with both the larger uptake of water and a hopping mechanism assisted by the acidic sites on the filler surface.

Fig. 12a-b shows the presence of clear relationships between the O-H polarization bonding in the surface functionalities as well as the stretching and bending frequencies of the physically adsorbed water and the pH of slurry of the fillers. Such features strongly influence the conductivity behaviour of the membranes and thus the maximum power density achieved at 145 °C in direct methanol fuel cells (Fig. 12b). Accordingly, it may be rationalised that water retention properties of composite membranes at high temperature are strictly related to the capability of the filler to adsorb water on the surface through a strong interaction with surface OH groups and consequent formation of hydrogen bonds. Such interaction is enhanced by the surface acidity and determines an increase of proton conduction in perfluorosulfonic membranes. It is pointed out that, during operation, the DMFC cell produces water at the cathode; water is also fed to the anode and it is transported through the membrane by the electro-osmotic drag. The filler particles distributed inside the membrane thus act as centers which retain water inside the system avoiding strong water loss by the temperature.

It appears clear that, as in bare Nafion (see Fig 5), water is the real conducting medium in these composite membranes. The water diffusion coefficient in such systems will depend on the average distance between nearest neighbour water hopping sites and their extent of interaction with water dipoles. In other words, the diffusion coefficient and thus the conductivity are directly related to the concentration and polarization (acidic strength) of water coordinating surface groups in the inorganic fillers. Suitable dispersion of the inorganic nanoparticles in the water channels of the polymer framework also plays an important role [28]. Upon increasing the concentration of the inorganic filler in the polymer at 5% wt. there is no significant change in the cell resistance values and further increase to 10% wt. content produces an increase of the cell resistance [29, paragraph III.2].

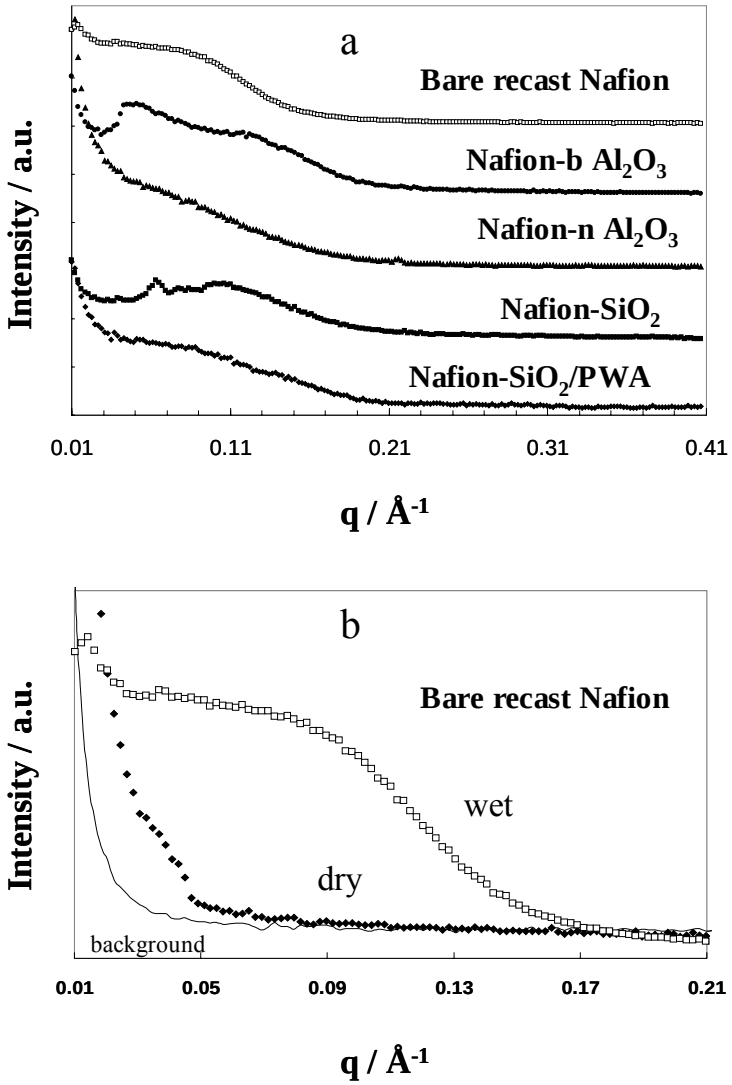

Fig. 13. (a) Small angle X-ray scattering patterns from the various membranes immersed in water. (b) SAXS profiles of bare recast Nafion membrane immersed in water and under vacuum (10^{-3} Torr). The SAXS pattern of the water background is reported for comparison.

The influence of the inorganic fillers on the membrane morphology and water self-diffusion coefficient was also investigated. SAXS data, collected for the various membranes while they were immersed in water, are reported in Fig. 13a. A comparison between the SAXS profile measured for the recast Nafion membrane immersed in water and under vacuum is reported in Fig. 13b. The dried membrane (fig. 13b) shows only the X-ray scattering due to the lamellar crystallites of the polymer at small values of the scattering vector (q) corresponding to an average spacing of 18 nm. On the other hand, the same membrane immersed in water mainly shows the X-ray scattering due to the ion clusters (water channels) at larger scattering angles corresponding to an average spacing of 7.9 nm. The swelling by water probably produces an increase of the Bragg spacing or a loss of the long identity period nof lamellar crystallites in the polymer [30, 31]. However, two membranes i.e. those based on SiO_2 and n Al_2O_3 fillers show two distinct peaks which can be attributed to the polymer lamellar crystallites and ion clusters at small and large q values, respectively. The average dimension of ion cluster spacings is reported in Table 2 for all the membranes. It appears that there is no relationship between such parameter and the observed electrochemical properties. WAXS measurements have allowed to compare the ratio between X-ray scattering due to the crystalline and amorphous components of the membranes at large and small Bragg angles, respectively. These values are reported in Table 2. Fig. 14 shows the WAXS profiles for some selected membranes. As previously observed for in the SAXS measurements, no relationship is envisaged between the morphology and the conductivity behaviour of the membranes under high temperature operation. Yet, it should be pointed out that such measurements (SAXS and WAXS) have been carried out at room temperature and further analysis in the high temperature range is required before to rule out any effect of the morphology.

Water self diffusion coefficients have been investigated by PFG-NMR in a few selected membranes. The results obtained at 140 °C are reported in Table 2 and as an Arrhenius plot in Fig. 15. The diffusion coefficients of the investigated composite membranes is slightly larger than the bare recast Nafion in the high temperature range from about 100 °C to 140 °C (Fig. 15, Table 2). Whereas, in the lower temperature range the trend is opposite (Fig. 15). It is observed that these measurements do not exactly reproduce the fuel cell operating conditions where water is generated at the cathode and supplied to the anode. As it has been shown by Kreuer [27] that the diffusion coefficient varies significantly with the hydration behaviour; thus, the observed differences could be amplified under real operating conditions.

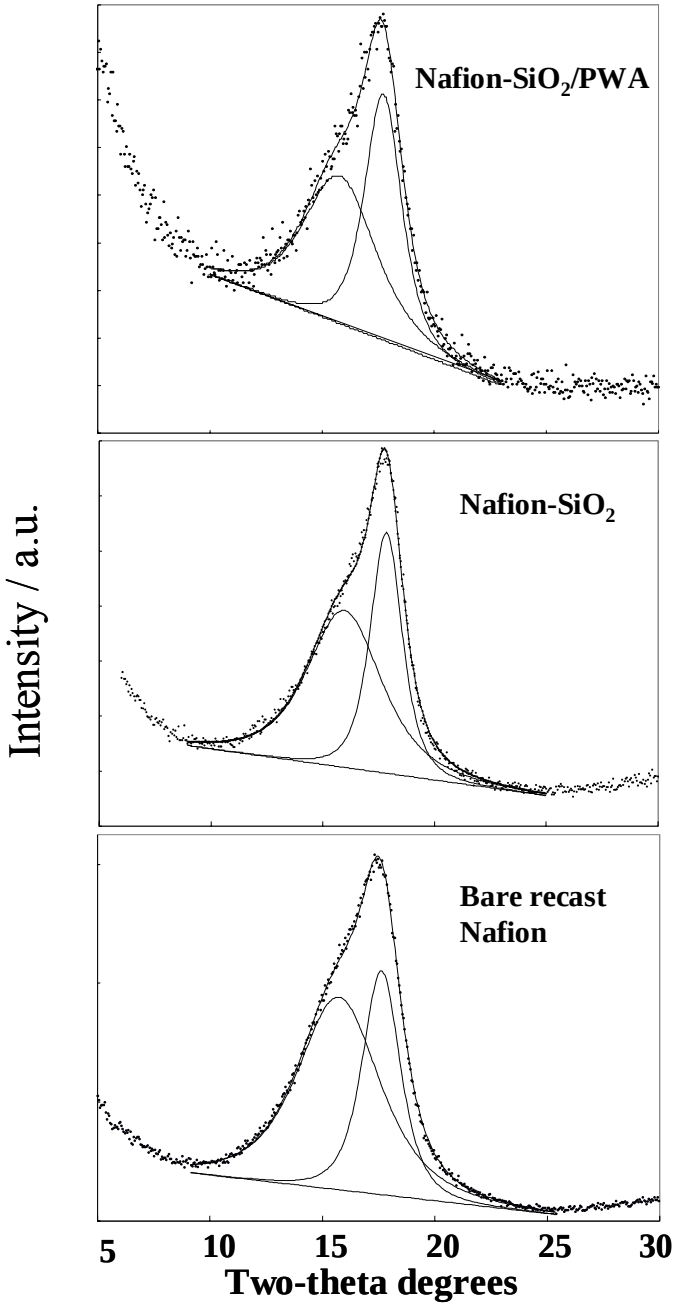

Fig. 14. WAXS patterns for selected membranes with deconvoluted amorphous and crystalline profiles.

Presently, the main drawback limiting a wide use of composite membranes in high temperature DMFCs is the high pressure operation requirement. In the present work, we have investigated the effect of pressure in order to understand if this requirement is strictly necessary to allow efficient membrane hydration (Fig. 16 a-b). Since both methanol oxidation

and oxygen reduction are positive-order reactions, a decrease of the operating pressure should negatively influence the reaction kinetics. Besides, mass transport at high current density is strongly affected by a variation in the operating pressure.

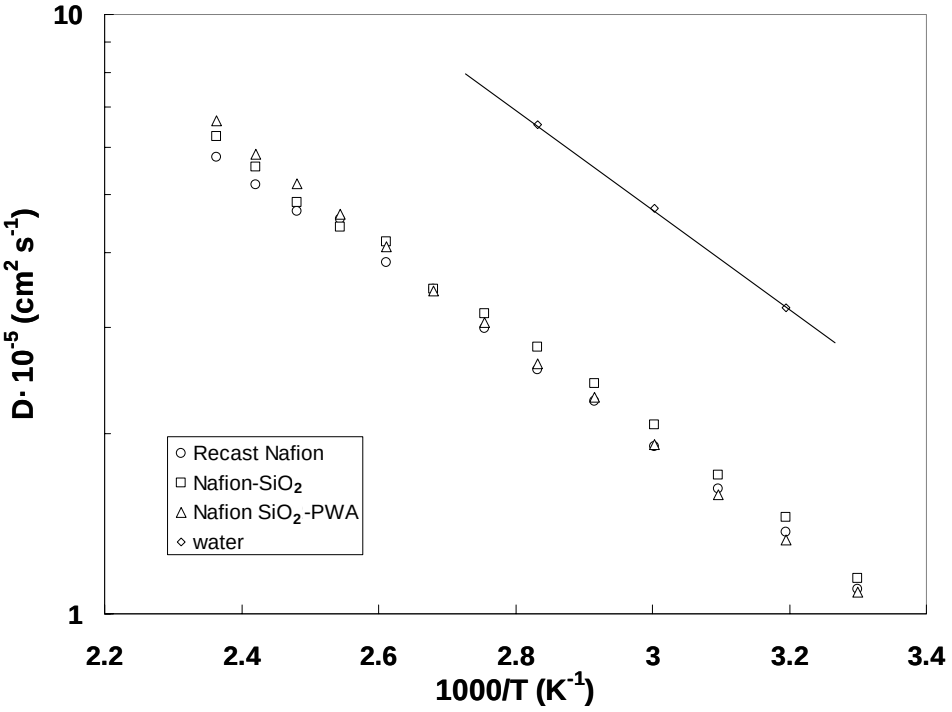

Fig. 15. Water diffusion as a function of temperature for selected membranes (R.H. = 30 %).

The effect of the anode pressure on the DMFC performance at 145° C is shown in Fig. 16a. In the potential range of technical interest above 0.4 V (i.e. at suitable values of cell efficiency), the decrease of performance is significant but not dramatic. At 0.4 V, a performance decrease of 40% is observed at 0.5 atm, but, the power density is still acceptable (200 mW cm^{-2}). Much more significant is the effect of the decrease of anode back pressure on the diffusion limiting current (see Fig. 16 a-b). By comparing the DMFC polarization curves in Fig. 16a-b it can be derived that a significant decrease of performance, in the region of technical interest, is recorded only when the cathode pressure is decreased. A decrease in the cathode pressure also produces a significant decrease of the diffusion limiting current. Interestingly, the decrease of pressure produces in all cases only a limited increase of cell resistance (see legend in Fig. 16a-b). On such basis we may suggest that the pressure does not play a dominant role in the hydration of the composite membranes since conductivity at 145 °C is only slightly affected by such effect. More likely, the observed decrease in cell performance as function of the cathode pressure is largely related to the cathode poisoning by methanol cross-over. A reduction in the oxygen partial pressure will favour the competitive

adsorption of methanol molecules at the cathode surface with consequent formation of a mixed potential on this electrode [32]. Such conjectures may find a better validation after a proper development of methanol tolerant oxygen-reduction catalysts [33].

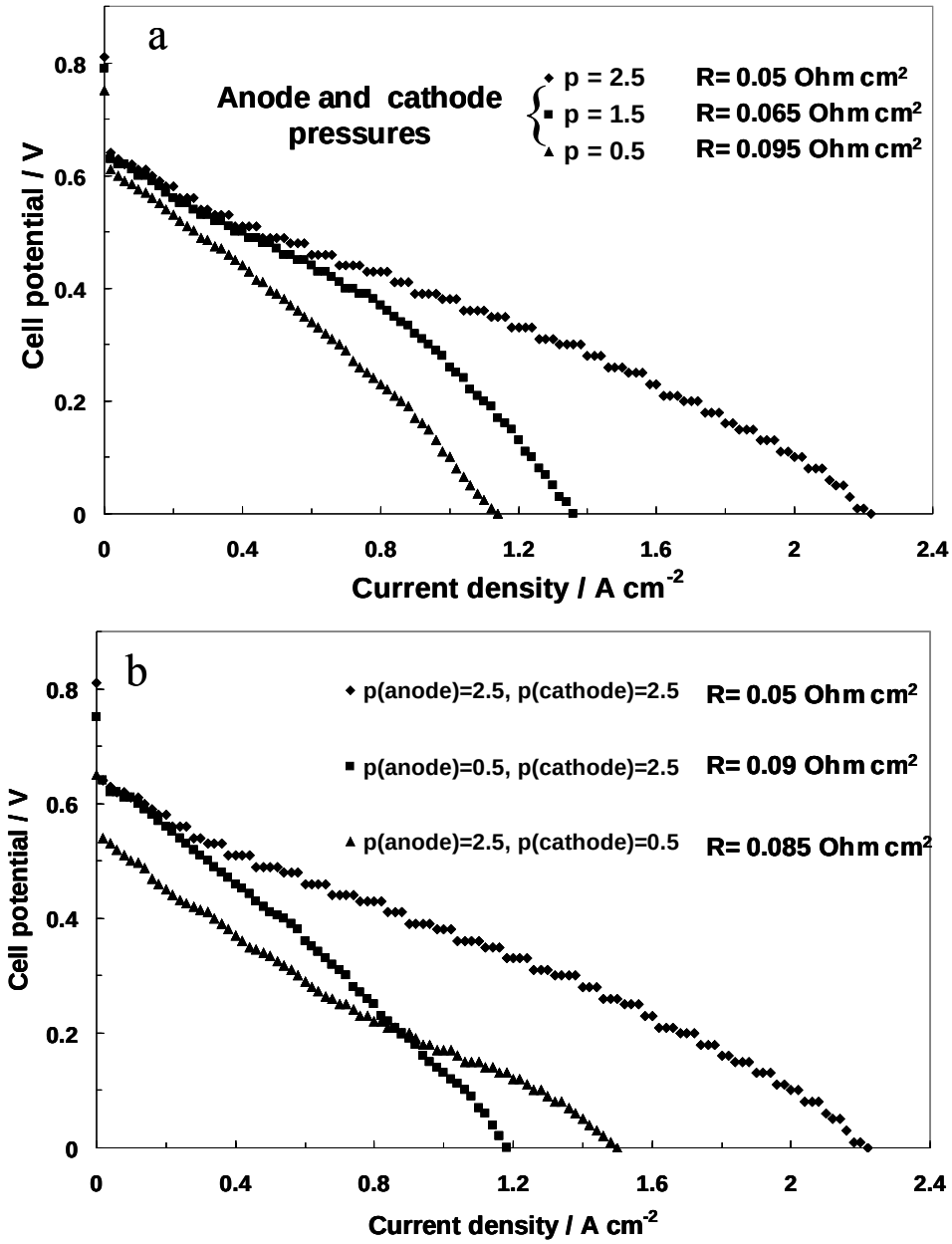

Fig. 16. Variation of the polarization behaviour at 145 °C for the PWA-SiO_2 based M&E assembly in DMFC as a function of the anode and cathode back pressures. Cell resistance values under various conditions are reported in the legend. Methanol feed 2M; oxygen feed. Pt loading 2 mg cm^{-2}.

Membrane	Crystalline /amorphous X-ray scattering ratio	Ion cluster spacing nm	Polymer lamellar crystallites spacing nm	Proton/water Self-diffusion coefficient at 150 °C 10^{-5} cm^2 s^{-1}	Estimated conductivity at 145 °C under operation (2.5 atm anode- 2.5 atm cathode) S cm^{-1}	Current density at 0.5 V and 145 °C (2.5 atm anode- 2.5 atm cathode) A cm^{-2}
Nafion-SiO_2	0.7	6.3 [a]	9.7 [a]	6.2	0.154	~0.48
Nafion-SiO_2/PWA	0.9	7.4 [a]	-	6.6	0.2	~0.5
Nafion-ZrO_2	-	-	-		0.11	0.44
Nafion- n Al_2O_3	0.7	8.3 [a]	-		0.083	0.2
Nafion- b Al_2O_3	0.5	5.2 [a]	12.5 [a]		0.08	0.16
Bare recast Nafion	0.6	7.9 [a]	18[b]	5.7	-	-

[a]Polymer in the wet form; [b]polymer in dry form

Table 2. Physico-chemical properties of composite membranes.

Determination of the methanol cross-over levels for the various composite membranes is outside the scope of the present work. These values have been already determined for some of them e.g. SiO_2 and SiO_2-PWA based composite membranes [6,9]. Fuel efficiency values between 80% and 90% have been determined at high temperature with the fuel cell working at appropriate current densities.

III.1.4 Conclusions

Acid-base properties of inorganic fillers play a key role in the water uptake of composite Nafion based-membranes at temperatures close to 150 °C by influencing the proton conductivity of the electrolyte. The presence of acidic OH groups on the particle surface facilitates water co-ordination which acts as vehicle molecule for proton migration. Physically adsorbed water is desorbed on the investigated inorganic fillers at around 140 °C. This determines a minimum in the value of cell resistance around this temperature. DMFC performances of various M&E assemblies based on composite membranes, containing fillers with different acid-base characteristics, increase as the pH of slurry of the inorganic filler decreases. These preliminary evidences indicate that the ionic conductivity of the composite

membranes and their range of operation may be increased by appropriate tailoring of the surface characteristics of the added ceramic oxides.

Operation at low pressures does not appear to introduce significant technical limitation for what concerns the hydration/conductivity characteristics of composite membranes in high temperature DMFCs (150 °C). Reduction of the applied pressure would, in any case, reduce the fraction of liquid water inside the system and, in some extent, the water retention capabilities. However, the saved electrical power needed for the auxiliaries passing from a compressor to an air blower would probably more than compensate for the power output losses due to the small increase in resistance. Yet, in absence of methanol tolerant oxygen reduction catalysts, high oxygen partial pressures are needed for proper cathode operation in presence of methanol cross-over.

The results shown in this work show that composite membranes with inorganic fillers are characterised in the high temperature range (100°C-150 °C) by larger water retention properties than the bare perfluorosulfonic membrane. The water retention capability appears to be mainly related to the surface acid-base properties of the inorganic fillers. Accordingly, the present approach can be used for membranes alternative to Nafion such as sulfonated polyetherketones and polysulfones as well as in high temperature hydrogen-air PEMFCs where water retention inside the electrolyte plays a role even more important than in DMFCs.

III.1.5 References

[1] L. Tchicaya-Bouckary, D. J. Jones, J. Rozière, Fuel Cells 2 (2002) 40.

[2] K.T. Adjemian, S.L. Lee, S. Srinivasan, J. Benziger, A.B. Bocarsly, J. Electrochem. Soc. 149 (2002) A256.

[3] O. Savadogo, J. New Mater. Electrochem. Syst. 1 (1998) 47.

[4] G. Alberti , M. Casciola, Solid State Ionics 97 (1997) 177

[5] J. Wang, S. Wasmus, R. F. Savinell, J. Electrochem. Soc. 142 (1995) 4218.

[6] A. S. Aricò, P. Creti, P. L. Antonucci, V. Antonucci, Electrochem. Solid-State Lett. 1 (1998) 66.

[7] K. D. Kreuer, J. Membr. Sci. 185 (2001) 29.

[8] C. Hasiotis, V. Deimede, C. Kontoyannis, Electrochim. Acta 46 (2001) 2401.

[9] P. Staiti, A.S. Aricò, V. Baglio, F. Lufrano, E. Passalacqua ,V. Antonucci, Solid State Ionics 145 (2002) 101.

[10] V. Antonucci, A.S. Aricò, Europ. Patent 1999, EP 0 926 754 A1, 1-5.

[11] P. Costamagna, C. Yang, A.B. Bocarsly, S. Srinivasan Electrochim. Acta 47 (2002) 1023.

[12] E. Traversa, M.L. Di Vona, S. Licoccia, M. Sacerdoti, M.C. Carotta, L. Crema, G. Martinelli, J. Sol-Gel Sci. Technol. 22 (2001) 167.

[13] A. S. Aricò, V. Antonucci, M. Minutoli and N. Giordano, Carbon, 27 (1989) 337.

[14] K. D. Kreuer, St. Adams, W. Munch, A. Fuchs, U. Klock, J. Maier, Solid State Ionics 145 (20019 295.

[15] N. Giordano, P. Staiti, S. Hocevar, A.S. Aricò, Electrochim. Acta 41 (1996) 397.

[16] R. K. Iler " The Chemistry of Silica", Wiley-Interscience, John Wiley and Sons, New York, 1979, pp 622-710

[17] A. J. Leonard, P. Ratnasamy, F. D. Declerck, J. J. Fripiat, Faraday Discussion, 52 (1971) 185484.

[18] C. Morterra, E. Giamello, L. Orio, M. Volante, J. Phys. Chem. 94 (1990) 3111.

[19] M. Cappadonia, J. W. Erning, U. Stimming, J. Electroanal. Chem., 376 (1994) 189.

[20] A. S. Aricò, P.L. Antonucci, N. Giordano, V. Antonucci, Materials letters 24 (1995) 399.

[21] I. Honma, O. Nishikawa, T. Sugimoto, S. Nomura, H. Nakajima, Fuel Cells 2 (2002) 52.

[22] M. Tatsumisago, T. Minami, J. Am. Ceram. Soc. 72 (1989) 484.

[23] K. Vikulov, G. Martra, S. Coluccia, D. Miceli, F. Arena, A. Parmaliana, E. Paukshtis, Catal. Lett. 37 (1996) 235.

[24] N. Chen, R. T. Yang, J. Catal. 157 (1995) 76.
[25] H.P. Boehm, Adv. Catal. 16 (1966) 226.
[26] J. R. Scherer " The vibrational spectroscopy of water" in "Advances in Infrared and Raman Spectroscopy" Vol. 5 Edited by R.J.H. Clark and R. E. Hester, Heyden & Son Ltd London 1980, p. 149.
[27] K. D. Kreuer, Solid State Ionics 97 (1997) 1.
[28] M. Watanabe, H. Uchida, Y. Seki, M. Emori, P. Stonehart, J. Electrochem. Soc. 143 (1996) 3847.
[29] V. Baglio, A. Di Blasi, A. S. Aricò, V. Antonucci, F. Serraino Fiory, S. Licoccia, E. Traversa, Mat. Res. Soc. Symp. Proc. Vol. 756 (2003) p. 345
[30] G. Gebel, P. Aldebert and M. Pineri, Macromolecules 20 (1987) 1525.
[31] R.B. Moore and C. R. Martin, Macromolecules 21 (1988) 1334.
[32] X. Ren, M. S. Wilson, S. Gottesfeld, J. Electrochem. Soc. 143 (1996) L12.
[33] N. Alonso-Vante, H. Tributsch, Nature (London) 323 (1986) 431.

III.2 Influence of TiO_2 nanometric filler on the behaviour of a composite membrane for applications in direct methanol fuel cells*

III.2.1 Introduction

At present, much attention is received by Direct Methanol Fuel Cells operating at temperatures close to 150°C and employing composite polymer electrolyte membranes. The relatively high protonic conductivities that perfluorosulfonic polymeric membranes exhibit at low temperatures (below 100°C), in addition to their chemical and mechanical stability, allow the use of these materials as electrolytes in Polymer Electrolyte Fuel Cells (PEFCs) [1-9]. In DMFCs, an increase in operation temperature up to 150°C is highly desirable to enhance the kinetics of methanol oxidation and to reduce the poisoning of the anode electrocatalyst due to the adsorbed methanolic residues. Accordingly, in the last years, significant efforts have been addressed to the development of high temperature polymer electrolyte membranes for DMFCs [10-14]. Recently, the use of Nafion membranes containing finely dispersed nanocrystalline ceramic oxide powders has been proposed [5, 7, paragraph III.1]. The role of the oxide powders is to improve the water retention characteristics of the membrane [15], allowing fuel cell operation at 145°C with low external humidification conditions. Yet, limited attention has been devoted to the investigation of structural and morphological properties of these oxides in relation to their use in composite membranes.

In the present work, the electrochemical behaviour of composite TiO_2-Nafion membranes has been studied to understand the influence of the inorganic filler content on the performance of a DMFC. An investigation of the influence of particle size and TiO_2 crystallographic phase transition (from anatase to rutile) on the electrochemical behaviour of a composite membrane for high temperature operation has also been carried out.

III.2.2 Experimental

TiO_2 nanometric powder was synthesized via a sol-gel procedure, starting from a $Ti(OiPr)_4$ (Aldrich) [16]. TG analysis of the obtained titania precursor was carried out in a Netzsch TG/DSC/DTA analyser. The precursor was then thermally treated at different temperatures (500°C, 650°C and 800°C) for 2 hours. XRD analysis was performed with a

* Two papers based on this study have been published on **J. New Materials for Electrochemical Systems 7 (2004) 275-280** and **Electrochimica Acta 50 (2005) 1241-1246**

Philips X-Pert diffractometer using Cu Kα source operating at 40 kV and 20 mA. Transmission electron microscopy (TEM) of the powders was carried out using a Philips CM12 microscope equipped with LaB_6 filament. XPS measurements were performed using a Physical Electronics (PHI) 5800-01 spectrometer equipped with a monochromatic Al source operating at 350 W. Element spectra were acquired with a pass energy of 11.75 eV. pH of slurry was measured at room temperature by an ATC compensated pH probe (Orion). The slurry was composed by 0.5 g of powder suspended in 0.1 L of bi-distilled water and stirred for 24 hrs in the presence of a stream of nitrogen. A steady pH value was typically obtained after a few tens of minutes and no significant pH drift was recorded after 24 hrs (< 0.05 pH units). The pH of slurry was sampled in any case after 24 hrs. Scanning electron microscopy (SEM) of the powders was carried out using a Cambridge Stereoscan 360 instrument equipped with LaB_6 filament and operating at an acceleration voltage of 20 kV.

The following membranes were prepared: 1) Recast Nafion, 2) Recast Nafion + 3 wt% TiO_2 calcined at 500°C, 3) Recast Nafion + 5 wt% TiO_2 calcined at 500°C, 4) Recast Nafion + 10 wt% TiO_2 calcined at 500°C, 5) Recast Nafion + 5 wt% TiO_2 calcined at 650°C, 6) Recast Nafion + 5 wt% TiO_2 calcined at 800°C. All the membranes were prepared by a recast procedure [6,7]. The Nafion ionomer was mixed with dimethyl-sulfoxide (DMSO) and TiO2 powder in an ultrasonic bath. The slurry was cast over a glass substrate. The solution was slowly evaporated at 80°C under vacuum to achieve a dense polymeric film. This latter was detached from the glass substrate by addition of distilled water and hot pressed between two PTFE foils at 160°C for 10 minutes. The thickness of all the membranes was about 100 μm. The catalyst used for methanol oxidation was a 60 wt% Pt-Ru (1:1)/Vulcan (E-TEK), whereas a 30 wt% Pt/Vulcan (E-TEK) was used for oxygen reduction. The platinum loading in all the electrodes was 2 mg cm^{-2}. For both anode and cathode, the reaction layer was prepared by directly mixing in an ultrasonic bath a suspension of Nafion ionomer in water with the catalyst powder (catalyst/dry ionomer = 2/1 wt.); the obtained paste was spread on carbon cloth backings. MEAs were prepared by hot pressing the electrodes onto the membrane at 130°C and 50 atm.

Fuel cell tests were carried out in a 5 cm^2 single cell (GlobeTech, Inc.) connected to a HP 6060B electronic load. Aqueous solutions of methanol of varying concentrations (0.5, 1 and 2 M) and oxidant (oxygen or air), preheated at 85°C, were fed to the cell. The methanol solution was fed into the cell at a flow rate of 2.5 ml/min. For the cathode feed, oxygen or air at a flow rate of 500 ml/min was passed through a humidification bottle maintained at 85°C. Different operating temperatures for the cell were settled in the range from 90° to 145°C. The

anode back-pressure was varied between 1 and 3.5 atm abs. as the temperature was increased from 90° to 145°C; the cathode compartment back-pressure was maintained constant at 3.5 atm abs. The cell resistance was determined at the various temperatures by the current interrupter method during cell operation at 400 mA cm^{-2}.

III.2.3 Results and Discussion

The TG scan of the precursor obtained by sol-gel shows that only a very slight weight loss (1% wt.) occurs above 450°C (Fig. 1). The powders were then calcined at 500°C, 650°C and 800°C to obtain crystalline TiO_2. Fig. 2 shows the X-ray diffraction patterns of the TiO_2 samples after thermal treatments at the three selected temperatures. The presence of the crystallographic structure of anatase was observed for the powders calcined at 500°C and 650°C while the crystallographic structure of rutile was observed for the sample calcined at 800°C [16]. The crystallite size for the three samples, determined using the Scherrer's equation, was 12, 22 and 39 nm, respectively. The inset of Fig. 2 shows the XRD pattern of the composite Nafion membrane containing 5 wt% TiO_2 calcined at 500°C. This composite membrane shows the typical diffraction pattern of Nafion and small reflections due to TiO_2 in the anatase phase.

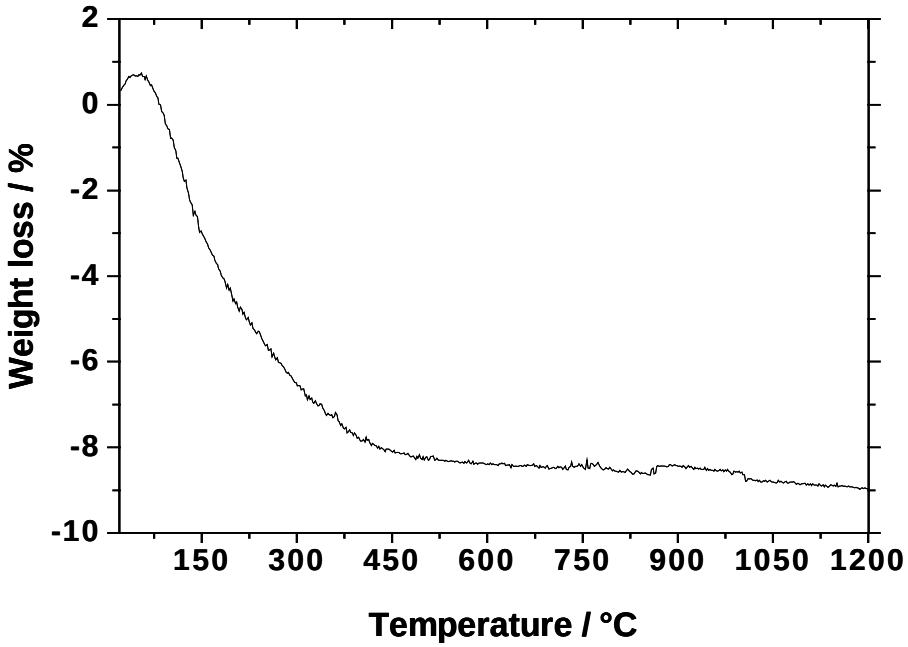

Fig. 1. TG analysis of the titania precursor obtained from the sol-gel procedure.

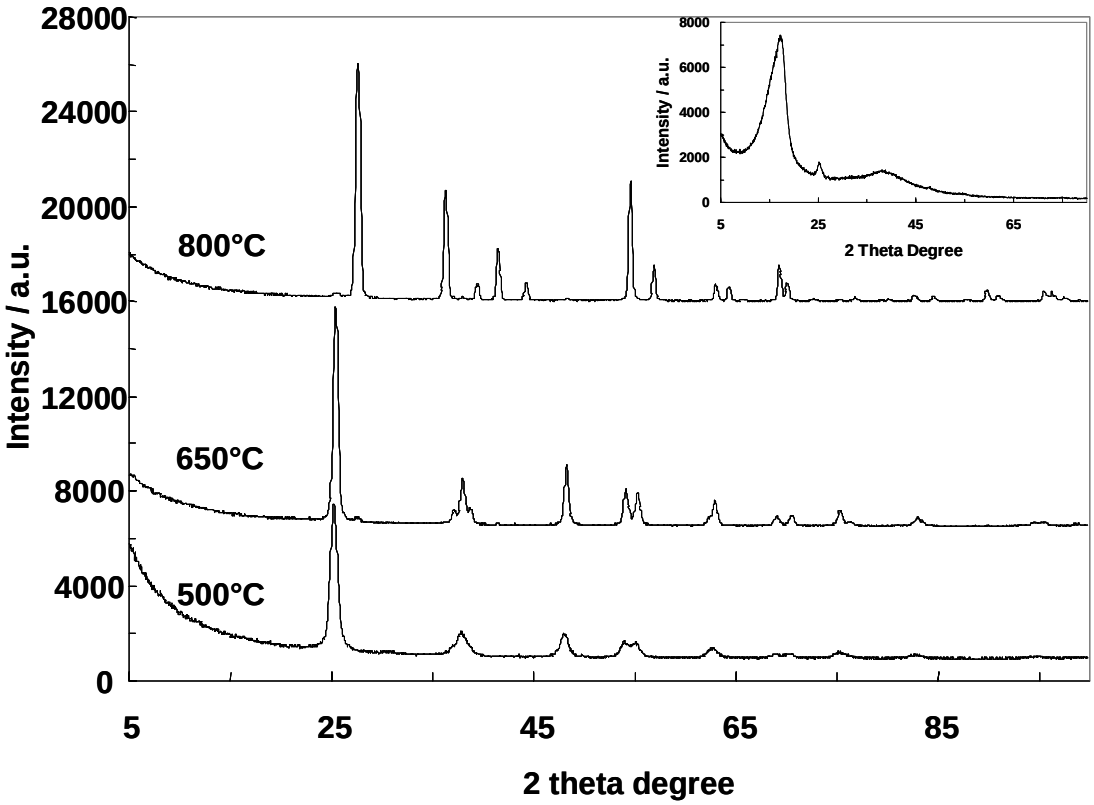

Fig. 2. X-ray diffraction patterns of TiO_2 powders calcined at different temperatures; inset: 5wt.% TiO_2 (calcined at 500°C) based recast Nafion membrane.

Scanning electron microscopy (SEM) analysis of the nanocrystalline powders evidenced a similar morphology for the oxides with the same crystallographic structure, whereas significantly larger particles and a different morphology were observed for TiO_2 calcined at 800°C (Fig. 3). Fig. 4 shows the TEM micrographs of the various TiO_2 samples. The particle size is in agreement with the XRD measurements for the powder calcined at the lowest temperature (500°C), although proper determination of the primary particle dimension was not possible because of the presence of agglomerates. Larger particles were observed in the TEM images of the samples fired at 650 and 800 °C; as expected, the particle size increases progressively with the thermal treatment temperature.

The surface chemistry of the TiO_2 powders was investigated by X-ray photoelectron spectroscopy (Figs. 5 and 6). The Ti $2p_{3/2}$ and Ti $2p_{1/2}$ photo-electron lines (Fig. 5) occurred at the same binding energies for the three samples (458.4 ± 0.2 eV and 463.94 ± 0.2 eV, respectively). This B.E. is typical of TiO_2 compounds; accordingly, the photo-electron peaks are mainly associated to the main Ti sites from the titania framework with small influence from surface defects. The O 1s region of the XPS spectra (Fig. 6) showed similar values of

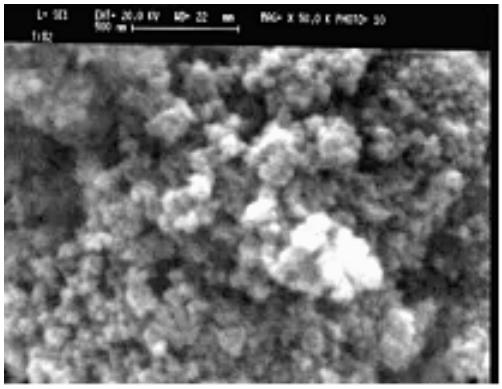

500°C

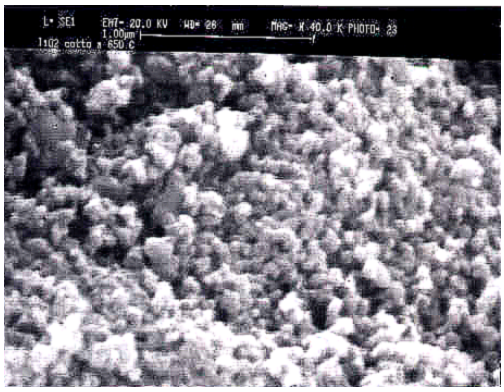

650°C

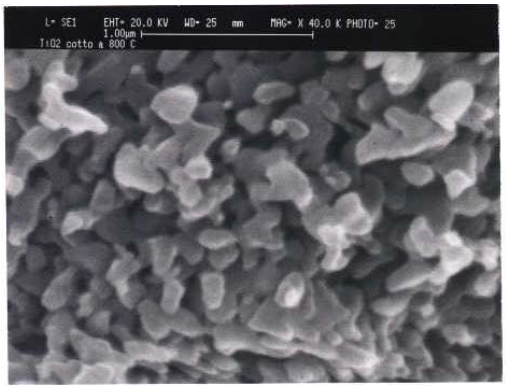

800°C

Fig. 3. Scanning electron micrographs of the TiO_2 powders calcined at different temperatures employed in the preparation of the composite membranes.

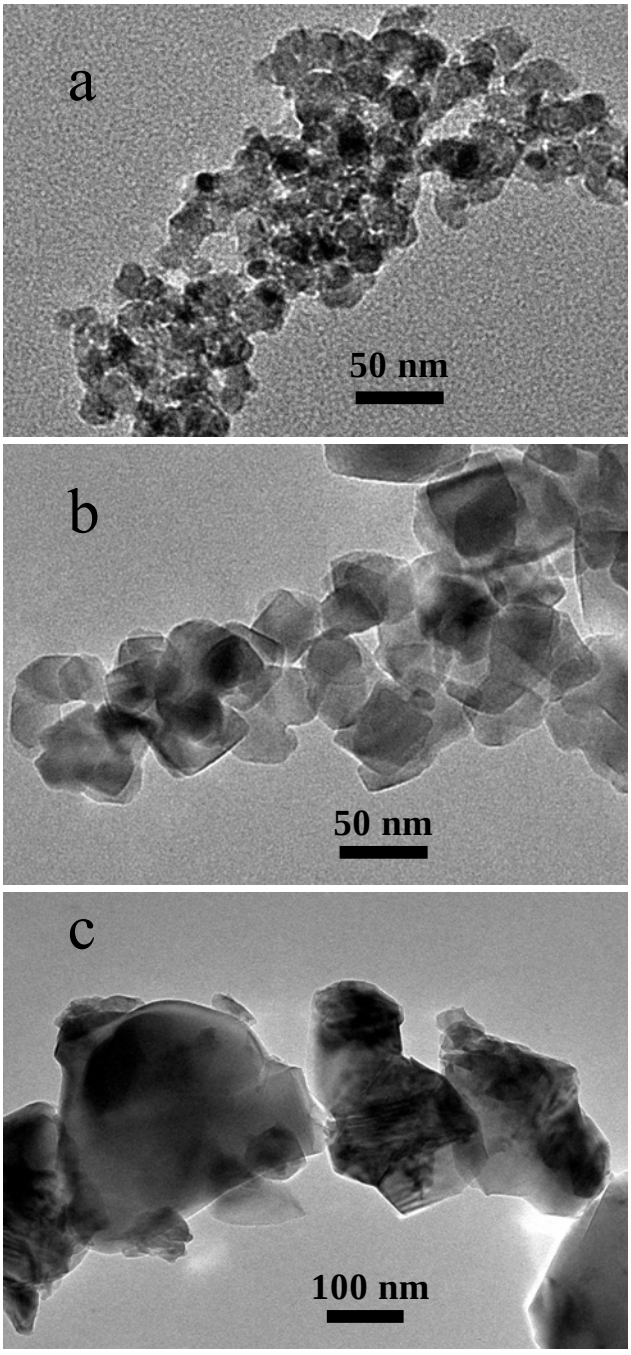

Fig. 4. Transmission electron micrographs of the TiO_2 powders calcined at 500°C (a), 650°C (b) and 800°C (c) employed in the preparation of the composite membranes.

B.E. for the main peak (Table 1) of the various TiO_2 samples (529.6 eV). However, the TiO_2 powders treated at 500°C and 650°C and characterized by the anatase structure showed a larger content of oxygen species at higher binding energies. These peaks, centered at about 530.8 eV (Fig. 6), are associated with the presence of surface OH groups. Their intensity is not very high with respect to the main O 1s peak deriving from crystalline TiO_2 framework. However the occurrence of Ti-OH groups on the surface imparts a slight acidic behaviour to the fillers [17]. This finding was confirmed by the measurements of the pH of slurry for the titania powders; the higher the temperature of the powder calcinations, the higher the measured values of the pH of slurry, up to basic value for the powder heated to 800°C (Table 2). The XPS analysis showed that the ratio between the intensities of the acidic Ti-OH surface species and the neutral -O-Ti-O- species from the framework was slightly larger for the sample treated at the lowest temperature (500°C). The more acidic behaviour of this sample with respect to the powder heated to 650°C can be also ascribed to its smaller particle size, and thus its larger surface area (Fig. 6a-b). The concentration of surface OH groups was lower for the sample calcined at 800°C and having the rutile structure, because of the water elimination reactions induced by the thermal treatment (Fig. 6c). Yet, a small peak was still present in the higher binding energies region of the O 1s spectrum.

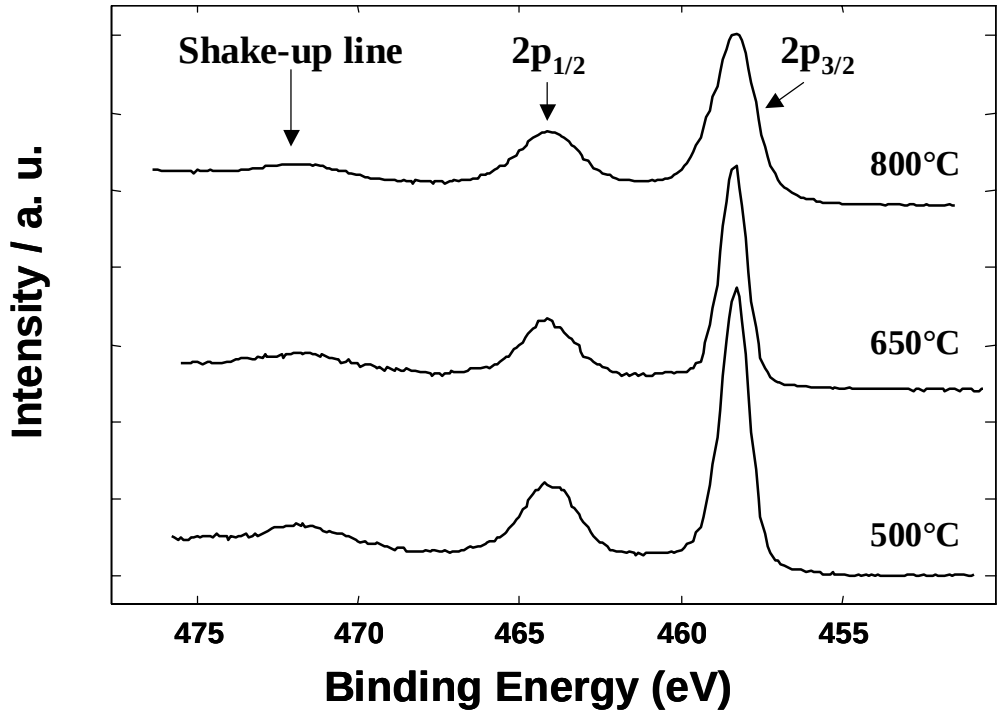

Fig. 5. Comparison of the Ti 2p X-ray photoelectron peaks for the TiO_2 powder calcined at different temperatures.

These surface oxygen species are believed to be responsible of the water co-ordination on the filler surface during membrane operation above 100°C, probably assisting at different extents the proton conduction [17, 18]. The XPS O 1s peak component at higher B.E.s (at about 532 eV) could be associated with the presence of surface oxygen containing carbonaceous species adsorbed from the atmosphere.

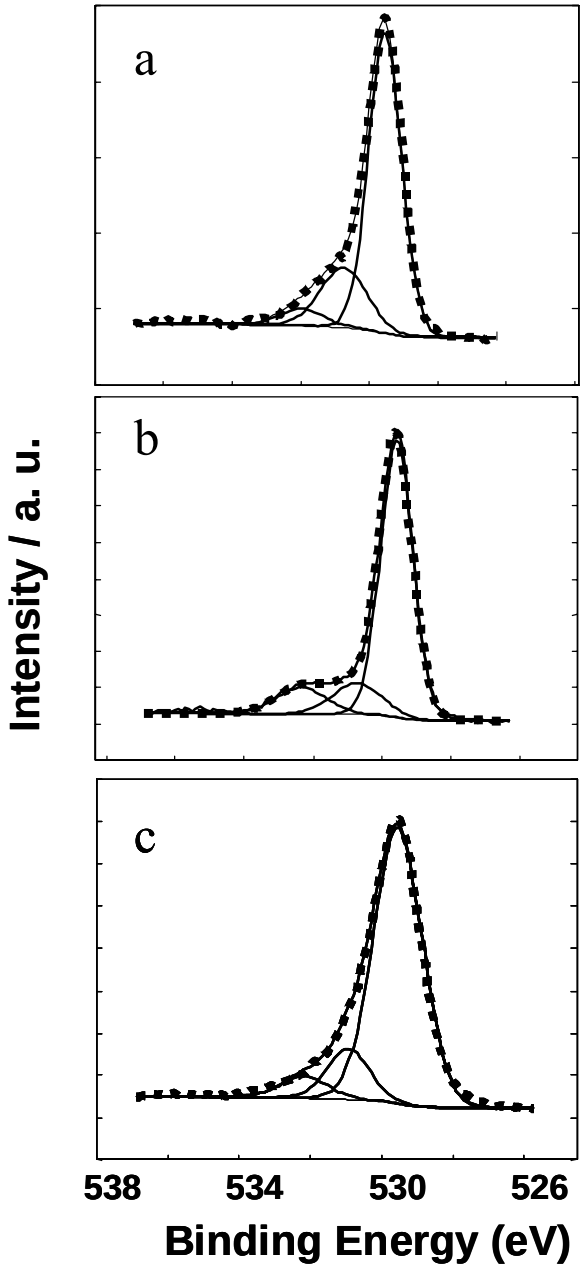

Fig. 6. Curve fitting of O 1s X-ray photoelectron peaks for the TiO_2 powder calcined at 500°C (a), 650°C (b) and 800°C (c).

Species	B.E. / eV	Relative peak area / %
TiO_2 calcined at 500°C		
O 1s	529.54	72.91
	530.76	21.08
	531.98	5.01
TiO_2 calcined at 650°C		
O 1s	529.56	75.52
	530.71	12.61
	532.33	11.87
TiO_2 calcined at 800°C		
O 1s	529.53	84.23
	530.93	11.20
	532.17	4.57

Table 1. B.E. and relative peak areas of O 1s species from curve-fitted XPS spectra for the various TiO_2 powders.

Filler	Crystallographic structure	Mean particle size* (nm)	pH of slurry
TiO_2 calcined at 500°C	Anatase	12	5.3
TiO_2 calcined at 650°C	Anatase	22	6.2
TiO_2 calcined at 800°C	Rutile	39	9.0

* From XRD; (101) reflection for anatase and (111) reflection for rutile.

Table 2. Physico-chemical properties of TiO_2 powders.

At first, the electrochemical behaviour of the various composite TiO_2-Nafion membranes was investigated to understand the influence of the inorganic filler content on the performance of a DMFC.

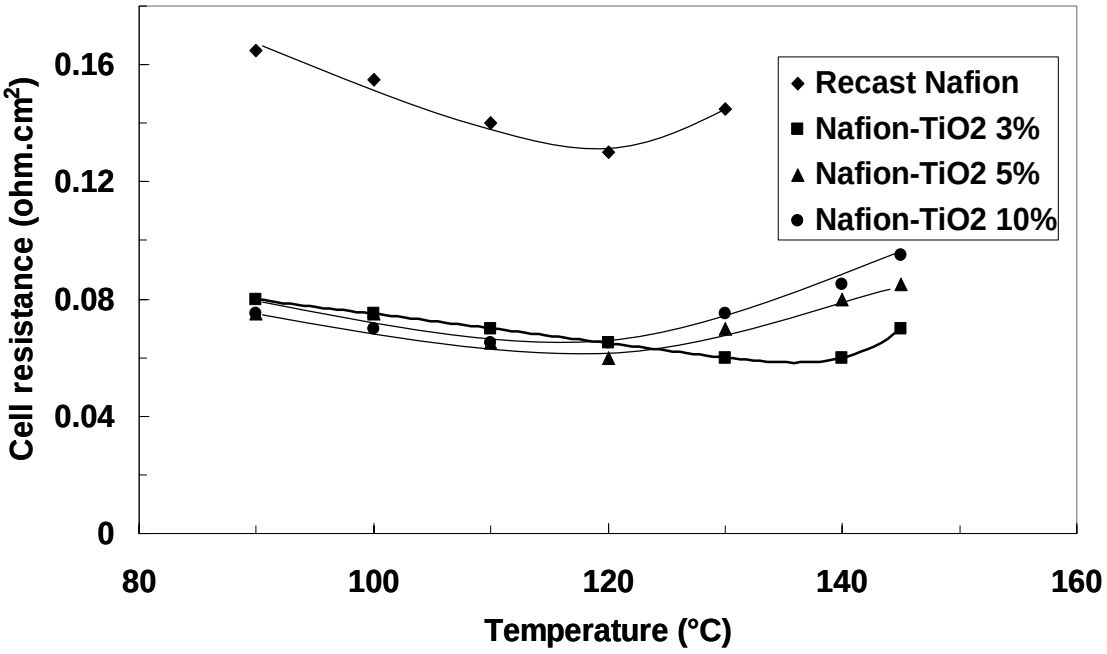

Fig. 7. Variation of cell resistance values as a function of the operating temperature for DMFCs employing the composite membranes containing different amounts of TiO_2 calcined at 500°C compared to bare recast Nafion.

All the MEAs equipped with the composite membranes containing TiO_2 calcined at 500°C were capable of operation at 145°C, whereas the cell using bare recast Nafion membrane reached the maximum performance at 120°C. This behaviour is due to the higher conductivity of the cell using TiO_2-containing membranes, as confirmed by cell resistance measurements. Fig. 7 shows the variation of the cell resistance as a function of the temperature for the assemblies equipped with composite membranes compared to bare recast Nafion. The cell resistance in the presence of composite membranes containing different amounts of titanium oxide did not vary in the range 90°-145°C, and it was lower than the resistance of the cell equipped with bare recast Nafion membrane. The cell resistance of the DMFC equipped with the bare recast Nafion membrane was not determined at 145°C since the cell showed very low current densities and an unstable behaviour at this temperature.

Figure 8a shows the polarization curves obtained for the fuel cell equipped with the different membranes in the presence of oxygen feed and 2 M methanol solution at 120°C. The

best electrochemical performances were obtained with membranes containing 3-5 wt% TiO_2 loading. The maximum power density recorded at 120°C was around 280 mW cm^{-2}. The composite membranes showed superior power densities at 120°C with respect to the recast Nafion membrane (Fig. 8b).

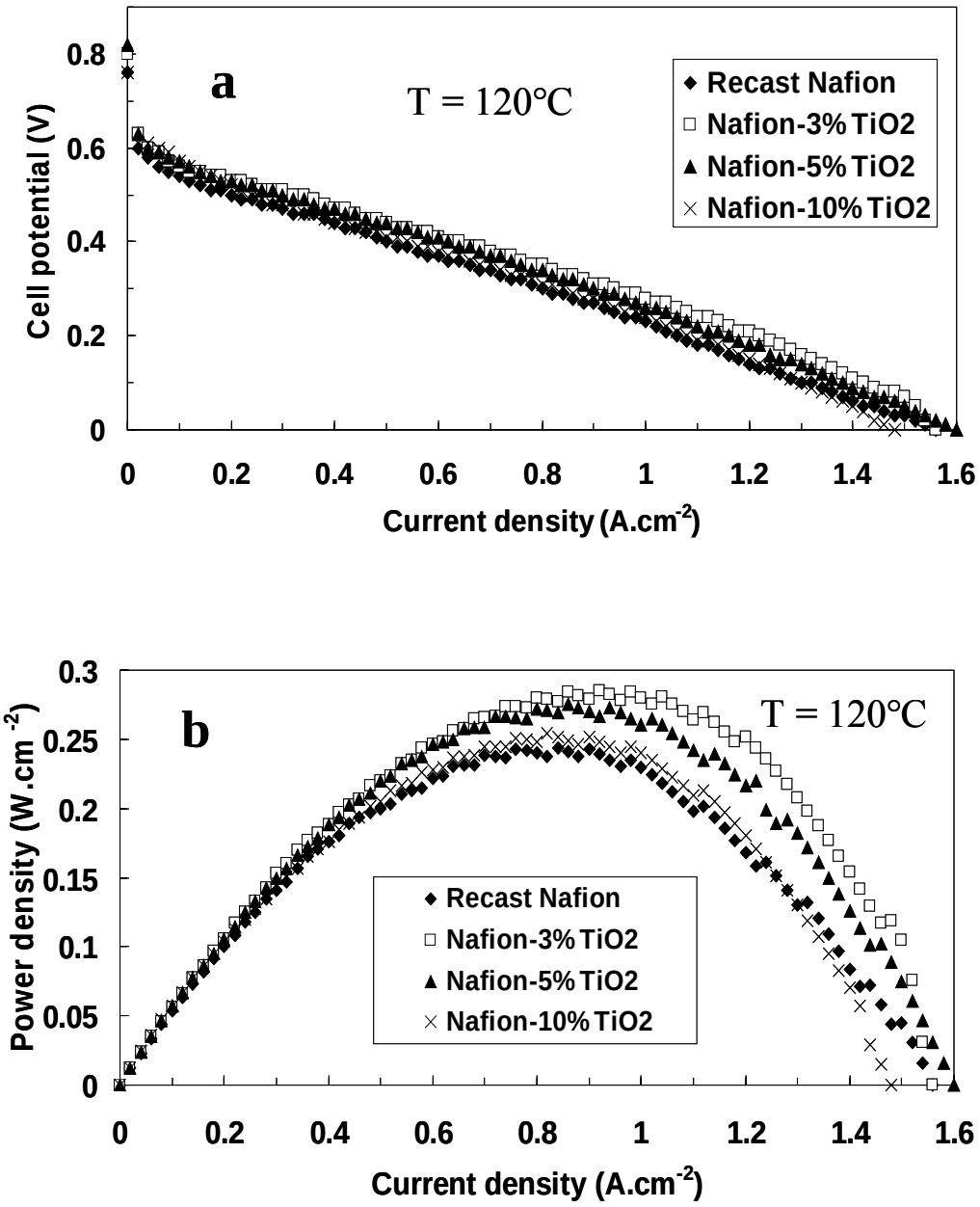

Fig. 8. DMFC polarization (a) and power density (b) curves at 120°C for various MEAs equipped with the composite membranes containing different amounts of TiO_2 calcined at 500°C compared to bare recast Nafion. 2M methanol feed, 1.5 atm rel.; oxygen feed, 2.5 atm rel.

It is well known that a high operating temperature, approaching 150°C, increases the catalyst tolerance towards adsorbed poisoning residues and reduces water and heat management. Fig. 9 shows the polarization and power density curves for the fuel cell equipped with the composite membranes containing the various amounts of titania, in the presence of oxygen feed and 2 M methanol solution at 145°C. The DMFC performance for the composite membranes further improved up to 145°C whereas the bare membrane did not show any capability to operate under such conditions, as already stated (not shown). This was due to a strong decrease in conductivity of the bare membrane. On the contrary, the cells equipped with composite membranes reached the operation temperature of 145°C (Fig. 9a).

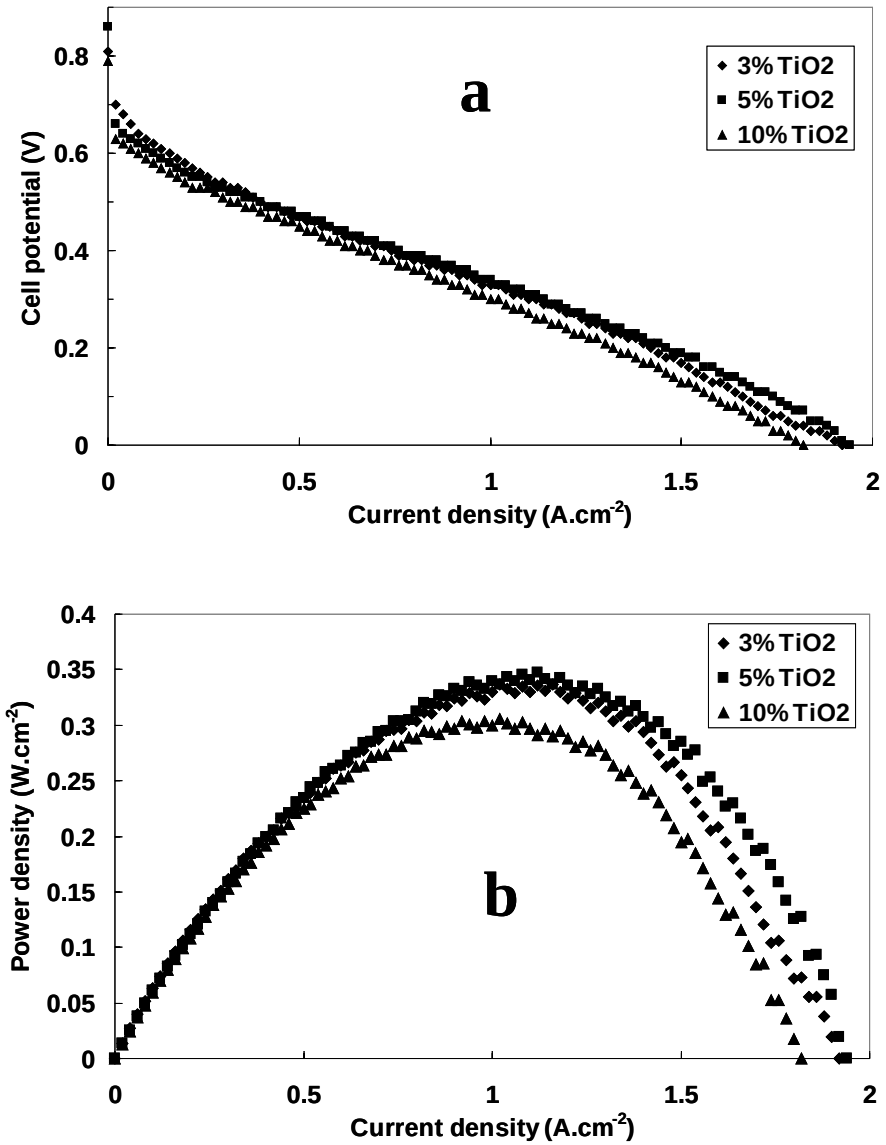

Fig. 9. DMFC polarization (a) and power density (b) curves at 145°C for various MEAs equipped the composite TiO_2-Nafion membranes. 2M methanol feed, 2.5 atm rel.; oxygen feed, 2.5 atm rel.

A maximum power density of 350 mW cm^{-2} was reached at a current density of about 1.1 A cm^{-2} with oxygen at 145°C (Fig. 9b). The performance of the composite membranes decreased with increasing the titanium oxide content up to 10 wt%, probably due to a unsuitable powder dispersion in the membrane; in this regard, the cell resistance also plays a considerable role.

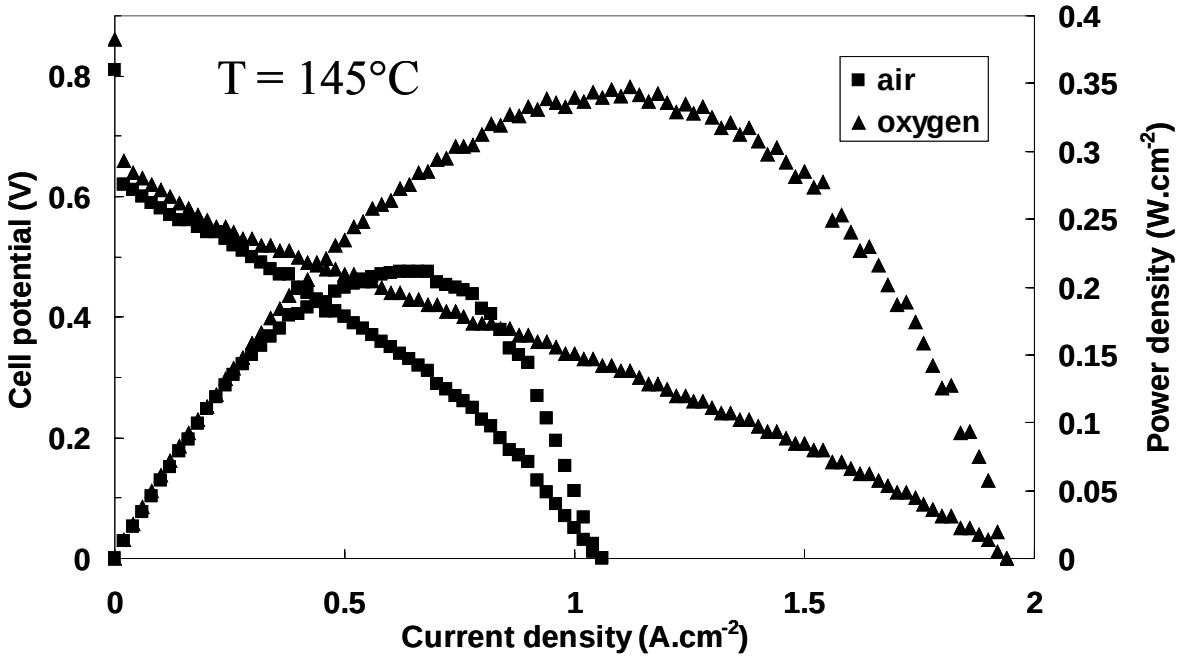

Fig. 10. Comparison of the polarization and power density curves in the presence of air and oxygen feed for the MEA equipped with recast Nafion + 5 wt% TiO_2 (calcined at 500°C) at 145°C. Operating conditions: oxygen feed, 2M methanol; air feed, 1M methanol.

Fig. 10 shows the comparison between the polarization and power density curves for the fuel cell equipped with the composite membrane containing 5 wt% TiO_2, at 145°C in the presence of air or oxygen feed. The best electrochemical performances were obtained, for all the membranes, with 2 M methanol solution feed at the anode when oxygen was used as oxidant; when air was fed to the cathode compartment, the best fuel cell performances were obtained with 1M MeOH solution. This can be attributed to the effect of methanol cross-over on cathode polarization, which is more significant in the presence of air as oxidant. The maximum power density obtained in air with the recast Nafion + 5 wt% TiO_2 (calcined at 500°C) was 210 mW cm^{-2} at 145°C; passing from oxygen to air the performance loss, in terms of maximum power density, was about 40%. Oxygen operation is useful to understand the fundamental properties of the membranes in absence of side effects such as mass transfer polarization constraints; air feed is important under practical operating conditions.

The 5 wt% TiO_2 loading was selected to investigate the influence of the ceramic oxide surface area on the electrochemical behaviour of DMFCs equipped with the composite membranes.

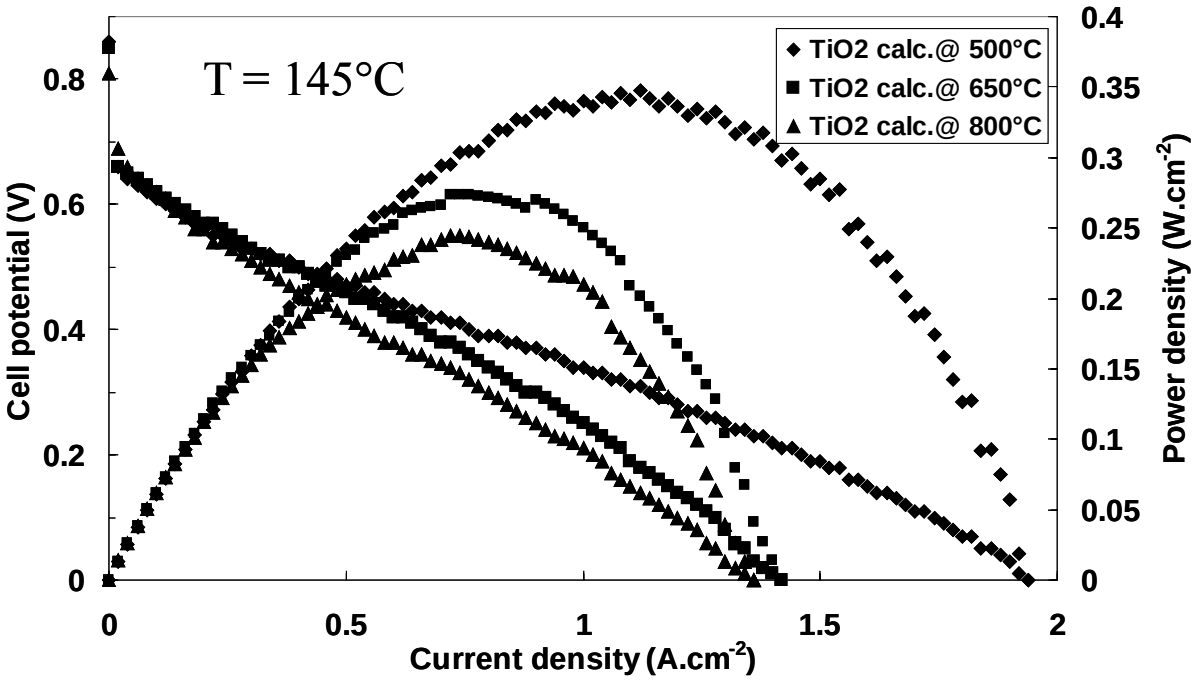

Fig. 11. Polarization and power density curves at 145°C for the various MEAs equipped with the composite Nafion membranes containing 5 wt% TiO_2 calcined at different temperatures. 2M methanol feed, 2.5 atm rel.; oxygen feed, 2.5 atm rel.

Fig. 11 shows the polarization and power density curves for the fuel cells equipped with recast Nafion membranes containing 5 wt% TiO_2 calcined at different temperatures. The best electrochemical performances, in terms of both power density and short circuit current density, were obtained with the cell equipped with the composite membrane including the smaller TiO_2 particles. The membranes with powder calcined at the highest temperature, having large crystallite dimensions, can also operate at 145°C but showed a poorer electrochemical behaviour, due to the higher cell resistance (Fig. 12). This indicates that the water retention properties of the composite membranes [15] are strictly related to the number of adsorbing sites. Nothing can be said about the influence of the different crystallographic structure of titanium oxide, because different particle sizes are associated with different crystalline phases. Most likely, the differences in cell resistance and, consequently, in performance are only due to the different surface areas. The high temperature operation capability of the composite membrane relies in the water adsorption properties of the

hygroscopic inorganic filler. The nature of the interaction between water molecules and the adsorbing sites on the filler surface has been previously investigated [17, 18, paragraph III.1]. The main difference between TiO_2 and other hygroscopic fillers, such as silica, is due to the nature and electronic environment of the surface functional groups. The present performances obtained with the TiO_2-composite membranes do not significantly differ from those recently reported for the Nafion-SiO_2 electrolytes [15]. It should be pointed out, however, that, in the case of the Nafion-SiO_2 membranes, amorphous silica has been mainly used. The TiO_2 powders offer the further advantage of tailoring the crystallographic structure allowing to modulate the physico-chemical characteristics and thus the water adsorption properties.

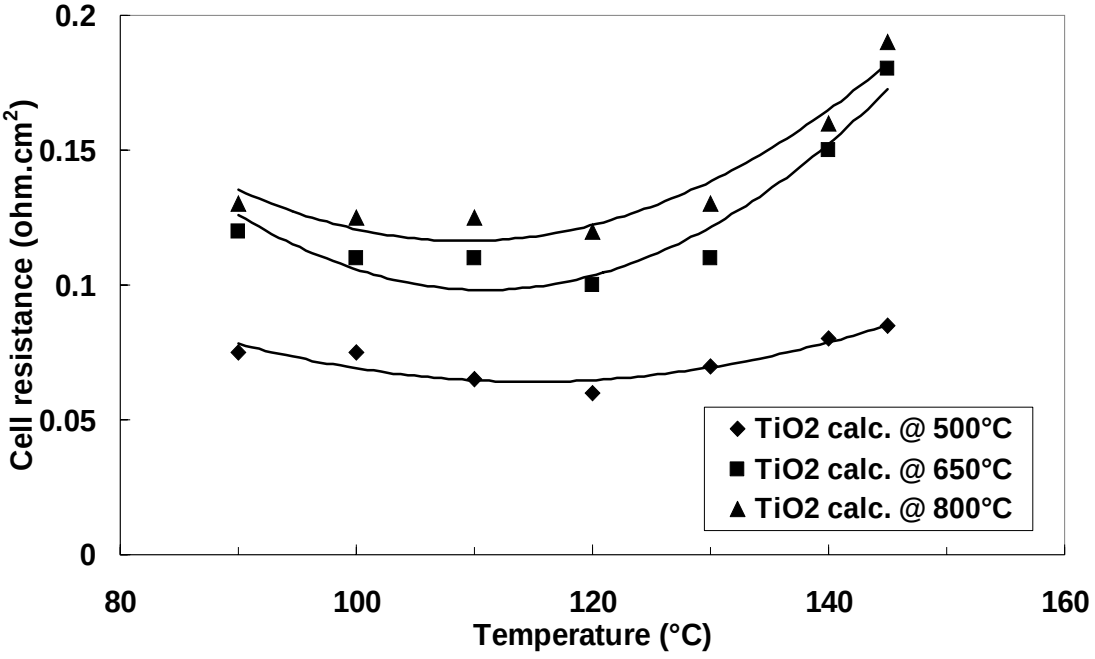

Fig. 12. Variation of cell resistance values as a function of the operating temperature for DMFCs employing the composite membranes containing 5 wt% TiO_2 calcined at different temperatures.

A considerable aspect for a successful application of a composite polymer electrolyte in fuel cell devices is the performance stability. In general, cycled operation is interesting for application in automotive systems where discontinuous operation is required. Accordingly, the DMFC equipped with Nafion membrane + 5 wt% TiO_2 (calcined at 500°C) was subjected to one month cycled operation. The cell was operated around 6 hours per day, including the start up and shut down procedures. Fig. 13 reports the recorded cell current density, at a cell potential of 0.4 V. A similar behaviour was recorded during all the days of operation. The

slight decrease of performance with time is due to the strongly adsorbed methanolic residues poisoning the anode catalyst. When the cell is discharged by feeding water at anode, the initial performance is regained the following day.

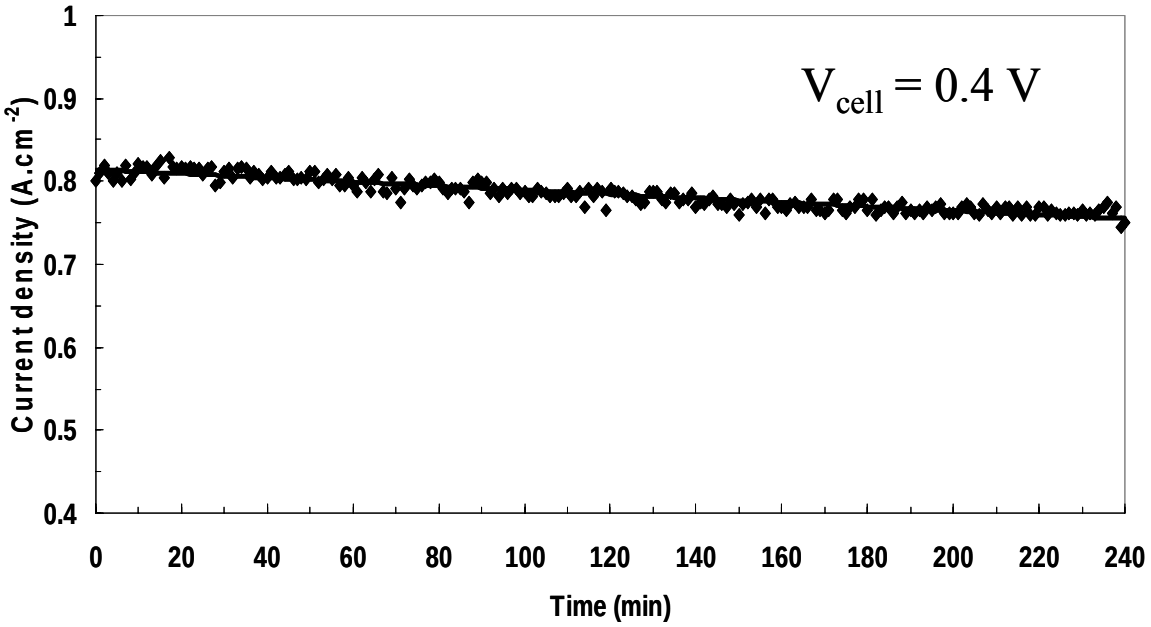

Fig. 13. Variation of DMFC current density for the MEA based on composite recast Nafion membrane + 5 wt% TiO2 calcined at 500°C as a function of time during a day operation under potentiostatic control. Cell voltage 0.4 V, temperature 145°C, 2M methanol feed, 2.5 atm rel., oxygen feed, 2.5 atm rel.

III.2.4 Conclusions

Composite Nafion-TiO_2 membranes have shown good properties for operation at 145°C in a Direct Methanol Fuel Cell, as a consequence of their improved water retention characteristics. DMFC investigation of these membranes reveals a significant influence of the ceramic oxide particle size and surface area on the electrochemical behaviour. This indicates that the water retention properties are related to the number of adsorbing sites. Further enhancement of such properties may be achieved through a proper tailoring of the filler morphology and structure.

III.2.5 References

[1] M. Neergat, D. Leveratto, U. Stimming, *Fuel Cells* 2, 25 (2002)

[2] S. Wasmus and A. Kuver, *J. Electroanal. Chem.* 40, 150 (1999)

[3] O. Savadogo, *J. New Mat. Electrochem. Systems* 1, 47 (1998)

[4] A. S. Aricò, S. Srinivasan and V. Antonucci, *Fuel Cells* 1, 133 (2001)

[5] K.T. Adjemian, S.L. Lee, S. Srinivasan, J. Benziger, A.B. Bocarsly, *J. Electrochem. Soc.* 149, A256 (2002)

[6] M. Watanabe, H. Uchida, Y. Seki, M. Emori, P. Stonehart, *J. Electrochem. Soc.* 143, 3847 (1996)

[7] A.S. Aricò, P. Cretì, P.L. Antonucci, V. Antonucci, *Electrochem. Solid State Lett.* 1, 66 (1998)

[8] C. Yang, S. Srinivasan, A.S. Aricò, P. Cretì, V. Baglio, V. Antonucci, *Electrochem. Solid State Lett.* 4, A31 (2001)

[9] B. Bonnet, D.J. Jones, J. Roziere, L. Tchicaya, G. Alberti, M. Casciola, L. Massinelli, B. Bauer, A. Peraio, E. Ramunni, *J. New Mat. Electrochem. Systems* 3, 87 (2000)

[10] J. Kerres, W. Zhang, L. Jorissen, V. Gogel, *J. New Mat. Electrochem. Systems* 5, 97 (2002)

[11] F. Meier, J. Kerres and G. Eigenberger, *J. New Mat. Electrochem. Systems* 5, 91 (2002)

[12] P. Staiti, A.S. Aricò, V. Baglio, F. Lufrano, E. Passalacqua, V. Antonucci, *Solid State Ionics* 145, 101 (2001)

[13] B. Tazi and O. Savadogo, *J. New Mat. Electrochem. Systems* 4, 187 (2001)

[14] K.D. Kreuer, J. Membr. Sci. 185, 29 (2001)

[15] A.S. Aricò, V. Baglio, A. Di Blasi, P. Cretì, P.L. Antonucci, V. Antonucci, *Solid State Ionics* 161, 251 (2003)

[16] E. Traversa, M.L. Di Vona, S. Licoccia, M. Sacerdoti, M.C. Carotta, L. Crema, G. Martinelli, *J. Sol-Gel Sci. Technol.* 22, 167 (2001)

[17] A.S. Aricò, V. Baglio, A. Di Blasi, E. Modica, P.L. Antonucci, V. Antonucci, *J. Power Sources*, 128, 113 (2004)

[18] A.S. Aricò, V. Baglio, A. Di Blasi, V. Antonucci, *Electrochemistry Comm.* 5, 862 (2003)

III.3 Zeolite-based composite membranes for high temperature direct methanol fuel cells*

III.3.1 Introduction

A direct methanol fuel cell based on a high temperature proton conducting membrane with suitable conductivity and stability up to 130°-150 °C and characterized by low thermal and water management would become a viable system for mobile applications [1-7]. In this regard, composite membranes with the filler exhibiting strong affinity towards water molecules are of particular interest. Various reports have dealt with the use of composite recast Nafion membranes containing finely dispersed ceramic oxide powders in high temperature direct methanol and H_2-air fuel cells [8-13, paragraphs III.1 and III.2]. In fact, the role of inorganic filler is to improve the water retention in the membrane, allowing an increase of fuel cell operation temperature in conjunction with low external humidification conditions. A further effect of the composite membrane is the reduction of methanol cross-over [14, 15]. It is well known that the physical adsorption of water by materials such as silica (one of the most used inorganic fillers) is mainly determined by the functional groups on the surface of these oxides that act as water co-ordination centers [16, paragraph III.1]; similar considerations can be made for other hygroscopic inorganic materials such as zeolites [17, 18].

To improve the proton conductivity of Nafion at high temperature, we have selected three natural zeolites as inorganic fillers in composite membranes, due to their characteristics of proton conductors and hygroscopic materials [15, 17, 19]. Thus, in the present study, we have prepared Nafion-zeolite composite membranes using Chabazite, Clinoptilolite and Mordenite as fillers. The behaviour of the composite membranes was evaluated under high temperature DMFC operation (140°C). A membrane/electrodes assembly (MEA) based on bare recast Nafion membrane was also investigated for comparison.

III.3.2 Experimental

The zeolites were received from GSA Resources Inc, Tucson AZ. The as-received zeolite materials were ground in an agate mill until an impalpable powder was obtained. The

* A paper based on this study has been accepted for publication on **J. Applied Electrochemistry** (in press)

zeolites were converted from Na^+ to H^+-form by treatment in a 0.01 M H_2SO_4 aqueous solution. X-ray diffraction (XRD) analysis of the zeolite powders before and after the acid treatment was carried out with a Philips X-Pert X-ray diffractometer using Cu Kα source operating at 40 kV and 20 mA. BET surface area measurements of the zeolite fillers were made by a Thermoquest 1990 series Sorptomatic. The fillers were compacted into pellets at 50 MPa and degassed in a sample holder at 140°C under vacuum before the measurement. Potentiometric titrations of the inorganic fillers were carried out as reported previously [20]; a Metrohm automated titration system equipped with an ATC compensated pH probe was used. The inorganic powder was suspended in aqueous electrolyte (KNO_3, 0.1 M) and continuously stirred in presence of N_2 purging. A defined amount of 0.1 N KOH was added for each sample and the slurry was back-titrated with 0.1 N HNO_3. The steady-state pH value was measured after each HNO_3 addition. The acid-base surface functional groups and the adsorption density function (OH^- - H^+) were determined from these measurements by a WinZPC software (Costech International).

The composite membranes were prepared using an alternative approach than that presented in our previous papers [16, 21]. 5 volumes of Nafion solution (5 wt.% Aldrich) were mixed with 5 volumes of ethanol and 3 volumes of N,N-dimethylformamide (DMF). The fine zeolite powder (in H^+-form) was then added to the resulting mixture and dispersed by stirring and sonication. The suspension was cast in a teflon dish; afterwards, it was treated at 80°C in a vacuum oven. Composite membranes with zeolite content of 3 and 6 vol.% were thus obtained. In order to evaluate the influence of the zeolite fillers on the electrochemical behaviour of the membrane for application in high temperature DMFC, a bare recast Nafion membrane was also prepared using the same procedure. The thickness of all the membranes was about 70 μm. The catalyst employed for methanol oxidation was a 60 wt% Pt-Ru (1:1)/Vulcan (E-TEK), whereas a 30 wt% Pt/Vulcan (E-TEK) was used for oxygen reduction. The platinum loading in all the electrodes was 2 ± 0.2 mg cm^{-2}. For both anode and cathode, the reaction layer was prepared by directly mixing in an ultrasonic bath a suspension of Nafion ionomer in water with the catalyst powder (catalyst/dry ionomer = 2/1); the obtained paste was spread on carbon cloth backings. Membrane & electrodes assemblies were prepared by hot pressing the electrodes onto the membrane at 130°C and 50 kg cm^{-2}.

Fuel cell tests were carried out in a 5 cm^2 single cell (GlobeTech, Inc.) connected to a HP 6060B electronic load. 2M aqueous solutions of methanol and oxygen, preheated at 85°C, were fed to the cell. The methanol solution was fed into the cell at a flow rate of 2.5 ml/min whereas for the cathode feed oxygen at a flow rate of 500 ml/min was passed through a

humidification bottle maintained at 85°C. Different operating temperatures for the cell were settled in the range from 90° to 145°C. The anode back-pressure was varied between 1 and 3.5 atm abs. as the temperature was increased from 90° to 145°C; the cathode compartment back-pressure was maintained constant at 3.5 atm abs.

III.3.3 Results and discussion

Fig. 1 shows the X-ray diffraction patterns of the three zeolite powders converted in H^+-form by treatment in diluted sulfuric acid. From a comparison between the diffraction patterns of the powders before (not shown) and after the treatment, no change in the crystallographic structure of the zeolites has been evidenced. The treated materials were used as fillers in the composite membranes in order to get advantage of the proton conduction as well as the water retention properties of these powders.

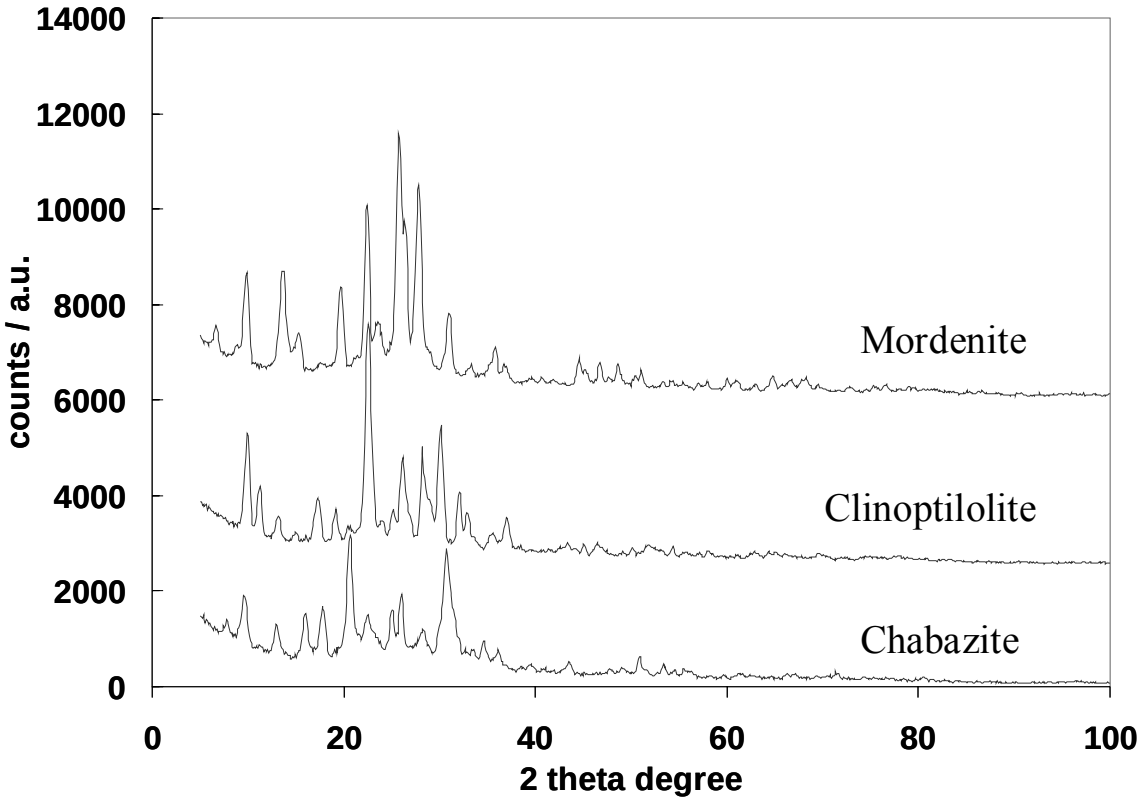

Fig. 1. X-ray diffraction patterns of the various zeolite powders after acid treatment.

The host environment of the inorganic filler particles inside the membrane may be considered, in a first approximation, as a solution of a diluted strong acid. The conductivity of Nafion® 1100 at room temperature is almost one order of magnitude lower than a 0.5 M

H_2SO_4 solution (6 10^{-2} S cm^{-1} vs. 4 10^{-1} S cm^{-1}). Accordingly, the adsorption density of OH^- species in the pH range around pH=2 as well as the zero point of charge (ZPC) may be indicative of the capability of the filler to adsorb water on the surface (Table 1). Fig. 2 shows the variation of the (OH^- - H^+) adsorption function versus pH for the H^+-exchanged zeolites in powder form. It is clearly observed that the adsorption density (OH^- - H^+) decreases in the low pH range according to the following series: mordenite>clinoptilolite>chabazite. The adsorption density appears to be related to the amount and strength of functional groups than to the BET surface area (Table 1).

Filler	BET Surface Area (m^2/g)	ZPC	Extra Ads. Function at pH 2.8 (ΓOH^- - ΓH^+) μmoles g-1	Basic or Acidic Functional Group Dissociation Constants	Basic or Acidic Functional Group Amounts (meq/g)
Mordenite	194.07	2.10	490.05	pKa= 8.03	1.053
				pKa= 3.56	0.965
Chabazite	341.25	3.43	-603.91	pKa= 8.02	0.650
				pKa= 4.16	0.950
Clinoptilolite	5.87	2.90	-31.11	pKa= 7.98	0.550
				pKa= 3.86	0.500

Table 1. Surface properties of zeolite fillers

The beneficial influence of the acid characteristics of the inorganic fillers on the high temperature performance of composite membranes in direct methanol fuel cells was already demonstrated in a recent paper [21]. The presence of acidic groups on the particle surface facilitates the co-ordination of water, that acts as vehicle for proton migration. Furthermore,

the characteristics of proton conduction of the zeolite materials can enhance the conductivity of the polymeric membranes.

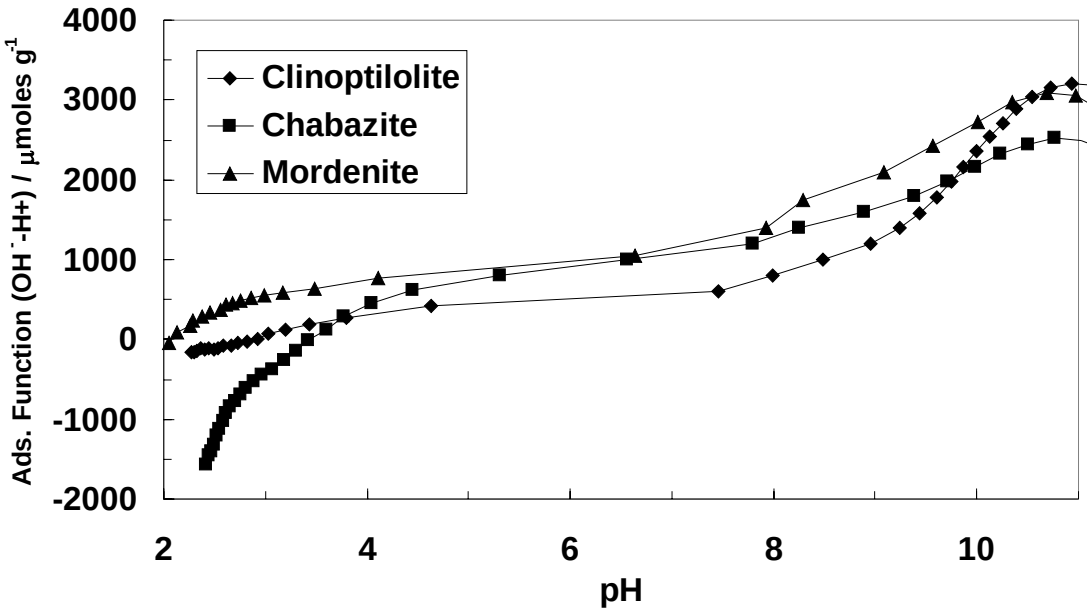

Fig. 2. Variation of the adsorption density function vs. pH for the various zeolite fillers.

Fig. 3 shows the variation of cell resistance as a function of temperature for the MEAs equipped with the composite membranes compared to bare recast Nafion. MEAs based on composite membranes containing 3 vol.% inorganic filler showed similar cell resistances for the three different zeolites. This resistance did not vary significantly in the range between 90° and 145°C. Effectively a small decrease from 90° to 130°C was observed followed by a slight increase at about 140°C. For what concerns the bare recast Nafion prepared by the same method, the cell resistance at 90° and 100°C was lower than that of composite membranes, whereas it increased significantly with the increase of temperature due to the dehydration of the membrane at high temperature. This probably indicates that the water retention effect is more significant with respect to the proton conduction behaviour of the zeolite powders.

All the MEAs equipped with the composite membranes were capable of operation at 140°C with an increase of cell performance as the temperature was increased from 90°C up to 140°C. Also the cell based on bare recast Nation membrane as electrolyte reached the operation temperature of 140°C, but the cell performance recorded at this temperature was equal to that obtained at 120° - 130°C due to the increase of cell resistance caused by dehydration (not shown).

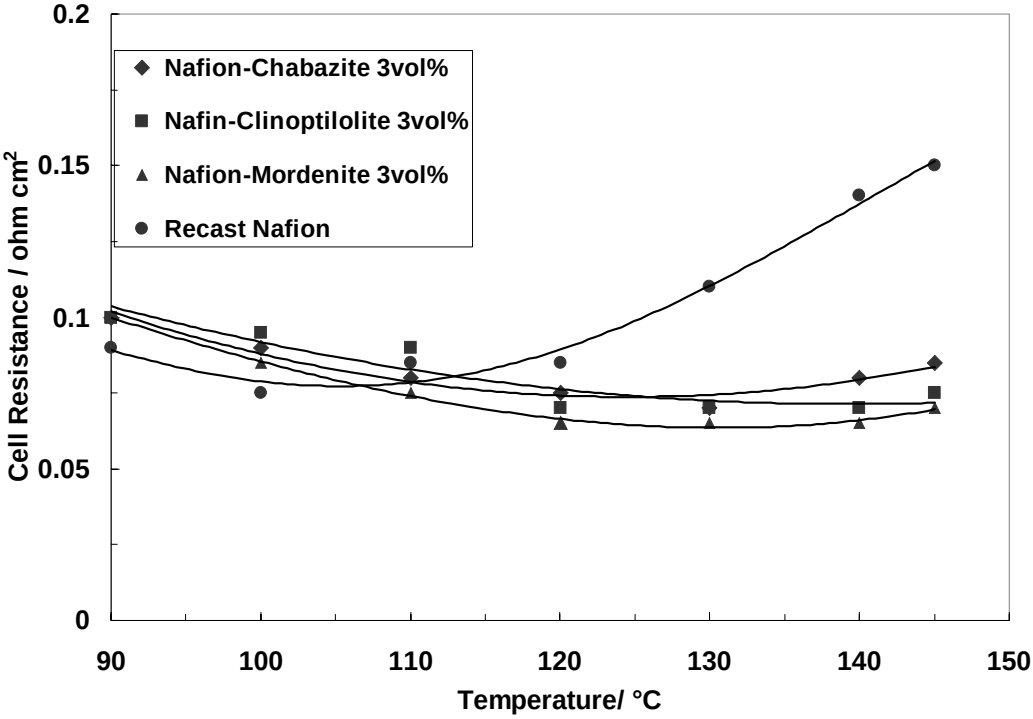

Fig. 3. Variation of cell resistance values as a function of the operating temperature for DMFCs employing the zeolite-based composite membranes compared to bare recast Nafion.

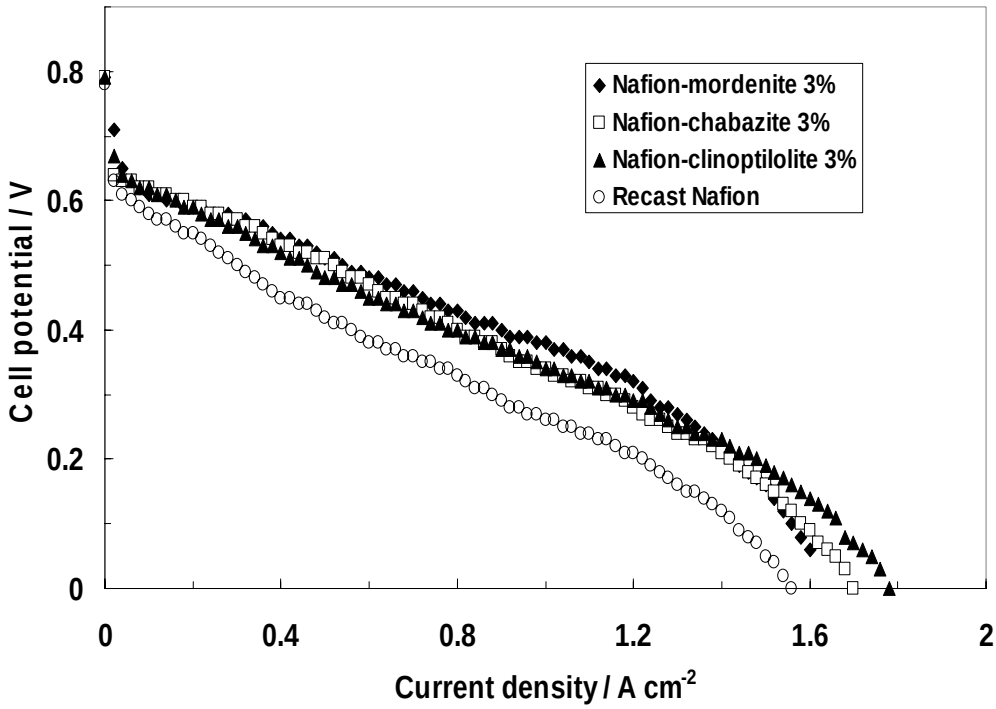

Fig. 4. DMFC polarization curves in the presence of oxygen feed at 140°C for various MEAs equipped with the composite membranes containing 3 vol.% zeolite powders compared to bare recast Nafion.

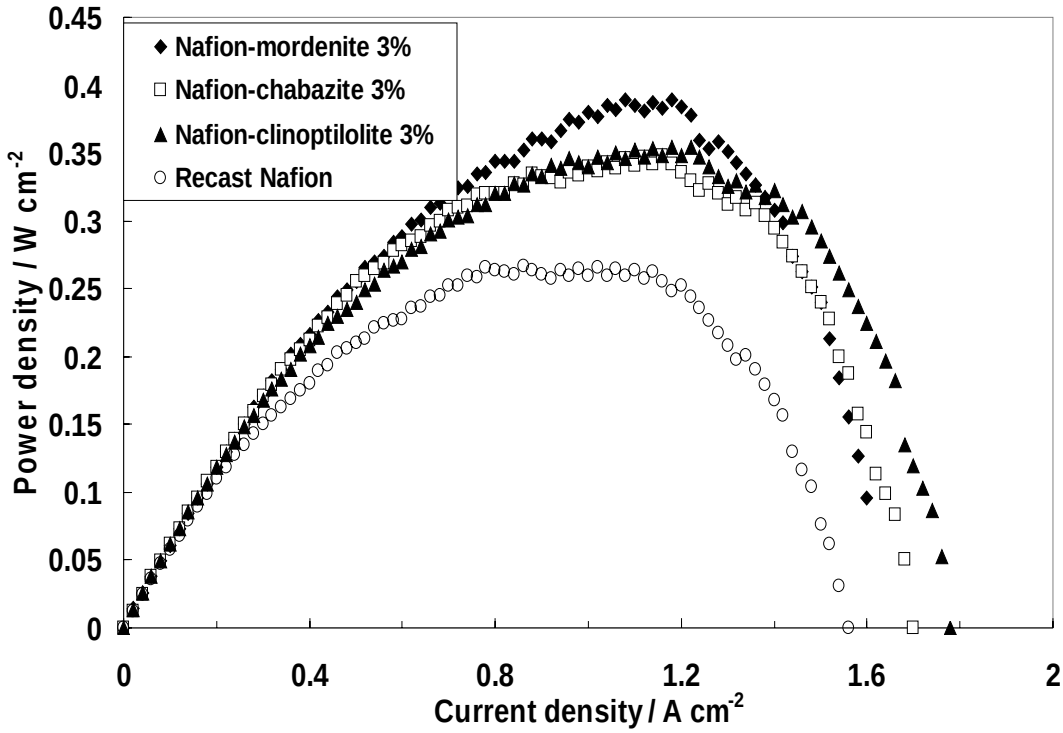

Fig. 5. DMFC power density curves in the presence of oxygen feed at 140°C for various MEAs equipped with the composite membranes containing 3 vol.% zeolite powders compared to bare recast Nafion.

The polarization curves obtained for the fuel cells equipped with the different membranes containing 3 vol.% zeolite filler at the temperature of 140°C in the presence of oxygen feed at cathode and 2M methanol solution at anode are reported in Fig. 4. A similar electrochemical behaviour was observed for the various composite membranes, whereas the polarization curve of the cell equipped with bare recast Nafion was significantly affected by a larger ohmic drop. The best electrochemical performance was obtained with the mordenite-based membrane, which gave a maximum power density of 390 mW cm^{-2} at current density of about 1.1 A cm^{-2} at 140°C under oxygen feed (Fig. 5). Similar performances were recorded for the DMFCs equipped with 6 vol.% zeolite-Nafion membranes (not shown); however, at larger loadings, the occurrence of pinholes inside the membrane was observed to be more probable.

The effect of temperature on the electrochemical polarization and power density behaviour of a fuel cell equipped with the mordenite-based membrane is reported in Fig. 6. The voltage loss in the activation control region decreases progressively as the temperature increases from 90°C to 140°C, indicating the strong activation nature of the methanol electro-oxidation process.

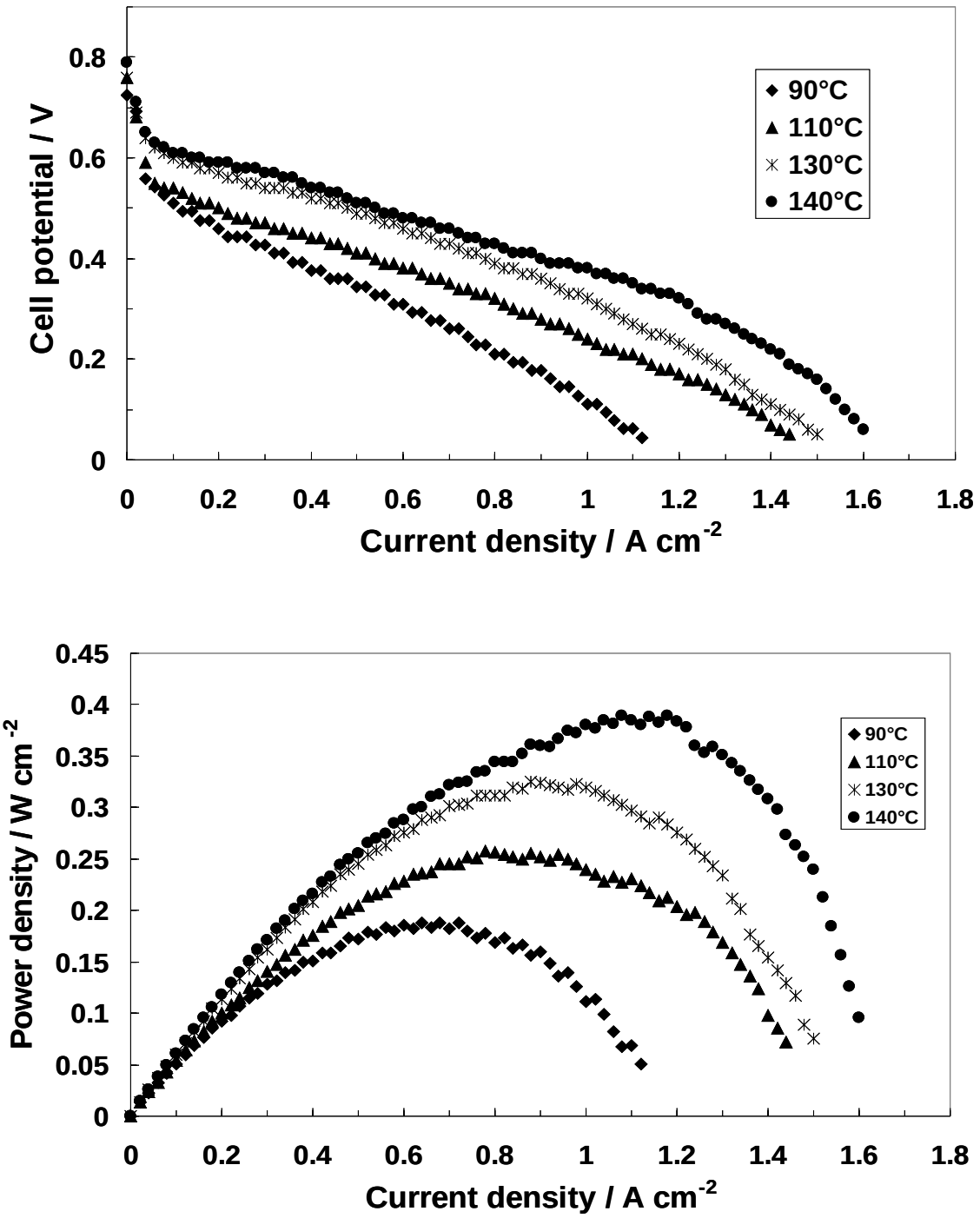

Fig. 6. Influence of operating temperature on the DMFC polarization and power density behaviour for the MEA equipped with mordenite-based membrane in the presence of oxygen and 2M methanol feed.

III.3.4 Conclusions

Composite Nation-zeolite membranes have shown good properties for high temperature DMFC operation, mainly due to their improved water retention characteristics. As observed with other inorganic fillers, the proton conduction properties [17] of the zeolite materials may also play a role in the enhanced conductivity of the DMFC at high temperature. However, this latter aspect need to be investigated more in depth. Maximum power densities comprised between 350 and 390 mW cm^{-2} were recorded at 140°C under oxygen operation and 2M MeOH with the 3 and 6 vol.% zeolite-based membranes. Such results indicate that an increase of the membrane conductivity and DMFC performance can be achieved through a proper tailoring of the surface acid-base properties of the inorganic filler in the composite membranes.

III.3.5 References

[1] M. Neergat, D. Leveratto and U. Stimming, *Fuel Cells* 2 (2002) 25.

[2] S. Wasmus and A. Kuver, *J. Electroanal. Chem.* 40 (1999) 150.

[3] A. S. Aricò, S. Srinivasan and V. Antonucci, *Fuel Cells* 1 (2001) 133.

[4] O. Savadogo, *J. New Mat. Electrochem. Systems* 1 (1998) 47.

[5] X. Ren, M. S. Wilson and S. Gottesfeld, *J. Electrochem. Soc.* 143 (1996) L12.

[6] V. Tricoli, N. Carretta and M. Bartolozzi, *J. Electrochem. Soc.* 147 (2000) 1286.

[7] B.S. Pivovar, Y. Wang and E.L. Cussler, *J. Membr. Sci.* 154 (1999) 155.

[8] A. S. Aricò, P. Creti, P. L. Antonucci and V. Antonucci, *Electrochem. Solid-State Lett.* 1 (1998) 66.

[9] P. Staiti, A.S. Aricò, V. Baglio, F. Lufrano, E. Passalacqua and V. Antonucci, *Solid State Ionics* 145 (2001) 101.

[10] V. Baglio, A. Di Blasi, A. S. Aricò, V. Antonucci, F. Serraino Fiory, S. Licoccia and E. Traversa, 202nd ECS meeting, Salt Lake City, Utah, October 20-24, 2002 Abstract C1-91.

[11] K.T. Adjemian, S.L. Lee, S. Srinivasan, J. Benziger and A.B. Bocarsly, *J. Electrochem. Soc.* 149 (2002) A256.

[12] M. Watanabe, H. Uchida, Y. Seki, M. Emori and P. Stonehart, *J. Electrochem. Soc.* 143 (1996) 3847.

[13] B. Bonnet, D.J. Jones, J. Roziere, L. Tchicaya, G. Alberti, M. Casciola, L. Massinelli, B. Bauer, A. Peraio and E. Ramunni, *J. New Mat. Electrochem. Systems* 3 (2000) 87.

[14] N. Miyake, J. S. Wainright and R.F. Savinell, *J. Electrochem. Soc.* 148 (2001) A905.

[15] B. Libby, W.H. Smyrl and E.L. Cussler, *Electrochem. and Solid State Letters* 4 (2001) A197.

[16] A.S. Aricò, V. Baglio, A. Di Blasi and V. Antonucci, *Electrochem. Comm.* 5 (2003) 862.

[17] D.W. Breck, "Zeolite Molecular Sieves", Wiley, 1974

[18] R. Szostak, "Handbook of Molecular Sieves", Van Nostrand Reinhold, New York, NY, USA, 1992

[19] D.H. Jung, S.Y. Cho, D.H. Peck, D.R. Shin and J.S. Kim, *J. Power Sources* 118 (2003) 205.

[20] A.S. Aricò, V. Antonucci, M. Minutoli and N. Giordano, *Carbon* 27 (1989) 337.

[21] A.S. Aricò, V. Baglio, A. Di Blasi, P. Cretì, P.L. Antonucci and V. Antonucci, *Solid State Ionics* 161 (2003) 251.

ACKNOWLEDGEMENTS

I express my deep sense of gratitude to the management of CNR-ITAE for kindly giving me permission to carry out this research work at CNR-ITAE Laboratories. I sincerely thank Dr. Vincenzo Antonucci for providing me all facilities and financial assistance through out my research carrier.

I wish to place on record my sense of gratitude to Dr. Antonino S. Aricò and Prof. Pier Luigi Antonucci for suggesting me these research topics and for their inspiring guidance. I am greatly indebted to them for their words of encouragement, unstinting support, involvement in the research work, valuable suggestions and for their critical evaluations at all stages.

I gratefully acknowledge the financial support of the European Commission through the DREaMCAR Project ENK6-CT2000-00315.

I deem it pleasure to thank Alessandra Di Blasi, Ester Modica, Irene Gatto, Daniela La Rosa for their constant encouragement, valuable suggestions and for offering critical comments during the preparation of the manuscript of this thesis.

I owe my sincere thanks to P. Cretì, G. Monforte, A. Stassi, C. D'Urso, L. Gullo, A. Carbone, A. Saccà, G. Urbani, R. Pedicini, A. Patti, M. Lo Faro for their help in various occasions.

I feel pleased to thank Prof. E. Traversa for giving me the opportunity to attend to this PhD course in Materials for Environment and Energy and all his group at University of Rome "Tor Vergata", in particular Prof. S. Licoccia, F. Serraino Fiory, V. Esposito, etc.

I take this opportunity to express my gratitude to my family members for their love and affection. I am thankful to my friends for giving me moral support, co-operation and encouragement all along.